Annexe 7

Modélisation du potentiel sismique du projet Horne 5

Ressources Falco Ltée
1100, avenue des Canadiens-de-Montréal, Bureau 300
Montréal, Québec, H3B 2S2

Ressources Falco Ltée
230, avenue Marcel-Baril
Rouyn-Noranda (Québec) J9X 7C1
Tél. : 819 917 3875
www.falcores.com

PAR COURRIEL

Rouyn-Noranda, le 5 août 2024

Monsieur Eric Chaize
Médecin conseil Santé et Environnement
Direction de santé publique
Centre Intégré de Santé et Services Sociaux de l'Abitibi-Témiscamingue (CISSSAT)
1, 9e Rue
Rouyn-Noranda (Québec) J9X 2A9

Objet : Modélisation du potentiel sismique du projet Horne 5
Ressources Falco Ltée

Monsieur Chaize,

À la suite de votre discussion avec Madame Hélène Cartier et Monsieur Martin Duclos, vous avez exprimé un intérêt pour les résultats de la modélisation numérique concernant le potentiel sismique du projet Horne 5. Vous trouverez ci-joints les documents suivants :

1. **Numerical Modelling and Risk Analysis** (2021_2158-HOR-002_RiskAnalysis_FINAL CORRECTED.pdf)

2. **Structure Response and Damage Produced by Ground Vibration From Surface Mine Blasting** (RI-8507-Blasting-Vibration-1989-Org-Scanned-Doc.pdf)

Dans le document « Numerical Modelling and Risk Analysis », il est indiqué que l'événement sismique le plus significatif modélisé pourrait survenir en fin de production, soit environ 13 ans et 10 mois après l'excavation du premier chantier, et pourrait atteindre une magnitude de 3,5 sur l'échelle moment-magnitude (Mw 3,5). Cette échelle, préférée à l'échelle Richter pour quantifier la magnitude des séismes, se base sur le moment sismique, lié à l'aire de rupture et au déplacement causé par l'événement. L'échelle moment-magnitude est comparable à l'échelle Richter pour des magnitudes allant jusqu'à 7 à 8.

…2

L'échelle de Richter étant logarithmique, chaque point supplémentaire correspond à une multiplication par dix de l'amplitude des ondes sismiques. Par conséquent, un événement de Mr 3,5 serait huit fois moins puissant que l'événement de Mr 4,1 survenu au complexe Laronde le 24 juin 2024.

La modélisation indique également que cet événement de Mr 3,5 pourrait générer des amplitudes vibratoires maximales de 70 mm/s. Bien que les séismes naturels produisent généralement des événements de longue durée et de basse fréquence, les événements sismiques induits par l'exploitation minière ont, par contre, une durée beaucoup plus courte, soit dans l'ordre de 2 à 3 secondes.

Pour une meilleure compréhension des impacts potentiels sur les structures, nous vous recommandons de consulter le document de la *United States Bureau of Mines* (USBM - *Structure Response and Damage Produced by Ground Vibration From Surface Mine Blasting*), notamment les pages 6 à 8. Par exemple, dans une étude, Richter indique que des dommages peuvent survenir à partir de vibrations de 156 mm/s à 1 Hz, ce qui serait bien au-delà des amplitudes anticipées pour un événement de Mr 3,5. Le potentiel de dommage dépend aussi de la durée des vibrations : des amplitudes de 156 mm/s à 1 Hz, telles qu'indiquées par Richter, pourraient ne pas causer de dommages si elles ne durent que quelques secondes, mais pourraient en provoquer si elles durent 25 à 30 secondes. En conséquence, un événement de Mr 3,5 (tel que modélisé pour le projet Falco Horne 5) générerait la moitié moins des amplitudes vibratoires considérées comme dommageables à une fréquence de 1 Hz, tout en étant d'une durée très courte ce qui limite d'autant plus le risque de bris.

Nous comprenons toutefois que le risque zéro n'existe pas et c'est pour cette raison qu'un programme d'inspection et d'intégrité des résidences et des infrastructures, associé à un programme de communication communautaire seraient mis en place avant le début des opérations.

Sachant que le potentiel d'événement plus significatif pourrait survenir environ 13 ans et 10 mois après l'excavation du premier chantier, nous nous sommes engagés à développer un programme d'instrumentation, de surveillance et de suivi de la sismicité qui permettrait de collecter de l'information sismique dès le début des opérations, ce qui permettrait de mieux comprendre la nature de la sismicité induite par le projet et mieux anticiper dans le temps le plus gros événement plausible en fonction des événements déjà enregistrés.

Bien entendu, si un tel événement survenait, un plan des mesures d'urgence préalablement défini avec les acteurs du milieu serait immédiatement déployé tant pour nos employé.es, le voisinage que pour la population rouynorandienne.

Nous demeurons à votre disposition pour toute question supplémentaire.

Veuillez agréer, Monsieur Chaize, nos plus cordiales salutations.

Julie Brassard

Julie Brassard, ing.
Directrice, services techniques

Ressources Falco Ltée
230, avenue Marcel-Baril
Rouyn-Noranda (QC) J9X 7C1
Tél. : 819 917-3875 poste 226
Cell. : 819 763-9400
Courriel : jbrassard@falcores.com

p. j.
- Numerical Modelling and Risk Analysis
- Structure Response and Damage Produced by Ground Vibration From Surface Mine Blasting

c. c. Madame Hélène Cartier, vice-présidente, environnement, développement durable et relations avec les communautés – Ressources Falco Ltée

Monsieur Martin Duclos, directeur, environnement et relations avec les communautés – Ressources Falco Ltée

ANDRIEUX & ASSOCIATES
GEOMECHANICS CONSULTING, L.P.

A²GC

Technical Report

(REVISED FINAL VERSION)

Horne 5 Project
Numerical Modelling and Risk Analysis

Friday 19 March 2021
A2GC Ref.: 2158-HOR-002-20210319-FR

Prepared For:

Osisko Gold Royalties, Ltd. – Falco Resources, Ltd.
Horne 5 Project

Prepared By:

Amélie Ouellet, Eng.
Thierry Lavoie, Eng.
Nicolas St-Onge, Eng.
André-Michel Maheux, Eng.
Patrick Andrieux, Eng.

Page left blank intentionally.

TABLE OF CONTENTS

Page

LIST OF FIGURES

LIST OF TABLES

Page

DISTRIBUTION LIST

(Names in alphabetical order)

Osisko Gold Royalties – Falco Resources

Mrs. Julie Brassard
Mr. Patrick Frenette
Mr. Victor Gauthier
Mr. François Girard
Mr. François Vézina

A2GC

Files.

Release Notes

A draft version of this report (A2GC ref. 2158-HOR-002-20201130-01) was released on 30 November 2020 for review and comments by Osisko Gold Royalties / Falco Resources engineering personnel.

A final version (A2GC ref. 2158-HOR-002-20210125-F) was released on 25 January 2021, which was found on 15 March 2021 to contain an error in Section 8.2.3 in the estimation of the vibration amplitudes from potential seismic events along the Andesite fault.

This revised final version supersedes both documents.

Twelve (12) interim presentations were delivered to Osisko Gold Royalties / Falco Resources following the progress meetings of 12 May, 26 May, 02 June, 16 June, 23 June, 30 June, 15 July, 11 August, 18 August, 28 August, 10 September and 25 September 2020. Results presented in this report supersede results presented in those progress meetings.

Disclaimer of Liability

This document was prepared by Andrieux and Associates Geomechanics Consulting, L.P. (A2GC) for the sole use of the persons listed in the distribution list and the firms they represent. The material presented in this report is the result of the utmost care by, and reflects the best judgement of, A2GC and its associates in light of the available information that had been provided to A2GC and its associates at the time it was prepared, and/or the data collected and/or derived by A2GC and its associates over the course of the project. A2GC accepts no responsibility for any errors and/or omissions in the information it has been provided with by the Client and/or other parties at the start and during the completion of this project. This document is comprised of text, tables and figures, all of which are to be read and interpreted in the context of the whole report. Any use of this document by a third party (any entity other than the Client), or any reliance on it, or any decision based on it, are the sole responsibility of that third party. A2GC accepts no responsibility for damages, if any, suffered by any third party as a result of decisions made, or actions taken, based upon the content of this document.

Please consider the environment before printing or photocopying this report.
If you must, two-sided printing on recycled paper is environmentally friendlier.

EXECUTIVE SUMMARY

The Horne 5 project is an underground gold project located within the city limits of the town of Rouyn-Noranda in the Abitibi region of northwest Quebec, in Canada. The main geomechanical challenges expected are related to a combination of strong and brittle rock mass conditions, deep mining (down to over 2 km below surface) and proximity to the historical Horne Mine above. The location on surface, nearly directly above, of the Glencore Horne smelter is another important aspect of the project.

Falco Resources, Ltd. has asked Andrieux and Associates Geomechanics Consulting, L.P. (A2GC) to conduct a numerical simulation of the entire Horne 5 feasibility study (FS) mining sequence and complete a geomechanical risk assessment based on the modelling results. The specific risk-related objectives were to: 1) evaluate the seismic potential at each modelling step; 2) establish a risk profile based on mining-induced stress and plasticity criteria; and, 3) verify that major infrastructure are planned in sectors unlikely to experience damaging mining-induced stress changes. Importantly, no additional geomechanical data were collected after the FS was published in 2017 – the analyses presented in this report are hence based on the same data.

The numerical modelling simulations were all completed using *FLAC3D*, an advanced explicit three-dimensional inelastic finite-difference program for continuum mechanics engineering applications. A mine-wide model was built, which encompassed all six dominant lithologies (Massive Sulphides, Semi-Massive Sulphides, Rhyolite, Diorite, Diabase and Andesite). Extensive work had been done during the FS to derive the mechanical properties of the various lithological units – in the absence of any new data, the same mechanical properties were retained. Four regional faults (the Andesite, Horne Creek, Strong and No Name) were also included in the model, represented by adding ubiquitous joints to the rock mass they intersected (while keeping the same intrinsic properties) based on the major faults general orientation. Paste backfill material was modelled as a strain-softening Mohr-Coulomb material with the mechanical properties derived during the FS. The in-situ stress regime was the same as was considered during the FS, installed tectonically to account for stiffer geological units attracting higher stresses than softer ones. The Horne 5 mining sequence analysed with the *FLAC3D* model is the one finalized during the FS, which encompasses 2,165 stopes. To limit computational time, as well as the storage of the model files, ten (10) stopes were mined at each modelling stage, for a total of 217 computed mining steps.

An analysis of the underground seismic potency was completed first, by quantitatively assessing the mining-induced energy released at each modelling step, based on the volume of rock undergoing inelastic deformation. The seismic potency can be related to the likelihood of seismic events. An associated relative risk level was derived for each modelling step. Note that no attempt was made to correlate the seismic potency results to the magnitude of possible seismic events. This remains an active field of research, which would have required significant field data to calibrate at Horne 5. This analysis concluded that 28 out of the 217 modelling steps (13%) were rated with a *High* seismic potency, with 26 occurring during Phase 2 mining mainly in stopes punching into a highly stressed, but not yet damaged, sill pillar. Modelling steps rated with a *Moderate* seismic potency were related to similar situations (e.g., punching of sill pillars, primary stopes causing shearing of secondary stopes), but were associated with less energy release.

Modelling results were also used to establish various mining risk profiles, in terms of mining conditions during stope recovery. The assessment of the mining conditions was meant to evaluate how challenging mining a given stope can be expected to be. Two types of mining challenges were considered: mining under high stress conditions (i.e., in highly stressed ground that is nearing its peak strength) and mining under low / residual conditions (i.e., in damaged and relaxed ground). Stopes excavated in highly stressed areas are likely to generate seismicity, require rehabilitation and/or be affected by drilling challenges, potentially resulting in production uncertainties and risks, such as schedule delays, rework, and possibly some ore losses in the worst cases. On the other hand, stopes mined in highly damaged areas are likely to cause production delays (from rework and rehabilitation) and experiment drilling challenges, which also can cause production uncertainties and risks. The risks of mining under high stress and residual conditions were first evaluated separately, then merged into a single production risk profile.

A total of 109 stopes out of the 2,165 Horne 5 stopes (5%) met the *High* rating threshold of the 'Mining Under High Stress Conditions' risk category: 34 during Phase 1 and 75 during Phase 2 mining. This represents 4% of the 866 Phase 1 stopes, and 6% of the 1,299 Phase 2 stopes. It is also interesting to note that out of the 109 stopes rated *High*, 100 constituted the first block (the southern-most stope) of a north-south panel of stopes. This represents 12% of the 863 "first block" stopes. Only 1% of the "second block" stopes were rated *High* (6 stopes out of 661), and this percentage dropped lower as the number of blocks increased. This suggests that where high stresses concentrate, opening one stope is sufficient to cut the stresses and generate a stress shadow area.

Considering mining under low / residual conditions, 83 stopes out of the 2,165 Horne 5 stopes (4%) are forecasted to be excavated under "residual conditions": 26 during Phase 1, and 57 during Phase 2, representing 3% of the 866 Phase 1 stopes, and 4% of the 1299 Phase 2 stopes.

The risks of mining under high stress conditions and under residual conditions were merged into a single global production risk profile, meant to capture the mining conditions under which the Horne 5 stopes are forecasted to be mined. Only stopes to which a *High* risk was assigned for either the high stress or the residual conditions hazards were considered in the global risk profile. Each Horne 5 stope can hence globally be flagged as a *High Stress* stope, a *Residual Conditions* stope, or an *OK* stope. A fourth category was added to highlight stopes that would have a portion highly stressed and another portion highly damaged. Those stopes were called *Combined* stopes.

Overall, a total of 202 stopes (9% of the 2,165 Horne 5 stopes) are expected to be mined under challenging conditions. Importantly, these risk estimates are based solely on the expected mining-induced stress changes during mining – the challenge associated with geological structures and discontinuities, which are always possible, was not considered in these analyses, themselves sensitive to the threshold values retained for the various risk categories.

The dilution risk was evaluated in terms of the expected behaviour of the stopes during mucking – post-blasting conditions were hence considered in this case. Note that the dilution potential was only evaluated in the hanging wall and footwall of the stopes. Numerical zones that were damaged and deconfined, and located within a pre-set geometrical range in the walls were counted as dilution. The total dilution associated with one stope was summed (in terms of tonnes) and the percentage of dilution for that stope was computed (tonnes of dilution / extracted tonnes). A dilution risk rating (*Low*, *Moderate* or *High*) was then assigned per stope based on the percentage of dilution computed. A total of 104 out of the 2,165 Horne 5 stopes (5%) were rated *High* in terms of the dilution risk: 30 during Phase 1 mining (representing 3% of the 866 Phase 1 stopes) and 74 during Phase 2 mining (representing 6% of the 1,299 Phase 2 stopes). Here as well, these analyses only considered the effects of stress on sound rock – the occurrence in the stope walls of adverse structures or patches of poor ground could significantly increase the dilution levels, as would poor mining practices.

Geomechanical aspects of the major infrastructures were also examined in terms of the mining-induced stress variations at their planned locations. The infrastructures evaluated were the crusher chambers, garage, shaft, ore passes and main ventilation raises. The haulage drifts between L1030 and L1310, planned to be driven within the ore body, were also assessed. The analysis was conducted through the examination of control points within the *FLAC3D* model. The selected infrastructures were hence not explicitly added in the model as physical voids, but, instead, mining-induced stress changes were tracked at their location, where control points were set, throughout the mining sequence. Stress paths in the σ_1-σ_3 space and deviatoric stress graphs were then extracted to verify that the stress state at the proposed location of each major infrastructure at each modelled mining step was not nearing the failure envelope of the local rock mass. If this stress state was deemed favourable, then the location was considered acceptable. Only small mining-induced stress changes were observed at the planned locations of the garage, shaft and Phase 2 crusher. The ore passes, ventilation raises and Phase 1 crusher locations showed stress changes, but these remained below the failure envelope and indicated no significant deconfinement (except for ventilation raises on L1150 and L1190, where σ_3 varies between 2 and 5 MPa). Stress variations at the haulage drift locations on levels 1030 to 1310 (driven within the ore body) were significantly larger. The failure envelope can be expected to be reached along these drifts, and very low confinement values are forecasted to develop at some point. In the FS, increased ground support requirements have been accounted for in the drifts located in ore. Still, maintaining these drifts throughout their required life span can be expected to be challenging. Planning for additional costs and delays (due to rehabilitation, ground support upgrades, and/or even bypasses) may be prudent.

Considering the importance of maintaining the integrity of the smelter, the mining-induced surface displacement was also evaluated from the *FLAC3D* modelling results. Less than 0.5 cm of total displacement was computed on surface at the smelter location due to mining at Horne 5. Note that the displacements due to the mining of the historical Horne mine were zeroed in the model prior to mining Horne 5. Therefore, the displacements subsequently computed are solely due to the mining of the Horne 5 ore body.

The volume of rock between the historical Horne mine and the upper Horne 5 stopes, referred to as the Barrier Pillar, will experience stress changes from Phase 1 mining, and fracturing of that barrier pillar due to stress increases was identified as a potential mining challenge. Consequently, the stress regime indicated by the numerical simulations within the barrier pillar was examined over the full mining sequence to establish whether conditions could develop in it, which could plausibly result in fracturing. At the end of Phase 1 (at mining step 99), about 250,000 m^3 of rock in the model have reached their residual strength in that sector, most of that volume being located north-west of the barrier pillar. But even with that large volume of damaged ground, a significant large-scale instability remains unlikely within the barrier pillar. Firstly, the volume of void open at any time (in the form of blasted stopes not yet backfilled) will remain small; secondly, by the time yielding will start in earnest, those Horne 5 stopes located nearest to the historical Horne workings will have long been excavated and backfilled; and, thirdly, the yielded volume sits mainly between the historical Horne workings and new Horne 5 stopes – it is not expected to connect with the development located to the north of the ore body. However, should the historical Horne excavations not be appropriately paste backfilled, water could reach the Horne 5 excavations through new fractures created in the barrier pillar. Note that this analysis did not account for possible large-scale persistent structural discontinuities within the barrier pillar.

Due to sensitive instrumentation installed in the smelter, it is important to assess whether a large seismic event could occur within the barrier pillar, which, being located at the top of the Horne 5 mine, would involve the shortest distance between the source and the smelter. One approach used to anticipate whether a rock mass subjected to stress changes will fail violently consists in examining how the stress path it is subjected to evolves over time. The likelihood of violent failure increases when the maximum (major, σ_1) principal stress (the driving stress) increases while the minimum (minor, σ_3) principal stress (the confining stress) remains near-constant or reduces slightly. For that purpose, stress paths in the σ_1-σ_3 space, as well as deviatoric stress values, were extracted at each mining step at control points purposely set up within the barrier pillar. The only area where the ratio of deviatoric stress magnitude over UCS was higher than 0.7 is located towards the top of the Horne 5 excavations and does not extend to the old Horne workings. The deviatoric stress magnitudes computed within the barrier pillar were also found to be similar to the values obtained in other pillars during mining. However, the major principal stress magnitude at control point '1036,' located by the "window" between the Horne 5 upper lobes, is expected to increase to about 150 MPa, with little reduction of the minor principal stress magnitude. This abutment sector could thus experience bouts of significant seismic activity and violent rock mass failure. Also, once the western sequence will have been completed, the stress towards the centre of the ore body will have increased. If possible, stopes in this sector should be mined sooner, shortly after the stopes to their east. Their extraction would then be easier due to the lower local stress levels. This would also provide the opportunity to have the area backfilled prior to the stress increase from the western mining front. Based upon the plastic deformations and stress paths computed at the control points within the barrier pillar, the FS assumption of a stress-induced seismic event with an upper magnitude around $M_N + 2.0$ in the barrier pillar appears credible. In the absence of large-scale geological structures within the barrier pillar, which could change the stress state and/or slip, a very large event would not be expected from stress change alone.

The plasticity state at the fault locations was also evaluated from the modelling results, which indicated that yielding of the rock mass at these locations due to Horne 5 mining activity occurred only over the mining depth range (i.e., not up to surface).

Because of its proximity to the planned Horne 5 stopes and the fact that it extends to surface, and given the current geological and structural knowledge, only the Andesite fault could realistically be a concern for severe adverse effects on surface. However, that fault lies in close proximity to the Horne 5 stopes (within about 10 m) only between levels 1194 and 1484. It then rapidly gains separation with elevation, above and below. The fault-slip potential of the Andesite fault was evaluated through a stress drop approach, and estimates of possible strain energy release levels and associated seismic event magnitudes were derived. For this purpose, the model was re-run without considering the weakened fault properties (without the ubiquitous joints), assigning instead the full Andesite mechanical properties to the numerical elements within the Andesite fault volume – this was deemed conservative because it allowed for larger stress drops to occur at failure. For the geological settings considered, the hypotheses retained in the various algorithms developed for this project and notwithstanding the intrinsic limitations of the analysis, the largest seismic event expected along the Andesite fault, originating at a depth of around 1,745 m below surface, would have a moment magnitude of about $M_W + 3.5$. To help assess the effects of the calculated seismic events on surface infrastructures, including the smelter, their vibration levels were estimated. The highest expected vibration amplitude occurred at Step 209 of the modelled mining sequence with a value of 70 mm/s, caused by the maximum moment magnitude event ($M_W + 3.5$) previously mentioned.

Note that a coalescence of events around solicited lock-up points along faults would normally appear in the seismic data, which would give advanced warning and allow for mitigating measures to be put in place. Mitigation measures could include a change of extraction sequence, a mining rate adjustment, additional ground support, destressing measures, etc. The aim would be to have these measures already planned and ready to deploy in the event that increased seismicity was detected, so they could be implemented without delay.

In reviewing the conclusions presented in this report, several important limitations must be kept in mind. Firstly, the *FLAC3D* model used in this work and the criteria retained for the various geomechanical risk assessment exercises were not calibrated on any field data. This is due to the absence of relevant data to conduct back-analyses. Also, in the absence of in-situ stress measurements at the Horne 5 site, the virgin stress regime implemented in the model was chosen from the literature, based on regional measurements. It must also be noted that *FLAC3D* being a continuum formulation, structurally controlled instabilities and failures along discontinuities were not systematically considered. Furthermore, no dynamic effects, from blast-induced vibrations for example, were considered, nor were water effects (e.g., potential pore pressures) considered. Finally, A2GC did not visit the site within the context of these analyses – all the input data used in this project were entirely supplied to A2GC by Osisko Gold Royalties / Falco Resources.

In parting, the Horne 5 project has several characteristics that increase the geomechanical risk it is associated with: it is deep (and, hence, will be subjected to high stress levels), its geological settings are expected to be stiff, strong and brittle (a combination that leads to seismic conditions), and its upper part will lie in close proximity to the large historical Horne mine. It targets high production levels, which, with the mining method retained, require large longhole stopes and multiple mining fronts (and the associated diminishing sill pillars between mining fronts). Being located in the City of Rouyn-Noranda, it also has numerous neighbours. All these aspects were considered in the geomechanical analyses. Still, close monitoring, including with a sufficiently sensitive seismic monitoring array, should be conducted right from the beginning of construction and throughout mining to verify that the stress analyses are reliable, and confirm that mining is proceeding as expected. The cause(s) of significant divergence between field observations and modelling-based expectations, if any, should be promptly investigated. Such divergence can have many causes, such as incorrect far-field stress assumptions, incorrect mechanical properties, the presence of geological horizons and structures that were not included in the model, differences between the sequence implemented and the one modelled, differences between the stope dimensions and geometry vs those modelled, and more. Once the causes of the discrepancies are identified and corrected, the model can be rerun to produce adjusted risk profiles and production "road maps."

SUMMAIRE EXÉCUTIF

Horne 5 est un projet aurifère souterrain localisé dans la ville de Rouyn-Noranda dans la région de l'Abitibi dans le nord-ouest de la Province de Québec. Les principaux défis géomécaniques anticipés sont liés à une combinaison de conditions rocheuses dures et fragiles, une grande profondeur de minage (jusqu'à 2 km) et la proximité de la vieille mine Horne juste au-dessus. La présence en surface, presque directement au-dessus, de la fonderie Horne de Glencore est un autre aspect important du projet.

Ressources Falco, ltée. a mandaté Andrieux et associés consultation géomécanique, s.e.c. (A2GC) pour effectuer des simulations numériques de la séquence de minage préconisée dans l'étude de faisabilité de Horne 5 et compléter une étude de risque géomécanique à partir des résultats de cette modélisation. Les objectifs spécifiques étaient 1) d'évaluer le potentiel de sismicité à chaque étape de minage simulée ; 2) d'établir un profil de risque basé sur les contraintes de terrain induites par le minage et des critères de rupture du massif rocheux ; et, 3) de vérifier que les infrastructures majeures seront localisées dans des secteurs peu propices à subir des dommages suite à des changements de contraintes. Il faut noter qu'aucunes nouvelles données géomécaniques n'ont été collectées ou produites depuis la publication de l'étude de faisabilité en 2017 – les analyses présentées dans ce rapport sont donc basées sur les mêmes informations.

Les simulations numériques discutées dans ce rapport ont toutes été réalisées avec *FLAC3D*, un code explicite tridimensionnel avancé basé sur la méthode des différences finies et largement utilisé en mécanique continue (*continuum mechanics*). Un modèle global à l'échelle de la mine a été construit, qui a inclus les six principales lithologies rencontrées à Horne 5 (Sulphures massifs, Sulphures semi-massifs, Rhyolite, Diorite, Diabase et Andésite). Un travail considérable a été effectué lors de l'étude de faisabilité pour établir les propriétés mécaniques des diverses unités géologiques – en l'absence de nouvelles données, les mêmes propriétés ont été utilisées dans le cadre des travaux décrits dans ce rapport. Quatre failles régionales (Andésite, Horne Creek, Strong et No Name) ont également été incluses dans le modèle numérique, représentées par l'ajout de joints répétitifs (*ubiquitous joints*) aux unités rocheuses qu'elles intersectent, orientés selon l'orientation des failles. Le remblai en pâte a également été considéré dans les travaux, représenté comme un matériel Mohr-Coulomb muni des propriétés mécaniques établies lors de l'étude de faisabilité. Le régime de contrainte *in situ* est demeuré similaire à celui utilisé lors de l'étude de faisabilité, installé tectoniquement pour tenir compte des différences de rigidité entre les diverses unités rocheuses et créer un chargement différentiel avant même de miner. La séquence d'extraction analysée avec *FLAC3D* est celle qui a été retenue suite à l'étude de faisabilité, qui comprend 2 165 chantiers. Pour limiter le temps de calcul et l'espace mémoire requis pour gérer les fichiers de résultats, dix (10) chantiers ont été minés simultanément à chaque étape modélisée, pour un total de 217 étapes distinctes analysées.

Une analyse du potentiel sismique (*Seismic Potency*) a d'abord été entreprise en examinant l'énergie libérée par le minage à chaque étape modélisée, basée sur le volume de roche soumis à des déformations inélastiques. Le potentiel sismique pouvant être relié au risque de générer des événements sismiques, un niveau de risque a ainsi pu être associé à chacune des 217 étapes de minage examinées. À noter qu'aucune tentative n'a été faite pour corréler les résultats des analyses de potentiel sismique à la magnitude possible des événements – cet aspect demeure un domaine de recherche actif, et des données historiques auraient été requises pour calibrer l'approche à Horne 5. Cette analyse a conclu que 28 des 217 étapes de minage modélisées (13%) sont associées à un 'Haut' potentiel sismique, 26 de ces étapes survenant durant le minage de Phase 2, et principalement dans des chantiers approchant des piliers de sole encore intacts et soumis à de hautes contraintes. Les étapes de minage associées à un potentiel sismique 'Moyen' étaient d'ailleurs reliées à des situations similaires, mais associées à moins de libération d'énergie.

Les résultats de modélisation ont également été utilisés pour établir divers profils de risque en termes des conditions de minage anticipées durant la production. L'évaluation des conditions de minage avait pour but d'estimer le degré de difficulté anticipé pour chaque chantier. Deux types de difficultés ont été considérés : le minage sous hautes contraintes de terrain (dans du roc soumis à de hautes pressions de terrain et approchant sa résistance mécanique ultime) et le minage dans des conditions de contraintes faibles à résiduelles (dans du terrain endommagé et en relaxation). Les chantiers extraits sous hautes contraintes sont susceptibles de générer de la sismicité, de requérir des travaux de réhabilitation et/ou d'être affectés par des problèmes de forage, pouvant causer des incertitudes et des fluctuations de production, ainsi que d'autres risques concernant le respect des cédules de production, des travaux de remédiation supplémentaires, voire des pertes de réserves dans les pires cas. D'un autre côté, des chantiers minés dans du terrain fortement abîmé peuvent causer des délais de production suite à des travaux de réhabilitation dans les accès, ou des problèmes de forage (incluant la perte de trous), qui peuvent eux-aussi résulter en des incertitudes et des fluctuations de production. Les risques de minage sous hautes contraintes et dans des conditions résiduelles ont d'abord été évalués séparément, puis combinés en un profil de risque unique.

Un total de 109 chantiers sur les 2 165 que compte Horne 5 (soit 5%) ont été associés à un 'Haut' niveau de risque de récupération sous hautes contraintes : 34 durant la Phase 1 et 75 durant la Phase 2 – cela représente 4% des 866 chantiers de la Phase 1 et 6% des 1 299 chantiers de la Phase 2. Des 109 chantiers répertoriés à haut niveau de risque de hautes contraintes durant leur récupération, 100 constituent le premier bloc (le chantier le plus au sud) de panneaux nord-sud, ce qui représente 12% des ces premiers blocs. Seulement 1% des chantiers constituant le second bloc d'un panneau de production (6 sur un total de 661) sont anticipés être affectés par de hautes contraintes, et ce pourcentage continue de diminuer pour les blocs subséquents plus au nord. Cette observation suggère que dans les secteurs hautement contraints, le minage d'un chantier à l'extrémité des panneaux suffit pour couper les contraintes et protéger le reste des blocs du panneau.

En ce qui concerne les chantiers récupérés en post-rupture, 83 des 2 165 chantiers à Horne 5 (4%) sont anticipés être soumis à ces conditions : 26 durant la Phase 1 et 57 durant la Phase 2, ce qui correspond à 3% des 866 chantiers de la Phase 1 et 4% des 1 299 chantiers de la Phase 2.

Les risques de minage sous hautes contraintes et en conditions résiduelles ont été combinés en un seul profil de risque global. Seuls les chantiers associés à des risques qualifiés de 'Haut' soit à cause de hautes contraintes soit à cause de conditions résiduelles ont été considérés dans le profil de risque global. Chacun des chantiers à Horne 5 peut donc être étiqueté 'À risque de hautes contraintes', 'À risque de conditions résiduelles' ou 'Ok'. Une quatrième catégorie de risque, nommée 'À risque de conditions combinées', a été ajoutée pour identifier des chantiers soumis à la fois à des conditions de hautes contraintes dans un secteur et à des conditions résiduelles ailleurs. Globalement, 202 chantiers (soit 9% des 2 165 chantiers de Horne 5) ont été identifiés comme étant associés à une forme de 'Haut' risque lors de leur extraction. À noter que ces estimations de risque sont basées uniquement sur les contraintes de terrain – les difficultés possiblement associées à des structures géologiques, toujours possibles, n'ont pas été considérées dans ces analyses, elles-mêmes sensibles aux seuils retenus pour les diverses catégories de risque.

Le risque de dilution a été évalué en termes du comportement des chantiers lors de leur marinage – les conditions post-sautage ont donc été considérées dans ce cas. À noter que la dilution n'a été évaluée que pour les épontes supérieure et inférieure des chantiers. Les éléments numériques endommagés (en post-rupture) et sous faible confinement, et localisés dans des volumes préétablis, ont été considérés comme contribuant à la dilution. La dilution totale associée à un chantier a été déterminée (en termes de tonnes) et les pourcentages de dilution calculés (sous forme du ratio tonnes de dilution / tonnes extraites). Une catégorie de dilution ('Faible', 'Moyenne' ou 'Haute') a subséquemment été assignée à chaque chantier en fonction du pourcentage calculé. Un total de 104 chantiers sur les 2 165 à Horne 5 (soit 5%) ont été catégorisés comme 'Hauts' en termes de dilution : 30 dans la Phase 1 (soit 3% des 866 chantiers de cette Phase) et 74 dans la Phase 2 (soit 6% des 1 299 chantiers de cette Phase). Ici encore, ces analyses considèrent uniquement les effets des contraintes sur du roc sain – la présence dans les épontes des chantiers de structures adverses ou de zones de mauvais terrain pourrait augmenter significativement la dilution, tout comme de mauvaises pratiques d'exploitation.

Les aspects géomécaniques reliés aux infrastructures majeures ont également été examinés en termes des contraintes induites par les opérations de minage à leurs localisations planifiées. Les infrastructures évaluées ont été les concasseurs, le garage, le puits, les chutes à minerai et les monteries de ventilation. Les galeries de roulage des niveaux 1030 à 1310, planifiées être localisées à l'intérieur même du gisement, ont également été examinées. L'analyse a été effectuée par le biais de points de contrôle installés dans le modèle *FLAC3D*. Les infrastructures n'ont donc pas été explicitement incluses dans le modèle sous forme de vides – ce sont seulement les changements de contraintes dus au minage aux points de contrôle placés à leurs localisations qui ont été analysés. Les cheminements de contraintes dans l'espace σ_1-σ_3 et les contraintes déviatoriques ont été extraits à ces points de contrôle et ont constitué les critères de l'analyse, elle-même sous forme de la vérification que les conditions de contraintes ne s'approchaient pas de l'enveloppe de rupture du massif rocheux local. Si tel était le cas, la situation était considérée favorable et la localisation proposée acceptable. Seuls de faibles changements de contraintes ont généralement été observés aux localisations proposées pour le garage, le puits et le concasseur de la Phase 2. Les localisations prévues pour les chutes à minerai, les monteries principales de ventilation et le concasseur de Phase 1 montrent des changements de contraintes, mais qui n'atteignent pas l'enveloppe de rupture et n'indiquent pas de pertes significatives de confinement, sauf pour les monteries de ventilation aux niveaux 1150 et 1190, où σ_3 varie de 2 à 5 MPa. Les variations de contraintes anticipées aux galeries de roulage aux niveaux 1030 à 1310 (foncées dans le minerai) sont plus significatives. L'enveloppe de rupture est atteinte à ces endroits et de très faibles niveaux de confinement sont prévus être atteints. Bien que du support de terrain supplémentaire ait été prévu pour ces galeries dans l'étude de faisabilité, leur maintien tout au long de leur durée de vie utile pourrait s'avérer ardu. Planifier des coûts et des délais additionnels (dus à de la réhabilitation, des ajouts de support de terrain, voire des voies de contournement) serait prudent.

Considérant l'importance de maintenir l'intégrité de la fonderie Horne, les déformations causées en surface par les opérations de minage ont également été examinées. Moins de 5 mm de déplacement total ont été calculés à la localisation de la fonderie suite aux opérations à Horne 5. À noter que les déplacements déjà causés par la vieille Horne ont été réinitialisés dans le modèle *FLAC3D* avant de miner le gisement Horne 5 – les déplacements rapportés sont donc seulement ceux causés par l'extraction des chantiers de Horne 5.

Le volume de roche entre les chantiers de la vieille mine Horne et ceux de Horne 5, appelé le « pilier de barrière », est prévu subir des changements de contraintes durant l'extraction de la Phase 1, et la fracturation de ce pilier a été identifiée comme étant un problème potentiel. L'évolution du régime de contraintes indiquée par les analyses numériques a donc été examinée sur toute la séquence pour établir si des conditions de contraintes propices à des ruptures sont susceptibles de se produire. À la fin de la Phase 1 (à l'étape modélisée N° 99), environ 250,000 m^3 de roche dans le modèle ont atteint leur résistance résiduelle dans ce secteur, ce volume se situant principalement au nord-ouest du pilier. Mais même avec ce fort volume de terrain endommagé, une instabilité significative de grande envergure demeure improbable dans le pilier. En premier lieu, le volume ouvert à tout moment (sous forme de chantiers dynamités non encore remblayés) demeurera limité. De plus, à partir du moment où l'endommagement est prévu commencer de manière significative, les chantiers de la mine Horne 5 localisés les plus proches des chantiers de la vieille mine Horne auront déjà été exploités et remblayés. Finalement, les volumes affectés sont surtout situés entre les chantiers historiques et de nouveaux chantiers – ils ne sont pas anticipés rejoindre le développement du côté nord du gisement. Toutefois, si les anciennes excavations à la mine Horne ne sont pas bien remplies de remblai en pâte, des infiltrations d'eau pourraient atteindre la Horne 5 par le biais de nouvelles fractures créées dans le pilier de barrière. À noter que cette analyse ne tient pas compte de la présence possible de grandes structures géologiques persistantes naturelles dans ce pilier.

Considérant la fragilité de certains instruments à la fonderie, un aspect du projet a consisté en l'estimation de la possibilité de forts événements sismiques émanant du pilier de barrière, qui impliqueraient les plus courtes distances d'atténuation à la surface. Une approche possible pour estimer si un massif rocheux soumis à des changements de contraintes subira des ruptures soudaines et violentes consiste à traquer le cheminement des contraintes jusqu'à l'enveloppe de rupture. Le risque de générer des ruptures de ce type augmente à mesure que la contrainte maximale (la contrainte principale majeure, σ_1, qui alimente le processus) augmente alors que la contrainte minimale (la contrainte principale mineure, σ_3, qui génère du confinement) demeure quasi-constante ou diminue faiblement. Dans cette optique, le cheminement des contraintes dans l'espace σ_1-σ_3, ainsi que la magnitude des contraintes déviatoriques à des points de contrôle insérés selon un patron régulier dans le pilier de barrière, ont été examinés. Le seul secteur où le rapport de la magnitude de la contrainte déviatorique sur la résistance en compression uniaxiale a dépassé 0.7 est localisé vers le haut des chantiers de la mine Horne 5 et ne s'étend pas jusqu'aux chantiers de la vieille mine Horne. Les contraintes déviatoriques calculées dans le pilier de barrière ont des magnitudes comparables à celles observées dans d'autres piliers de sole ailleurs dans la mine durant la séquence de minage. Toutefois, la contrainte principale majeure calculée au point de contrôle N^o 1036, localisé dans la « fenêtre » entre les lobes supérieurs de Horne 5, est prévue augmenter jusqu'à une magnitude de près de 150 MPa, accompagnée d'une faible réduction de la magnitude de la contrainte principale mineure. Ce secteur pourrait donc être soumis à des épisodes de forte sismicité et à des ruptures violentes. De plus, une fois que la séquence à l'ouest aura été complétée, les contraintes vers le centre du gisement auront augmenté. Si cela s'avère possible, les chantiers dans ce secteur auraient avantage à être minés plus tôt dans la séquence, peu de temps après les chantiers à l'est. Leur extraction serait alors plus facile étant donné les niveaux de contraintes plus faibles. Cela offrirait aussi l'opportunité de remblayer l'endroit avant que les augmentations de contraintes causées par le minage à l'ouest ne surviennent. D'après les déformations plastiques et les cheminements de contraintes obtenus aux points de contrôle dans le pilier de barrière, l'hypothèse formulée lors de l'étude de faisabilité, faisant état d'un événement sismique maximum en provenance de ce pilier (suite aux redistributions de contraintes) de l'ordre de M_N (magnitude Nuttli) + 2.0, demeure crédible. D'après ces analyses, et en l'absence de grandes structures géologiques dans le pilier de barrière qui pourraient changer l'état de contraintes et/ou glisser, un très fort événement sismique n'est pas anticipé en provenance de cet endroit suite au seul changement des contraintes.

L'état de plasticité a été évalué numériquement dans le modèle aux endroits où les failles sont localisées. Cette analyse a indiqué de l'endommagement causé par les contraintes induites par les opérations de minage à Horne 5 à ces endroits est localisé dans la fenêtre verticale de minage et ne s'étend pas jusqu'en surface.

Dû à sa proximité aux chantiers du gisement Horne 5 et au fait qu'elle s'étend jusqu'en surface, et selon les connaissances géologiques et structurales actuelles, seule la faille Andésite pourrait vraisemblablement avoir de fortes répercutions en surface. Toutefois, cette faille est à proximité des chantiers (en-deçà d'environ 10 m) seulement entre les niveaux 1194 et 1484 – elle s'en éloigne ensuite rapidement avec l'élévation, vers le haut et vers le bas. Le potentiel de glissement soudain (*fault-slip*) de la faille Andésite a été évalué avec une approche de chute de contraintes, et une estimation a été effectuée des niveaux de libération d'énergie de déformation et de la magnitude d'événements sismiques associés. À ces fins, le modèle numérique a été relancé, mais sans les propriétés affaiblies des failles (sans la présence des joints répétitifs), assignant plutôt les propriétés de l'Andésite aux éléments numériques à l'intérieur de la faille – cette approche est considérée conservative puisqu'elle a permis de générer de plus grandes chutes de contraintes à la rupture. Pour les conditions géologiques considérées, les diverses hypothèses retenues dans les algorithmes numériques développés pour cette étude et les limites intrinsèques de la méthode, le plus gros événement sismique anticipé le long de la faille Andésite, originant d'une profondeur de 1 745 m, aurait une magnitude de près de M_W (moment magnitude) + 3.5. Afin d'évaluer les effets de ces événements sismiques sur les infrastructures en surface, incluant la fonderie, les vibrations qu'ils sont susceptibles d'y engendrer ont été estimées. Les plus hautes vibrations calculées sont survenues à l'étape de minage 209, d'une amplitude de 70 mm/s, associées au plus gros événement sismique (de magnitude maximale M_W + 3.5) discuté précédemment. Une coalescence d'événements sismiques devrait apparaître autour de points de verrouillage (qui résistent au glissement) le long de la faille, qui devrait normalement être détectée par le système de surveillance sismique et avertir suffisamment d'avance pour que des mesures de mitigation soient mises en place. Ces mitigations pourraient inclure des ajustements à la méthode et/ou la séquence et/ou la vitesse de minage, du support de terrain supplémentaire, des mesures de relaxation des contraintes (*destressing*), etc. L'objectif serait alors d'avoir ces mesures déjà en place et prêtes à être rapidement déployées dès que la sismicité devient significative.

Diverses limitations importantes reliées aux analyses effectuées dans le cadre de ce projet doivent être gardées en tête lors de la lecture de ce rapport. Tout d'abord, the modèle *FLAC3D* et les critères retenus pour les divers types de risques géomécaniques n'ont pas pu être calibrés avec des observations de terrain. Cela est dû à l'absence de données historiques locales fiables avec lesquelles effectuer des rétro-analyses. Aussi, en l'absence de mesures de contraintes *in situ* à Horne 5, le régime de contraintes naturelles pré-minage a été établi suite à une revue littéraire et basé sur des mesures régionales. De plus, *FLAC3D* étant un modèle en formulation continue, les instabilités et ruptures contrôlées par des structures géologiques n'ont pas été systématiquement examinées. Aucun effet dynamique, causé par exemple par les vibrations de sautage, n'a non plus été considéré, ni aucun effet résultant de la présence d'eau (comme des pressions interstitielles, par exemple). Finalement, A2GC n'a pas visité le site de Horne 5 dans le cadre de ces travaux – tous les intrants utilisés dans les diverses analyses ont été fournis à A2GC par Royautés aurifères Osisko / Ressources Falco.

En conclusion, le projet Horne 5 est associé à des conditions qui augmentent le risque géomécanique auquel il est associé : il est situé en grande profondeur (et, donc, sera soumis à de hautes contraintes de terrain), ses caractéristiques géologiques sont anticipées être rigides, résistantes et fragiles (une combinaison favorable au développement de conditions sismiques) et sa partie supérieure est à proximité de la vieille mine Horne. Ses cibles de production sont élevées, ce qui requiert, avec la méthode de minage choisie, d'assez gros chantiers longs-trous et de multiples fronts de minage (et, donc, la présence de piliers qui seront progressivement réduits entre ces fronts de minage). Étant localisée dans la ville de Rouyn-Noranda, la mine aura aussi plusieurs voisins. Tous ces aspects ont été considérés dans les analyses géomécaniques. Néanmoins, un suivi serré devra être effectué dès le début de la construction de la mine et durant toute son extraction, incluant avec un système de surveillance sismique suffisamment sensible, pour vérifier que les analyses géomécaniques demeurent fiables et confirmer que le minage procède selon les conditions anticipées. Les causes de divergences entre les observations de terrain et les prévisions des analyses numériques, s'il y en a, devraient être rapidement investiguées. De telles divergences peuvent avoir de nombreuses causes, comme un champ de contraintes naturelles incorrect, de mauvaises propriétés mécaniques, la présence d'horizons géologiques et/ou de structures qui n'étaient pas inclus dans le modèle, des différences entre la séquence appliquée et celle modélisée, des changements de géométrie et de dimensions des chantiers par rapport à ceux modélisés, et autres. Une fois les causes des écarts entre les observations et les prédictions identifiées, le modèle peut alors être corrigé et relancé pour produire des profils de risque ajustés et des anticipations de production révisées.

1. INTRODUCTION AND BACKGROUND

The Horne 5 project is an underground gold project located in Rouyn-Noranda, in the Abitibi region of northwest Quebec, in Canada. The mining complex will be located on the site of the former Québmont Mine, within the city limits of the town of Rouyn-Noranda. A feasibility study (FS) was published for the project on 05 October 2017 (Falco Resources, 2017), at which time production was planned to start in 2021.

The main geomechanical challenges expected at the Horne 5 project are related to a combination of strong and brittle rock mass conditions, deep mining (at depths between 710 and as much as 2060 m below surface) and proximity to the historical Horne Mine above. The location on surface, nearly directly above, of the Glencore Horne smelter is another important aspect of the project.

Numerical simulations were conducted as part of the FS study in 2016-2017 by Golder Associates, Ltd. (Golder) in support of the mine design. Stress and plasticity analyses were conducted to help derive stopes dimensions and to provide guidelines regarding the mining sequence (including for the management of the sill pillars, converging fronts, diabase dyke and barrier pillar). Results from the Golder modelling work were used to establish the FS mining sequence. However, the final mining sequence derived during the FS was not entirely simulated at the time.

Falco Resources, Ltd. (Falco) has asked Andrieux and Associates Geomechanics Consulting, L.P. (A2GC) to conduct a numerical simulation of the entire Horne 5 FS mining sequence and to complete a geomechanical risk assessment based on the modelling results. A2GC sent a proposal to that effect on 03 February 2020, which was accepted by Falco on 21 February 2020.

Based on the modelling results, the specific objectives of the project were to:

1. Evaluate the seismic potential at each modelling step;
2. Establish a risk profile based on mining-induced stress and plasticity criteria; and,
3. Verify that major infrastructure (crushers, garage, shaft, ventilation raises, ore passes) are planned in sectors that will not experience major mining-induced stress changes.

In the following report, the data available for the study are first presented in Section 2. The *FLAC3D* model built is then described in Section 3. The seismic potential analyses are discussed in Section 4. The geomechanical risk assessment is explained and its results are presented in Section 5. The stress paths experienced by the major infrastructures are shown in Section 6. A discussion about the stresses in the barrier pillar is given in Section 7. Finally, the fault-slip potential on major faults is discussed in Section 8. Limitations and recommendations are then summarised in sections 9 and 10.

2. AVAILABLE DATA

No additional geomechanical data were collected after the FS was published in 2017. The assessments presented in this report are based on the following data provided by Falco:

- Bedrock topography – dated 18 February 2016
- Historical Horne Mine openings – dated 24 February 2016
- Major faults model – dated 14 September 2016
- Lithological model – dated 05 December 2016
- Extensive rock strength testing and interpretation – from the Golder (2016) FS work
- Mining sequence – from the FS, dated 05 October 2017
- Major infrastructure location – from the FS, dated 05 October 2017

The CAD input data files used are detailed in Table 1.

Table 1. CAD input data files used in the project.

Data type	File name	Date	Comments
Lithological model	Massive Sulphide_ELV-4300.dxf	20-Feb-17	–
	Gems_H5_GG_CC_Granite_surf_2016_PEA.dxf	05-Dec-16	Rhyolite was assigned by default. A visual check was done.
	Gems_H5_GG_CC_Rhy_ALL_surf_2016_PEA.dxf	05-Dec-16	
	Gems_H5_GG_CC_Rhy_BR_surf_2016_PEA.dxf	05-Dec-16	
	Gems_H5_GG_CC_Rhy_DYKE_surf_2016_PEA.dxf	05-Dec-16	
	Gems_H5_GG_CC_Rhy_Quem_surf_2016_PEA.dxf	05-Dec-16	
	Gems_H5_GG_CC_Rhy_TU_surf_2016_PEA.dxf	05-Dec-16	
	Gems_H5_GG_CC_Syenite_surf_2016_PEA.dxf	05-Dec-16	–
	Gems_H5_GG_CC_Diabase_D_surf_2016_PEA_EW.dxf	05-Dec-16	–
	Gems_H5_GG_CC_Diabase_D_surf_2016_PEA_NS.dxf	05-Dec-16	–
	M_diabase.dxf	03-May-16	Andesite was prioritised over M-Diabase where they overlapped
	Gems_H5_GG_CC_Andesite_surf_2016_PEA.dxf	05-Dec-16	
Major faults	FLT_Andesite_surf_ff_20160914_ext.dxf	14-Sep-16	In Major_2016 1028b.dxf
	FLT_HorneCreek_surf_ff_20160914_ext.dxf	14-Sep-16	
	FLT_Unknown_surf_ff_20160914_ext.dxf	14-Sep-16	
	FLT_Strong_surf_ff_20161025_SHZ.dxf	25-Dec-16	

Table 1 (cont.). CAD input data files used in the project.

Data type	File name	Date	Comments
Home openings	HORNE_DRIFTS.dxf	04-Mar-20	HORNE_ DRIFTS was not imported in the model
	HORNE_REMBLAIS_ELV-4300_EXP_2020-03-06.dxf	06-Mar-20	
	HORNE_VIDES_ELV-4300_EXP_2020-03-06.dxf	06-Mar-20	
Topo-graphy	TOPO_ELV-4300_2020-03-06.dxf	06-Mar-20	–
Mining sequence	Stope Name and Blast Date.xlsx	05-Oct-17	One (1) dxf per stope in the sequence – received on 03-Mar-20
Infra-structure	Horne 5_Infrastructure Location.dxf	05-Oct-17	Polylines – received on 09-Apr-20

A total of twenty-nine (29) unconfined compressive strength (UCS) tests, thirty-two (32) Brazilian indirect tensile strength (BTS) tests and fifty-two (52) triaxial compressive strength (TCS) tests were conducted during the FS study. From this testing campaign, a set of mechanical properties was derived for the FS – note that the mechanical properties used in the model presented in this report were not modified from the FS. Details regarding the mechanical properties are given in Section 3.3.

During the FS study, Golder attempted to find calibration data from the historical Horne Mine to validate the numerical model, but no such data could be found. Therefore, neither the FS model nor the model presented in this report have been checked against field data.

3. *FLAC3D* MODEL CONSTRUCTION

This section discusses the choice of numerical modelling code for the project, as well as the geometry of the model constructed for the analyses.

3.1 CHOICE OF NUMERICAL MODELLING CODE – *FLAC3D*

The numerical modelling simulations presented in this report were all completed using *FLAC3D*™ (Fast Lagrangian Analysis of Continua in 3 Dimensions) version 7.00 (Itasca, 2019), a software package developed and commercialised by Itasca Consulting Group, Inc. (Itasca). *FLAC3D* is an advanced explicit three-dimensional inelastic finite-difference program for continuum mechanics engineering applications.

The basis for this program is the well-established numerical formulation used by the two-dimensional program *FLAC*™. *FLAC3D* extends the analysis capability of *FLAC* (Itasca, 2017) into three dimensions, simulating the behaviour of three-dimensional structures made of soil, rock or other materials that undergo plastic flow once their yield limits are reached. Materials are represented by polyhedral elements within a three-dimensional grid. Each element behaves according to a prescribed linear or non-linear (inelastic) stress-strain law in response to applied forces or boundary restraints. Because no matrices are formed, large three-dimensional calculations can be achieved with reasonable memory requirements.

Because of the hard and brittle massive nature of the rock mass, and the deep mining conditions, mining-induced stresses were expected to be the main mining challenge at Horne 5. The dominant failure mechanism anticipated was stress-related, rather than structurally controlled. For that reason, *FLAC3D* was selected as it is a continuum formulation fundamentally designed to simulate stress changes throughout a rock mass with a plastic behaviour. The Itasca proprietary *FISH*™ coding language allows for extended customisation and automatization of *FLAC3D* to be achieved, in terms of input formulation, failure modes, post-peak behaviours and results visualisation.

Note that *FLAC3D*, and by extension the modelling results presented in this report, do not explicitly account for wedge failure or other discrete structurally controlled instabilities, such as unravelling or strata delamination. A discontinuum formulation would be required for this type of analysis (e.g., *3DEC*™ or *PFC3D*™) – however, given the rock mass conditions, this type of instability was not expected to be prevailing.

3.2 MODEL GEOMETRY

To achieve the project objectives listed in Section 1, a mine-scale *FLAC3D* model was constructed. The objective was to simulate the FS mining sequence to capture the mining-induced stress, deformation and yielding changes in the rock mass as the sequence unfolds.

The model geometry was prepared from a series of referenced 3D dxf files with the various lithological contacts, large-scale geological structures, and existing and future excavations (Table 1). Rhino3D™ was used to collate all the dxf files, after which the end-result was imported into *FLAC3D*. The model dimensions were 3,072 m in the North-South direction, 4,096 m in the East-West direction and 2,785 m vertically. The dimensions of the smallest numerical zones towards the core of the model were 4 m × 4 m × 8 m, with the largest dimension being vertical. The dimensions of the largest zones, furthest from the mining excavations and geological contacts of interest, were 256 m × 256 m × 256 m. The total number of numerical zones in the model was 2,691,365. Outside and inside views of the *FLAC3D* model are shown in Figure 1 (isometric views looking north-west) and Figure 2 (front elevation views looking north), respectively.

The smallest 4 m × 4 m × 8 m zone size was assigned to volumes within and immediately around planned Horne 5 stopes and in sectors of interest where high resolution was required. Having non-cubic zones (twice as high as wide) greatly reduced the number of zones in the model, which significantly accelerated processing time. The planned stopes at Horne 5 being higher than wide and long, the number of elements per stope remained between 4 and 6 in all directions. The Horne 5 stopes ranged between depths of approximately 710 m to 2,060 m below surface – the modelled future Horne 5 stopes are is shown in Figure 2a.

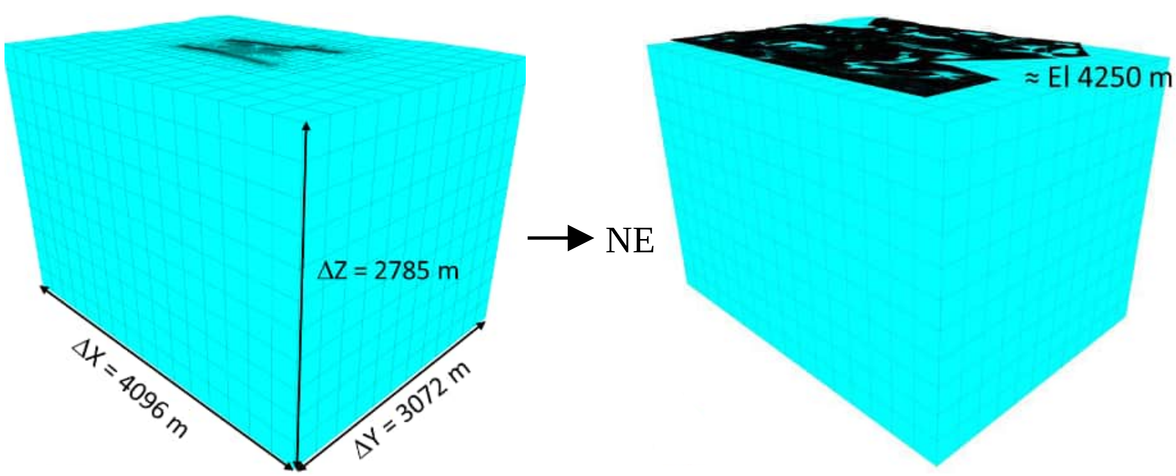

(a) Overall model extent. (b) Available topographic data.

Figure 1. Views of the external *FLAC3D* model extent.

(a) Future Horne 5 excavations.

(b) Historical and future mining.

Figure 2. Views of the inside *FLAC3D* geometry.

The smallest numerical zones within the historical Horne mine were 8 m × 8 m × 8 m, or 8 m × 8 m × 16 m if located near Horne 5 stopes, which were fitted with non-cubic zones. There are Horne 5 stopes adjacent to the historical Horne mine at depths of between approximately 685 m and 950 m. The historical Horne openings are shown in Figure 2b with respect to Horne 5 stopes.

The *FLAC3D* model was built up to surface. The topography CAD file (referred to in Table 1) was used. However, the coverage of the available topography file was not as wide as the extent of the *FLAC3D* model, and therefore, surface was fixed at z = 4,250 m where no topography data were available. The extent of the topography data available is shown in Figure 1b.

Four (4) major faults were included in the *FLAC3D* model: the regional Andesite, Horne Creek, Strong and No Name. The Andesite and Horne Creek faults were modelled up to surface whereas the Strong and No Name faults did not extend to surface.

The fault interpretations available were 3D surfaces that included no information on thickness. However, it is believed (Golder, 2017c) that major faults are associated with shear zones of varying thicknesses. As a result, all four faults were fitted with a thickness (instead of being modelled as interfaces). All faults were defined in thickness by a minimum of 4 to 5 numerical zones, the smallest zones at fault locations being 8 m × 8 m × 8 m, or 8 m × 8 m × 16 m if located near Horne 5 stopes. The major faults included in the *FLAC3D* model are shown in Figure 3 (the views are looking approximately west).

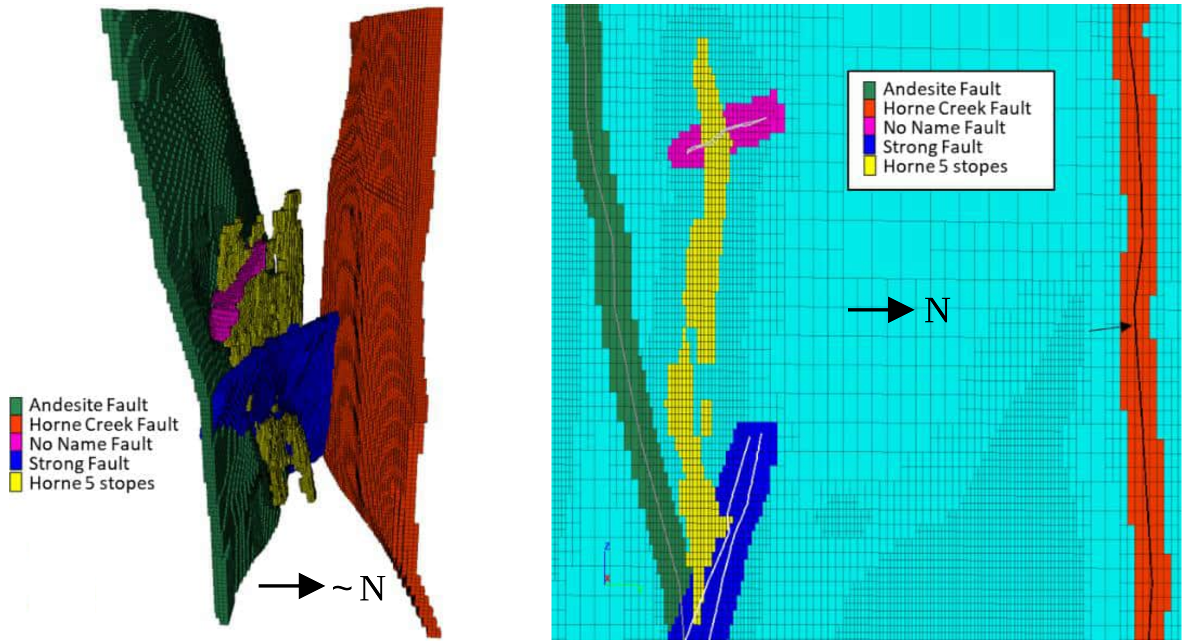

(a) General view of the major faults. (b) Faults representation.

Figure 3. Major faults included in the *FLAC3D* model.

Six (6) simplified lithological groups were included in the model: Massive Sulphides (MS), Semi-Massive Sulphides (SMS), Rhyolite (RHY), Diorite (DIO), Diabase (DIA) and Andesite (AND). The MS and SMS groups correspond to the ore material, whereas RHY and DIO are the main and secondary host rocks, respectively. The DIA group represents two main diabase dykes that cross the ore body. The AND group bounds the ore body to the South. The same groupings were made for the FS: the RHY group included Granite and all Rhyolite types (e.g., Brecciated and Quemont), and the DIO group included the Syenite units.

The available geology solids extended slightly above the Horne 5 stopes, but not up to surface – in the absence of geological interpretation, Rhyolite was assigned by default in this part of the model. The dimensions of the numerical zones within the diabase dykes (DIA group) were reduced to 4 m × 4 m × 8 m to ensure the presence of a minimum of 4 to 5 zones across their width. As there was no geological interpretation for the SMS group, SMS was assigned to numerical zones that were part of the Horne 5 stopes but did not belong to the MS group. The representation in the model of the MS and SMS groups is shown in Figure 4.

Additional zone densification (to 4 m × 4 m × 8 m) was done around or along major infrastructures (crushers, garages, shaft, ventilation raises, ore passes) to capture the stress paths at these locations.

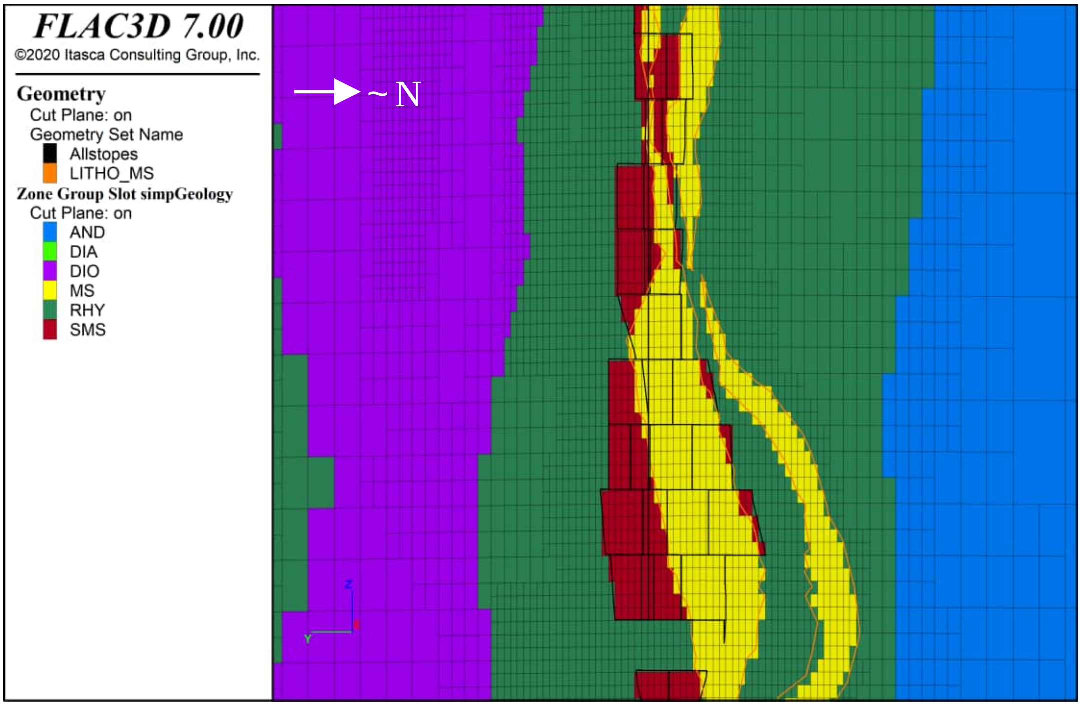

Figure 4. Representation of the MS and SMS groups in the *FLAC3D* model.

3.3 Mechanical Properties

Extensive work was done by Golder during the FS to derive the mechanical properties of the various lithological units at the Horne 5 project. In the absence of any new data, the same properties were retained in the analyses presented in this report. Theoretical considerations on the trilinear strength envelope are summarised in Section 3.3.1. The mechanical properties used for the Horne 5 rock groups are then shown in Section 3.3.2. Precisions on the mechanical properties assigned to the faults are provided in Section 3.3.3, followed in Section 3.3.4 by the properties used for the paste backfill.

3.3.1 Trilinear Strength Envelope

To account for the change of failure mode that accompanies increasing confining pressures, the rock mass scale strength envelopes of the brittle rock horizons at Horne 5 were considered trilinear (Kaiser *et al.*, 2000). The first segment of the envelope corresponds to the spalling strength, which corresponds to a Hoek-Brown curve with σ_{ci} = 0.33 to 0.50 × UCS, m = 0 and s = 1. The second segment is the spalling limit, which corresponds to the spalling-to-shear rupture transition and is typically represented by a line σ_1 / σ_3 = 10 to 20. The third segment is the confined strength, typically taken to be 80% of the intact rock strength. A trilinear field strength envelope is shown graphically in Figure 5.

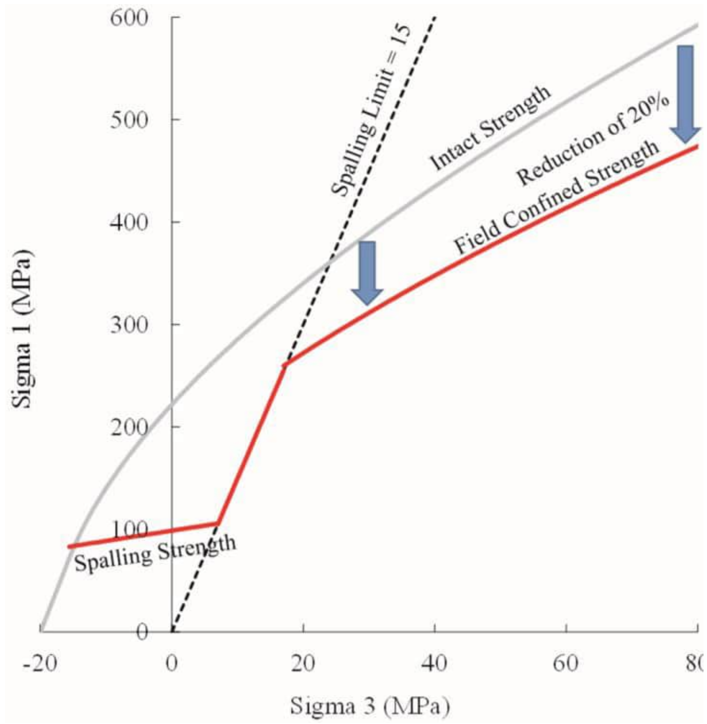

Figure 5. Trilinear strength envelope (after Bewick *et al.*, 2017).

3.3.2 Rock Mass Scale Strength

In the FS study, the following steps were followed by Golder to derive rock mass scale strength envelopes for *FLAC3D* from laboratory testing data.

1. A total of twenty-nine (29) unconfined compressive strength (UCS) tests, thirty-two (32) Brazilian indirect tensile strength (BTS) tests and fifty-two (52) triaxial compressive strength (TCS) tests were conducted during the FS study. From this dataset, intact rock Hoek-Brown strength envelopes were derived for the six (6) following rock types: MS, SMS, RHY, DIO, DIA and. An example is shown in Figure 6a (this example is for the Massive Sulphides [MS] unit).

   Values of Young's modulus, Poisson's ratio, density and UCS were also obtained from laboratory testing. Intact rock parameters are shown in Table 2, and intact rock Hoek-Brown curves for the six geology groups are compared in Figure 7.

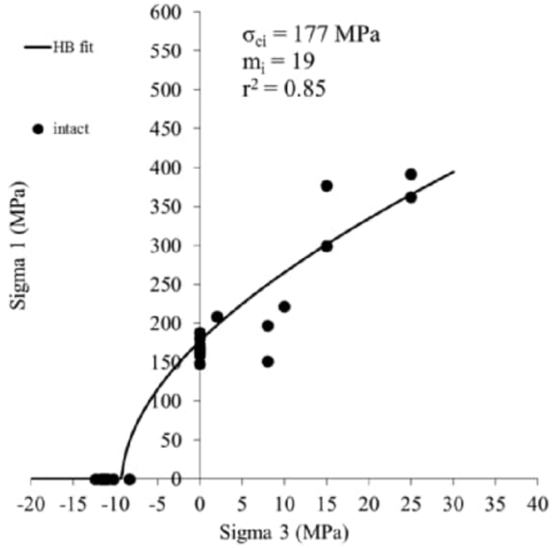

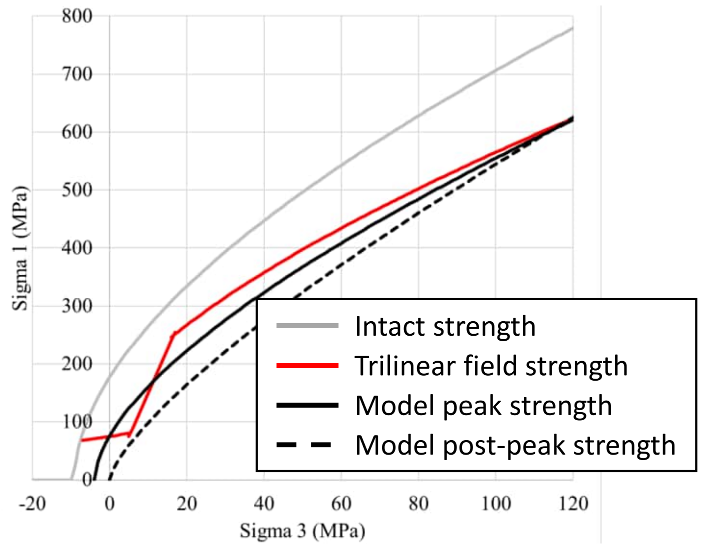

(a) Intact rock strength Hoek-Brown curve fitted through laboratory test results (after Golder, 2016).

(b) Rock mass (model) scale Hoek- Brown peak and post-peak curves fitted through the tri-linear strength envelope.

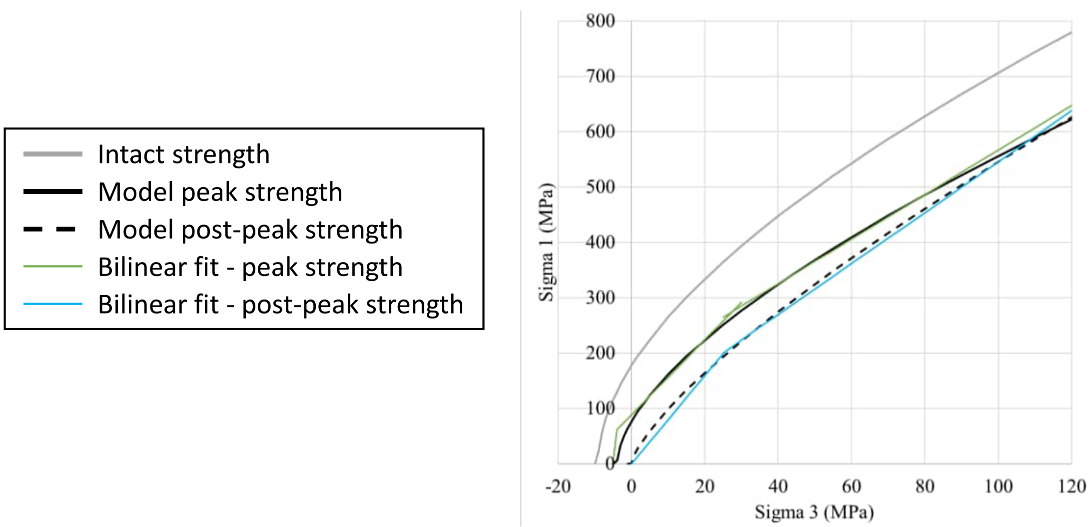

(c) Bilinear Mohr-Coulomb failure envelope fitted through the rock mass scale peak and post-peak strength envelopes.

Figure 6. Methodology followed by Golder during the FS to derive the rock mass scale strength envelopes implemented in the *FLAC3D* model (example of the MS unit).

Table 2. Intact rock mechanical properties.

Unit	Elastic properties			UCS (MPa)	Hoek-Brown properties	
	Density (kg/m^3)	Young's modulus (GPa)	Poisson's ratio (–)		σ_{ci} (MPa)	m_i
MS	4,700	145	0.23	168	177	19
SMS	3,400	144	0.21	157	148	10
RHY	2,800	94	0.22	205	234	13
DIO	2,900	110	0.27	247	286	20
DIA	3,000	106	0.28	258	260	20
AND	2,900	103	0.25	221	222	12

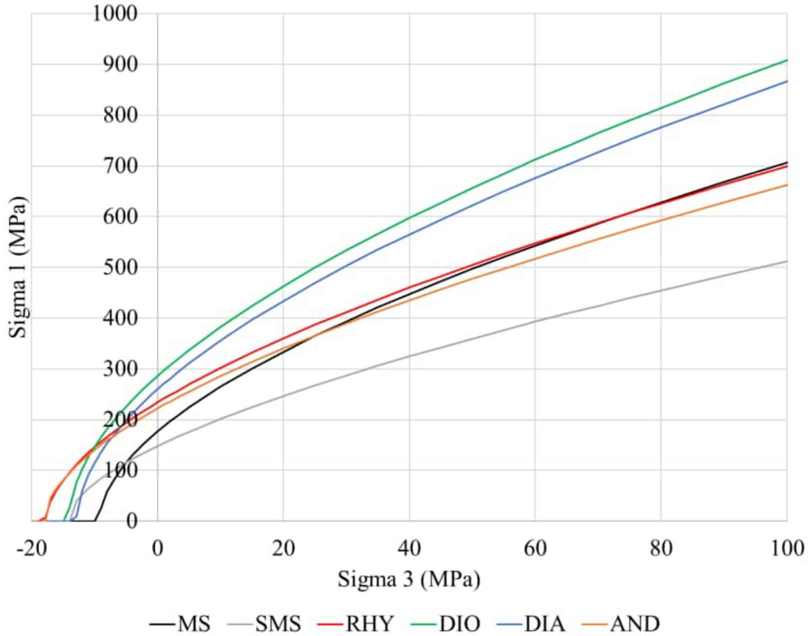

Figure 7. Intact rock Hoek-Brown curves for the six geology groups.

2. From the intact rock strength envelopes, trilinear strength envelopes were derived using a rock mass scale spalling strength of 0.45 × UCS and a spalling limit of $\sigma_1 / \sigma_3 = 15$.
3. For modelling purposes, Hoek-Brown curves were fitted through the trilinear strength envelope. An example is shown in Figure 6b for the MS unit. The corresponding rock mass scale parameters are given in Table 3.
   - The peak strength envelope was adjusted to intersect:
     - The spalling strength;
     - The mid-point of the spalling limit; and,
     - The field strength at a confinement of around 100 MPa.

- The model post-peak strength assumed:
  - The Hoek-Brown parameter s is nearly zero (0.001), such that σ_1 is close to zero when σ_3 = 0 MPa; and,
  - The post-peak strength curve intersects the peak strength curve at a confinement of around 100 MPa. This implied that at a confinement of 100 MPa, the rock mass will not lose strength when the peak strength is reached.

4. For implementation purposes in *FLAC3D*, the model peak and post-peak strength envelopes were then approximated with bilinear Mohr-Coulomb curves – those bilinear Mohr-Coulomb curves are the ones implemented in *FLAC3D*. An example is shown for the MS unit in Figure 6c. The Mohr-Coulomb parameters implemented in *FLAC3D* are given in Table 4.

As proposed by Golder during the FS study (Golder, 2017a), the critical cumulative plastic shear strain interval, over which the rock drops from peak to post-peak strength, was taken to be 0.1%.

Table 3. Field (rock mass scale) Hoek-Brown properties.

Unit	GSI	Elastic properties		Peak strength (Hoek-Brown)				Post-peak strength (Hoek-Brown)			
		Young's modulus (GPa)	Poisson's ratio (–)	σ_{ci} (MPa)	m	s	a	σ_{ci} (MPa)	m	s	a
MS	87	136	0.23	76	19	1	0.55	76	9.5	0.001	0.70
SMS	87	136	0.21	71	10	1	0.54	71	6.0	0.001	0.67
RHY	80	83	0.22	92	13	1	0.59	92	7.5	0.001	0.75
DIO	80	97	0.27	111	17	1	0.60	111	10.0	0.001	0.75
DIA	75	87	0.28	116	17	1	0.58	116	10.0	0.001	0.73
AND	80	91	0.25	99	12	1	0.57	99	7.0	0.001	0.72

Table 4. Bilinear Mohr-Coulomb envelopes implemented in the *FLAC3D* model.

Unit	Model peak strength (Mohr-Coulomb)						Model post-peak strength (Mohr-Coulomb)					
	First segment			Second segment			First segment			Second segment		
	c (MPa)	ϕ (°)	σ_t (MPa)	c (MPa)	ϕ (°)	σ_t (MPa)	c (MPa)	ϕ (°)	σ_t (MPa)	c (MPa)	ϕ (°)	σ_t (MPa)
MS	17	48	– 4	41	37	N/A	0	51	0	20	40	N/A
SMS	19	39	– 6	36	29	N/A	0	46	0	17	33	N/A
RHY	21	46	– 7	41	37	N/A	0	51	0	16	41	N/A
DIO	22	50	– 6	46	42	N/A	0	54	0	19	45	N/A
DIA	24	49	– 6	48	41	N/A	0	54	0	20	45	N/A
AND	23	44	– 8	43	35	N/A	0	50	0	17	39	N/A

3.3.3 Mechanical Properties of the Major Faults

Major faults were modelled by adding ubiquitous joints to the rock mass they intersected (while keeping the same intrinsic properties). The ubiquitous joints properties were set as follows: no cohesion (0 MPa), no tensile strength (0 MPa) and a friction angle of 35°. The orientation of the ubiquitous joints was based on the major faults general orientation, given in Table 5.

Table 5. Orientation of major faults (after Golder, 2017c).

Major fault	Dip (°)	Dip direction (°)
Horne Creek	80	165
Andesite	80	005
Strong	70	200
No Name	45	110

Notes:

- Dip is measured downwards from horizontal.
- Dip direction is measured clockwise from geographic North.
- Both conventions were maintained throughout the project.

3.3.4 Paste Mechanical Properties

The paste material was modelled as a strain-softening Mohr-Coulomb material. The mechanical properties implemented in *FLAC3D* were derived from the planned unconfined compressive strength of 1 MPa suggested by Golder (Golder, 2017b). The mechanical properties retained for the paste backfill material are given in Table 6.

Table 6. Paste mechanical properties implemented in the *FLAC3D* model.

Type of properties		Property	Value
Elastic Properties		Density[1] ρ (kg/m^3)	2,300
		Young's modulus[2] E (GPa)	0.20
		Poisson's ratio[3] ν	0.30
Strain-softening Mohr-Coulomb properties	Peak properties	Friction angle[4] ϕ_p (°)	30
		Cohesion[5] c_p (kPa)	290
		Tension[6] σ_{Tp} (kPa)	72
	Residual properties	Friction angle[7] ϕ_r (°)	45
		Cohesion c_r (kPa)	0
		Tension σ_{Tr} (kPa)	0
		Dilation angle[8] (°)	10

Please note the following concerning Table 6:

1. The density was assumed to be 2,300 kg/m^3.
2. $E = 72 \times UCS + 2 \times 10^8$, based on experience, UCS being expressed in Pa.
3. The Poisson's ratio was assumed to be 0.30.
4. The peak friction angle was assumed to be 30°.
5. $c_p = UCS / (2 \tan [45° + \phi / 2])$, the analytical form of the relation between the Mohr-Coulomb and Hoek-Brown failure envelopes.
6. $\sigma_{Tp} = 0.072 \times UCS$, based on experience.
7. The residual friction angle was assumed to be 45°. This is higher than the peak value to capture the friction increase that can result from fill material breaking apart.
8. The dilation angle was assumed to be 10°.

3.4 Stress Conditions

The in-situ stress regime implemented in the *FLAC3D* model was the same as for the FS model. It was chosen from the literature, based on regional measurements (Maloney & Yong, 2006). The stress gradients used are shown in Table 7.

Table 7. In situ stress regime implemented in the *FLAC3D* model (after Golder, 2017a).

Principal stress magnitude (MPa)	Orientation
$\sigma_1 = 23.6 + 0.026 \times z$	Horizontal, NE-SW
$\sigma_2 = 17.1 + 0.016 \times z$	Horizontal, NW-SE
$\sigma_3 = 0.021 \times z$	Vertical

Please note the following symbols and abbreviations used in Table 7:

- σ_1, σ_2 and σ_3 are the major, intermediate and minor principal stress components, respectively, expressed in MPa;
- z is the depth below ground surface, expressed in metres; and,
- N is North, S is South, E is East and W is West.

The stress profiles are graphically shown in Figure 8, where the principal stress magnitude values at the base of the *FLAC3D* model are given, for reference. Concerning the stress tensor orientation, as for the FS, the minimum principal stress (σ_3) was assumed vertical, and the major principal stress (σ_1) was assumed horizontal and oriented north-east–south-west (NE-SW). A plan view showing the orientation of σ_1 with respect to the Horne 5 ore body is shown in Figure 9. Note that no in situ stress measurements have been conducted on the Horne 5 site to confirm the validity of the selected in situ stress profile.

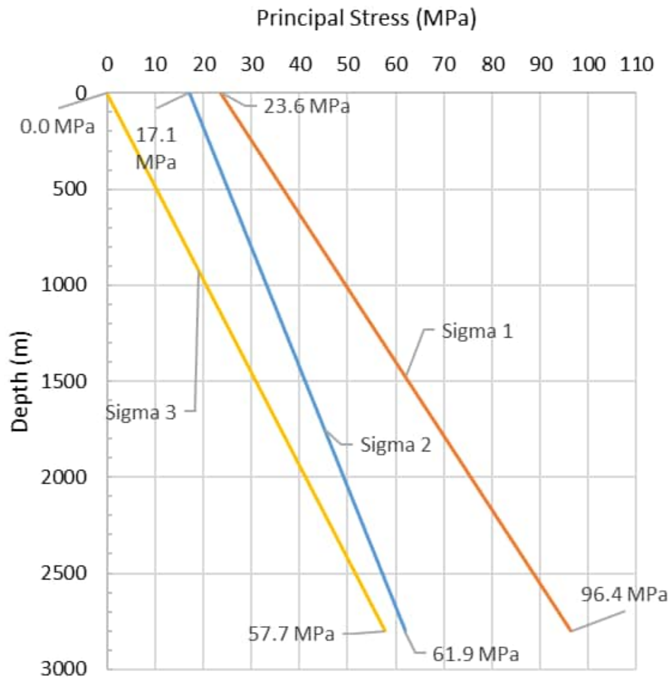

Figure 8. Principal in situ stress gradients implemented in the *FLAC3D* model.

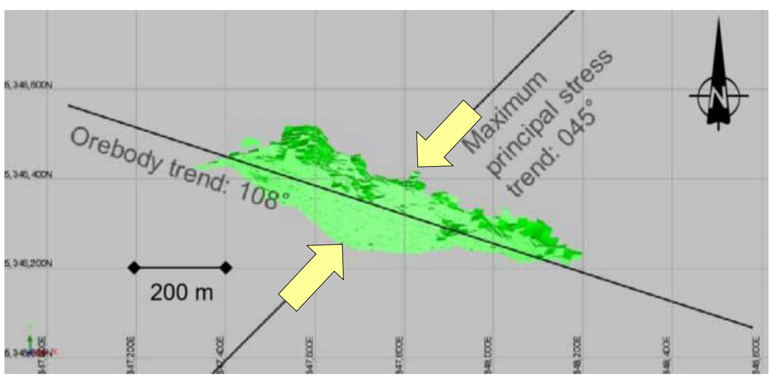

Figure 9. Plan view showing the orientation of σ_1 relative to the Horne 5 ore body (after Golder, 2017a).

Ground stresses were installed tectonically in the *FLAC3D* model, i.e., the model was simultaneously compressed in two axes, parallel to the maximum and minimum horizontal stress directions (σ_H and σ_h, respectively, which are also σ_1 and σ_2). The stresses at the model boundaries were increased gradually until they matched the stress gradients reported in Table 7. This methodology has the advantage of accounting for stiffer geological units (with a higher Young's modulus) attracting higher stresses than softer units. The stiffness contrast between the ore body (around 145 GPa) and the main host rock (94 GPa) justified this approach.

3.5 Mining Sequence

Prior to starting the analysis of the Horne 5 FS stopes, the mining and backfilling of the historical Horne mine above had to be simulated. The historical voids were filled in the model with paste material with a UCS value of 500 kPa (mine scale results are not overly sensitive to this value).

The Horne 5 mining sequence implemented in the *FLAC3D* model is the sequence finalized during the FS, which encompasses 2,165 stopes. To limit the computational time, as well as the storage of the model save files, ten (10) stopes were mined at each modelling stage (and five [5] stopes at the last stage). Therefore, a total of 217 mining steps were computed for the Horne 5 stopes. An example of a computed mining step (step 52 of 217) is shown in Figure 10.

Figure 10. Elevation view looking north showing one mining step (stopes in red) within the global mining sequence.

Some important aspects and challenges concerning the mining sequence are highlighted below – the reader is referred to the FS study (Falco Resources, Ltd., 2017) for additional information regarding the mining sequence.

- The main mining method is transverse longhole stoping with a bottom-up primary-secondary sequence.

- Mining is planned in two (2) phases: Phase 1 (from Level 710 down to Level 1310) and Phase 2 (from Level 1340 down to Level 2060), as shown in Figure 11.

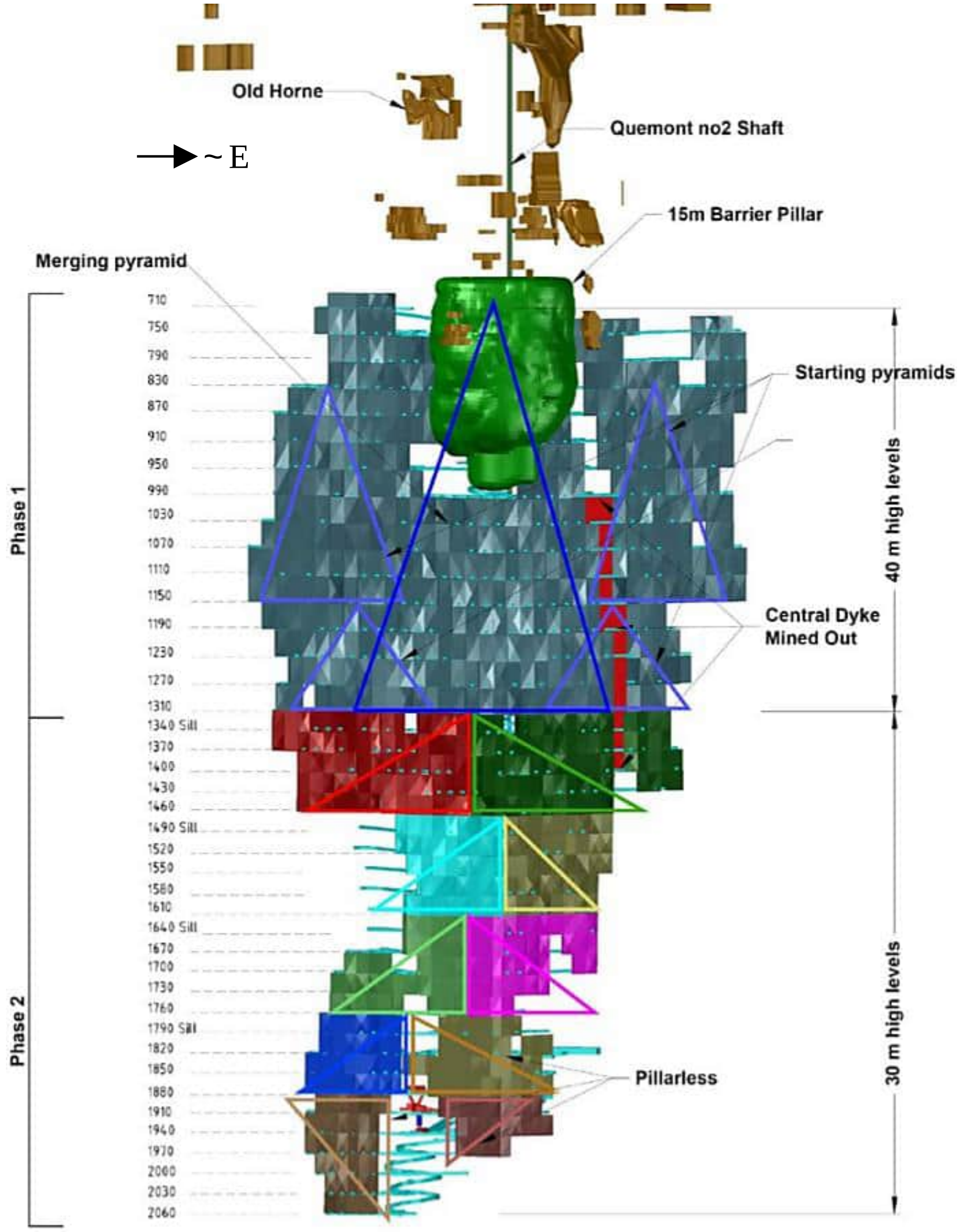

Figure 11. Elevation view looking approximately north showing the two mining phases and the various pyramids planned at Horne 5 (after NI 43-101 [Falco Resources, Ltd., 2017]).

Phase 1

- Phase 1 is recovered with four pyramids: two on L1310 and two on L1150. The four pyramids are progressively merged into a single large pyramid. Converging mining fronts in Phase 1 were identified as a potential mining challenge due to the associated stress concentrations.
- Mining in Phase 1 will induce stress changes in the vicinity of the historical Horne mine. The area between the historical Horne mine and the Horne 5 stopes is referred to as the *barrier pillar*. Fracturing of the barrier pillar due to stress increase was identified as a potential mining challenge. A 15 m-thick stand-off distance between the new and historical mine workings was planned for in the FS.
- A north-south-striking diabase dyke cuts through the Phase 1 mining zone. To avoid high stresses developing in this dyke and to avoid mining stopes in high stresses close to it, destress slots in the dyke were planned for during the FS.
- To reduce development costs, haulage drifts on levels 1030 to 1310 are planned to be developed within the ore body. The main challenge identified regarding this method is the potential for stress increases around the drifts as the mining front will approach. To mine the ore body at the drift location on these levels, *longitudinal* stopes are required.

Phase 2

- Phase 2 is divided into five mining zones: Phase 2A (from L1340 to L1460), Phase 2B (from L1490 to L1610), Phase 2C (from L1640 to L1760), Phase 2D (from L1790 to L1880) and Phase 2E (from L1910 to L2060).
- In Phase 2A, the main mining challenge is related to the diabase dyke discussed above, which cuts through the ore body. Destress slots have been planned for during the FS.
- In Phase 2B, the main mining challenge is related to the diabase dyke located in the eastern abutment – a thin pillar of host rock will remain between that dyke and the mining front. The recovery of the stopes located in the eastern abutment of this mining zone was identified as a potential mining challenge.
- Phase 2C consists of a primary-secondary half-chevron progressing to the West from the centre of the ore body and another primary-primary half-chevron progressing to the East (stopes excavated in a “primary-primary” sequence are referred to as *pillarless* stopes). Mining of the lead stopes was identified as a potential mining challenge.
- Phase 2E consists of a primary-primary full-chevron front progressing from top to bottom (underhand mining). Mining of the lead stopes was again identified as a potential mining challenge.

4. SEISMIC POTENCY ANALYSIS

Based upon the *FLAC3D* modelling results, an analysis of the underground seismic potency is presented in this section. Seismic risk on surface is discussed later in sections 7 and 8.

The objective of this analysis was to quantitatively assess the energy release at each modelling stage. The analysis was based on the *Seismic potency* P, which is associated with the volume of rock undergoing inelastic deformation (Ben-Menahem & Singh, 1981; King, 1978). The seismic potency can be interpreted as an indicator of mining-induced energy release, which in turn can be associated with seismic events. The scalar seismic potency (expressed in m^3) is the product of the strain change by the yielded volume, as follows:

$$P = \Delta\varepsilon \times V \qquad \text{… Eq. [1]}$$

Where: $\Delta\varepsilon$ is the incremental plastic shear strain (%); and,
V is the yielded volume (m^3).

4.1 METHODOLOGY

The seismic potency was computed for each modelling step. It was then normalized to the extracted tonnes at each modelling step. The unit of the value reported is therefore expressed in terms of m^3/mined tonnes. The criteria described in Table 8 were then applied to determine the risk level associated with each modelling step. Since no formal criteria have been established, the ones in Table 8 were set by A2GC based on multiple spot checks at numerous locations and mining steps, to ensure that potency ratings provide a sensible qualitative match with the numerical stress results.

Table 8. Definition of the risk categories associated with the seismic potency analysis.

Seismic potency analysis risk category	Criterion
Low	(Seismic potency / tonnes extracted) ≤ 0.001 m^3/t
Moderate	0.001 m^3/t < (Seismic potency / tonnes extracted) ≤ 0.002 m^3/t
High	(Seismic potency / tonnes extracted) > 0.002 m^3/t

The following limitations should be noted:

- As discussed in Section 3.5, ten (10) stopes were mined per modelling step. This was done to limit the computational time, as well as the storage requirements for the result files. Therefore, the seismic potency values reported considers the collective effect of all ten stopes together.

- No attempt was made to correlate the seismic potency obtained from the *FLAC3D* model to the magnitude of possible seismic events. This remains an active field of research and it would require significant field data to calibrate *FLAC3D* results to seismic magnitudes.

4.2 Results and Comments

The risk profile obtained for the seismic potency analysis is presented in Figure 12. The number of modelling steps associated with each risk category is given in Table 9.

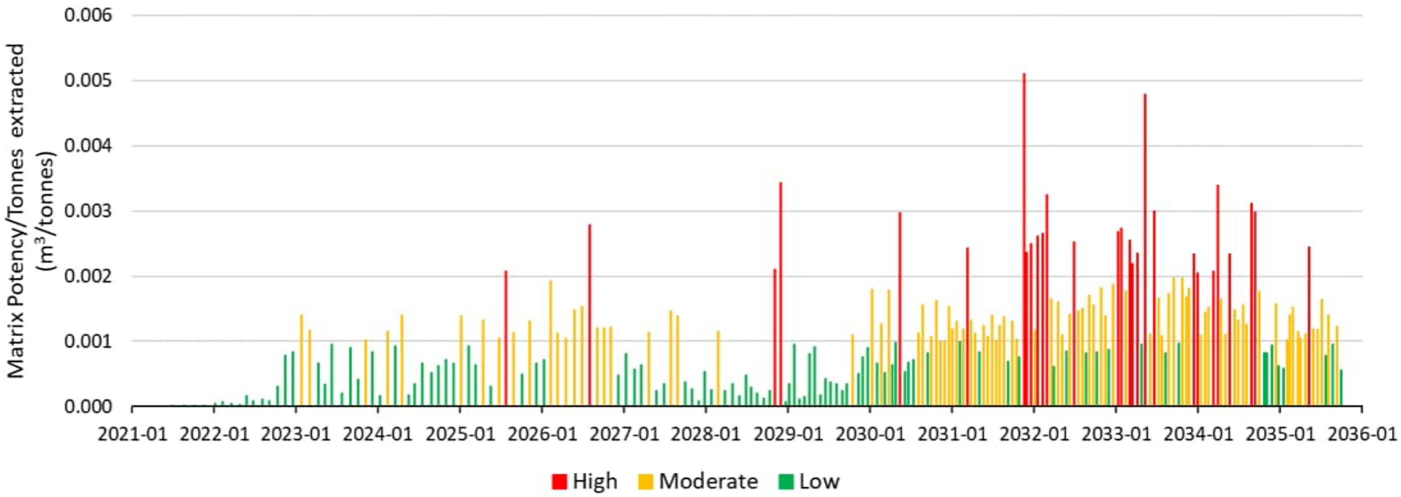

Figure 12. Seismic potency-based risk profile.

Table 9. Number of mining steps per seismic potency risk category.

Seismic potency risk category	Number of mining steps	Percentage of the total number of steps
High	28	13%
Moderate	89	41%
Low	100	46%
Total	217	100%

The following observations can be made:

- Twenty-eight (28) out of 217 modelling steps (13%) were rated with a *High* seismic potency.
- From those 28 steps, 26 occur during Phase 2 mining.
- Modelling steps rated with a *High* seismic potency seem to occur in the situations listed below (this list is not exhaustive):
  - Stopes punching into a highly stressed, but not yet damaged, sill pillar, causing a deconfinement area and shearing. An example is shown in Figure 13.

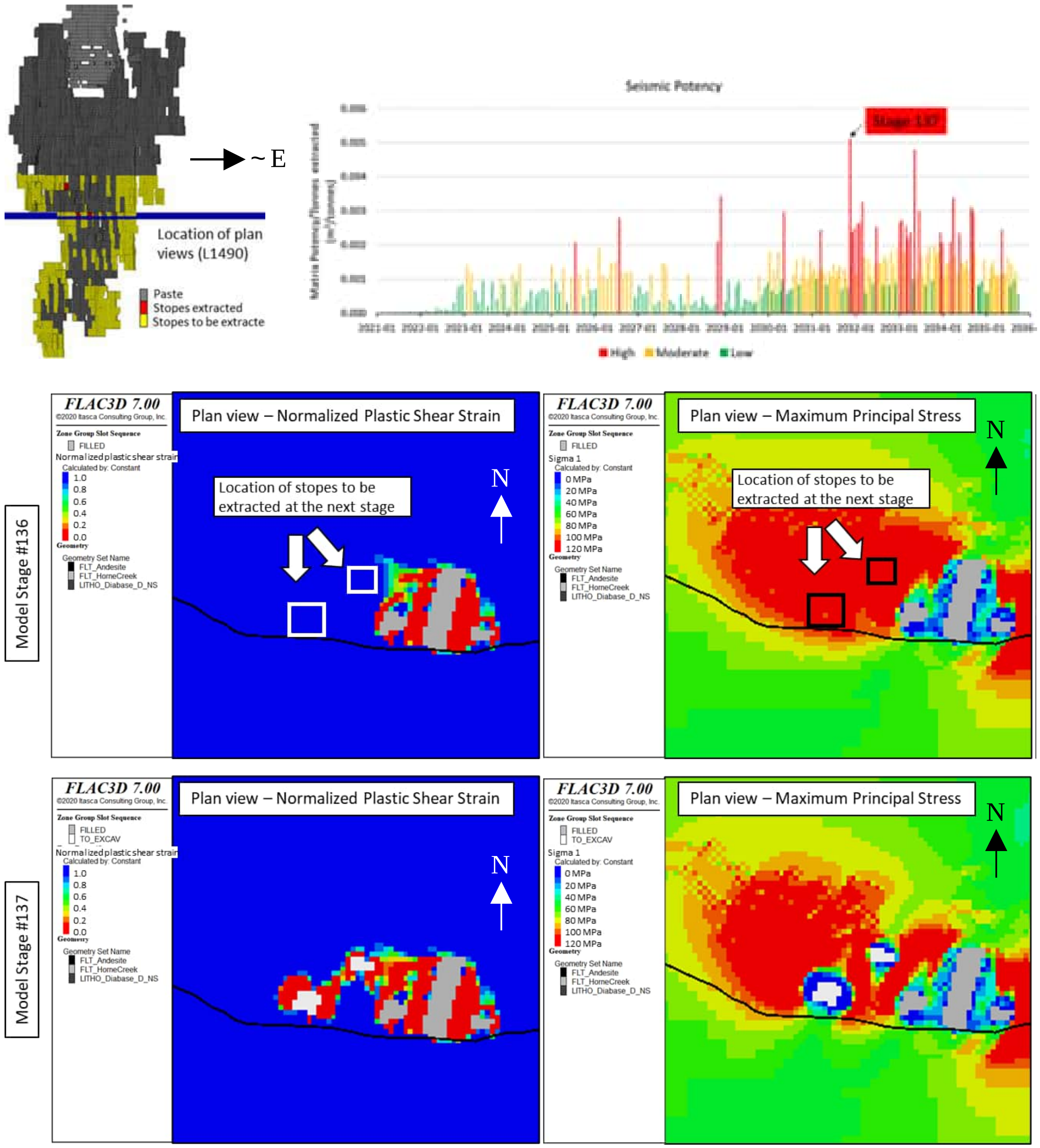

Figure 13. Plan views showing an example of stopes extracted at a sill pillar level that are generating a high seismic potency (L1490 at steps 136 and 137).

– Stopes mined in a highly stressed abutment, further propagating the failure and causing the stresses to be pushed away.

– Stopes mined in high stresses due to converging mining fronts (merging pyramids in Phase 1), therefore cutting the stresses and shearing the remaining pillar between the converging fronts. An example is shown in Figure 14.

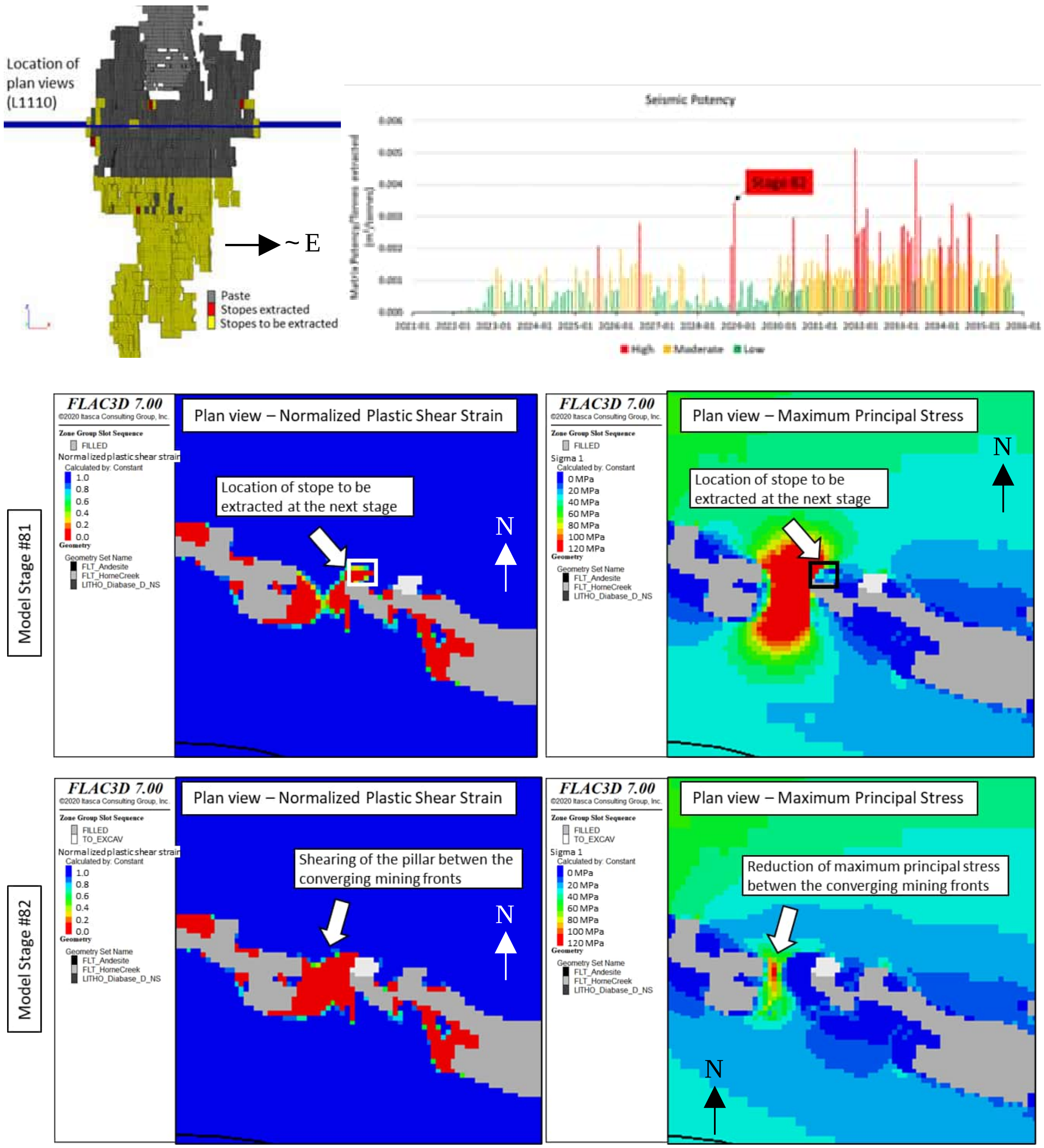

Figure 14. Plan views showing the example of a stope extracted in a converging mining front that is generating a high seismic potency (L1110 at steps 81 and 82).

  - Primary stopes not necessarily mined in high stresses but with a geometry configuration that enables the shearing of secondary stopes. This seems to happen mostly in primary stopes in the second panel or later (i.e., not in the first panel).
- Modelling steps rated with a *Moderate* seismic potency seem to occur in similar situations (e.g., punching of a sill, primary stopes causing shearing of secondary stopes), but the damage occurs over a lesser extent either because of the stope configuration or the stress level being slightly lower (*Moderate* instead of *High*).

It should be reminded that ten (10) stopes were mined per modelling step. Consequently, the seismic potency values reported consider the seismic potency generated by all ten stopes considered together – it does not mean that all the stopes mined in one step that is rated with a *High* seismic potency are expected to all radiate high energy levels in the rock mass.

5. GEOMECHANICAL RISK ASSESSMENT

Modelling results were used to establish mining risk profiles associated with the FS mining sequence. Mining conditions and dilution risks were investigated from a production perspective over the mine life. Mining-induced stresses and plasticity criteria guided the analyses. Results are presented in this section.

5.1 Mining Conditions Assessment

The mining conditions assessment is meant to evaluate how challenging mining a given stope can be expected to be. Two types of mining challenges were considered, as follows:

1. Mining under high stress conditions
2. Mining under low / residual conditions (i.e., in relaxed and damaged sectors)

Stopes excavated in highly stressed areas are likely to generate some local seismicity, require more rehabilitation and/or be affected by drilling challenges, potentially causing in turn production uncertainties and risks, such as schedule delays, rework, and possibly some ore losses in the worst cases. On the other hand, stopes mined in highly damaged areas are likely to cause production delays (from rework and rehabilitation) and experiment drilling challenges, which also can result in production uncertainties and risks.

The risks of mining under high stress and residual conditions were first evaluated separately, then merged into a single production risk profile. The following sections describe the methodology and results.

5.1.1 Risk of Mining Under High Stress Conditions

High stress conditions during mining were inferred from the *FLAC3D* modelling results in terms of the stress levels within the numerical zones of each stope. The global level of stress in each stope was then derived just prior to mining it, to estimate how highly stressed it will be at the moment it will be recovered.

5.1.1.1 Methodology

Each numerical zone within each stope in the model was assigned a *Low*, *Moderate* or *High* risk rating, based upon its deviatoric stress magnitude normalized by the local UCS ($[\sigma_1 - \sigma_3] / UCS$) just prior to mining. A global risk rating was then assigned to each stope based on the percentage of numerical zones that were assigned a *Low*, *Moderate* or *High* risk rating.

The criteria shown in Table 10 were applied to determine the risk rating for each numerical zone within the stopes (Cotesta *et al.*, 2014). Other authors (e.g., Board *et al.*, 2001) have suggested lower category thresholds, but those in Table 10, being higher, provide in our view a more realistic and reliable risk profile.

Table 10. Definition of the risk categories for high stress conditions (after Cotesta *et al.*, 2014).

Risk category	Criterion
Low	$(\sigma_1 - \sigma_3) / UCS < 0.5$
Moderate	$0.5 \leq (\sigma_1 - \sigma_3) / UCS < 0.7$
High	$(\sigma_1 - \sigma_3) / UCS \geq 0.7$

For each stope, the percentage of numerical zones rated *Low*, *Moderate* and *High* were computed, and a stope risk rating was assigned based on the criterion shown in Figure 15a. In this graphical representation, one stope is represented by a single point, with the percentages of *Low*, *Moderate* and *High* zones being read on each axis.

An example is given in Figure 15b – that particular stope would be assigned a *Low* high stress rating based on the categories shown in Figure 15a.

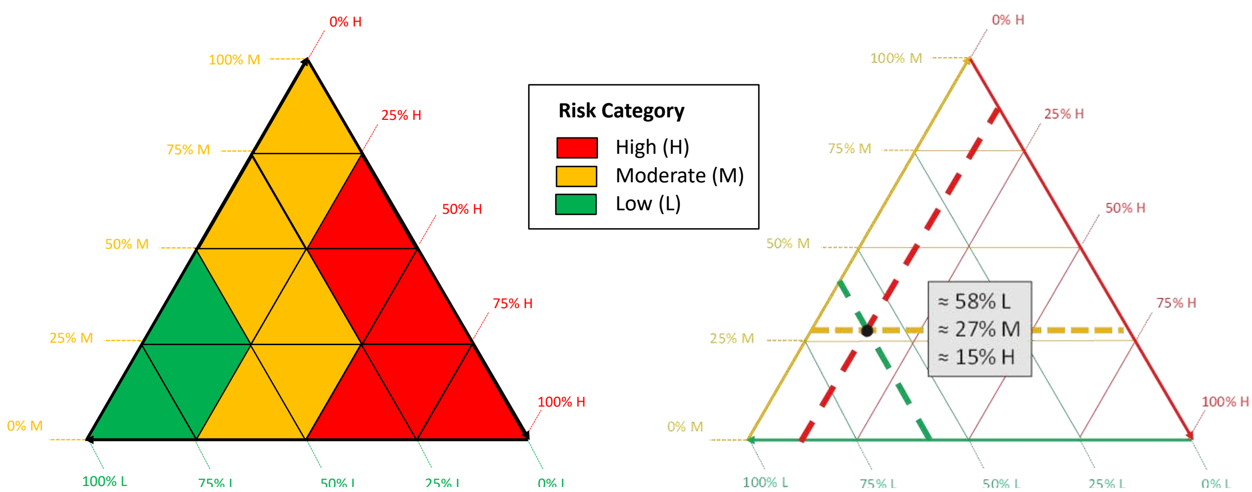

(a) Stope risk rating criterion. (b) Data point example.

Figure 15. Methodology implemented to assign a high stress risk rating to each stope from the normalized deviatoric stress in each of its numerical zones.

The decision tree used to establish the global risk ratings shown in Figure 15a is presented in Figure 16.

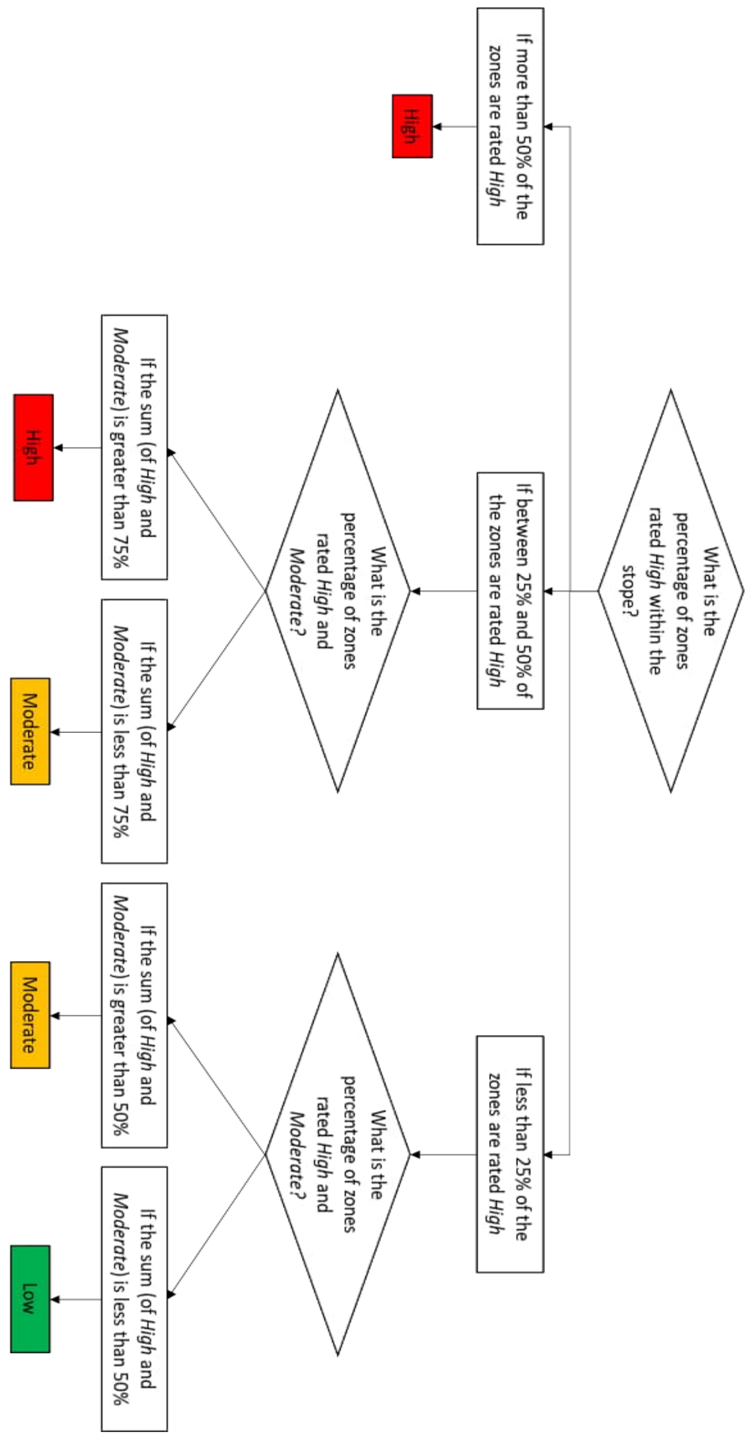

Figure 16. Decision tree to establish the global high stress risk rating categories.

5.1.1.2 Results and Observations

Figure 17 shows the complete dataset of stopes superimposed on the stope high stress risk rating criterion.

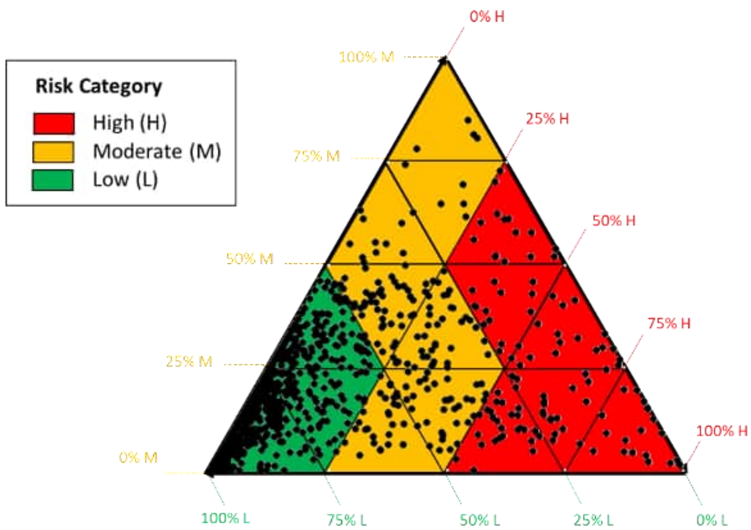

Figure 17. Dataset (individual stopes) superimposed on the stope high stress risk rating criterion.

The risk profile obtained from the evaluation of the high stress hazard is presented in Figure 18. This bar chart shows time (represented by the time stamp of each mining step) on the *x*-axis and the tonnes of ore planned at each of these mining steps on the *y*-axis, subdivided by *Low* (green), *Moderate* (yellow) and *High* (red) categories of high stress conditions.

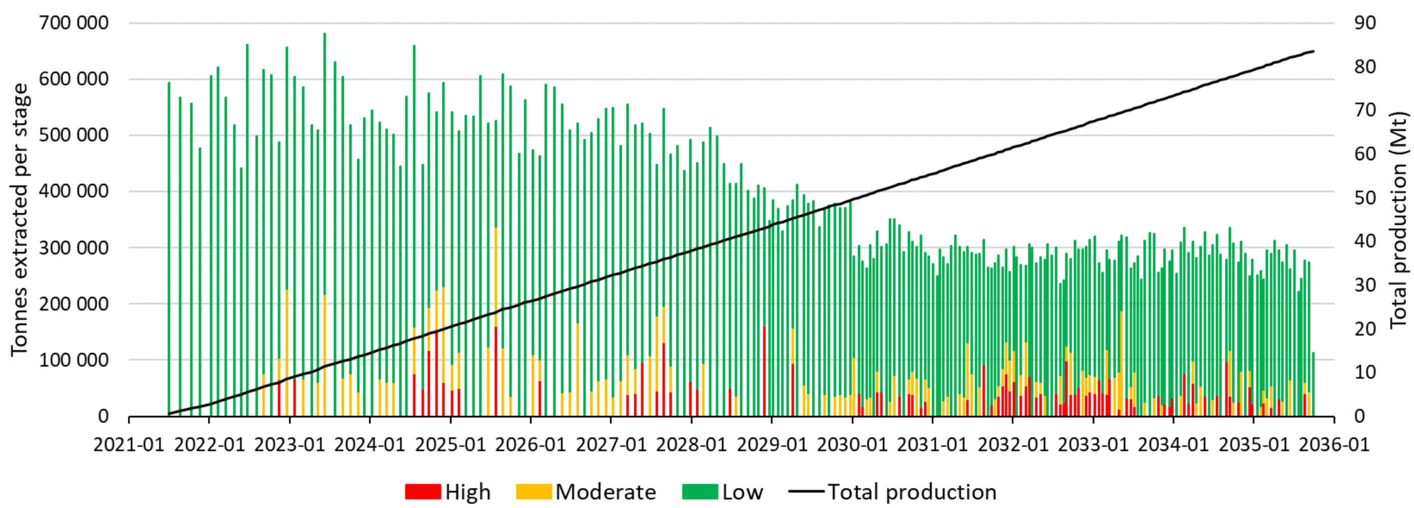

Figure 18. Risk profile for high stress mining conditions.

Each vertical bar in Figure 18 represents the extraction of ten (10) stopes. As the stopes become smaller at depth, more 10 stope-steps are required per annum to maintain production, which explains why the bars become smaller and denser during later mining. The total number of stopes in each risk category is given in Table 11.

Table 11. Number of stopes per high stress risk category.

High stress risk category	Number of stopes	Percentage of the total number of stopes
High	109	5%
Moderate	165	8%
Low	1,891	87%
Total	2,165	100%

The following observations can be made:

- One-hundred and nine (109) stopes out of the 2,165 Horne 5 stopes (5%) are forecasted to be excavated under high stress conditions. Out of those 109 stopes rated *High*, 34 were extracted during Phase 1, and 75 during Phase 2 mining. This represents 4% of the 866 Phase 1 stopes, and 6% of the 1,299 Phase 2 stopes.
  - Out of the 34 stopes rated *High* in Phase 1:
    - Eleven (11) were extracted during the period of August 2024 through to March 2025. This corresponds to the period when the Phase 1 pyramids merge together. Those 11 stopes were all secondary stopes. An example is shown in Figure 19.
    - Twelve (12) were longitudinal stopes extracted between the period of July 2027 through to April 2029. This represents 5% of the 226 longitudinal stopes. Longitudinal stopes in Phase 1 are stopes mined where haulage drifts are planned to be developed in the ore body (on levels 1030 to 1310).
    - All the other stopes rated *High* in Phase 1 were secondary stopes (11 stopes). This suggests that the capacity of the Phase 1 secondary stopes to retain high stress levels is a key design factor, but lead stopes are not expected to be challenging from a stress magnitude point of view.
  - Out of the 75 stopes rated *High* in Phase 2:
    - Sixteen (16) were pillarless stopes extracted between the period of November 2031 through to April 2035. This represents 7% of the 237 pillarless stopes in horizons 2D and 2E.
    - The majority of the other stopes rated *High* in Phase 2 were primary stopes (53 stopes). Only six (6) secondary stopes in Phase 2 were rated *High*. This suggests that lead stopes

in Phase 2 can be expected to be more challenging than in Phase 1, but that the secondary stopes in Phase 2 should not retain high stress levels.

- The FS mining sequence was designed to minimise the ground stresses retained in the diabase dyke through the in-sequence mining of a destress slot. Based on the *FLAC3D* modelling results, all destress slots in the diabase dyke are forecasted to be excavated in *Low* stress conditions. This suggests the destress slot planned during the FS should be sufficient to prevent to dyke from remaining a long-term stress-carrying rib pillar.

- It is also interesting to note that out of the 109 stopes rated *High*, 100 were the first panel (the southern-most stope) of a north-south row of stopes. This represents 12% of the 863 "first panel" stopes. Only 1% of the "second panel" stopes were rated *High* (6 stopes out of 661), and this percentage dropped lower as the number of panels increased. This suggests that where high stresses concentrate, opening one stope is sufficient to cut the stresses and generate a stress shadow area.

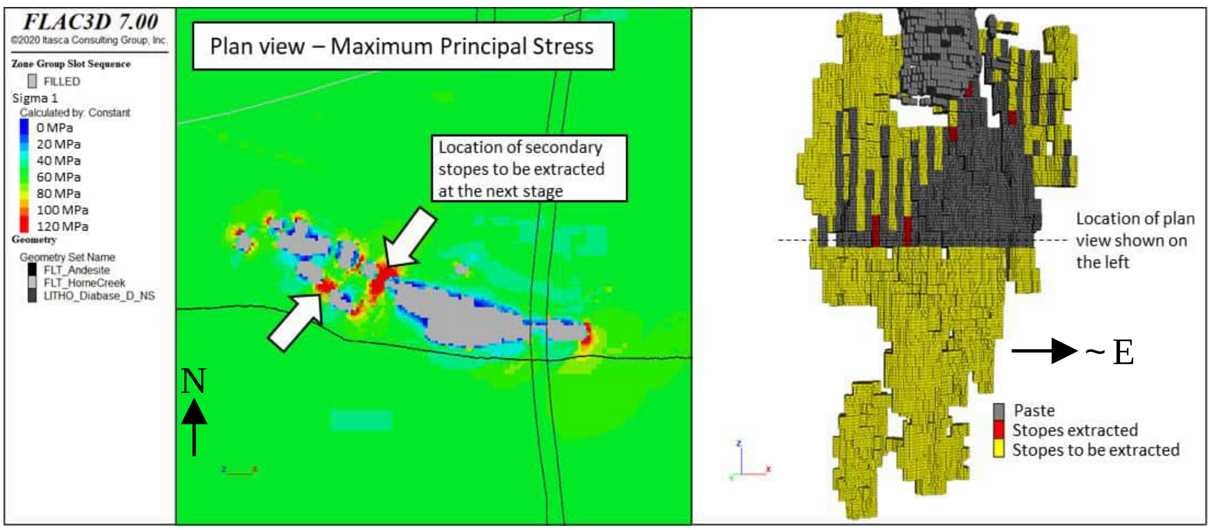

Figure 19. Example of stopes extracted under high stress conditions during the merging of the Phase 1 pyramids.

5.1.1.3 Discussion on a Proximity to Peak Criterion

An alternative approach to the deviatoric stress-based criterion just discussed was considered to assess mining under high stress conditions. The objective of this alternative approach was to establish how close to peak strength mining will be conducted in each stope. Instead of only comparing the deviatoric stress to the UCS of the rock (as discussed in Section 5.1.1.1), the focus was on how close to the peak strength the rock mass (either pre-peak or post-peak) mining is expected to occur. This approach was considered because of the high brittleness of the Horne 5 rock mass.

This alternative approach was explored, but was ultimately not retained – the risk of mining under high stress conditions remained associated to the criterion based on the deviatoric stress, as discussed in sections 5.1.1.1 and 5.1.1.2. The approach based on the proximity to peak strength is however briefly summarised for completeness, along with the reasons it has not been retained.

The 'proximity to peak' was evaluated in two different ways, depending on whether the numerical zone is pre-peak or post-peak.

If the zone is pre-peak (i.e., if it did not reach its peak strength), the following steps were followed:

- For each 'pre-peak' numerical zone, the major principal stress at peak ($\sigma_{1\text{-peak}}$) was computed based on the Hoek-Brown criterion equation for the σ_3 magnitude of the zone.
- The ratio $\sigma_{1\text{-zone}} / \sigma_{1\text{-peak}}$ was computed for each numerical zone.
- A risk rating was assigned to each numerical zone according to the following criteria:
  - If $\sigma_{1\text{-zone}} / \sigma_{1\text{-peak}} \geq 80\%$, then the zone was rated *High* (i.e., close to peak);
  - If $70\% \leq \sigma_{1\text{-zone}} / \sigma_{1\text{-peak}} < 80\%$, then the zone was rated *Moderate*; or,
  - If $\sigma_{1\text{-zone}} / \sigma_{1\text{-peak}} < 70\%$, then the zone was rated *Low*.
- In addition to the criteria described above, all numerical zones where σ_1 was under UCS/2 were rated *Low*, regardless of their proximity to peak.

If the zone is post-peak (i.e., if it has passed its peak strength), the following steps were followed:

- The normalized plastic shear strain (explained further in Section 5.1.2.1) was computed for each post-peak numerical zone.
- A risk rating was assigned to each numerical zone according to the following criteria:
  - If the normalized plastic shear strain was $\geq 90\%$, then the zone was rated *High* (i.e., close to peak);
  - If the normalized plastic shear strain was between 70% and 90%, then the zone was rated *Moderate*; or,
  - If the normalized plastic shear strain was $< 70\%$, then the zone was rated *Low*.
- In addition to the above criteria, all numerical zones in which σ_1 was under UCS/2 were rated *Low*, regardless of their proximity to peak.

The idea was then to assign a global risk rating per stope based on the percentage of its numerical zones that were assigned *Low*, *Moderate* and *High* risk ratings, using the same methodology as for the deviatoric stress criterion.

However, a concern was that the alternative approach based on the proximity to peak, in its current formulation, likely under-estimates the mining risk at high confinement levels. An example is shown in Figure 20, where a data point would be rated *High* based on the deviatoric stress criterion (i.e., it would land above the purple line), but it would be rated *Low* based on the proximity to peak criterion (i.e., it would locate below the green line (and even the blue line). The stress level at this data point is intuitively high (with σ_1 = 200 MPa and σ_3 = 50 MPa), and as such it was felt it should be flagged in the risk analysis.

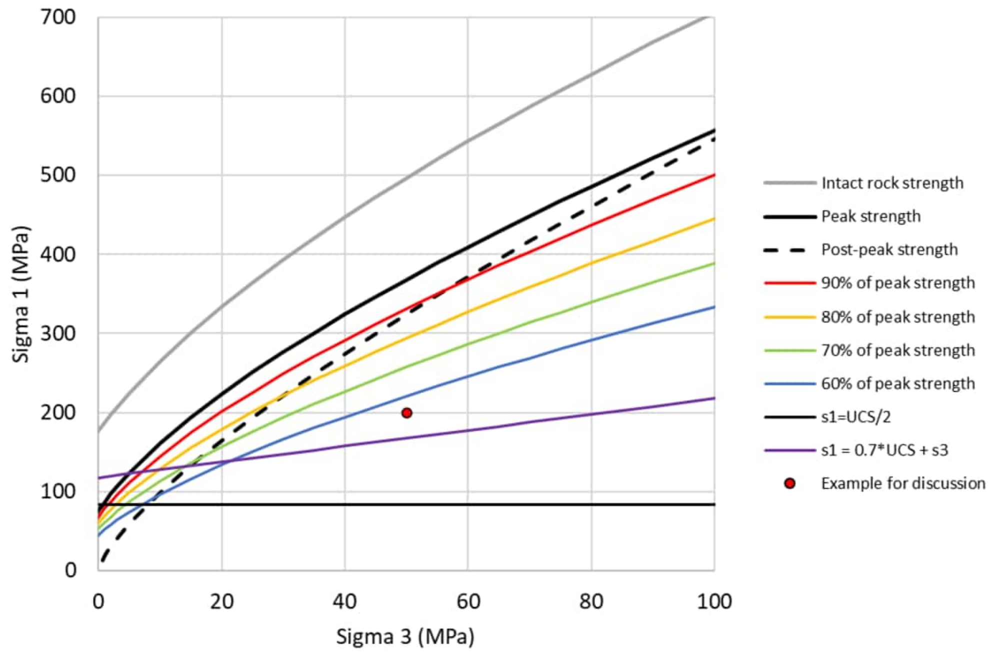

Figure 20. Comparison of the stress criterion based on the deviatoric stress and the alternative approach based on the proximity to peak.

Defining proximity to peak criteria based upon a percentage of the peak strength might not be the best approach without also considering the actual confinement level. However, calibration data would be required to better adjust this additional criterion. Therefore, in the absence of such calibration data, the criterion based on the deviatoric stress has been retained at this stage.

5.1.2 Risk of Mining Under Residual Conditions

At the other end of the spectrum lies the situation where mining is conducted under residual post-peak conditions, far past its peak strength, and under low stress and in significantly damaged rock. Under such circumstances, the damaged rock mass can be expected to require rehabilitation, produce difficult production drilling conditions (e.g., due to blastholes collapsing) and cause production delays.

5.1.2.1 Methodology

As for the high stress mining conditions discussed in Section 5.1.1, the objective of this analysis was to assess the rock mass conditions of each stope prior to it being mined. The goal was to flag stopes that will be mined in highly damaged ground. The damage of each numerical zone in each stope in the model was evaluated at the mining step just prior to its extraction. A global risk rating (again *Low*, *Moderate* or *High*, to remain consistent) was then assigned to each stope based upon the percentage of its numerical zones that were classified as "damaged."

To evaluate the level of damage, the following term was computed for each numerical zone at the step just prior to mining the stope:

Normalized plastic shear strain = 1 – (Plastic shear strain / Critical strain) … Eq. [2]

The normalized plastic shear strain is hence a value between 0 and 1. It equals 1 if the zone is intact, and it is equal to 0 if the zone has reached its residual properties. If the plastic shear strain exceeds the critical strain, the normalized plastic shear strain is capped at zero. The normalized plastic shear strain concept is illustrated in Figure 21.

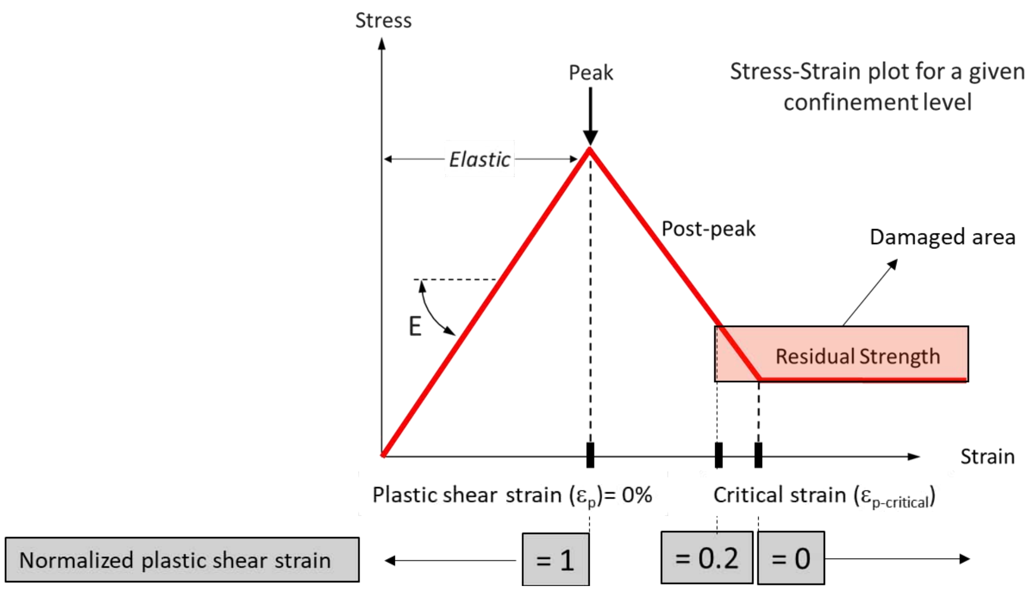

Figure 21. Representation of the normalized plastic shear strain and damage limits.

To be considered "damaged," a numerical zone in the model had to meet the following two criteria:

1. The normalized plastic shear strain is below 0.2 ("Damaged area" illustrated in Figure 21); and,
2. The minimum principal stress σ_3 magnitude is less than 1 MPa.

When these two criteria are met, the rock mass is expected to be significantly damaged, and the confinement insufficient to retain the unstable ground together. A stope risk rating was then assigned to each stope, based on the percentage of damaged and deconfined numerical zones it contains. The stope risk rating criterion is shown in Table 12.

Table 12. Definition of the risk categories for residual conditions.

Risk category	Criterion
Low	Damaged and deconfined stope volume < 50%
Moderate	50% ≤ Damaged and deconfined stope volume < 80%
High	Damaged and deconfined stope volume ≥ 80%

5.1.2.2 Results and Observations

The risk profile obtained from the evaluation of the residual condition hazard is presented in Figure 22. The number of stopes per risk category is given in Table 13.

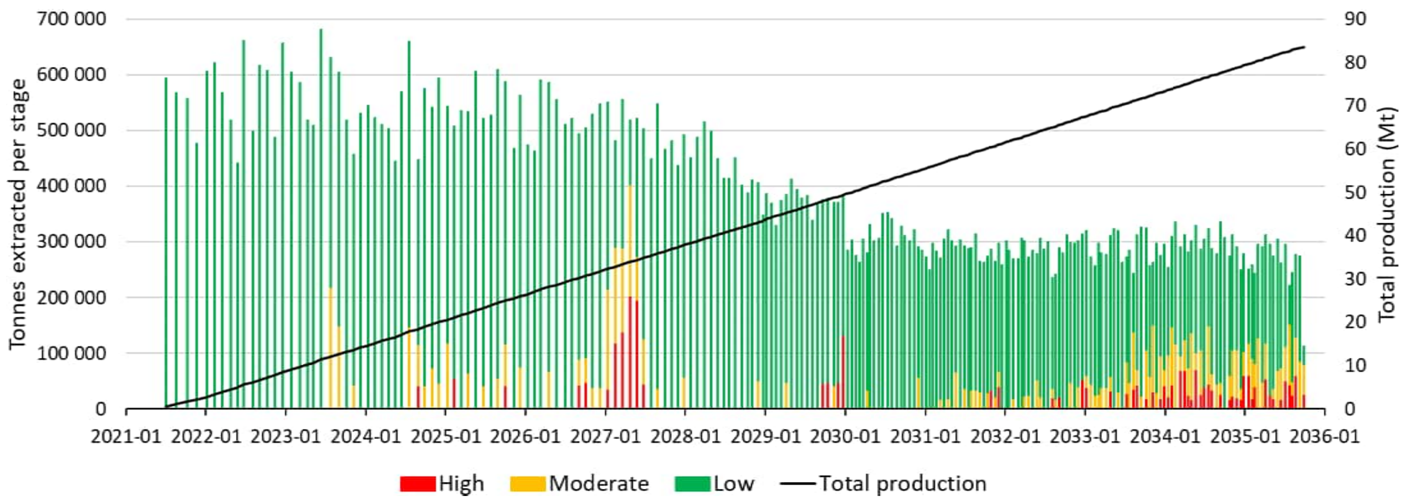

Figure 22. Risk profile for mining under residual conditions.

Table 13. Number of stopes per residual conditions risk category.

Residual conditions risk category	Number of stopes	Percentage of the total number of stopes
High	83	4%
Moderate	175	8%
Low	1,907	88%
Total	2,165	100%

The following observations can be made:

- 83 stopes out of the 2,165 Horne 5 stopes (4%) are forecasted to be excavated under "residual conditions."
- Out of those 83 stopes that are rated *High*, 26 were extracted during Phase 1 mining, and 57 during Phase 2 mining. This represents 3% of the 866 Phase 1 stopes, and 4% of the 1299 Phase 2 stopes.
  - From the 26 stopes rated *High* in Phase 1:
    - 17 were extracted during the period between August 2026 and June 2027. This corresponds to the time interval when the upper portion of Horne 5 is mined, west of the historical Horne mine. Those 17 stopes were mostly secondary stopes from shallow levels (L0830 to L0950). An example is shown in Figure 23.

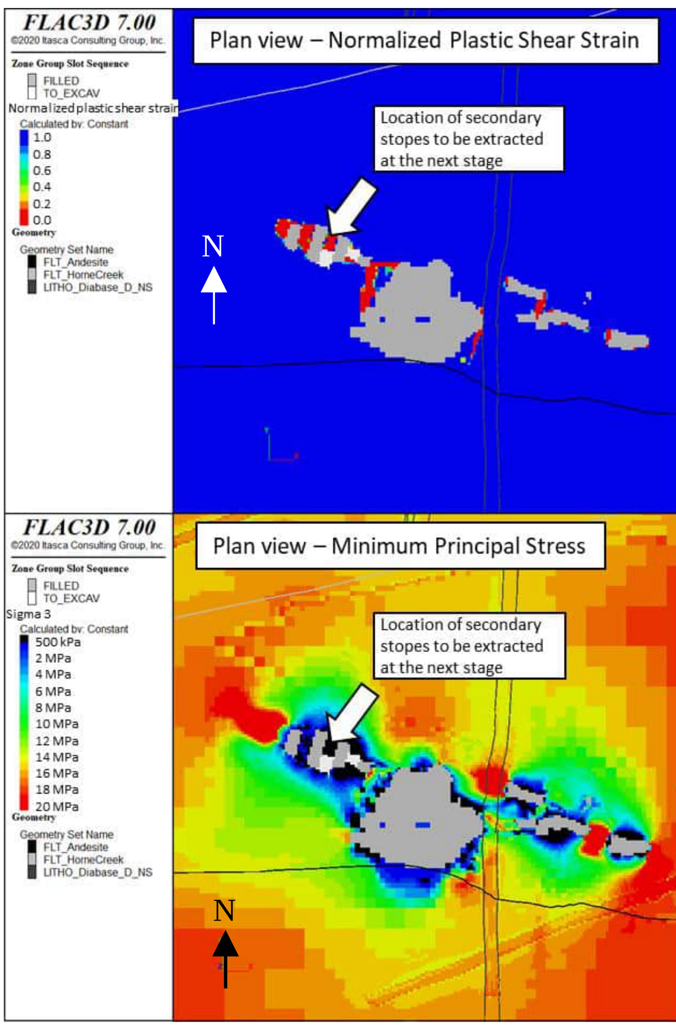

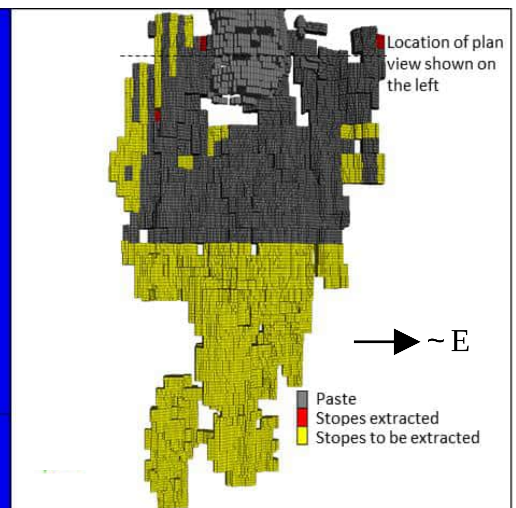

These 17 stopes lie in the vicinity of the old Horne mine, but beyond the barrier pillar planned to remain in place. As a result, they are not expected to be an issue in terms of interacting with the old workings.

Figure 23. Example of a stope extracted under residual conditions.

  - Six (6) stopes were extracted between September and December 2029. Those were all longitudinal stopes, which represent 3% of the 226 longitudinal stopes.
  - The three (3) other stopes rated *High* in Phase 1 were secondary stopes.
- From the 57 stopes rated *High* in Phase 2:
  - 14 were pillarless stopes from the second and third panels. This represents 6% of the 237 pillarless stopes.
  - 39 stopes were secondary stopes, mostly from the second, third and fourth panels. This represents 9% of the 450 secondary stopes in Phase 2.
  - The remaining four (4) stopes rated *High* in Phase 2 were primary stopes from the second panel.
  - It is interesting to note that the majority of stopes rated *High* in Phase 2 (50 stopes out of 57) are planned to be extracted towards the end of the Horne 5 mine life, from July 2033 through to September 2035. As a reference, the first Phase 2 stope is planned to be extracted in July 2028.

5.1.3 Global Assessment

The objective of this section is to merge the risk of mining under high stress conditions with the risk of mining under residual conditions into a single global production risk profile. This global risk profile is meant to capture the mining conditions under which Horne 5 stopes are forecasted to be mined.

5.1.3.1 Methodology

Only stopes to which a *High* risk was assigned for either the high stress or the residual conditions hazards were considered in the global risk profile. A given stope can obviously not be rated *High* for both hazards: the rock mass needs to be close to intact to sustain high stresses, and, inversely, a damaged rock mass cannot sustain high stresses. To simplify the interpretation of this analysis, *Moderate* stopes were not considered, and the reader is referred to the individual analyses (sections 5.1.1 and 5.1.2).

Accordingly, each Horne 5 stope can globally be flagged either as a *High Stress* stope, a *Residual Conditions* stope, or an *OK* stope. A fourth category was added to highlight stopes that would have a portion highly stressed and another portion highly damaged. Those stopes were called *Combined* stopes. The decision tree to establish the *Combined* category is shown in Figure 24.

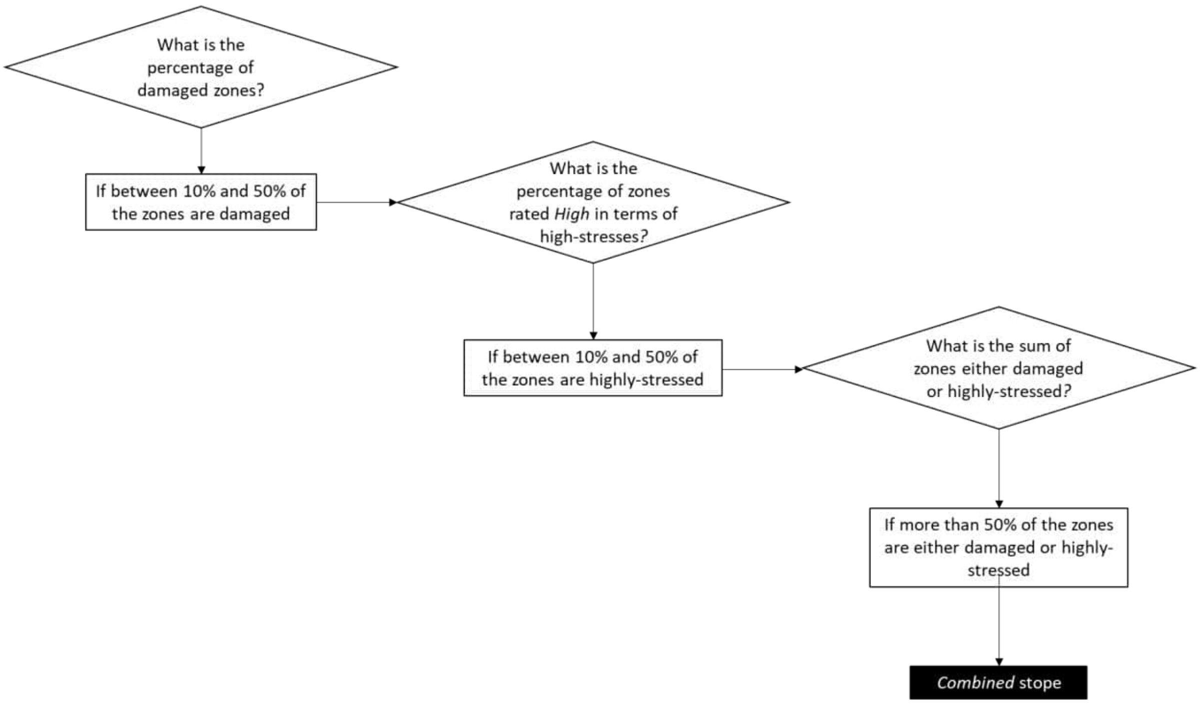

Figure 24. Decision tree to establish the *Combined* global risk rating category.

5.1.3.2 Results and Observations

The global mining conditions risk profile is presented in Figure 25. The number of stopes per risk category is given in Table 14. An annotated global risk profile is given in Figure 26.

The following observations can be made:

- A total of 202 stopes (9% of the 2,165 stopes) are expected to be mined under challenging conditions.
- In Phase 1:
  - Lead stopes in Phase 1 are not expected to be extracted under high stress conditions.
  - The stope dimensions were designed during the FS in order to minimise high stress concentrations in the secondary stopes. The analyses presented in this report confirm this design criterion has been met in most cases, except for a few secondary stopes when the pyramids merge, as well as for some longitudinal stopes. Those are highlighted in Figure 26.

  - Another aspect that could be challenging in Phase 1 is the mining of stopes under residual conditions. This concerns some shallow secondary stopes, as well as some longitudinal stopes planned to be extracted towards the end of Phase 1.

- In Phase 2:
  - Lead stopes (primary and pillarless) in Phase 2 are expected to be more challenging than in Phase 1 in terms of high ground stresses.
  - During the FS, stope dimensions were designed in Phase 2 to also minimise high stress concentrations in the secondary stopes. Here as well, the analyses confirm this design criterion has been met in most instances. This criterion also explains why the majority of stopes extracted under residual conditions are secondary stopes. This is expected to occur towards the end of the mine life.

- From the ten (10) stopes flagged as *Combined*, five (5) were pillarless (in Phase 2), and three (3) were located at shallow depth (L0830, L0750 and L0790) towards the western abutment. An example of a *Combined* stope is given in Figure 27.

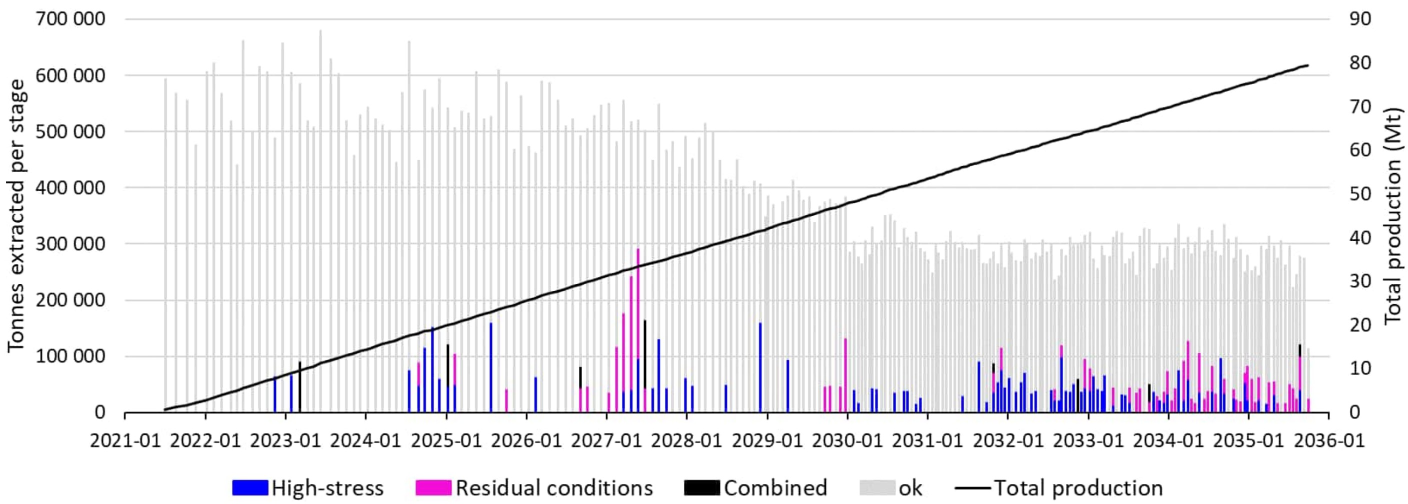

Figure 25. Global risk profile.

Table 14. Number of stopes per global mining risk category.

Global mining conditions risk category	Number of stopes	Percentage of the total number of stopes
High stress	109	5.0%
Residual conditions	83	3.8%
Combined	10	0.5%
No risk tagged	1,963	90.7%
Total	2,165	100%

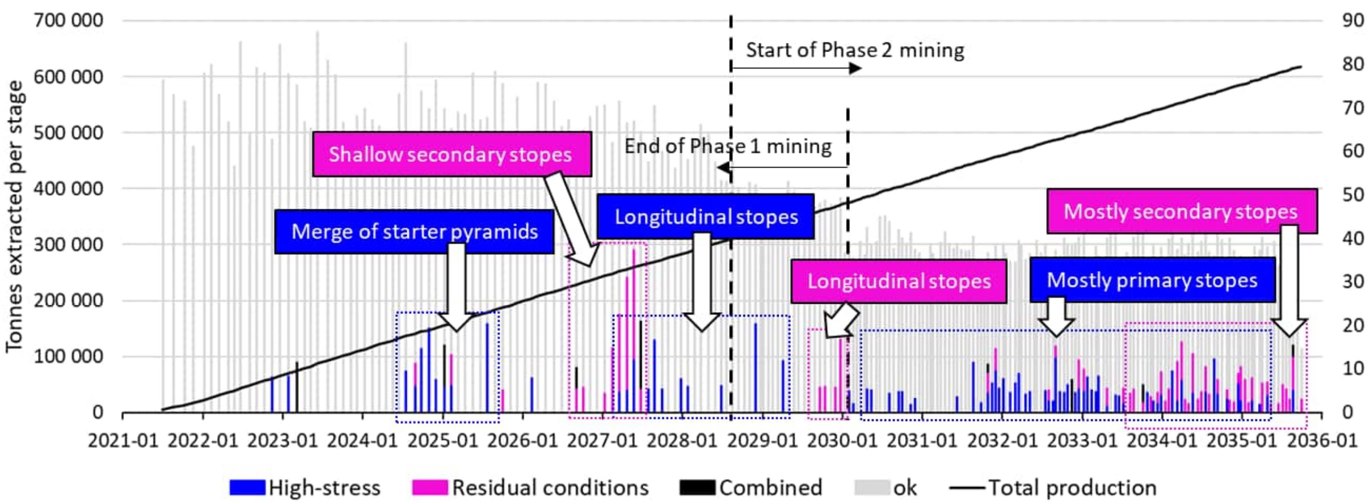

Figure 26. Annotated global risk profile.

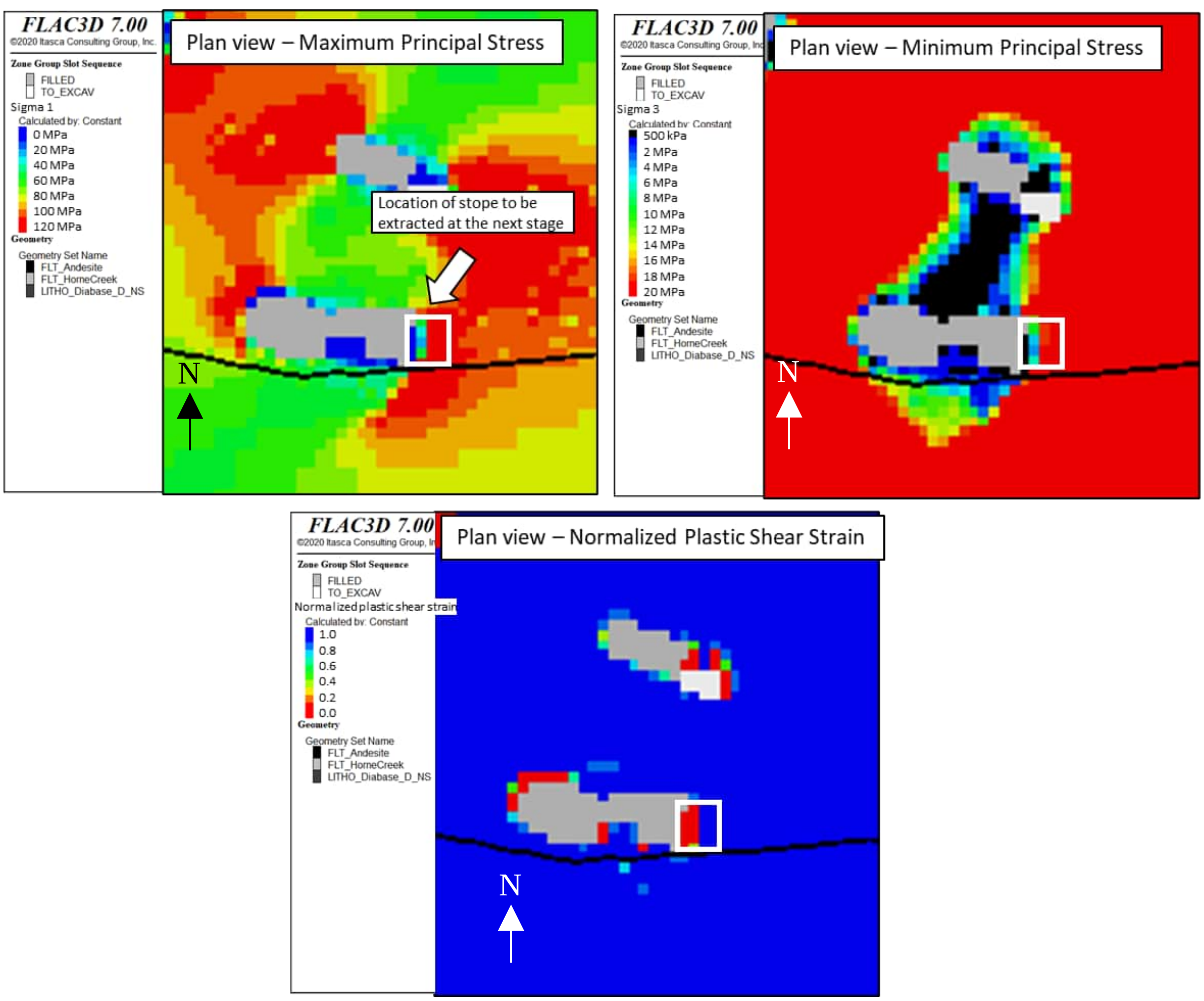

Figure 27. Example of a stope with a *combined* risk (Stope 1790-0724-1).

5.2 Dilution Risk

The mining conditions assessment discussed in Section 5.1 was meant to evaluate how challenging a stope can be expected to be – as a result, pre-mining conditions (just prior to excavation) were evaluated. The evaluation of the dilution risk presented in this section describes the behaviour of a stope during mucking, after blasting – post-mining (or, more accurately, post-blasting) conditions are hence evaluated in this case.

5.2.1 Methodology

The objective of this particular analysis was to assess the dilution potential for each stope. The dilution potential was evaluated in the hanging wall and footwall of the stopes. For scripting purposes in *FLAC3D*, a "possible dilution" group of numerical zones was defined for each stope. That group included the hanging wall and footwall areas (it excluded the end walls and the back), and included only waste rock material (it excluded paste backfill and ore). Those numerical zones that were damaged and deconfined, and located within the "possible dilution" group were counted as dilution. The total dilution associated with one stope was summed (in terms of tonnes) and the percentage of dilution for that stope was computed (tonnes of dilution / extracted tonnes). A dilution risk rating (*Low*, *Moderate* or *High*) was then assigned per stope based on the percentage of dilution computed.

More specifically, in order to be considered as dilution, a numerical zone in the model had to meet the three (3) following criteria:

1. Be located within the "possible dilution" group;
2. Have a normalized plastic shear strain of less than 0.5; and,
3. Have a minor principal stress σ_3 of less than 1 MPa.

Base on this analysis, the following remarks can be made:

- Because the ore body is sub-vertical, dilution was evaluated similarly in the hanging wall and in footwall of the stopes.
- Furthermore, the dilution levels in the hanging wall and footwall were summed during the data extraction process. This implies that the potential for dilution was evaluated on one or two walls, depending on the stope configuration. For example, if paste was present in the hanging wall, then only the footwall was considered in the dilution risk analysis. An example of the "possible dilution" group definition is shown in Figure 28.
- Potential for dilution was not computed for the destressing slots in the diabase dyke.

The criteria described in Table 15 were then applied to determine the risk label for each numerical zone.

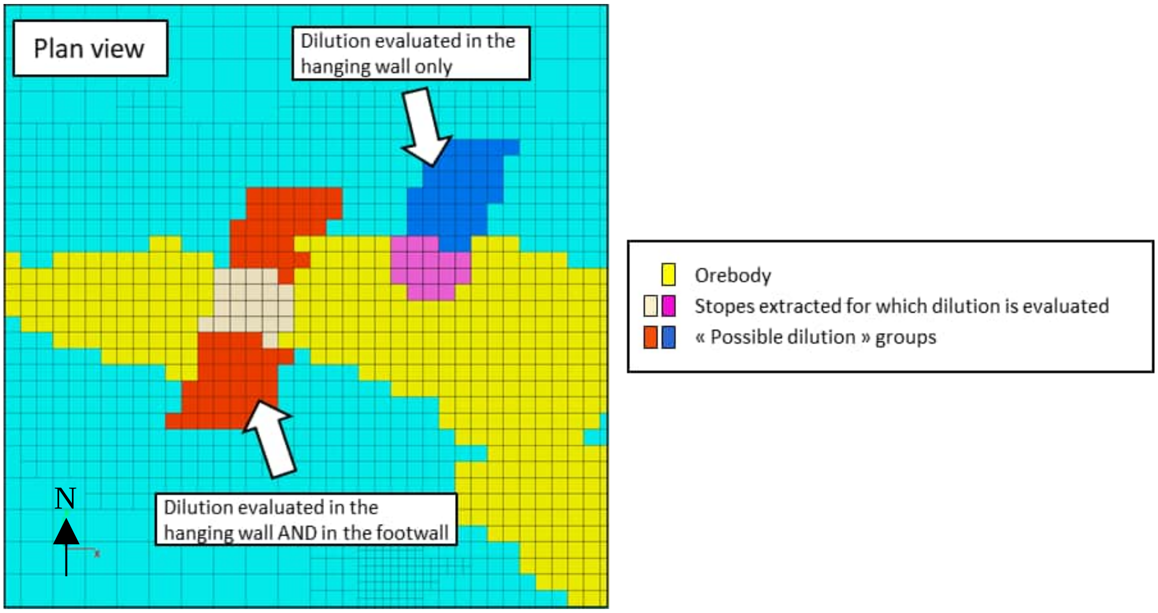

Figure 28. Plan view showing examples of the "possible dilution" group definition.

Table 15. Definition of the risk categories for dilution.

Dilution risk category	Criterion
Low	Tonnes of dilution / Extracted tonnes < 10%
Moderate	10% ≤ Tonnes of dilution / Extracted tonnes < 30%
High	Tonnes of dilution / Extracted tonnes ≥ 30%

5.2.2 Results and Observations

The dilution risk profile obtained is presented in Figure 29. The number of stopes per risk category is shown in Table 16.

The following observations are made:

- 104 stopes out of the 2,165 Horne 5 stopes (5%) were rated *High* in terms of the dilution risk.
- Out of those 104 stopes rated *High*:
  - 30 were extracted during Phase 1 mining. This represents 3% of the 866 Phase 1 stopes.
    - 21 stopes were longitudinal stopes extracted between August 2027 and January 2030 – this represents 9% of the 226 longitudinal stopes.
    - The other nine (9) stopes rated *High* in Phase 1 were secondary stopes extracted between September 2024 and May 2027.

- 74 stopes were extracted during Phase 2 mining. This represents 6% of the 1,299 Phase 2 stopes.
  - 42 stopes were secondary stopes extracted between March 2033 and September 2035. This represents 9% of the 450 secondary stopes in Phase 2.
  - 18 stopes were pillarless stopes extracted between January 2033 and September 2035. This represents 8% of the 237 pillarless stopes.
  - 14 stopes were primary stopes extracted between March 2031 and May 2035. This represents 2% of the 612 primary stopes in Phase 2.

Sensitivity analyses were conducted to evaluate the effects of the minor principal stress threshold (initially set at 1 MPa) and the normalized plastic shear strain (initially set at 0.5). It was found that setting the σ_3 magnitude threshold between 500 kPa and 2 MPa did not have a significant impact on the analysis results. Furthermore, setting the normalized plastic shear strain threshold between zero to 0.75 did not have a significant effect on the results. However, considering all the deconfined zones that have passed peak (i.e., with a normalized plastic shear strain < 1.0) would have a greater impact on the results. It is however believed that considering all zones that have passed peak would be too conservative.

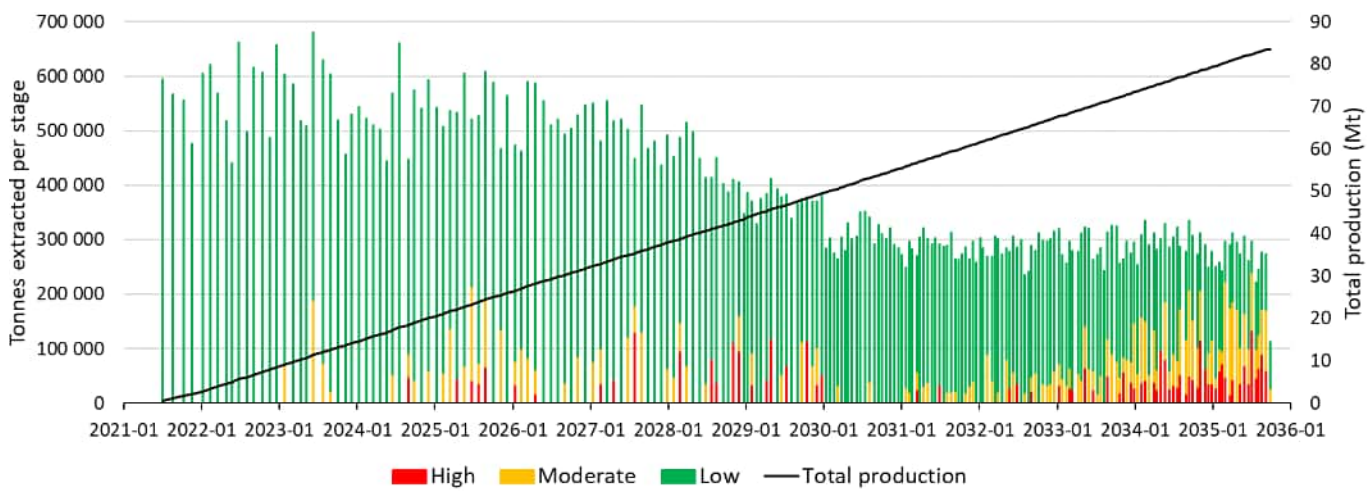

Figure 29. Dilution risk profile.

Table 16. Number of stopes per dilution risk category.

Dilution risk category	Number of stopes	Percentage of the total number of stopes
High	104	5%
Moderate	204	9%
Low	1,857	86%
Total	2,165	100%

Note that average dilution levels (in percentage) may be derived from this type of analysis.

Figure 30 shows examples of stopes rated with a *High* and a *Low* dilution risk.

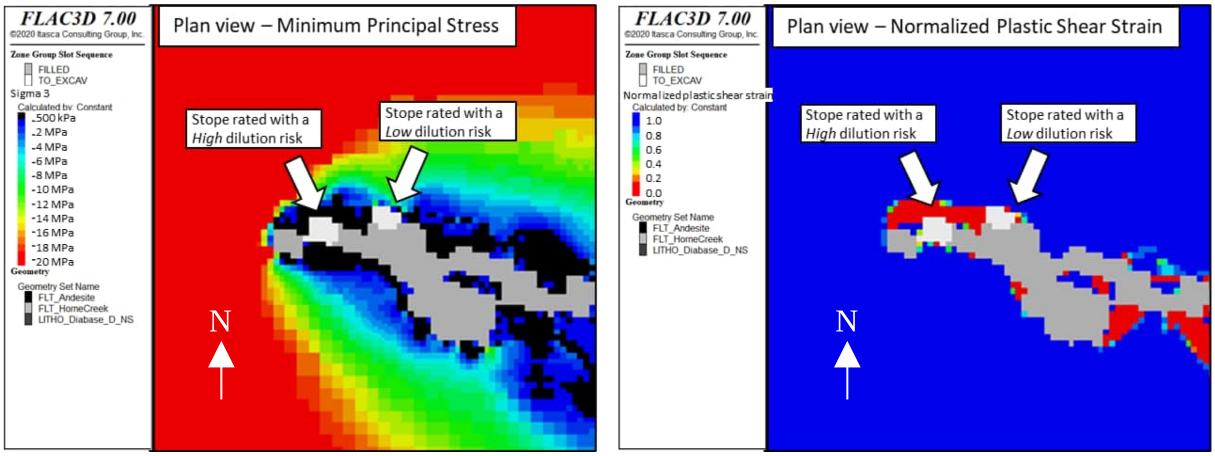

Figure 30. Plan views showing examples of stopes rated with a *High* and *Low* dilution risk.

6. EVALUATION OF MAJOR INFRASTRUCTURE LOCATION

The objective of the work described in this section was to assess the mining-induced stress variations at the location of various planned major infrastructures. The following infrastructures were evaluated: crushers, garage, shaft, ore passes and ventilation raises. Haulage drifts from L1030 to L1310 – all planned to be driven within the ore body – were also assessed.

This analysis was conducted through the examination of control points specified within the *FLAC3D* model. In other words, the infrastructures were not explicitly added in the model as physical voids. Instead, major and minor principal stress (σ_1 and σ_3) magnitudes were tracked at these points of interest throughout the entire simulation. Stress paths (in the σ_1–σ_3 space) and deviatoric stress graphs were then extracted. Those stress paths do not consider the infrastructure presence, nor geometry. The objective of this approach was to hasten the process. What was verified was the stress state at the proposed location of each major infrastructure at each modelled mining step. If this stress state was deemed favourable, then the location was considered adequate.

In order to establish the adequacy of the stress state, the path of the deviatoric stress was examined, in combination with its proximity to the failure envelope of the local rock mass and the confinement level. To minimise stress damage, an infrastructure should ideally be in an area that experiences minimal deviatoric stress variations (taken to be a variation of less than 10 MPa) and which remains sufficiently confined (i.e., with a σ_3 magnitude ≥ 5 MPa). If the stress path extracted from the *FLAC3D* model indicates an increase in deviatoric stress, then the proximity to failure envelope needs to be evaluated. If the stress state becomes too close to the failure envelope, stress damage should be expected at that location once the infrastructure is excavated. If an increase in deviatoric stress is forecasted but the stress regime remains far from the failure envelope, then the forecasted stress conditions (once the infrastructure is excavated) should be considered in the ground support design, taking into account the geometry of the infrastructure. Dedicated small-scale numerical models would then be considered for a more detailed analysis, which explicitly accounts for the infrastructure.

The observations and conclusions for the infrastructure analyses are presented hereafter.

6.1 CRUSHERS

There are two crushers planned in Phase 1 on L1310 and one crusher planned in Phase 2 on L1910. These three crushers are planned to be located between 100 and 125 m from stopes. The following observations were made at their locations:

- The failure envelope was not reached at any point.

- The Phase 1 crusher location towards the west of the ore body experienced the largest deviatoric stress increase (of + 15 MPa) during its operational period, as observed in Figure 31a.
- The two other crusher locations sustained smaller stress changes, as observed in Figure 31c and d, where the stress path at the location of the Phase 2 crusher is shown.

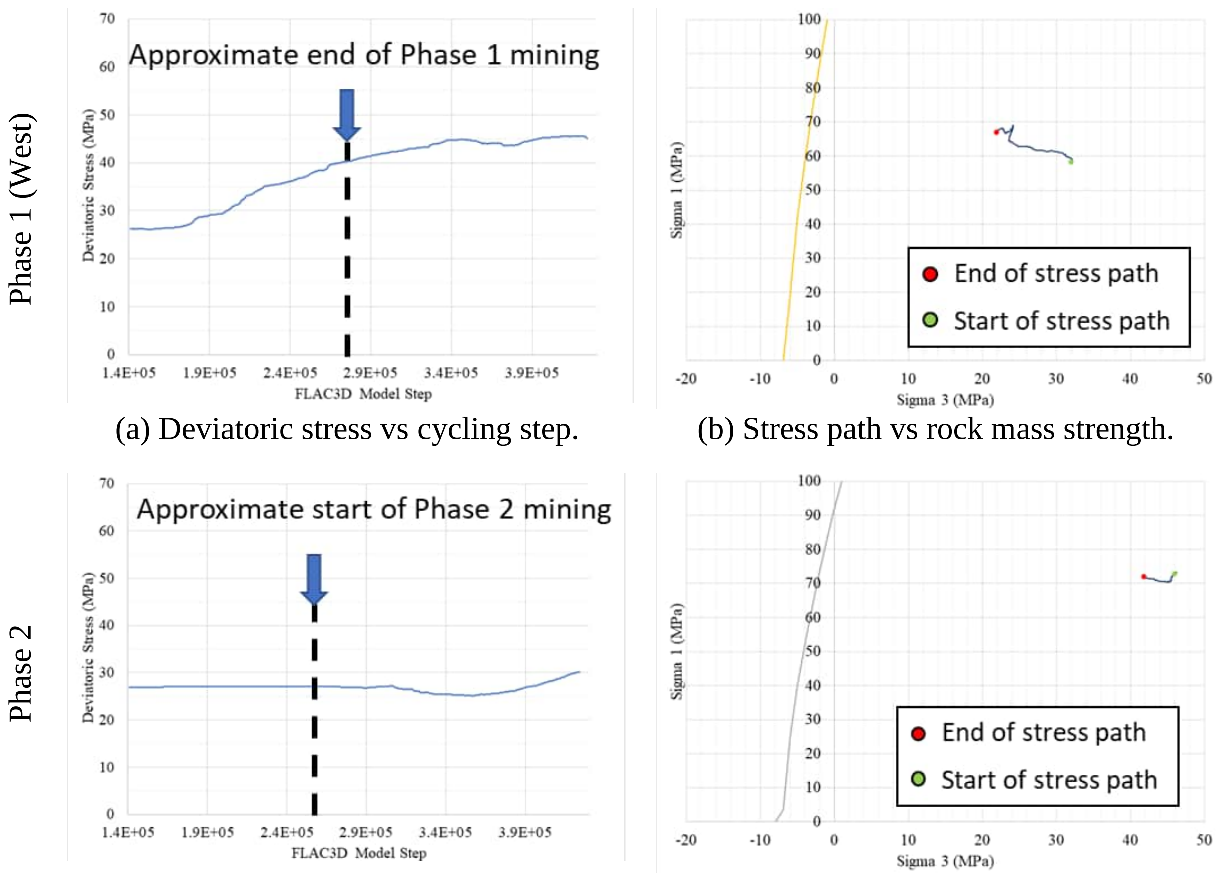

(a) Deviatoric stress vs cycling step.
(b) Stress path vs rock mass strength.
(c) Deviatoric stress vs cycling step.
(d) Stress path vs rock mass strength.

Figure 31. Deviatoric stress and stress path at Phase 1 West and Phase 2 crusher location.

6.2 Garage

The garage is planned on Level 1230. It is located at approximately 500 m from the nearest stopes. The following observations were made at this location:

- The failure envelope was not reached.
- Minimal stress changes are forecasted (the deviatoric stress decreases by 10 MPa), as seen in Figure 32.

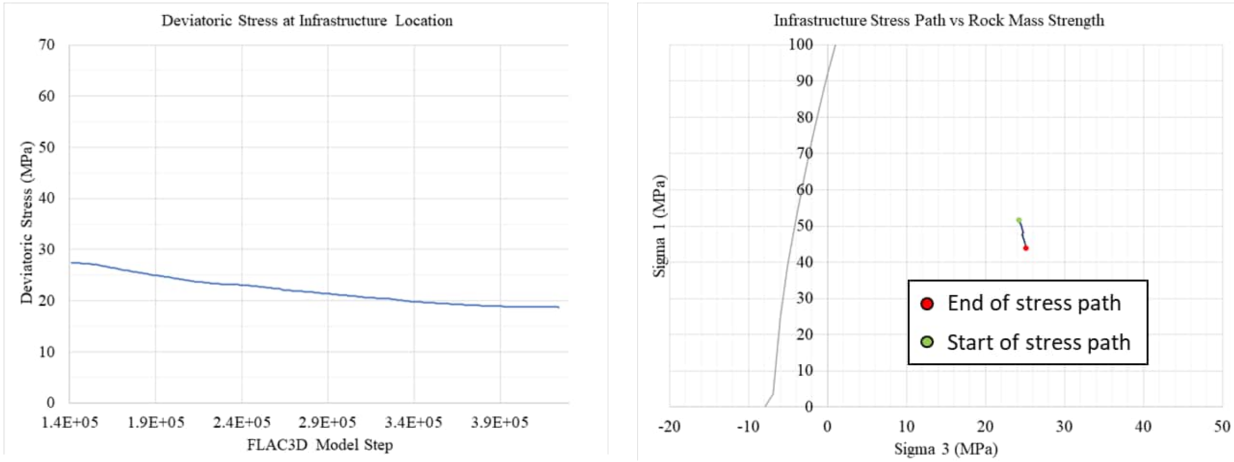

(a) Deviatoric stress vs cycling step. (b) Stress path vs rock mass strength.

Figure 32. Deviatoric stress and stress path at the garage location.

6.3 Shaft

The shaft is planned from surface down to L1970. It is located at approximately 700 m from the nearest stopes. The following observations were made along its location:

- The failure envelope was not reached at any point.
- Minimal stress changes are forecasted (the deviatoric stress decreases by 10 MPa), as observed in Figure 33 , where a representative example is shown on Level 1270.

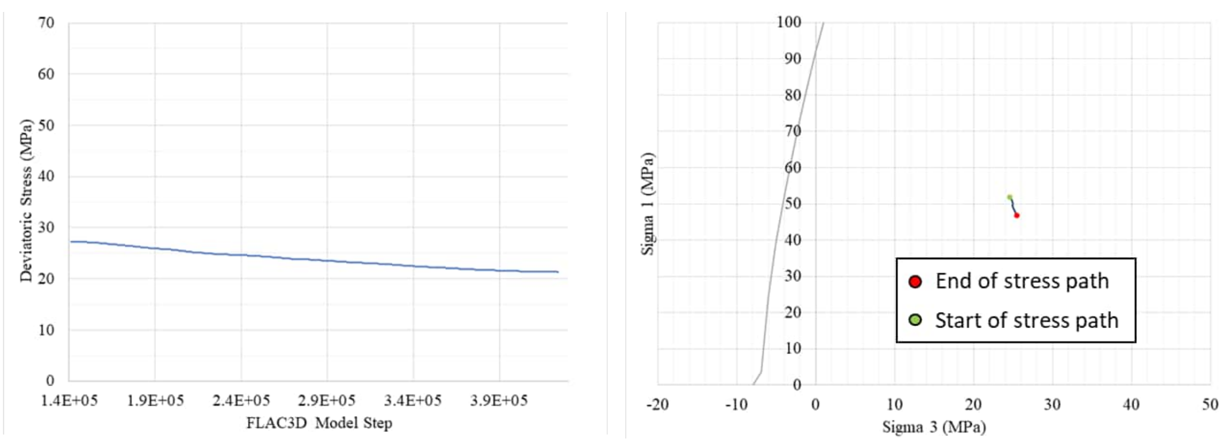

(a) Deviatoric stress vs cycling step. (b) Stress path vs rock mass strength.

Figure 33. Deviatoric stress and stress path at the shaft location (on Level 1270).

6.4 Ore Passes

The ore passes were arranged in four groups: Phase 1 West, Phase 1 East, Phase 2 West and Phase 2 East (Figure 24).

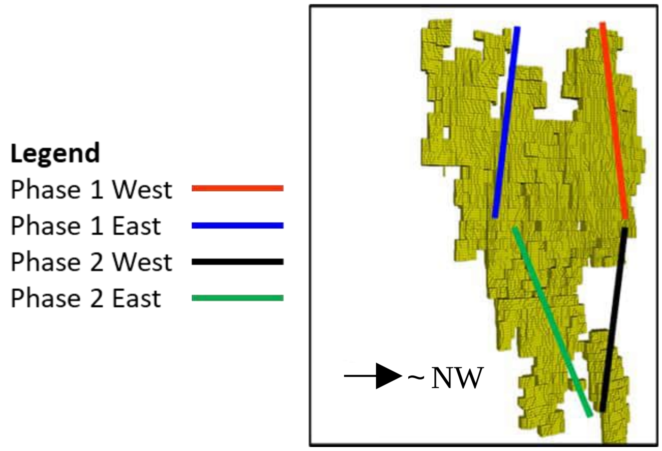

Figure 34. View looking approximately south-west showing the ore pass groups.

The following observations can be made at the ore pass locations:

- The failure envelope was not reached at any point.
- Phase 1 West ore passes:
  - Levels towards the bottom of Phase 1 (levels 1110 to 1270) experienced the largest deviatoric stress increases (up to 20 MPa) during Phase 1 mining, as shown in Figure 35a and b.
  - Smaller stress changes were observed at shallower levels, where deviatoric stress variations remained within 10 MPa with lower σ_3 values, but always greater than 5 MPa. A representative example is shown in Figure 35c and d.
- Phase 1 East ore passes:
  - Deviatoric stress variations during mining remained within 10 MPa with lower σ_3 values, but always greater than 5 MPa.
- Phase 2 West ore passes:
  - Levels towards the top of Phase 2 (levels 1270 to 1640) experienced the largest deviatoric stress increase (between 10 and 20 MPa) during Phase 2 mining, as observed in Figure 36, where a representative example is shown (on Level 1520).
  - Smaller stress changes were observed in deeper levels (L1760 to L1880). Deviatoric stress variations remained within 10 MPa.

- Phase 2 East ore passes
  - Levels towards the top of Phase 2 (levels 1340 to 1490) experienced the largest deviatoric stress variations (within 20 MPa) during Phase 2 mining. Decreasing tendencies were mainly observed, leading to lower σ_3 values but always greater than 5 MPa, as visible in Figure 37, which shows a representative example on Level 1370.
  - Smaller stress changes were observed on deeper levels (L1550 to L1880). Variations of deviatoric stress remained within 10 MPa.

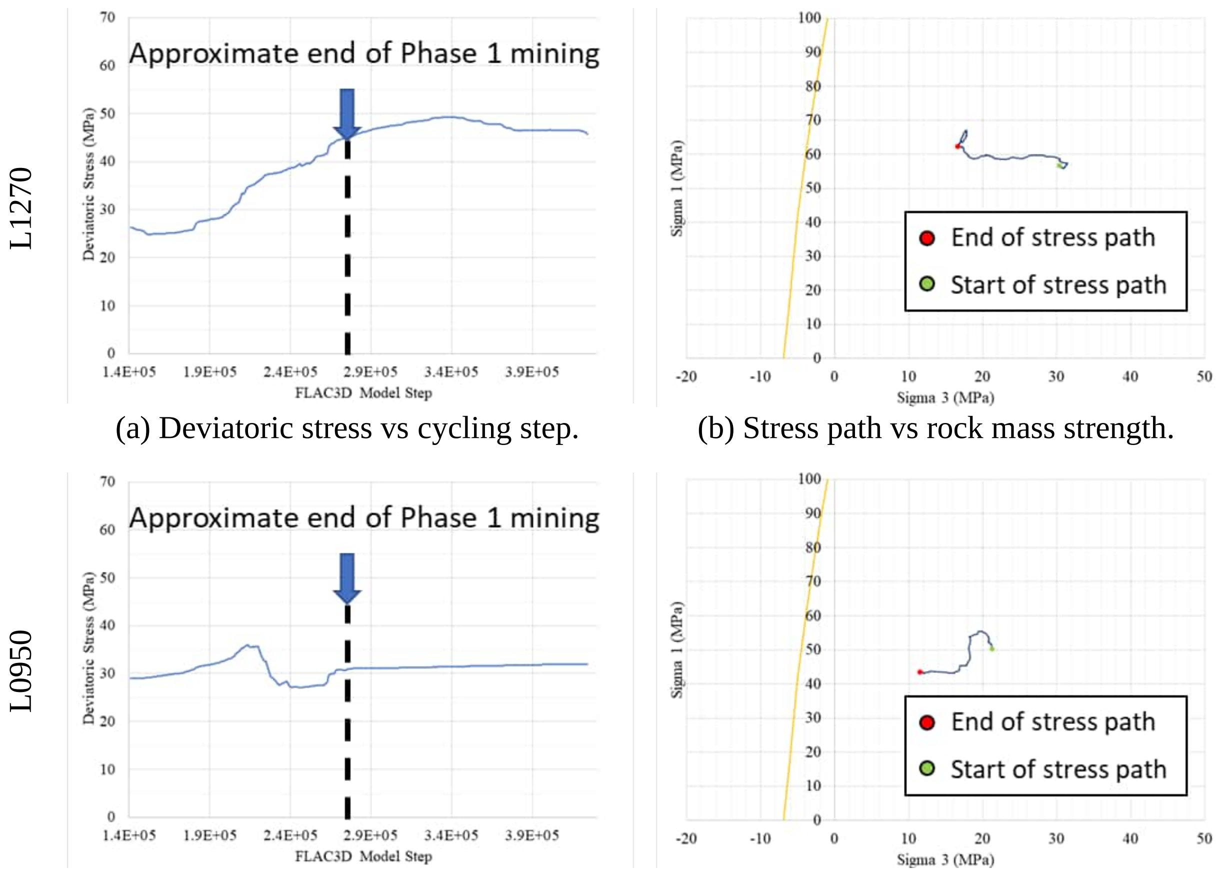

(a) Deviatoric stress vs cycling step. (b) Stress path vs rock mass strength.

(c) Deviatoric stress vs cycling step. (d) Stress path vs rock mass strength.

Figure 35. Deviatoric stress and stress path at the Phase 1 West ore passes location (on levels 1270 and 950).

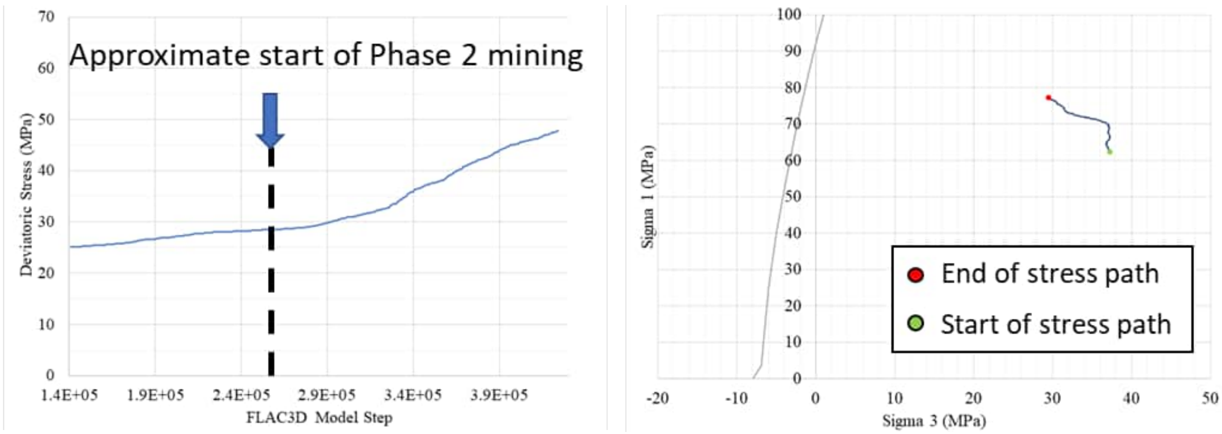

(a) Deviatoric stress vs cycling step. (b) Stress path vs rock mass strength.

Figure 36. Deviatoric stress and stress path at Phase 2 West ore passes location (on L1520).

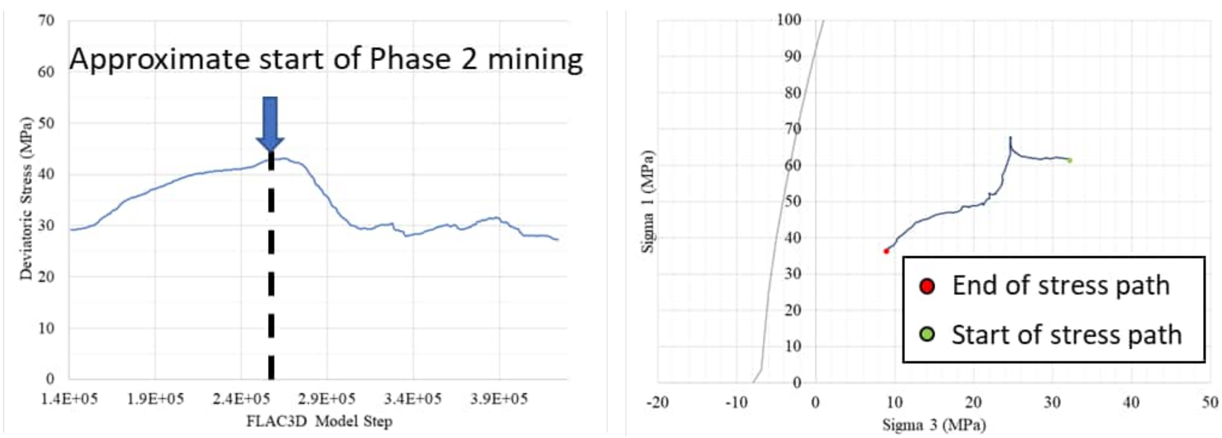

(a) Deviatoric stress vs cycling step. (b) Stress path vs rock mass strength.

Figure 37. Deviatoric stress and stress path at Phase 2 East ore passes location (on L1370).

6.5 Ventilation Raises

The ventilation raises were arranged in three groups: raises above Phase 1, raises within Phase 1 and raises within Phase 2. These groups are shown in Figure 38.

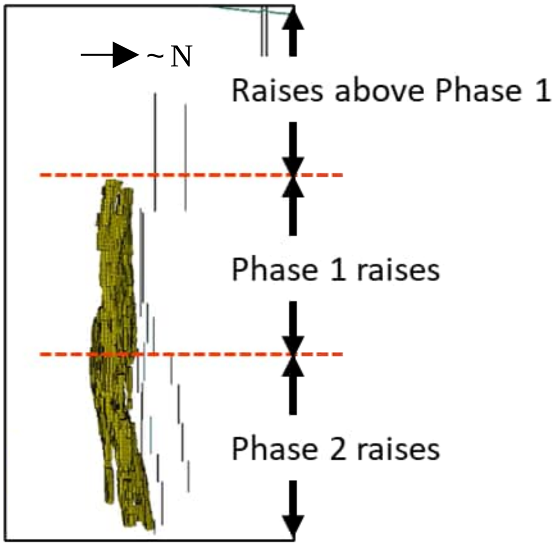

Figure 38. View looking approximately west showing the three ventilation raise groups.

The following observations were made at the ventilation raise locations:

- The failure envelope was not reached at any point.
- Raises above Phase 1: small stress changes (close to zero) were observed, as shown in Figure 39 (cut at Level 322).
- Phase 1 raises:
  - The level at the bottom of Phase 1 (L1370) experienced the largest deviatoric stress variation. A 30 MPa deviatoric stress increase was first recorded, followed by a stress decrease (with σ_3 reaching 5 MPa), as shown in Figure 40a and b.
  - On the other Phase 1 levels, ventilation raise locations experienced deviatoric stress variations (increases and/or decreases) of 15 MPa or less. On levels 1150 and 1190, σ_3 became lower than 5 MPa, but remained above 2 MPa. An example is shown in Figure 41a and b (on Level 1150). At that point, the raise is located approximately 50 m from the stopes.
- Phase 2 raises:
  - In Phase 2, some planned raise locations are close to the ore body (around 50 m) while others are further away (around 175 m).
  - At the location of those raises closer to the ore body deviatoric stress increases of up to 35 MPa were computed. An example is shown in Figure 42a and b (on Level 1880). At that point, the raise trajectory is located approximately 50 m from the stopes. However, not all raises closer to the ore body experienced such a high deviatoric stress increase.

- Minimal stress changes were observed at the location of the raises located further away from the ore body. An example is shown in Figure 42c and d (on Level 1610). At that point, the raise is located approximately 180 m from the stopes.
- The confinement (σ_3) magnitude was not observed to decrease under 5 MPa at any of the Phase 2 raise locations.

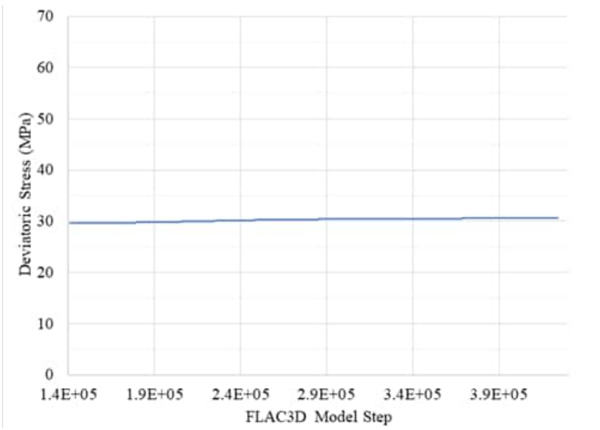

(a) Deviatoric stress vs cycling step.

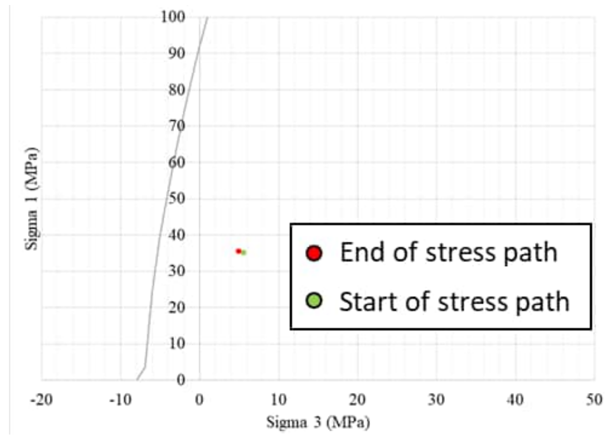

(b) Stress path vs rock mass strength.

Figure 39. Deviatoric stress and stress path at the location of ventilation raises above Phase 1 (on L0322).

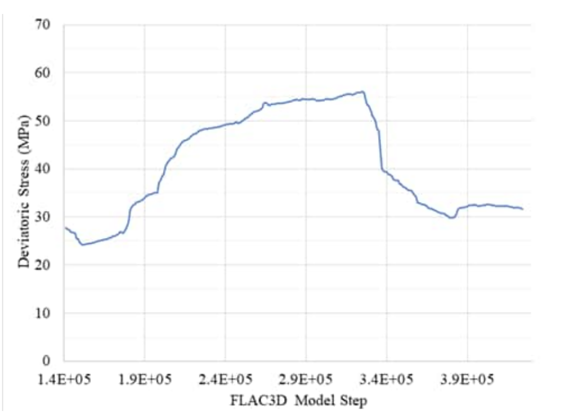

(a) Deviatoric stress vs cycling step.

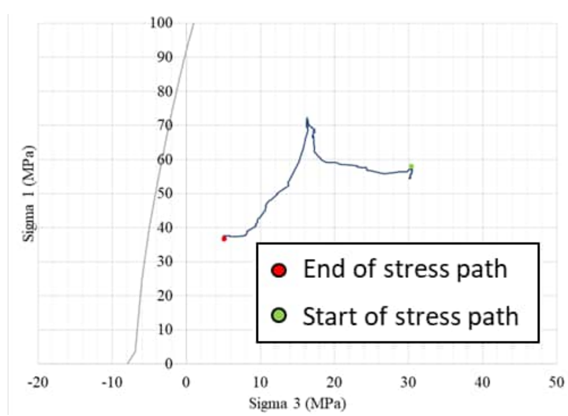

(b) Stress path vs rock mass strength.

Figure 40. Deviatoric stress and stress path at Phase 1 ventilation raises location (on L1310).

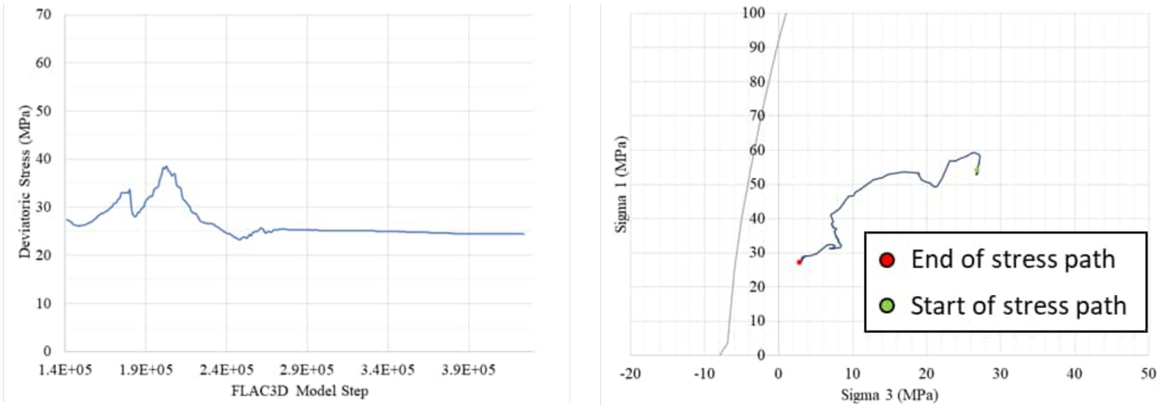

(a) Deviatoric stress vs cycling step. (b) Stress path vs rock mass strength.

Figure 41. Deviatoric stress and stress path at Phase 1 ventilation raises location (on L1150).

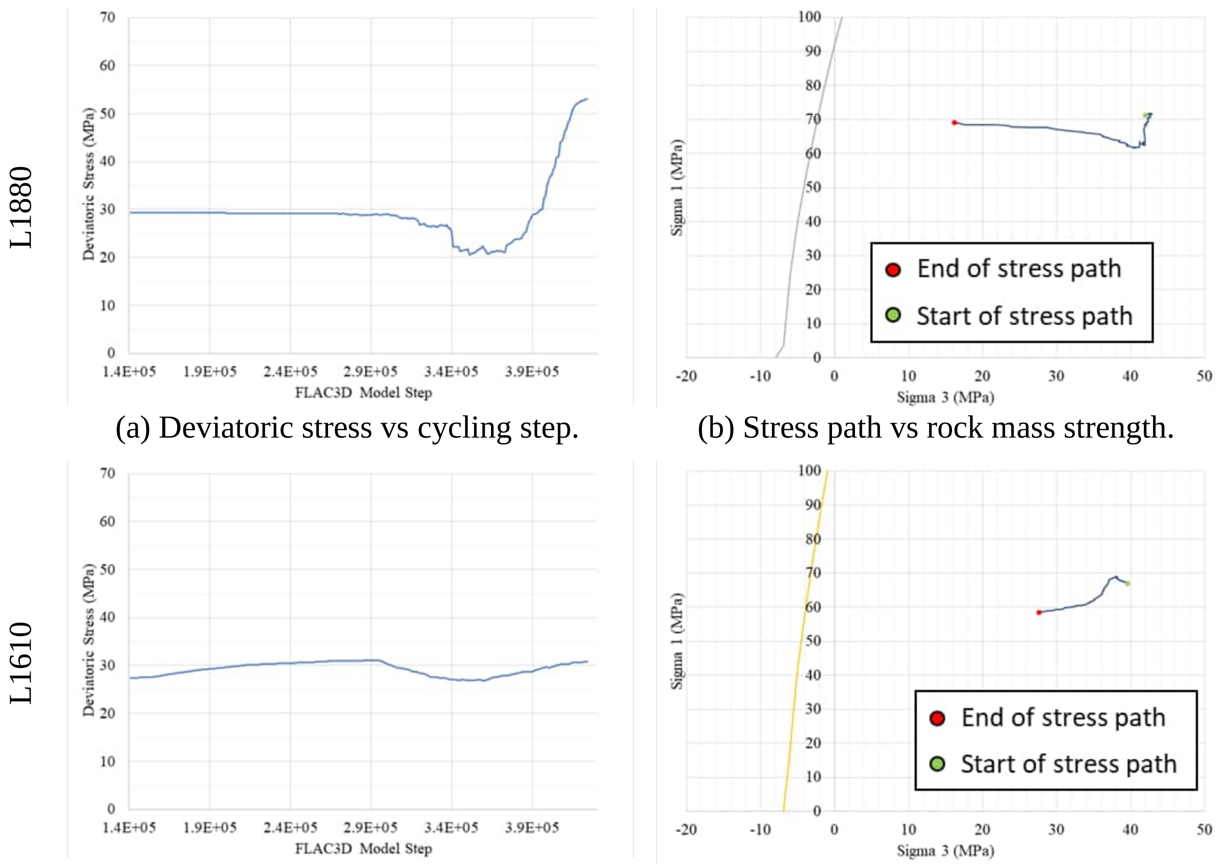

(a) Deviatoric stress vs cycling step. (b) Stress path vs rock mass strength.

(c) Deviatoric stress vs cycling step. (d) Stress path vs rock mass strength.

Figure 42. Deviatoric stress and stress path at Phase 2 ventilation raises location (on L1880 and L1610).

6.6 Haulage Drifts Within the Ore Body

To reduce development costs, haulage drifts from Level 1030 to Level 1310 (corresponding to the eight bottom levels of Phase 1) are planned to be driven within the orebody rather than in waste rock some distance away. At these locations, stress changes due to the approaching, then passing, mining front is the main challenge expected. The stress paths (in the σ_1–σ_3 space) extracted from the model at these locations eventually reached the origin (0,0) once the longitudinal stope is mined at the drift location. The following observations were made along these drift locations.

- Towards the ore body abutments (east and west), haulage drifts can be expected to experience significant deviatoric stress increases (up to 120 MPa) prior to the longitudinal stope being mined at that location. The stress regime will however remain below the failure envelope. An example is shown in Figure 43 (on Level 1110). It should be noted that because the stress variations forecasted at the haulage drift locations are significantly larger, the scale of Figure 43a has been changed compared to the scale used for the deviatoric stress graphs of other infrastructures. For reference, at the control point shown in Figure 43c, $0.7 \times (\sigma_1 - \sigma_3) / UCS$ = 110 MPa (threshold over which a zone was considered "highly stressed," as per Table 10).

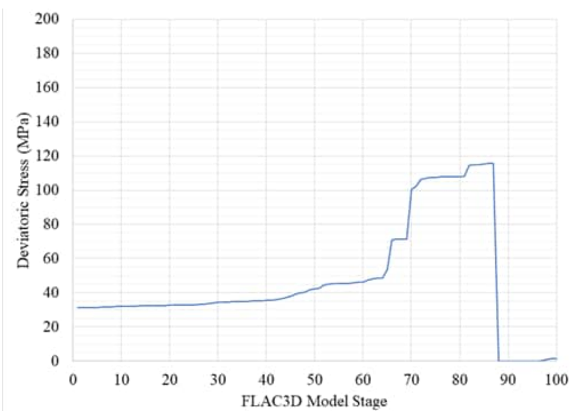

(a) Deviatoric stress vs modelling step.

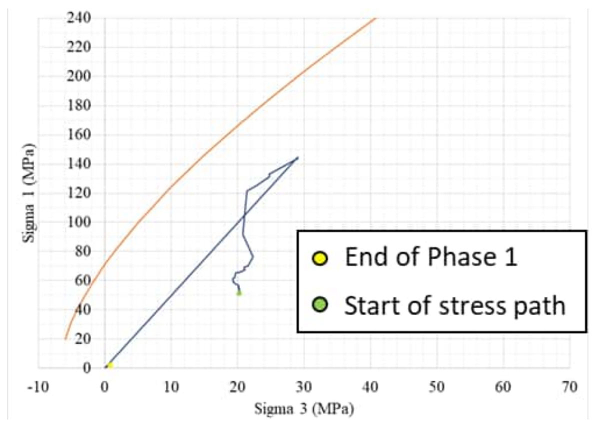

(b) Stress path vs rock mass strength.

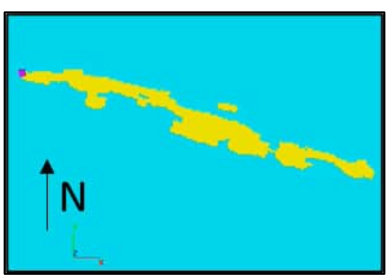

(c) Control point location (plan view).

Figure 43. Deviatoric stress and stress path at the location of the haulage drift on L1110 (driven in the ore body).

- On all the levels assessed, except on Level 1310 where the failure envelope was not reached, stress paths towards the centre of the ore body (starting at about 100 m from the abutments) either reached the failure envelope or, if not, very low confinement values were forecasted (below 2 MPa). An example of a stress path reaching the failure envelope is given in Figure 44a and b (on Level 1070). An example of a stress path reaching very low confinement values is given in Figure 44c and d (on Level 1230).

L1070

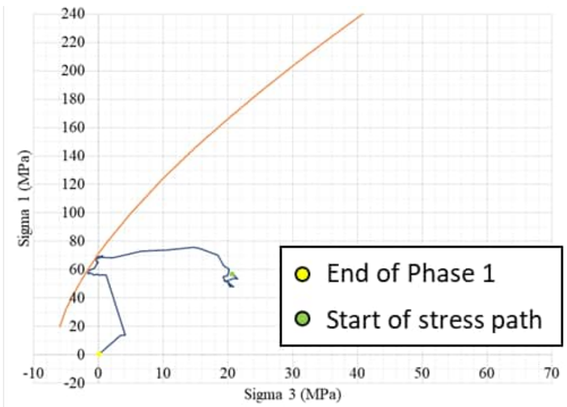

(a) Stress path vs rock mass strength.

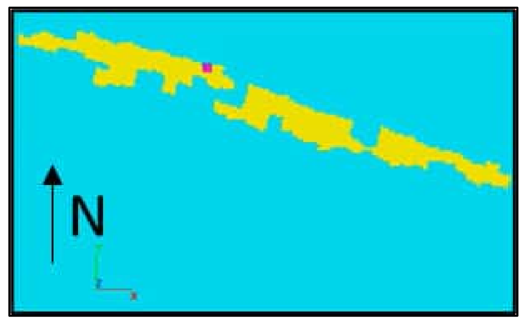

(b) Control point location (plan view).

L1230

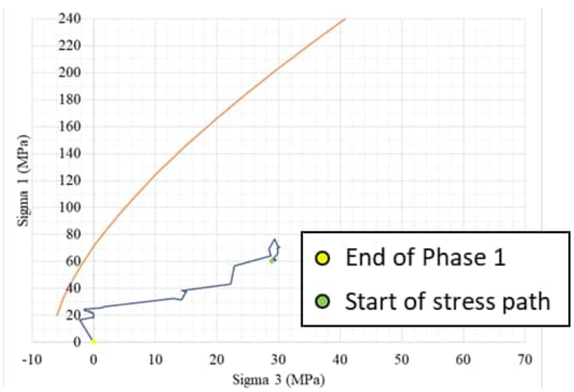

(c) Stress path vs rock mass strength.

(d) Control point location (plan view).

Figure 44. Deviatoric stress and stress path at the location of haulage drifts on L1070 and L1230 (driven in the ore body).

6.7 Note on the Smelter

The smelter on surface, located almost directly above the Horne and Horne 5 mines, is a critical long-term asset whose stability and integrity must be maintained. Mining-induced surface displacements were hence extracted from the *FLAC3D* modelling results to ensure they remain low. A longitudinal view, as well as a close-up view of displacement to surface, are shown in Figure 45.

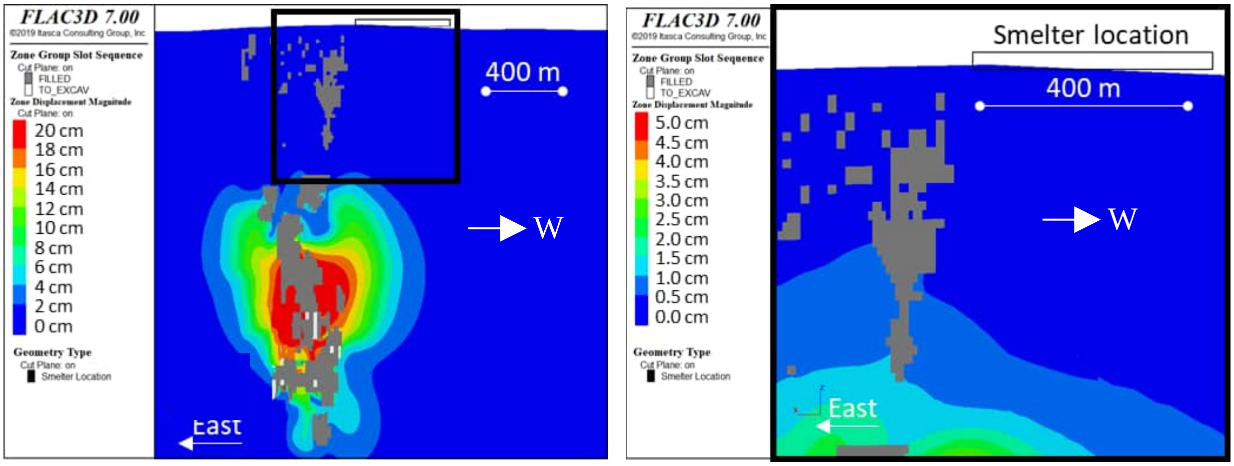

(a) Longitudinal view, showing historical Horne and Horne 5 workings.

(b) Longitudinal view, focusing on the first 700 m below surface (black square in [a]).

Figure 45. Views looking south showing total displacement at the end of Horne 5 mining.

Less than 0.5 cm of total displacement was computed on surface at the smelter location due to mining at Horne 5. Note that the displacements due to the mining of the historical Horne mine were zeroed in the model prior to mining Horne 5. Therefore, the displacements shown in Figure 45 are solely due to the mining of the Horne 5 ore body. It should be reminded that *FLAC3D* is a continuum code, which therefore does not account for discrete block movement (i.e., ravelling, wedge failure, or other discrete mechanisms).

6.8 Summary of Conclusions

The following conclusions were reached following the infrastructure analyses:

- The garage, shaft and Phase 2 crusher should experience minimal stress changes.
- Phase 1 crushers, ore passes and ventilation raises can be expected to experience stress changes, but these should remain below the failure envelope and should not be severely de-confined (σ_3 remained > 5 MPa at all points, except for ventilation raises on L1150 and L1190 where 2 MPa < σ_3 < 5 MPa).
- Stress variations at the haulage drift locations on levels 1030 to 1310 (driven within the ore body) were significantly larger. The failure envelope can be expected to be reached along these drifts, and very low confinement values are forecasted to develop at some point. In the FS, increased ground support requirements have been accounted for in the drifts located in ore. Note however that maintaining these drifts throughout their useful life span will be chal-

lenging. Planning for additional costs and delays (due to rehabilitation, ground support upgrades, and/or even bypasses) may be prudent.

- Less than 0.5 cm of total displacement was computed on surface at the smelter location due to mining at Horne 5.

7. BARRIER PILLAR

The shallowest levels of the Horne 5 project (between levels 710 and 950) will be located near the historical Horne mine. The volume of rock between the historical Horne mine and the Horne 5 stopes is referred to as the *Barrier Pillar*. Mining in Phase 1 will induce stress changes in the vicinity of the historical Horne mine, and, consequently, within the barrier pillar. Fracturing of the barrier pillar due to stress increases was identified as a potential mining challenge. In the FS, several mitigation measures were planned to reduce the risk of fracturing the core of the barrier pillar. Those measures are listed below for reference:

- The mining sequence was designed to reduce the potential for stress fracturing.
- A minimum 15 m stand-off distance was planned between the mined-out historical Horne mine from the new Horne 5 mining.
- A higher backfill binder content, resulting in higher strength, was planned for the Horne 5 stopes within 65 m of historical workings.
- The historical Horne mine openings between levels 474 and 1310 are planned to be backfilled prior to Horne 5 mining.

The stress regime indicated by the numerical simulations within the barrier pillar was examined over the entire mining sequence to establish whether conditions could develop in it, which could plausibly result in fracturing within the pillar.

7.1 BARRIER PILLAR STABILITY

The objective of this analysis was to evaluate the stability of the barrier pillar formed between the historical Horne mine and the Horne 5 stopes. The normalised plastic shear strain was the tracking parameter used for this analysis. During Phase 1 of the mining sequence, zones that reached their residual strength were identified. As discussed in Section 5.2, these zones are associated with damaged ground. Figure 46 shows steps 49, 50, 51 and 99 of the mining sequence.

The following observations can be made:

- Steps 0 to 49: damaged areas are limited to sectors abutting existing excavations and there is no increase during these mining steps. The affected volume remains constant at ~ 20,000 m^3.
- Step 50: following the excavation of Stope 0790-0640-1, the damaged volume increases by more than 64,000 m^3. This represents 26% of the affected volume at the end of Phase 1. That stope and the historical excavations are only approximately 11 m apart. The yielded volume is located between levels 0830 and 0750.
- Steps 51 to 62: as the mining sequence progresses in the western part of the mine, the major principal stress magnitude increases in the pillar and causes the volume of damaged ground to grow by 143,000 m^3. The yielded zone reaches Level 0910.

- Steps 63 to 99: from Step 63 until the end of Phase 1, the yielded volume variations remain low.
- Step 99: at the end of Phase 1, about 250,000 m^3 of rock have reached their residual strength. Most of that volume is located north-west of the barrier pillar.

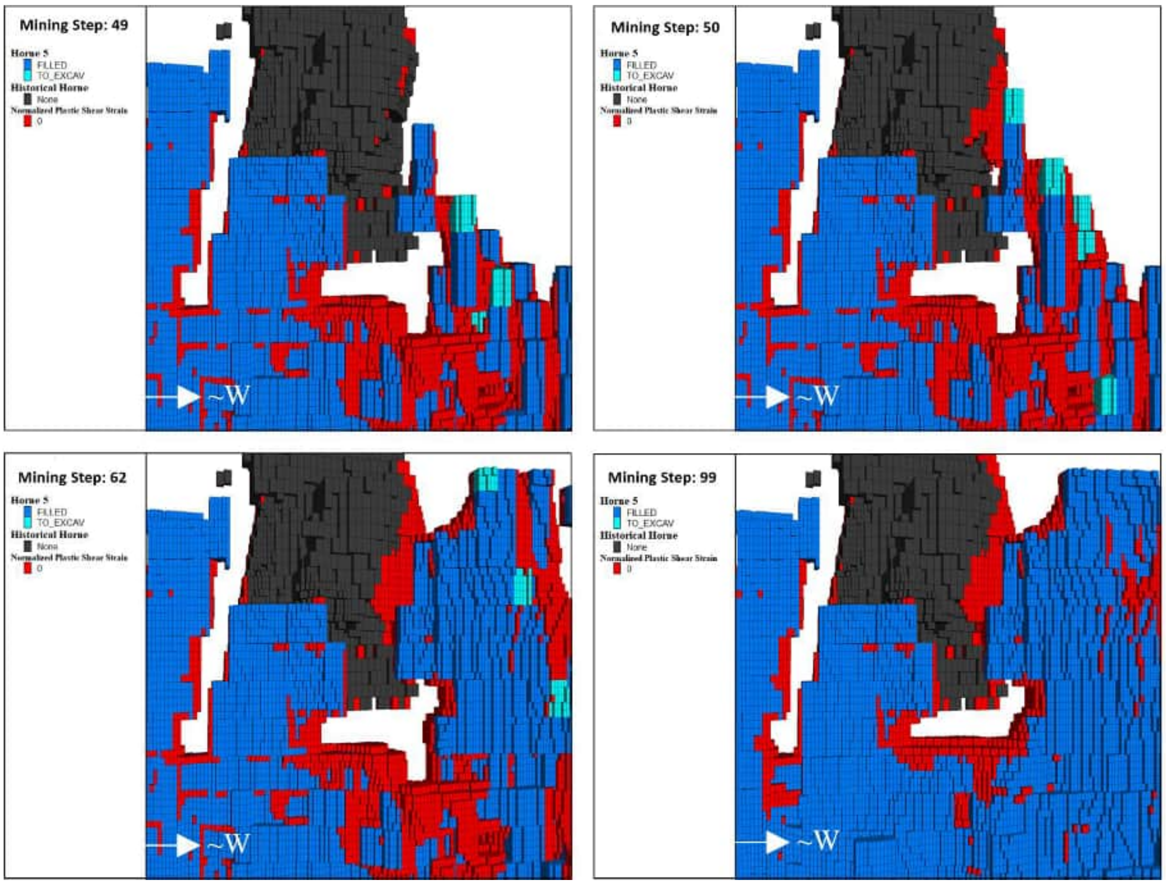

Figure 46. Elevation views looking approximately south, showing the normalised plastic shear strain values in the barrier pillar for mining steps 49, 50, 62 and 99.

Even with that large volume of damaged ground, a significant large-scale instability remains unlikely within the barrier pillar for the following reasons:

- The volume of void open at any time (in the form of blasted stopes not yet backfilled) remains small.
- By the time yielding starts in earnest, those Horne 5 stopes located nearest to the historical Horne workings have long been extracted and backfilled.
- The yielded volume sits mainly between the historical Horne workings and the new Horne 5 stopes. It is not expected to connect with the development located to the north of the ore body (Figure 47a).

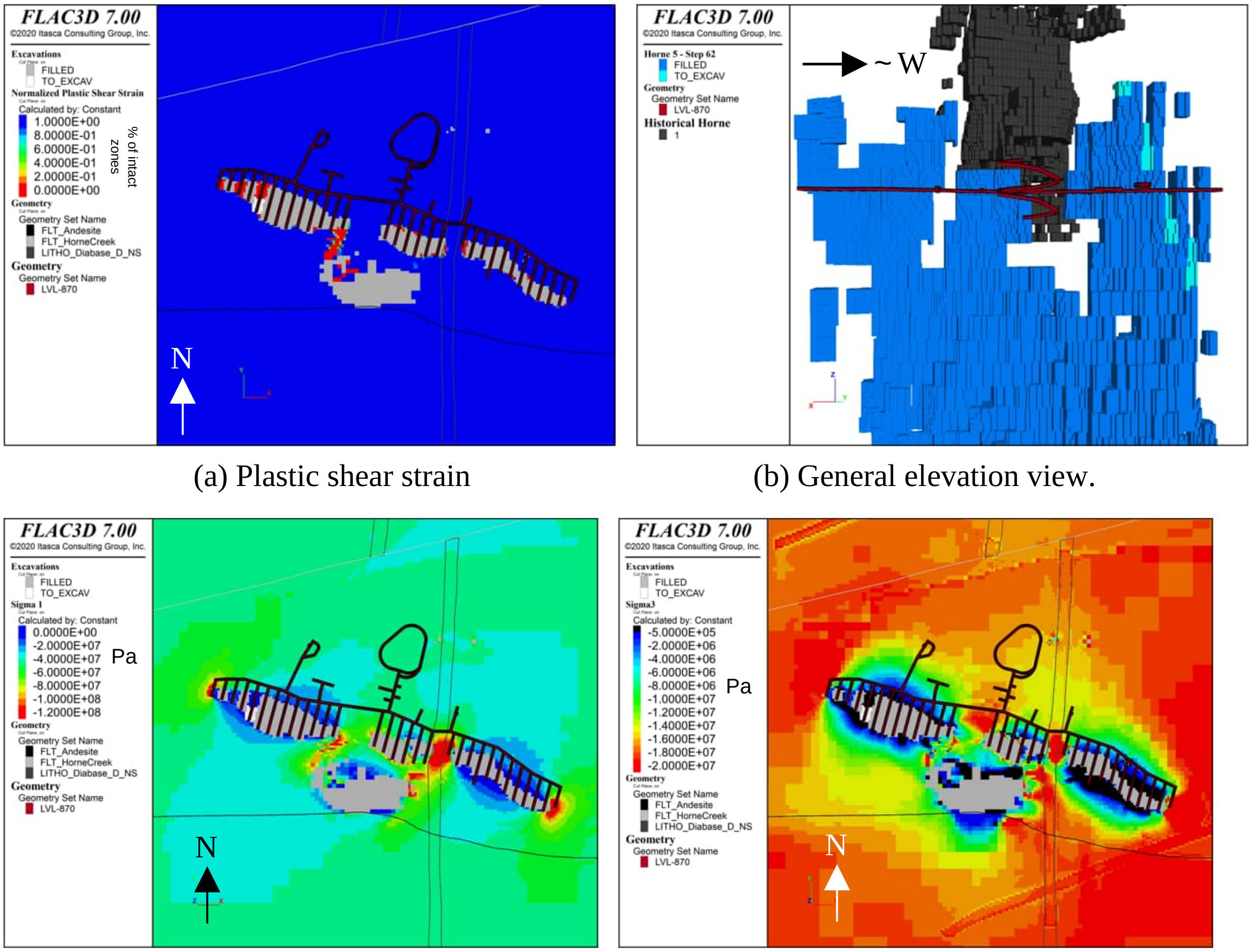

(a) Plastic shear strain (b) General elevation view.

(c) σ_1 magnitude. (d) σ_3 magnitude.

Figure 47. Plastic shear strain, and σ_1 and σ_3 magnitudes after Step 62 on Level 0870.

However, increased dilution could be expected during the exploitation of Stope 0790-0640-1. The installation of extra ground support (cablebolts) could help control dilution and help stabilise its south wall. Close monitoring during the mucking and paste backfilling cycles is recommended. Furthermore, should the historical Horne excavations not be appropriately paste backfilled, water could reach the Horne 5 excavations through new fractures created in the barrier pillar.

7.2 Large Seismic Events

Due to sensitive instrumentation installed in the smelter, it is important to assess whether a large seismic event could occur within the barrier pillar. For that purpose, stress paths (in the σ_1-σ_3 space), as well as deviatoric stress plots were extracted. One approach – described by Board *et al*. (2001) – to anticipate whether a rock mass subjected to stress changes will fail violently consists in examining how the stress path evolves in that volume of rock over the mining sequence. As shown in Figure 48, the likelihood of violent failure increases when the maximum (major) principal stress (the driving stress) increases while the minimum (minor) principal stress (the confining stress) remains near-constant or reduces. More energy will be released if the failure is caused by an increase in major principal stress without a loss of confinement – a non-violent / more progressive yielding response is expected with a rapid drop of confinement.

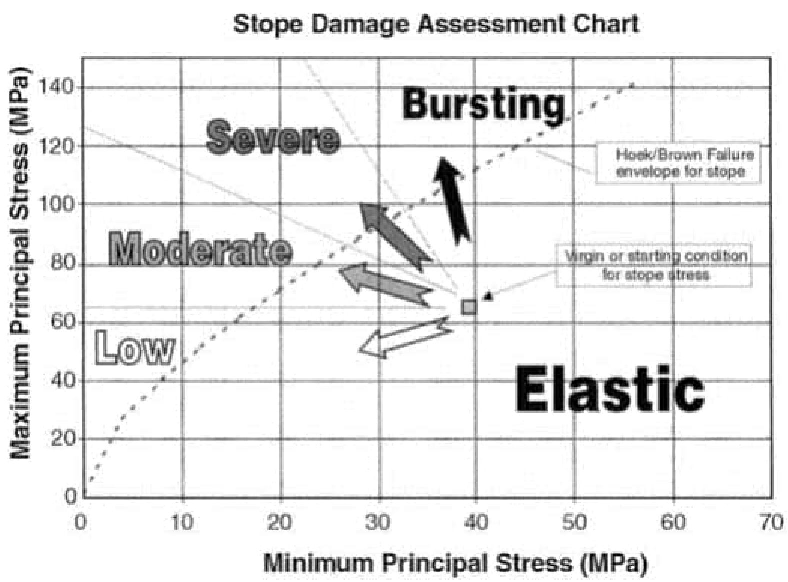

Figure 48. Generalised stress path plot showing the approximate correlation between stress path and failure violence, based on 80 stope case histories at Kidd Mine (from Board *et al.*, 2001).

Several control points were specified inside the barrier pillar and the value of the deviatoric stress divided by UCS ($[\sigma_1 - \sigma_3]$ / UCS) was extracted at each mining step at each of these points. The location of these control points is show in Figure 49.

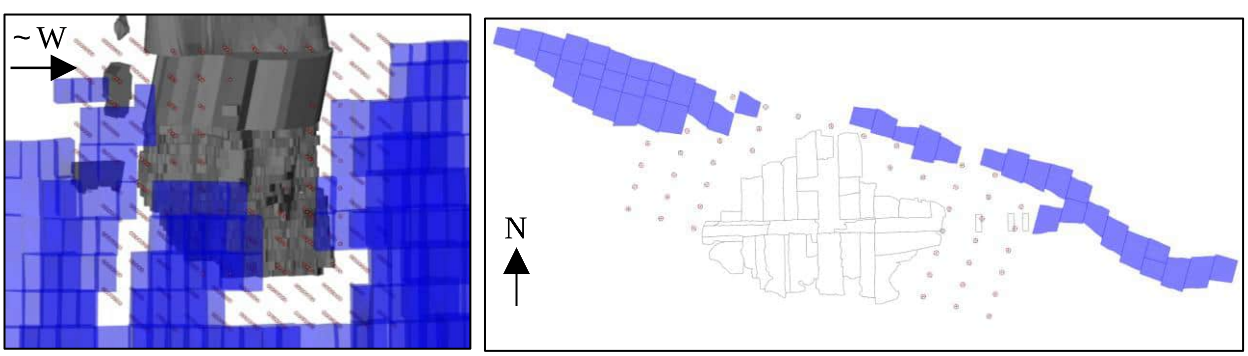

Figure 49. Isometric view looking approximately south-west and plan view (at elevation 3,460 m) showing the location of the control points.

Figure 50 shows the > 0.5 and > 0.7 isocontours of the ([$\sigma_1 - \sigma_3$] / UCS) ratio at Step 99, as well as the associated stress paths.

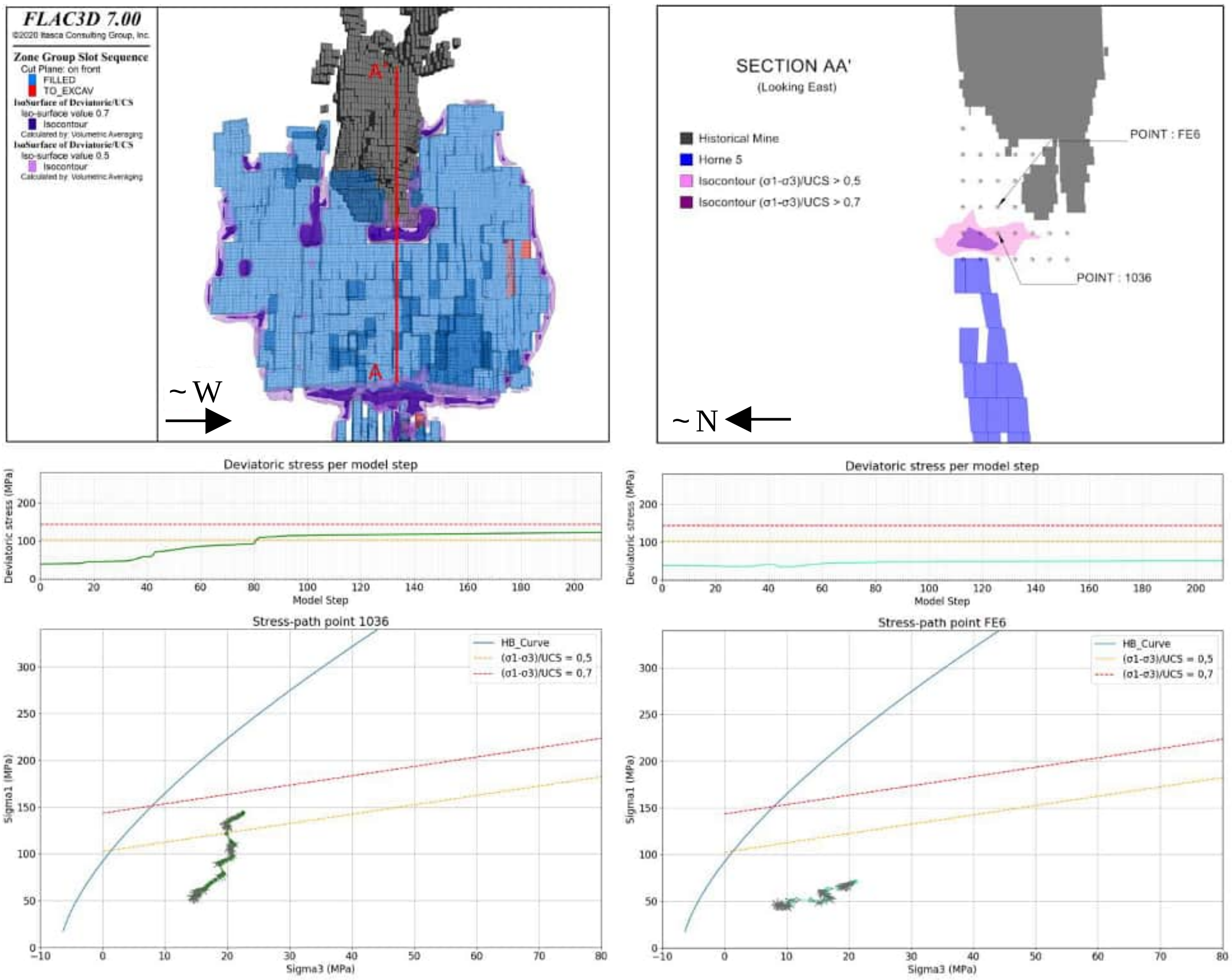

Figure 50. Isometric view looking south-west and plan view (cut at elevation 3,460) showing control points, > 0.5 and > 0.7 isocontours of the ([$\sigma_1 - \sigma_3$] / UCS) ratio at Step 99, as well as the stress path at two selected control points.

The following observations can be made:

- The area where the ratio of deviatoric stress magnitude over UCS is higher than 0.7 is located towards the top of the Horne 5 excavations and does not extend to the old Horne workings.
- The deviatoric stress magnitudes computed within the barrier pillar are similar to the values obtained in other pillars during the sequence.
- The stress path at control point FE6 shows a relatively constant σ_1 magnitude throughout the sequence – this is indicative of the anticipated conditions within most of the barrier pillar.

- The major principal stress magnitude at control point 1036 is expected to increase to about 150 MPa, with little reduction of the minor principal stress magnitude. This abutment sector could thus experience bouts of significant seismic activity and violent rock mass failure.
- The 0.5 isocontour of deviatoric stress magnitude over UCS reaches the bottom of the old Horne 5 mine. However, as shown by the stress path associated with control point 1036, the deviatoric ratio will reach this threshold at around the 80th mining step in the sequence, increasing only slightly from then on. This deviatoric stress increase at step 81 is caused by mining in the central pillar after the mining of the western part (Figure 51).

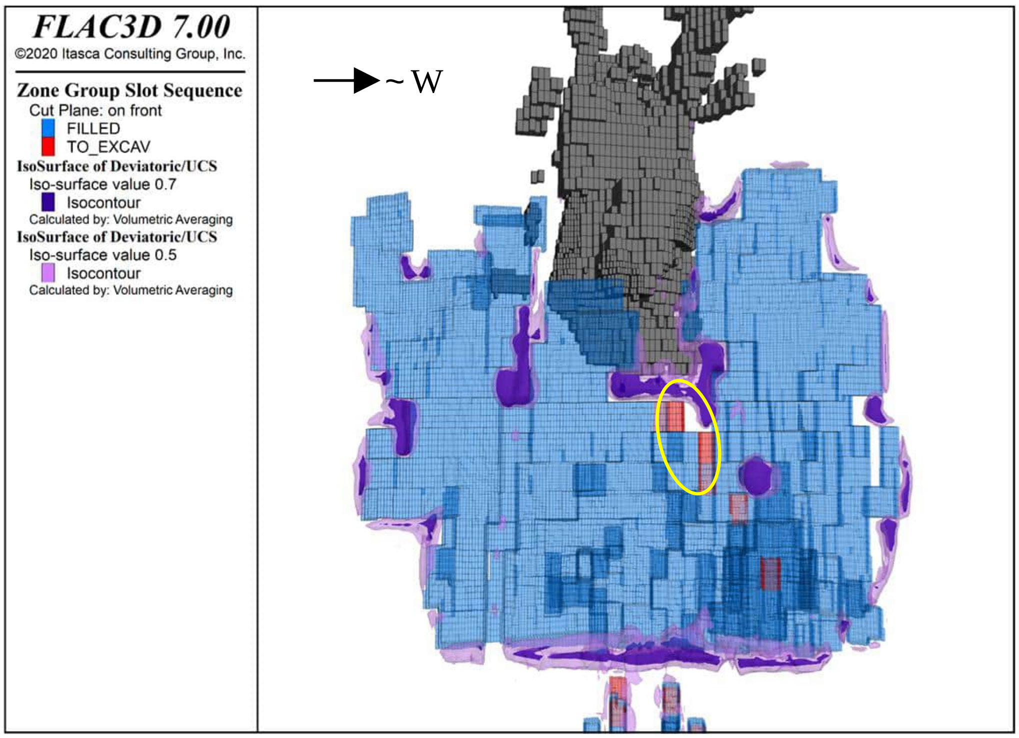

Figure 51. Isometric view looking approximately south showing the excavated stopes at Step 81.

Mining steps 81 and 82 have already been flagged in Section 4 as high risk seismic potency-wise. Once the western sequence will have been completed, the stress towards the centre of the ore body will have increased. If possible, stopes in this sector (in red and highlighted in yellow in Figure 51) should be mined sooner, shortly after the stopes to their east. Their extraction would then be easier due to the lower local stress levels. This would also provide the opportunity to have the area backfilled prior to the stress increase from the western mining front.

Based on the plastic deformations and stress paths computed at the control points within the barrier pillar, the assumption by Golder (Bewick, 2017) of an upper magnitude around M_N + 2.0 in the barrier pillar appears credible. A mining-induced stress change occurs in the barrier pillar, but it is located in a limited volume and is of the same magnitude as the changes in other sill pillars and ribs during the life of mine. Without large-scale geological structures within the barrier pillar, which could change the stress state and/or slip, a very large event would not be expected from stress change alone.

8. BEHAVIOUR OF THE MAJOR FAULTS

The potential effects on surface from mining activities at depth at the Horne 5 mine were discussed in a technical memorandum issued by A2GC in July 2020 as part of this project (Andrieux, 2020). Considerations about the largest seismic event that could be generated and the associated vibrations felt on surface were discussed in that document. One of the aspects considered was the potential for slipping to occur along some of the large-scale faults in the vicinity of the mine. This topic is further developed in this section.

8.1 PLASTIC STATE

First, the plastic state at the fault locations was evaluated from the *FLAC3D* modelling results. Isometric views after historical Horne mining and future Horne 5 mining are shown in Figure 52a and b, respectively.

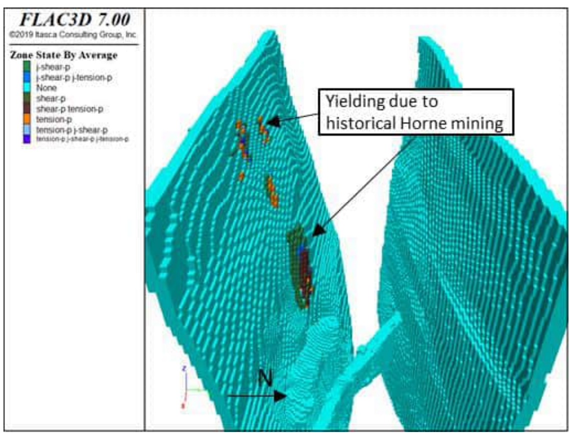

(a) After historical mining.

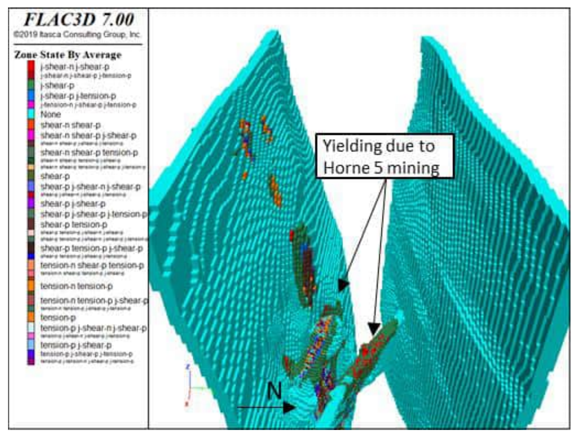

(b) After Horne 5 mining.

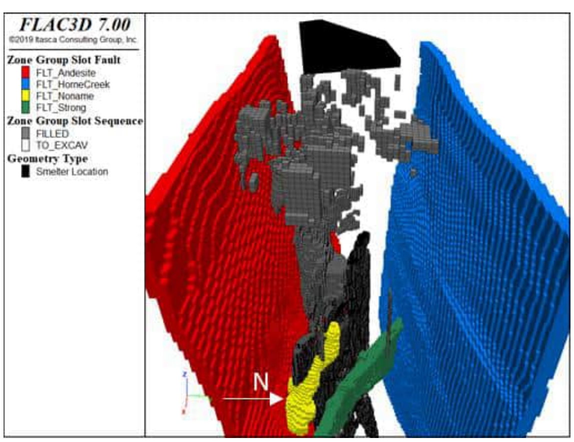

Notes:

- *All the numerical zones coloured cyan in the plots in figures (a) and (b) have not reached their failure envelope.*
- *All views look approximately west from above.*

(c) Reference plot showing the location of the various faults.

Figure 52. Plastic state plots at the location of the major faults.

It was observed that yielding of the rock mass at the location of major faults due to Horne 5 mining activity occurred only over its range of mining depth (i.e., not up to surface).

8.2 Stress Drop Analysis

As mentioned by Andrieux (2020), because of its proximity to the planned Horne 5 stopes and the fact that it extends to surface, only the Andesite fault could, with the current geological and structural knowledge, credibly be a concern for direct severe adverse effects on surface. Still, that fault lies in close proximity to the Horne 5 stopes (within about 10 m) only between levels 1194 and 1484. It then rapidly gains separation with elevation, above and below.

The fault-slip potential of the Andesite fault was evaluated through a stress drop approach, and estimates of possible strain energy release levels and associated seismic event magnitudes were derived.

8.2.1 Introduction to the Stress Drop Approach

The stress drop approach is based upon the Excess Shear Stress (*ESS*) method described by Ryder (1987, 1988) and (Board, 1994), and can be used to estimate the size of seismic events associated with fault slips. It considers the stress drop in the following terms:

$$\Delta\tau = \tau_s - \tau_d \qquad \text{... Eq. [3]}$$

Where: $\Delta\tau$ is the stress drop;
τ_s is the static shear strength along the slip plane; and,
τ_d is the dynamic shear strength along the slip plane.

The dynamic shear strength considers that once the peak static shear strength τ_s of the fault (or the encasing rock material in cases where undulations cause local locking points in it) is reached, sliding starts, which instantly removes all cohesive strength. Resistance to motion then relies entirely on friction, which is now controlled by the dynamic coefficient of friction, as follows:

$$\tau_d = \mu_d \times \sigma_n \qquad \text{... Eq. [4]}$$

Where: τ_d is the dynamic shear strength;
μ_d is the dynamic coefficient of friction; and,
σ_n is the normal stress acting upon the slip plane.

In terms of rock mass properties, τ_s can be seen as the peak strength and τ_d as the residual strength. The stress drop expressed by Eq. [3] is the result of the near-instantaneous transition from static (pre-slip) to dynamic (slip) conditions. For a given confining stress σ_{ni}, $\Delta\tau$ is the difference between the relevant static and the transient dynamic shear strength envelopes (Figure 53).

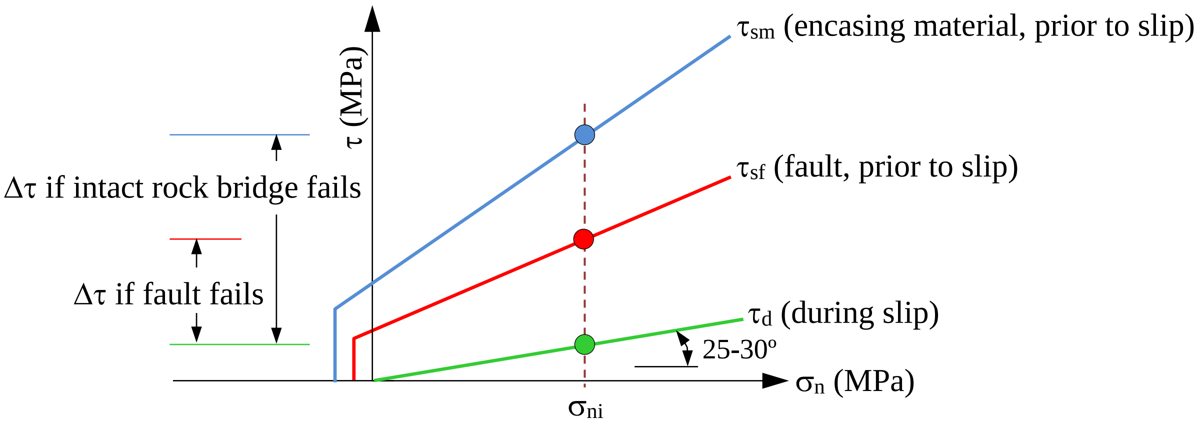

Figure 53. Conceptual (not to scale) Mohr-Coulomb failure envelopes and peak stress drops ($\Delta\tau$) for various types of failure.

Using Eq. [3] and Eq. [4], the stress drop can be calculated from the numerical modelling outputs for any location along a fault. Once obtained, that stress drop can in turn be used to infer the mean ride, which is the slip vector averaged over the slipping surface.

For a circular dislocation in an elastic rock mass, the mean ride (u_{ave}) can be estimated with the following analytic expression, assuming a constant shear stress drop (Salamon, 1964):

$$U_{ave} = (8 \times [1 - \nu] \times \check{T} \times Ls) / (3\pi \times [1 - (\nu / 2)] \times G) \qquad \text{… Eq. [5]}$$

Where: ν is the Poisson's ratio.

$\check{T}$ is the peak stress drop ($\Delta\tau_{max}$), defined as the largest difference between the static and the dynamic shear strength envelopes encountered in all the numerical elements considered in the analysis (the difference at the highest encountered normal stress magnitude). McGarr (1981) described this peak stress drop as representing the shearing of the "most energetic asperity" along the fault. $\check{T}$ can in turn be used to assess energy release and seismic event magnitude.

L_s is the rupture radius.

G is the shear modulus of the rock mass (equal to $E / [2 \times (1 + \nu)]$, E and ν being the Young's modulus and Poisson's ratio, respectively).

Finally, the following equations can be used to calculate the moment of such an event (Board, 1994):

$$M_o = G \times u_{ave} \times A \qquad \text{… Eq. [6]}$$

Where: M_o is the seismic moment of the event;
G is again the shear modulus of the rock mass;
u_{ave} is the mean ride and,
A is the area of the slipping surface, which can be inferred from the *FLAC3D* model by summing the surface of the elements where the stress drop is positive.

Once the seismic moment M_o has been calculated, the moment magnitude M_W of the event can be estimated with the following equation (Kanamori, 1977):

$$M_W = 2/3\,(\log_{10} M_o) - 6.07 \qquad \text{… Eq. [7]}$$

8.2.2 Methodology

As mentioned, the objective was to evaluate the fault-slip-related seismic potential of the Andesite fault at each modelled step of the mining sequence, as well as the area affected on the fault surface. For this purpose, the model was re-run without considering the fault properties (without the ubiquitous joints), assigning instead the full Andesite mechanical properties to the numerical elements within the Andesite fault volume – this was deemed conservative because it allowed for larger stress drops to occur at failure.

Theoretically, τ_d and τ_s would be extracted for each mesh element on the Andesite fault surface, and the stress drop calculated by subtracting the two. But since very little is reliably known about the fault strength properties (at both the large and small scales, as well as in terms of variability, presence of rock bridges, etc.) and to remain conservative, simplifications were required in the stress drop calculations.

Consequently, τ_s was taken to be equal to the shear stress calculated on the fault surface (as long as the value was higher than τ_d). In other words, no specific static fault strength envelope was considered for this exercise. When the shear stress acting upon a numerical element was above its dynamic shear strength, that element was assumed to have reached its static shear strength at that value. Since the Andesite fault was not explicitly represented in the model, τ_s was only bound by the strength of the rock mass at its location, and the static shear strength could thus readily exceed τ_d. This simplification allowed to simultaneously account in a simplified manner for very weak and very strong fault strength properties.

For this study, the dynamic shear strength was calculated with a dynamic friction angle of 30° and zero cohesion. The maximum of the $\Delta\tau$ values obtained for a "patch" of adjoined slipping numerical elements (discussed in more detail in the next paragraph), was retained as the peak shear stress drop $\check{T}$ for that patch.

To calculate the slip area and associated potential event radius, the stress drop contours were divided into patches, or, less colloquially, “mobilised sectors” defined as connected mesh elements that form a cohesive uninterrupted area that could slip as one entity. An algorithm was devised to automatically define these mobilised sectors based on the connectivity of the mesh elements with a $\Delta\tau$ greater than zero. The radius of a mobilised sector was then approximated as the radius of a circle of equal area.

Mobilised sector extents and areas, equivalent radii, as well as associated $\check{T}$ peak stress drops and M_o event magnitudes were calculated for every simulated mining step.

8.2.3 Results and Observations

When reviewing the analysis results, one should keep in mind the following considerations. The results show the largest expected events based on the numerical modelling results. Stresses (and energy) fluctuate throughout the mine life in the numerical zones where the Andesite fault lies, and can accumulate without being dissipated – however, progressive slippage on the fault, if it occurred as mining progresses, would dissipate some of the energy. In other words, the stress drop analysis results assume that the fault accumulates all the energy without moving until it releases it all at once and produces one single large seismic event. This represents a worst-case scenario, although a plausible one. It should also be noted that the model computed mobilised sectors of potential seismic events after mining in their vicinity was completed – there is always a risk that seismic events will happen later, as mining will have progressed further. Also, the results apply solely to the Andesite fault – any other structure(s) not identified at this point, and not covered by this study, including possible interactions, could potentially produce yet larger events.

The mobilised sectors, which represent areas of slip surfaces, also deserve a few comments. As shown in Eq. [6], A is a multiplier in the seismic moment calculation and, consequently, weighs heavily on the moment magnitude estimates from Eq. [7]. Theoretically, any element with $\Delta\tau > 0$ could potentially slip and be considered as part of a slip surface. However, this results in many elements being selected and, hence, very large mobilised sectors, very large areas A and, ultimately, very large corresponding seismic events.

These very large mobilised sectors also often have geometries that do not form cohesive surfaces that would realistically slip as one entity due to the presence of individual slip areas connected by thin isthmuses of mesh elements with very small $\Delta\tau$ values. Consequently, a critical aspect of the mobilised sectors identification algorithm consists in being able to automatically differentiate between groups of elements that form a cohesive mobilised sector that could credibly slip as a single entity.

To do so, several hypotheses needed to be made on the following aspects:

- ***The Δτ threshold.*** A critical parameter is the Δτ threshold that triggers the selection of a numerical element in the process. As discussed, as that threshold decreases, more numerical elements are tagged as potential slip points, and the area *A* and magnitude of possible associated seismic events increase. Furthermore, and as mentioned, the narrow isthmuses connecting larger coherent slip areas are often made of mesh elements with very small Δτ values. Increasing the Δτ threshold reduces the occurrence of such narrow strips and results in more realistic slip surfaces. Figure 54 illustrates both concepts.

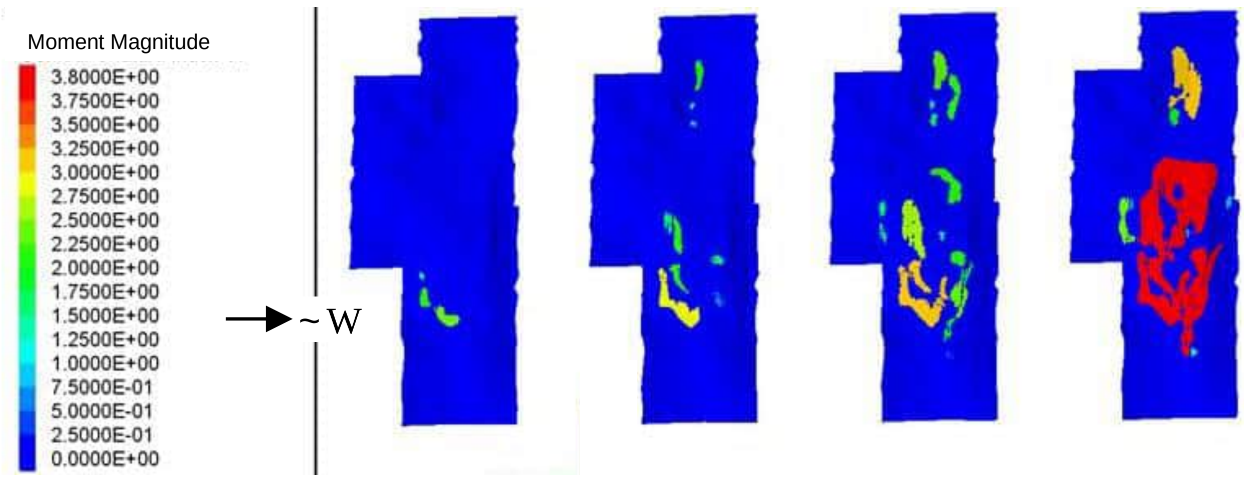

(a) $\Delta\tau \geq 8$ MPa. (b) $\Delta\tau \geq 4$ MPa. (c) $\Delta\tau \geq 2$ MPa. (d) $\Delta\tau > 0$ MPa.

Figure 54. Elevation views looking approximately south, showing mobilised sectors along the Andesite fault, colour-coded by the moment magnitude M_W of the maximum seismic event they can generate, for various Δτ threshold values.

In our case, we settled on a threshold of $\Delta\tau \geq 2$ MPa, which allowed to: 1) eliminate many irrelevant connecting strips; 2) still generate large mobilised sectors, which is conservative since it generates in turn large seismic moments; and, 3) provide lower, perhaps less overestimated event magnitudes than with a threshold of $\Delta\tau \geq 0$ MPa.

- ***The search cell characteristics.*** Mobilised sectors were automatically derived with a moving cell algorithm that searched for numerical elements meeting the Δτ threshold previously discussed. The search cell is an important parameter with several influential settings:
  - ***Its shape:*** in our analysis, that shape was taken to be square.
  - ***Its size:*** a 40 m edge size ended up being retained in our work, which corresponds to 8 numerical elements on the Andesite fault mesh. Several tests were conducted on that pa-

rameter, and 40 m provided the best qualitative compromise between sensitivity, continuity and regular elliptical or rectangular shapes that could credibly slip.

In the absence of historical seismicity to back-analyse against, it was not possible to reliably calibrate these various hypotheses. As a result, once mining-induced seismicity will start to be recorded, they should be revisited and validated, or adjusted.

Figure 55 shows the calculated moment magnitudes M_W from each mobilised sector at mining step 209 (the step associated with the largest moment magnitude event anticipated). Figure 56 shows the largest calculated moment magnitude for each modelled step throughout the life of mine, whereas Figure 57 shows the depth at which the seismic events are expected to occur based on this analysis, again for the life of mine.

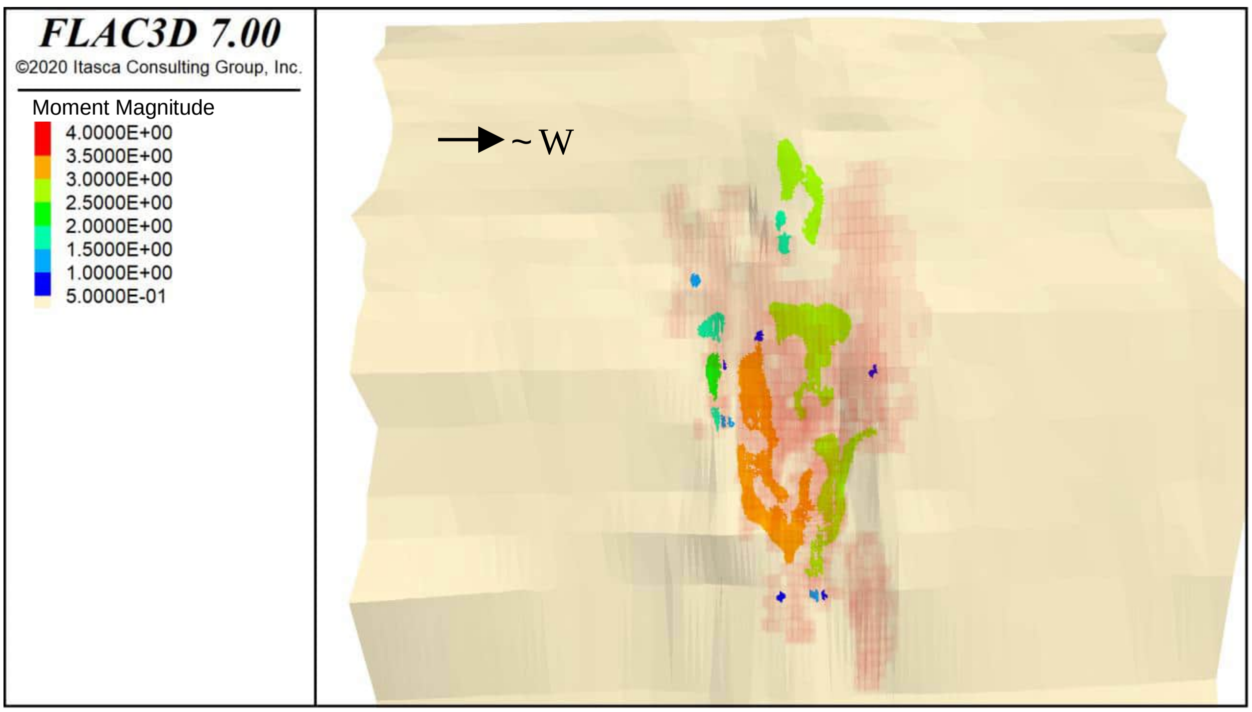

Figure 55 Elevation view looking approximately south showing contours of calculated moment magnitudes M_W from each mobilised sector at Step 209. Stopes are shown in light red in front of the Andesite fault.

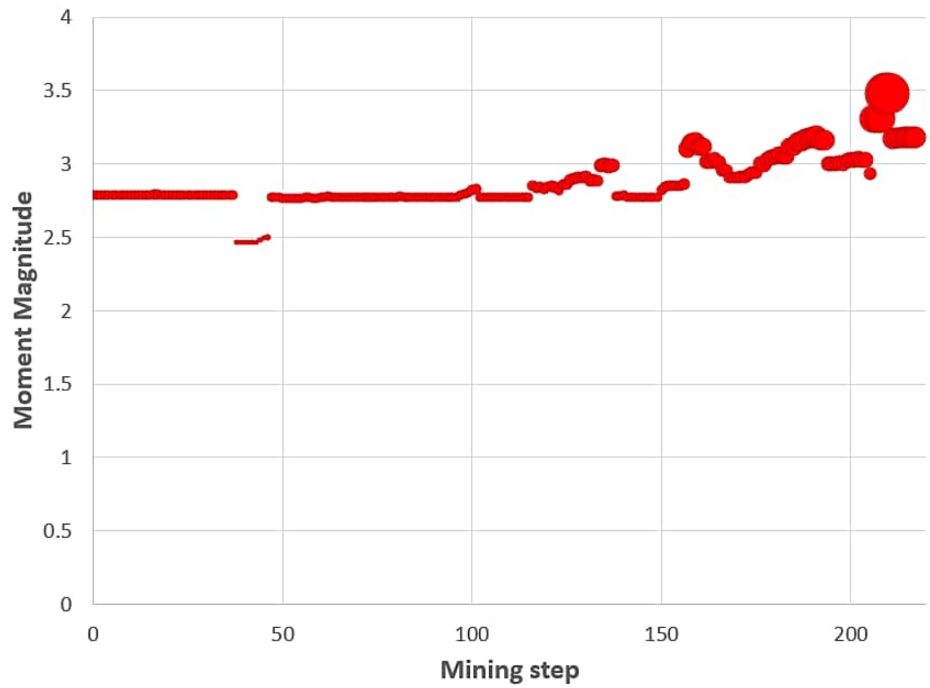

Figure 56. Graph showing the maximum calculated moment magnitude Mw along the Andesite Fault over the life of mine. The size of the circles reflects the magnitude of the events.

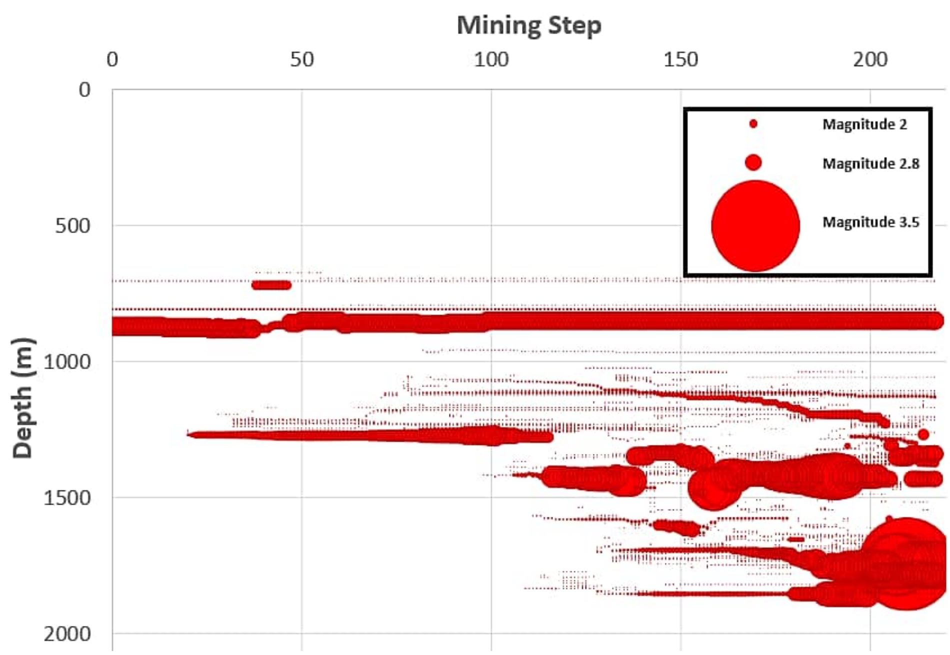

Figure 57. Graph showing the depth of the mobilised sectors (locations where seismic events are expected to occur) along the Andesite Fault over the life of mine. The size of the circles reflects the magnitude of the events.

Based on this analysis, the largest event expected – related to a mobilised sector located at a depth of 1,745 m below surface – would have a moment magnitude of about M_W + 3.5.

The plots also show that a mobilised sector is present along the Andesite fault from the onset of Horne 5 mining, from right after the extraction of the old Horne mine in the model, at a depth of 850 m – this mobilised sector is associated with a maximum seismic event with a calculated moment magnitude M_W of + 2.8. The loading on the fault at that location is attributable to the mining of the old Horne ore body, and it remains mostly unaffected by the mining of the Horne 5 ore body. The potential for this event remains throughout the time period examined, even once mining in the area will have been completed and the local stresses will remain constant.

To help assess the effects of the calculated seismic events on surface infrastructures, including the smelter, vibration peak particle velocity (*PPV*) values were estimated on surface for each mobilised sector, again for the entire mine life. To do so, the following equation, proposed by Kaiser *et al.* (1996), was used:

$$PPV = (C \times 10^{[0.5 \times (M_L + 1.5)]}) / (R + R_o) \qquad \text{… Eq. [7]}$$

Where: *PPV* is the vibration peak particle velocity, in m/s;
C is a constant between 0.2 and 0.3, as recommended for design purposes (0.25 was used for this project);
M_L is the local magnitude (derived with Eq. [9] further down);
R is the distance between the top of the mobilised sector (nearest to surface, to remain conservative) and the ground surface, in metres; and,
R_o is the source radius, in metres, estimated using Eq. [8] below.

To calculate R_o (in metres), one can use:

$$R_o = \alpha \times 10^{[0.33 \times (M_L + 1.5)]} \qquad \text{… Eq. [8]}$$

Where: α is a constant between 0.53 and 1.14 (0.84 was used for this project); and,
M_L is the local magnitude of the event, as in Eq. [7].

The local magnitude M_L was itself derived from the seismic moment M_o as follows:

$$M_L = \log_{10} M_o - (1.5 \pm 0.15) \qquad \text{… Eq. [9]}$$

With M_o expressed in GN.m (after Kaiser *et al.*, 1996).

Figure 58 shows the calculated *PPV* values (in mm/s) anticipated on the ground surface from the various mobilised sectors at mining step 209. For example, the largest seismic event from a mobilised sector shaded in yellow would be expected, based on Eq. [7], to produce on surface a peak vibration amplitude of around 75 mm/s.

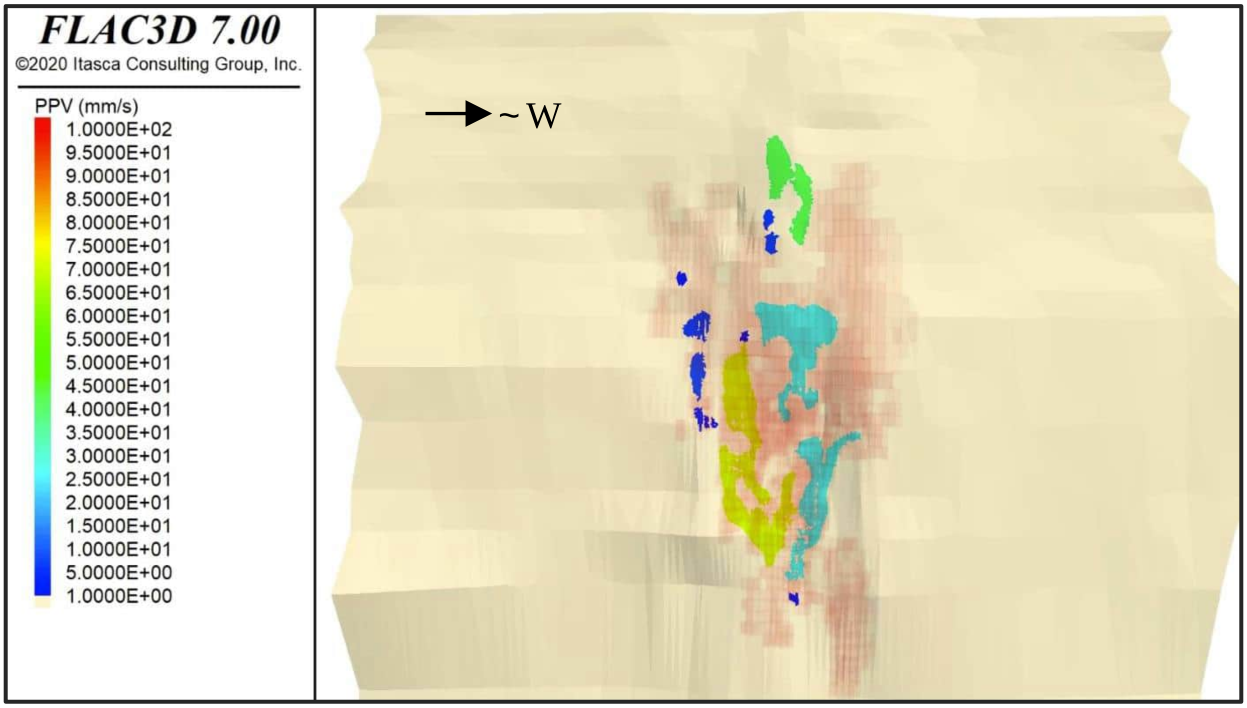

Figure 58. Elevation view looking approximately south showing contours of calculated *PPV* values (in mm/s) expected on the ground surface from each mobilised sector at Step 209. Stopes are shown in light red in front of the Andesite fault.

Figure 59 next page is a graph showing the highest expected *PPV* values (again in mm/s) on surface at each mining step. It shows that the highest expected *PPV* value occurred at Step 209 with a value of 70 mm/s. This was generated by a seismic event computed from a mobilised sector located 1,745 m below surface, with a calculated moment magnitude of M_W + 3.5 (the strongest seismic event expected along the Andesite fault, based on the results of the numerical stress drop analyses).

8.2.4 Mitigation

A coalescence of events around solicited lock-up points along faults would normally appear in the seismic data, which would give advanced warning and allow for mitigating measures to be put in place. Mitigation measures could include a change of extraction sequence, a mining rate adjustment, additional ground support, destressing measures, etc. This is important and should be noted in mining plans, and sensitivity studies should be conducted around these mitigation measures.

The aim would be to have these measures already planned and ready to deploy in the event that increased seismicity was detected, so they could be implemented without delay.

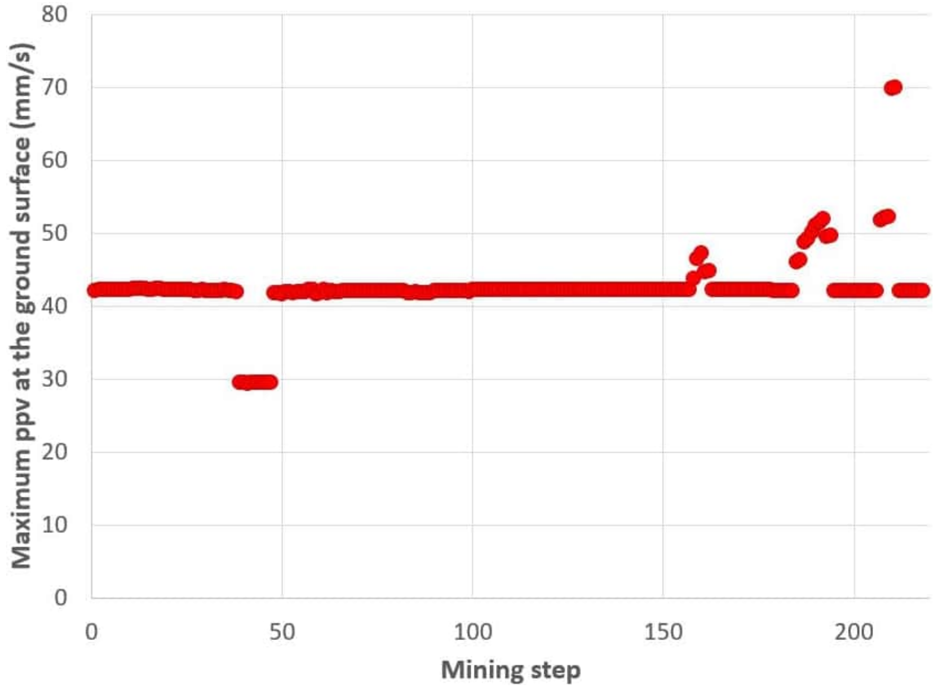

Figure 59. Graph showing the maximum calculated *PPV* values (in mm/s) expected on surface over the life of mine.

9. LIMITATIONS

In reviewing the conclusions presented in this report, the following limitations must be kept in mind:

- The *FLAC3D* model and geomechanical risk assessment presented were not calibrated on any field data. This is due to the absence of relevant data to conduct back-analyses.
- The lack of calibration data affects, amongst other aspects, the thresholds fixed between risk categories (*Low*, *Moderate*, *High*). Once field data will become available, these thresholds may be reviewed. However, the tendencies observed on the risk profiles are reliable.
- The in-situ stress regime implemented in the *FLAC3D* model was chosen from the literature, based on regional measurements. No in-situ stress measurements have been conducted at the Horne 5 site to confirm the validity of the selected in-situ stress characteristics. The orientation of this stress field is of particular importance as it controls where stress increases and relaxations can be expected to occur.
- Residual mechanical properties, as well as critical plastic strains (the cumulative volumetric plastic strains at which residual properties are reached for the various rock units) can have a significant effect on the results. Those were fixed by Golder during the FS, based on observations that suggested a very hard and brittle rock mass behaviour. Note also that mechanical properties were considered constant throughout each lithological unit (no strength variations were considered within lithologies).
- To limit computational time, as well as the storage of the model save files, ten (10) stopes were mined at each successive modelling step. Therefore, the seismic potency and the dilution analyses for each modelling step consider ten stopes together, which can have the effect of "diluting" peaks in the risk profiles obtained. For the mining conditions assessment (mining under high stresses and mining under residual conditions), it was possible to evaluate stopes individually, but it should still be kept in mind that the stresses and plasticity states in the model resulted from the simultaneous mining of ten stopes (and not only one). For the detailed engineering design phase, the model could be refined in such a way to mine one stope per modelling steps, and particularly for time periods where significant changes occur at successive ten-stope steps.
- *FLAC3D* being a continuum formulation, structurally controlled instabilities and failures along discontinuities were not systematically considered.
- The location and geometry of the Andesite fault considered in the ESS analyses were based upon interpreted drilling results.
- The geometry of the major infrastructures was not explicitly modelled in *FLAC3D*. Therefore, the stress paths at the infrastructure locations do not consider the effects (e.g., stress redistributions) due to the actual presence of these excavations.

- No dynamic effects, from blast-induced vibrations for example, were considered.
- No water effects (e.g., pore pressures) were considered.
- A2GC did not visit the site within the context of these analyses. All the input data used in this project were entirely supplied to A2GC by Osisko Gold Royalties / Falco Resources.

10. RECOMMENDATIONS

In closing, the following recommendations are given:

- As underground developments will progress prior to starting production at Horne 5, stress measurements should be conducted. Should the stress regime differ significantly from the one assumed, the effect on the risk profile should be re-examined.
- As mining will start at Horne 5 and the seismic monitoring system is deployed, the risk ratings should be reviewed and possibly adjusted.
- The structural model should be kept up to date, based on further diamond drilling, as well as underground mapping and observations. Advanced knowledge of the presence of large-scale discontinuities is of paramount importance when mining at depth under high stress conditions.
- The Horne 5 project has several characteristics that increase the geomechanical risk it is associated with: it is deep (and, hence, will be subjected to high stress levels), its geological settings are expected to be stiff, strong and brittle (a combination that leads to seismic conditions), and its upper part will lie in close proximity to the large historical Horne mine. It targets high production levels, which, with the mining method retained, require large longhole stopes and multiple mining fronts (and the associated diminishing sill pillars between mining fronts). Being located in the City of Rouyn-Noranda, it also has numerous neighbours. All these aspects were considered in the geomechanical analyses.

  Still, close monitoring, including with a sufficiently sensitive seismic monitoring array, should be conducted right from the beginning of construction and throughout mining to verify that the stress analyses are reliable, and confirm that mining is proceeding as expected. The cause(s) of significant divergence between field observations and modelling-based expectations, if any, should be promptly investigated. Such divergence can have many causes, such as incorrect far-field stress assumptions, incorrect mechanical properties, the presence of geological horizons and structures that were not included in the model, differences between the sequence implemented and the one modelled, differences between the stope dimensions and geometry vs those modelled, and more. Once the causes of the discrepancies are identified and corrected, the model can be rerun to produce adjusted risk profiles and production "road maps."

We trust this report meets your needs and expectations. Please do not hesitate to contact us if you have questions or require more details on some of the topics discussed in this document.

Sincerely,

Amélie C. Ouellet, M.A.Sc., Eng. §
Project Engineer
E-mail: amelie@a2gc.ca
Mobile: (int.) +1-514-266-0689

Thierry Lavoie, M.A.Sc., Eng.
Principal Engineer
E-mail: thierry@a2gc.ca
Mobile: (int.) +1-418-998-3146

Nicolas St-Onge, Eng., P.Eng.
Senior Engineer
E-mail: nicolas@a2gc.ca
Mobile: (int.) +1-514-293-1623

André-Michel Maheux, Eng.
Project Engineer
E-mail: andre-michel@a2gc.ca
Mobile: (int.) +1-581-998-4420

Patrick Andrieux, Ph.D., Eng., P.Eng.
PEO Designated Consulting Engineer
Principal Engineer
E-mail: patrick@a2gc.ca
Mobile: (int.) +1-514-953-2773

ANDRIEUX & ASSOCIATES GEOMECHANICS CONSULTING, L.P.
81 De Brésoles Street, Suite 309
Montreal, Quebec, H2Y 0A1, Canada.
Tel.: (int.) +1-514-379-1789
info@a2gc.ca
www.a2gc.ca

© 2021

§: *principal corresponding author.*

Notes:

3DEC, *FISH*, *FLAC*, *FLAC3D*, and *PFC3D* are registered trademarks of Itasca Consulting Group, Inc., Minneapolis, MN, USA.

Rhino is a registered trademark of McNeel North America, Inc., Seattle, WA, USA.

Internal Review

The draft version of this document was internally reviewed in Quebec City, Quebec, on 28 November 2020 as per the established A2GC quality assurance / quality control program. Its content has been found to meet the A2GC quality guidelines for technical documentation.

Sebastien Guido, M.Sc., Eng.
Project Engineer
E-mail: sebastien@a2gc.ca
Mobile: (int.) +1-418-905-1789

11. REFERENCES

Andrieux, P. (2020). *Potential Horne 5 Mining-Induced Seismic Tremors on Surface.* Technical memorandum from Andrieux and Associates Geomechanics Consulting, L.P. to Osisko Gold Royalties, Ltd., Falco Resources, Ltd., Horne 5 Project, ref. No 2158-HOR-002-20200709-F, 11 p. Montreal, QC, Canada. (09 July.)

Ben-Menahem, A., and S. Singh (1981). *Seismic Waves and Sources.* Published by Springer-Verlag, 1127 pp. New York, NY, USA.

Bewick, R. (2017). *Seismicity.* Presentation by Golder Associates, Inc. to Osisko Gold Royalties, Ltd., in preparation for the Horne 5 Feasibility Study external peer review, 7 slides. Sudbury, ON, Canada. (08 June.)

Bewick, R., A. Ouellet, S. Otto, and D. Gaudreau (2017). *Importance of Understanding Laboratory Strength and Modulus Testing Data for Deep Mining in Hard Brittle Rocks*. Proceedings of the 8th International Conference on Deep and High Stress Mining, Perth, Australia, pp. 827-842. Australian Centre for Geomechanics: Perth, WA, Australia.

Board, M. (1994). *Numerical Examination of Mining-Induced Seismicity*. Doctoral thesis, University of Minnesota, Department of Civil, Environmental and Geo-Engineering, 255 pp. Minneapolis, MN, USA.

Board, M., R. Brummer, and S. Seldon (2001). *Use of Numerical Modeling for Mine Design Evaluation.* In "Underground Mining Methods – Engineering Fundamentals and International Case Studies," Handbook of the Society of Mining Engineers (W. Hustrulid and R. Bullock, Eds.), Chapter 58, pp. 483-491. Published by the American Institute of Mining and Exploration. Littleton, CO, USA.

Cotesta, L., C. O'Connor, R. Brummer, and A. Punkkinen (2014). *Numerical Modelling and Scientific Visualisation – Integration of Geomechanics into Modern Mine Designs*. Proceedings of the 2014 Deep and High Stress Mining conference, Sudbury, Canada, pp. 377-395. Australian Centre for Geomechanics: Perth, WA, Australia.

Falco Resources, Ltd. (2017). *Feasibility Study – Horne 5 Gold Project.* NI 43-101 Technical report, 1000 pp. Rouyn-Noranda, QC, Canada. (05 October.)

Golder Associates, Ltd. (2016). *Horne 5 Feasibility Study – Intact Rock Strength Testing.* Technical report from Golder Associates, Ltd. to Osisko Gold Royalties, Ltd., Falco Resources, Ltd., Horne 5 Project, ref. No GAL101-1541337-21130-TM-H5FS-Rev0, 17 pp. Montreal, QC, Canada. (24 August.)

Golder Associates (2017a). *Horne 5 Feasibility Study – Modelling Basis for Rock Mechanics Assessment.* Technical report from Golder Associates, Ltd. to Osisko Gold Royalties, Ltd., Falco Resources, Ltd., Horne 5 Project, ref. No GAL002-1774165-Rev0, 23 pp. Montreal, QC, Canada. (17 November.)

Golder Associates (2017b). *Horne 5 Feasibility Study – Geotechnical Paste Backfill Strength Recommendations*. Technical report from Golder Associates, Ltd. to Osisko Gold Royalties, Ltd., Falco Resources, Ltd., Horne 5 Project, ref. No GAL010-1774165-2100-TM-Rev0, 4 pp. Montreal, QC, Canada. (20 November.)

Golder Associates (2017c). *Horne 5 FS – Characterization of Interpreted Primary and Secondary Faults*. Technical report from Golder Associates, Ltd. to Osisko Gold Royalties, Ltd., Falco Resources, Ltd., Horne 5 Project, ref. No GAL012-1774165-2100-TM-Rev0, 10 pp. Montreal, QC, Canada. (17 November.)

Itasca (2019). FLAC3D *Version 7.00 – Theory and Background.* Published by Itasca Consulting Group, Inc., 176 pp. Minneapolis, MN, USA.

Itasca (2017). FLAC *Version 8.00 – Theory and Background.* Published by Itasca Consulting Group, Inc., 304 pp. Minneapolis, MN, USA.

Kaiser, P., D. Morrison, G. Swan, M. Neumann, V. Kazakadis, and S. Talebi (1996). *Rockburst Research Handbook.* Published by the Mining Research Directorate, 976 pp. Sudbury, ON, Canada.

Kaiser, P., M. Diederichs, C. Martin, J. Sharp, and W. Steiner (2000). *Underground Works in Hard Rock Tunneling and Mining*. Proceedings of the International Conference on Geotechnical and Geological Engineering, Invited Papers, Vol. 1, pp. 841-926. Melbourne, VIC, Australia.

Kanamori, H. (1977). *The Energy Release in Great Earthquakes.* Journal of Geophysics Research, American Geophysical Union, Vol. 82 (20), pp. 2981-2987. Washington, DC, USA.

King, G. (1978). *Geological Faults, Fractures, Creep and Strain*. Philosophical Transactions of the Royal Society of London. Series A, Mathematical and Physical Sciences, 288(1350), pp. 197-212. London, U.K.

McGarr, A. (1981). *Analysis of Peak Ground Motion in Terms of a Model of Inhomogeneous Faulting.* Journal of Geophysical Research, Vol. 86 (B5), pp. 3901-3912. Washington, DC, USA.

Maloney, S., and S. Yong (2006). *A Re-Assessment of In Situ Stresses in the Canadian Shield*. American Rock Mechanics Association, ARMA/URMS 06-1096, 9 pp.

Ryder, J. (1987). *Excess Shear Stress (ESS): An Engineering Criterion for Assessing Unstable Slip and Associated Rockburst Hazards*. Proceedings of the 6th ISRM Congress, pp.1211-1214. Rotterdam: A.A. Balkema.

Ryder, J. (1988). *Excess Shear Stress in the Assessment of Geologically Hazardous Situations.* Journal of the South African Institute of Mining and Metallurgy, Vol. 88, Issue 1, pp. 27-39. Johannesburg, South Africa. (January.)

Salamon, M. (1964). *Elastic Analysis of Displacements and Stresses Induced by Mining of Seam or Reef Deposits – Part I, Inclined Reefs.* Journal of the South African Institute of Mining and Metallurgy, Vol. 65, Issue 5, pp. 319-338. Johannesburg, South Africa. (December.)

MASTER

Report of Investigations 8507

Structure Response and Damage Produced by Ground Vibration From Surface Mine Blasting

By D. E. Siskind, M. S. Stagg, J. W. Kopp,
and C. H. Dowding

UNITED STATES DEPARTMENT

Cecil D. Andrus, Secretary

BUREAU OF MINES

Lindsay D. Norman, Director

US Department of Interior

Office of Surface Mining

Reclamation and Enforcement

Kenneth K. Eltschlager

Mining/Blasting Engineer

3 Parkway Center

Pittsburgh, PA 15220

Phone 412.937.2169

Fax 412.937.3012

Keltschl@osmre.gov

This publication has been cataloged as follows:

United States. Bureau of Mines
Structure response and damage produced by ground vibration from surface mine blasting.

(Report of investigations • Bureau of Mines ; 8507)

Bibliography: p. 69-70.

1. Blast effect. 2. Buildings–Vibration. 3. Soils–Vibration. 4. Strip mining–Environmental aspects. I. Siskind, D. E. II. Title. III. Series: United States. Bureau of Mines. Report of investigations ; 8507.

TN23.U43 [TA654.7] 622s [690'.21] 80-607825

CONTENTS

ILLUSTRATIONS

ILLUSTRATIONS—Continued

TABLES

STRUCTURE RESPONSE AND DAMAGE PRODUCED BY GROUND VIBRATION FROM SURFACE MINE BLASTING

by

D. E. Siskind[1], M.S. Stagg[2], J. W. Kopp[3], and C. H. Dowding[4]

ABSTRACT

The Bureau of Mines studied blast-produced ground vibration from surface mining to assess its damage and annoyance potential, and to determine safe levels and appropriate measurement techniques. Direct measurements were made of ground-vibration-produced structure responses and damage in 76 homes for 219 production blasts. These results were combined with damage data from nine other blasting studies, including the three analyzed previously for Bureau of Mines Bulletin 656.

SAFE ~~Save~~ levels of ground vibration from blasting range from 0.5 to 2.0 in/sec peak particle velocity for residential-type structures. The damage threshold values are functions of the frequencies of the vibration transmitted into the residences and the types of construction. Particularly serious are the low-frequency vibrations that exist in soft foundation materials and/or result from long blast-to-residence distances. These vibrations produce not only structure resonances (4 to 12 Hz for whole structures and 10 to 25 Hz for midwalls) but also excessive levels of displacement and strain.

Threshold damage was defined as the occurrence of cosmetic damage; that is, the most superficial interior cracking of the type that develops in all homes independent of blasting. Homes with plastered interior walls are more susceptible to blast-produced cracking then modern gypsum wallboard; the latter are adequately protected by a minimum particle velocity of approximately 0.75 in/sec for frequencies below 40 Hz.

Structure response amplification factors were measured; typical values were 1.5 for structures as a whole (racking) and 4 for midwalls, at their respective resonance frequencies. For blast vibrations above 40 Hz, all amplification factors for frame residential structures were less than unity.

The human response and annoyance problem from ground vibration is aggravated by wall rattling, secondary noises, and the presence of airblast. Approximately 5 to 10 pct of the neighbors will judge peak particle velocity levels of 0.5 to 0.75 in/sec as "less than acceptable" (i.e., unacceptable) based on direct reactions to the vibration. Even lower levels cause psychological response problems, and thus social, economic, and public relations factors become critical for continued blasting.

[1] Geophysicist, Twin Cities Research Center, Bureau of Mines, Twin Cities, Minn.
[2] Civil engineer, Twin Cities Research Center, Bureau of Mines, Twin Cities, Minn.
[3] Mining engineer, Twin Cities Research Center, Bureau of Mines, Twin Cities, Minn.
[4] Civil engineer; Professor of Civil Engineering, Northwestern University, Evanston, Ill.

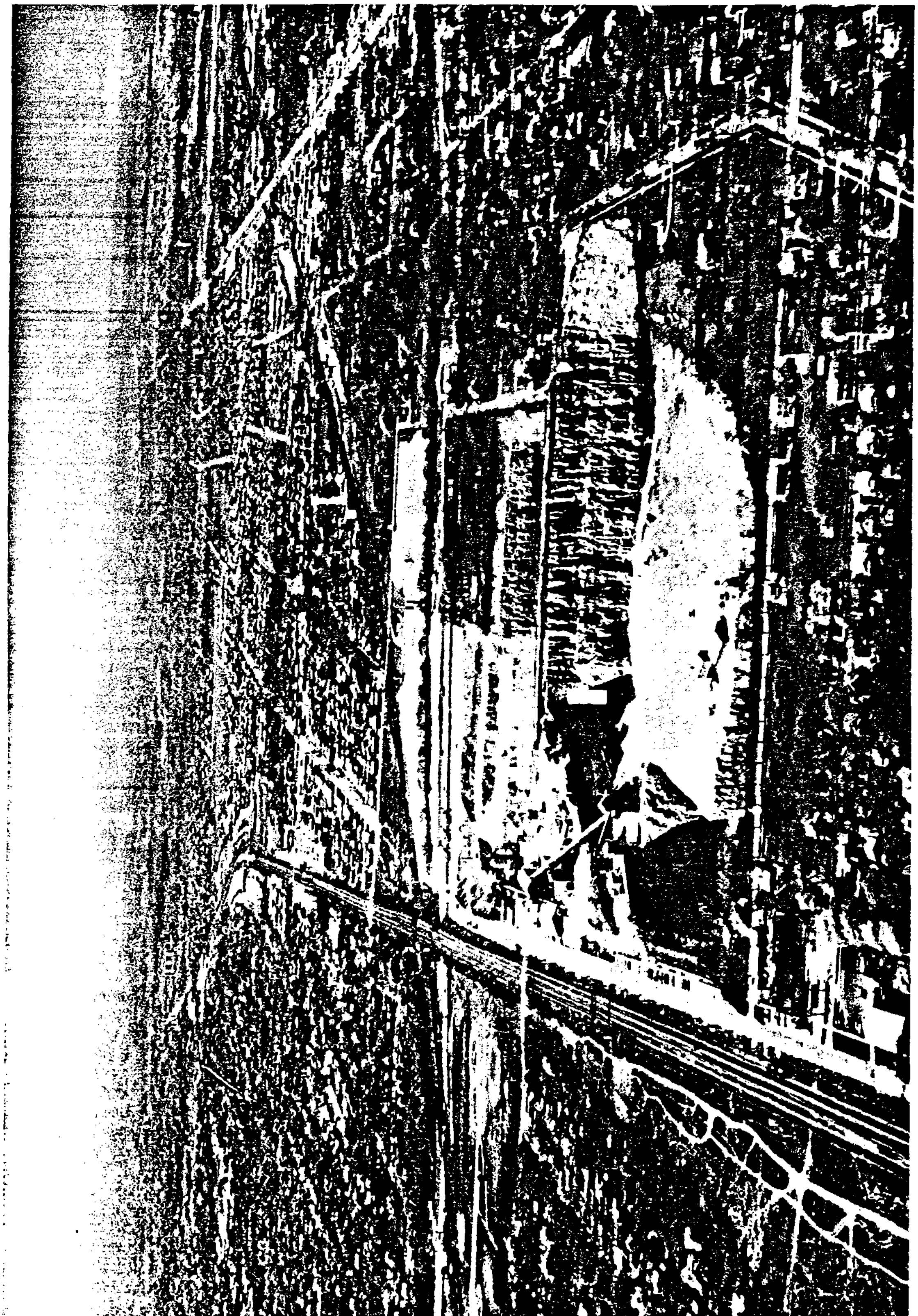

Figure 1.—Occupied residences near operating surface mine.

INTRODUCTION

Gound vibrations from blasting have been a continual problem for the mining industry, the public living near the mining operations, and the regulatory agencies responsible for setting environmental standards. Since 1930, the Bureau of Mines has studied various aspects of ground vibration, airblast, and instrumentation, culminating in Bulletin 656 in 1971(*37*)[5].

In that publication, Nicholls extensively reviewed blast design effects on the generation of vibrations, ground vibration and airblast propagation, and seismic instrumentation. Bulletin 656 established the use of peak particle velocity in place of displacement, a minimum delay interval of 9 msec for scaled distance calculations, and a safe scaled distance design parameter of 50 $ft/lb^{1/2}$ for quarry blasting in the absence of vibration monitoring. The authors also included a damage summary analysis originally published in 1962 by Duvall and Fogelson as Bureau of Mines Report of Investigations 5968 (*14*). New data available since the 1962 report were described in Bulletin 656, but a new analysis to include these data was not performed.

Recommended was the use of peak particle velocity to assess the damage potential of the ground vibrations, and 2.0 in/sec as an overall safe level for residential structures. These recommendations have been widely adopted by the mining and construction industry and incorporated into numerous State and local ordinances that regulate blasting activity. Soon after publication of the 2.0-in/sec safe level criterion, it became apparent that it was not practical to blast at this high vibration level. Many mining operations with nearby neighbors were designing their blasts to keep velocities as low as 0.40 in/sec. Severe house rattling caused fear of property damage below the 2.0-in/sec level, and many homeowners were attributing all cracks to the blast vibrations.

Pennsylvania was the first State to adopt the 2.0-in/sec peak particle velocity criterion as a safe standard in 1957. However, in 1974 it was forced to adopt stricter controls because of citizen pressure and lawsuits involving both annoyance and alleged damage to residences. There existed no technologically based and supportable criteria for mine, quarry, and construction blasting other than the 2.0-in/sec criteria from Bulletin 656 and RI 5968. The general growth of mining, the proximity of mining and quarrying to their residential neighbors, and greater environmental awareness have all required reexamination of blasting regulations and justified further research.

In 1974 the Bureau of Mines began to reanalyze the blast damage problem, expand the Duvall and Fogelson 1962 study, and overcome its more serious shortcomings through the following efforts:

1. Direct measurements were made of structural response, and damage was observed in residences from actual surface-mine production blasting.
2. Damage data from six additional studies, not available in 1962, were combined with three studies analyzed by Duvall and Fogelson, plus the new Bureau of Mines measurements.
3. Probabilistic analysis techniques were used on various sets of data, as well as the conventional statistical derivation of mean square fit and standard deviation for the various damage thresholds.
4. Particular emphasis was placed on the frequency dependence of structure response and damage, recognizing that the response characteristics and frequency content of the vibrations are critical to response levels and damage probabilities.
5. An analysis was made of various studies of human tolerance to vibrations, although most data are from steady-state rather than impulsive sources.

Italic

[5] ~~Underlined~~ numbers in parentheses refer to items in the list of references preceding the appendixes.

An understanding of how houses respond to ground vibration and the vibration characteristics most closely related to this response will enable operators to design blasts to minimize adverse effects. The mining industry needs realistic design levels and also practical techniques to attain these levels. At the same time, environmental control agencies responsible for blasting and explosives need reasonable, appropriate, and technologically established and supportable criteria on which to base their regulations. Finally, neighbors around the mining operations and other blasting, as shown in figure 1, require protection of their property and health so that they do not bear an unreasonable personal cost.

This report summarizes the state of knowledge on damage to residences from surface mine, quarry, and construction blasting. Included are discussions of applicable data on fatigue and human response, although work is continuing in these areas. An analysis was also made on vibration production from mining blasts. The generation and propagation data in Bulletin 656 are for smaller quarry blasts, which are also typically characterized by thin overburden layers.

The damage criteria presented herein were developed to quantify the response of and damage to residential-type structures from small to intermediate-sized blasts as used in mining, quarrying, construction, and excavation. Application of these criteria by regulatory agencies will require an analysis of social and economic costs and benefits for the coexistence of blasting and an enviromentally conscious society.

ACKNOWLEDGMENTS

The authors acknowledge the generous assistance of many regulatory agencies, engineering consultants, powder companies, homeowners, and mine and quarry operators. Special thanks are due to the Pennsylvania Department of Environmental Resources for demonstrating the need for this ground vibration research. Much of the fieldwork and data reduction was done by Virgil J. Stachura, Alvin J. Engler, Steven J. Sampson, Michael P. Sethna, Bryan W. Huber, Eric Porcher, and John P. Podolinski. Valuable technical support was provided by G. Robert Vandenbos for all stages of the blasting research.

GROUND VIBRATION CHARACTERISTICS

Ground vibrations from blasting are an undesirable side product of the use of explosives to fragment rock for mining, quarrying, excavation, and construction. This ground vibration or seismic energy is usually described as a time-varying displacement, velocity, or acceleration of a particular point (particle) in the ground. It can also be measured as various integrated (averaged) energy levels. Three mutually orthogonal time-synchronized components are required to characterize the motion fully. Alternatively, the three components can be combined into a true vector sum for any instant in time or a pseudo vector sum derived from vector addition of the maximums of each component, independent of time (*50*).

The descriptors for motion are related by integration and differentiation:

$$V = \frac{d}{dt} D = \int A dt.$$

$$\text{and } A = \frac{d}{dt} V = \frac{d^2}{dt^2} D$$

where D is displacement, V is velocity, and A is acceleration. When the vibrations can be approximated by a sine wave (simple harmonic motion), the relationships above become:

$$\begin{aligned} D &= D_0 \sin(2\pi ft), \\ V &= D_0 (2\pi ft)\cos(2\pi ft) = V_0\cos(2\pi ft), \\ \text{and } A &= -D_0(2\pi ft)^2\sin(2\pi ft) \\ &= -A_0\sin(2\pi ft). \end{aligned}$$

where f is frequency, t is time, and, D_0, V_0, and A_0 are constants. Peak values correspond to the time when the trigonometric functions equal unity, and the relationships for these peaks values then become:

$$\begin{aligned} D_0 &= \frac{V_0}{2\pi f} = \frac{A_0}{(2\pi f)^2} \\ V_0 &= 2\pi f D_0 = \frac{A_0}{2\pi f} \\ \text{and } A_0 &= (2\pi f)^2 D_0 = 2\pi f V_0 \end{aligned}$$

Complex vibrations cannot be approximated by the simple harmonic motion, and either electronic or numeric (computer) integration and differentiation become necessary for conversions.

Interactions between the vibrations and the propagating media give rise to several types of waves, including direct compressional and shear body waves, refracted body waves, and both horizontally and vertically polarized surface waves. These vibrational waves are of primary importance in studies of the earth's interior and earthquake characteristics, but their individual effects have been totally neglected in blasting seismology. Analysis of damage to structures does not require knowledge of what happens between the source and the receiver or of the type of wave. It requires only the vibrational input to the house at its foundation. Additionally, multiply-delayed shots are sufficiently complex vibration sources to make identification of individual waves difficult, if not impossible, under most conditions.

TIME AND FREQUENCY PROPERTIES OF MINING BLASTS

The amplitude, frequencies, and durations of the ground vibrations change as they propagate, because of (a) interactions with various geologic media and structural interfaces, (b) spreading out the wave-train through dispersion, and/or (c) absorption, which is greater for the higher frequencies. Close to the blast the vibration character is affected by factors of blast design and mine geometry, particularly charge weight per delay, delay interval, and to some extent direction of initiation, burden, and spacing (*56*). At large distances the factors of blast design become less critical and the transmitting medium of rock and soil overburden dominate the wave characteristics.

Particle velocity amplitudes are approximately maintained as the seismic energy travels from one material into another (i.e., rock to soil), probably from conservation of energy. However, the vibration frequency and consequently the displacement and acceleration amplitudes depend strongly on the propagating media. Thick soil overburden as well as long absolute (as opposed to scaled) distances create long-duration, low-frequency wave trains. This increases the response and damage potential of nearby structures.

Frequencies below 10 Hz produce large ground displacement and high levels of strain, and also couple very efficiently into structures where typical resonant frequencies are 4 to 12 Hz for the corner or racking motions. Racking is whole-structure distortion with characteristic shear stresses and failures. Previous studies described the frequency character of vibration from quarry (*37*) and coal mine blasts (*56*), and a recent report by Stagg on instrumentation for ground vibration summarized the frequency characteristics of vibrations from small to moderate-sized blast sources (*50*). Ground vibration frequencies from three types of blasts are shown in figure 2, all measured at the closest residence where peak particle velocities were within 0.5 to 2.0 in/sec. Although the shot types in figure 2 are labeled coal mine, quarry, and construction, the frequency-determining factors are the shot sizes, distances, and rock competence. The coal mine and quarry blasts were all more than 200 lb/delay at distances exceeding 350 ft. The construction (and excavation) shots ranged from 1¼ to 12¾ lb at distances of 30 to 160 ft. Soil overburdens were 0 to 5 ft for construction, under 10 ft for quarries, and generally above 5 to 10 ft for coal mines.

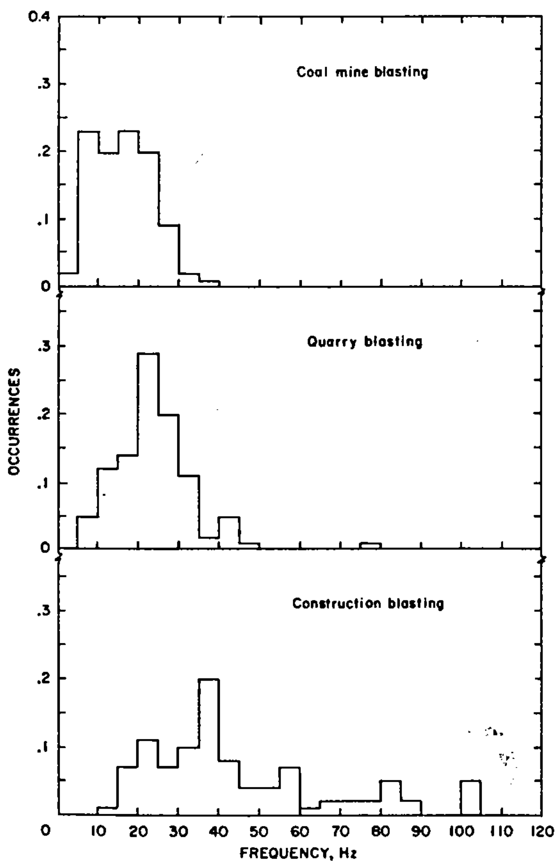

Figure 2.—Predominant frequencies of vibrations from coal mine, quarry, and construction blasting.

Time histories and Fourier frequency amplitude spectra from three typical blasts measured by a buried three-component transducer are shown in figures 3 to 5 (*50*). The coal mine shot is characterized by a trailing large-amplitude, low-frequency wave, which is probably a surface wave generated in the overburden layers. Quarry blasts do not usually show this low-frequency tail for one or more of the following reasons: smaller charge weights, smaller shot to instrument distances, and thinner soil overburdens. The combination of large shots, thick soil and sedimentary rock overburdens, relatively good confinement, and long-range propagation make coal mine blast vibrations potentially more serious than quarry and construction blasts because of their low frequencies. By contrast, coal mine highwall blasts are inefficient generators of airblast (*46*). Hard rock construction and excavation blasts tend to be shorter in duration and contain higher frequency motions than those of either coal mine or quarry.

Frequency characteristics of blast vibrations depend strongly on the geology and blast delay intervals. Except for the short-distance, all-rock case, they are difficult to predict and vary widely. Therefore, it is desirable to obtain complete time histories rather than simple peak values in any sensitive areas. Many examples of continual complaints about severe rattling at levels below 0.5 in/sec are attributable to the low frequencies. Research is continuing on the effects of blast design, face orientation, and near-surface geology on the character of both the ground vibrations and airblast.

OTHER VIBRATION SOURCES

Earthquakes, nuclear blasts, and very large scale, in situ mining shots all produce potentially damaging ground vibrations, as well as do other static and quasistatic vibration sources (traffic, pile driving, sonic booms, etc.). The first Bureau of Mines blast vibration summary in 1942 examined the levels of earthquake vibrations and the corresponding Mercalli intensities for damage, and concluded these did not apply to blasting (*51*). Earthquakes produce long-duration and very low frequency events.

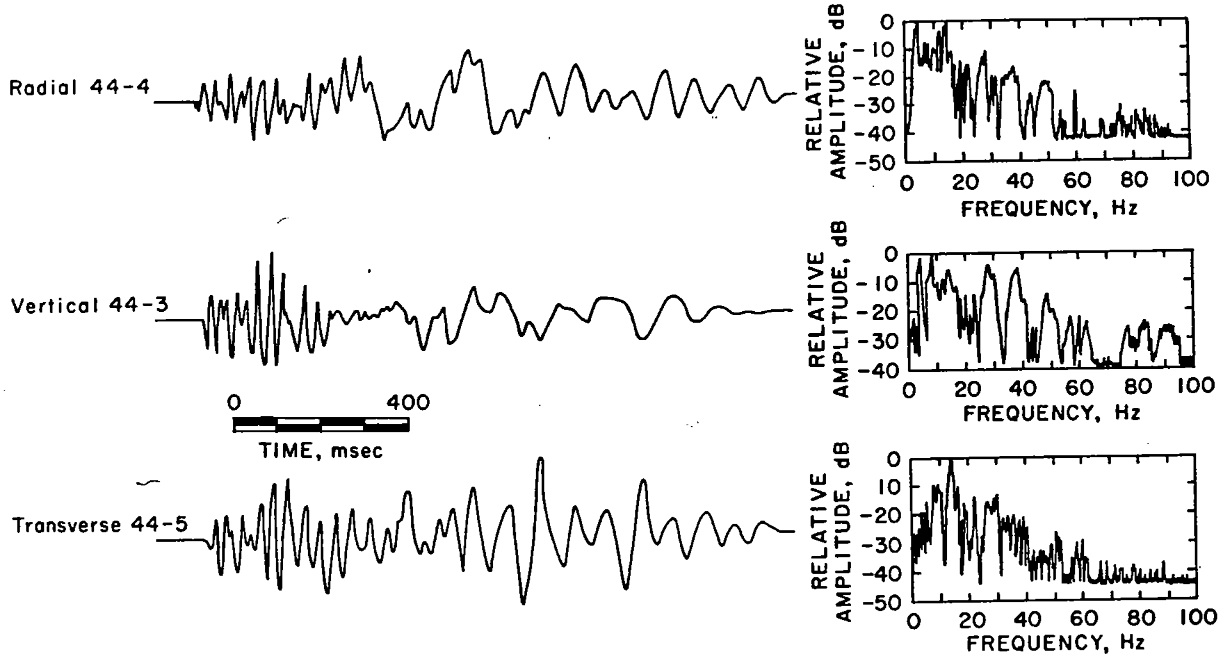

Figure 3.—Coal mine blast time histories and spectra measured at 2,287 ft.

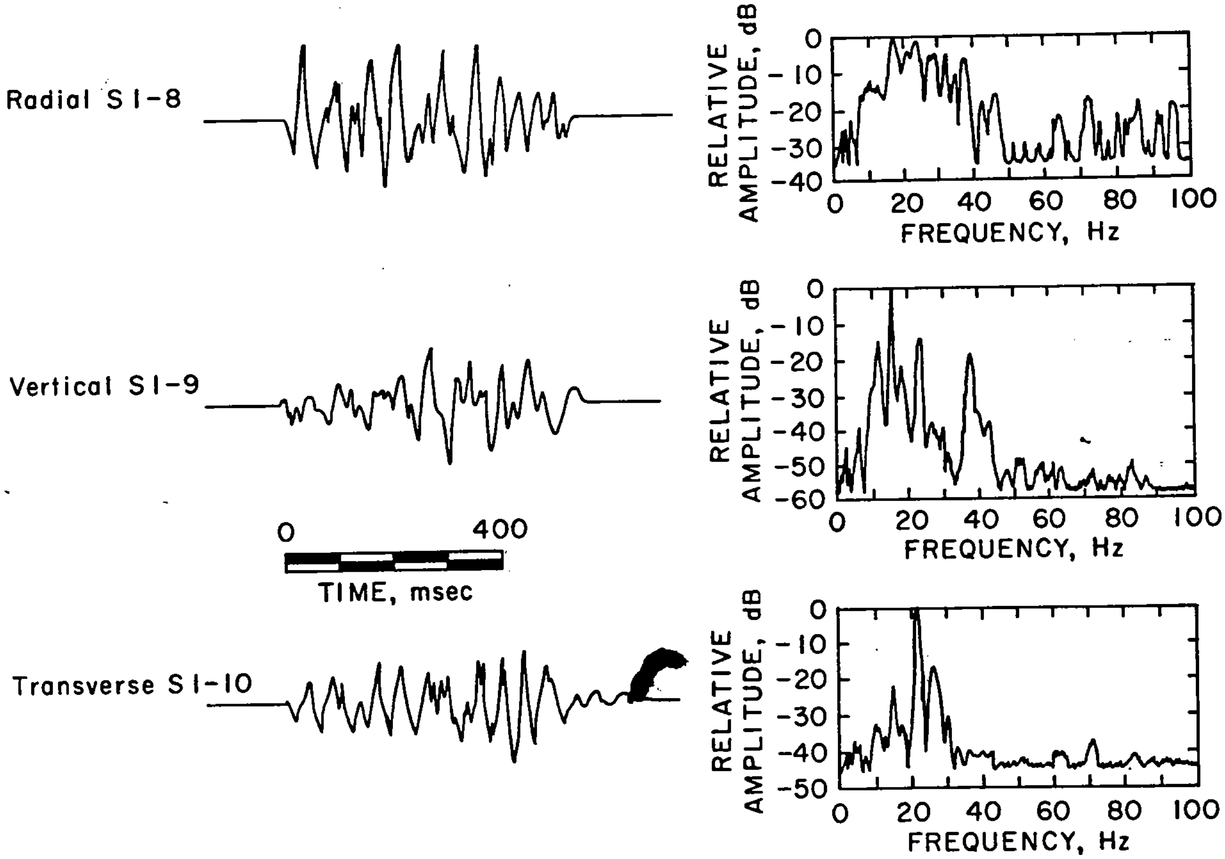

Figure 4.—Quarry blast time histories and spectra measured at 540 ft.

Acceleration levels are typically used by seismologists to quantify damage potential. These may be of moderate and even lower levels than found in blasting; however, their low frequencies produce large particle velocities and enormous displacements. As an example, Richter states that a 0.1 g acceleration at 1 Hz is ordinarily considered damaging in earthquake seismology (*41*). The corresponding particle velocity and displacement are 6.15 in/sec and 0.98 in, respectively, assuming simple harmonic motion. The same acceleration at 20 Hz would only produce 0.308 in/sec particle velocity and 0.0025 in displacement. Richter also observes that the damage potential of a given vibration is dependent on its duration, with 0.1 g at 1 Hz likely not to produce damage for events of a few seconds, but very serious for earthquake-type events of 25 to 30 sec (*41*).

A similar case is provided by the Salmon nuclear study and similar large blasts (*5, 35, 39, 42-43, 45*). These blasts all produced low-frequency and long-duration ground vibrations resulting from their sizes and distances. The Salmon vibration time history was 90 sec long at the structures (18 to 31 km) that were alleged to have been damaged. These durations are hardly comparable to those in mine, quarry, and construction blasting. Consequently, damage data of this kind cannot justifiably be correlated with the scale of blasting of concern in this analysis. However, the dynamic modeling techniques developed during the extensive research of earthquake and nuclear blast response can be applied to the study of blasting and the mechanisms of structural response.

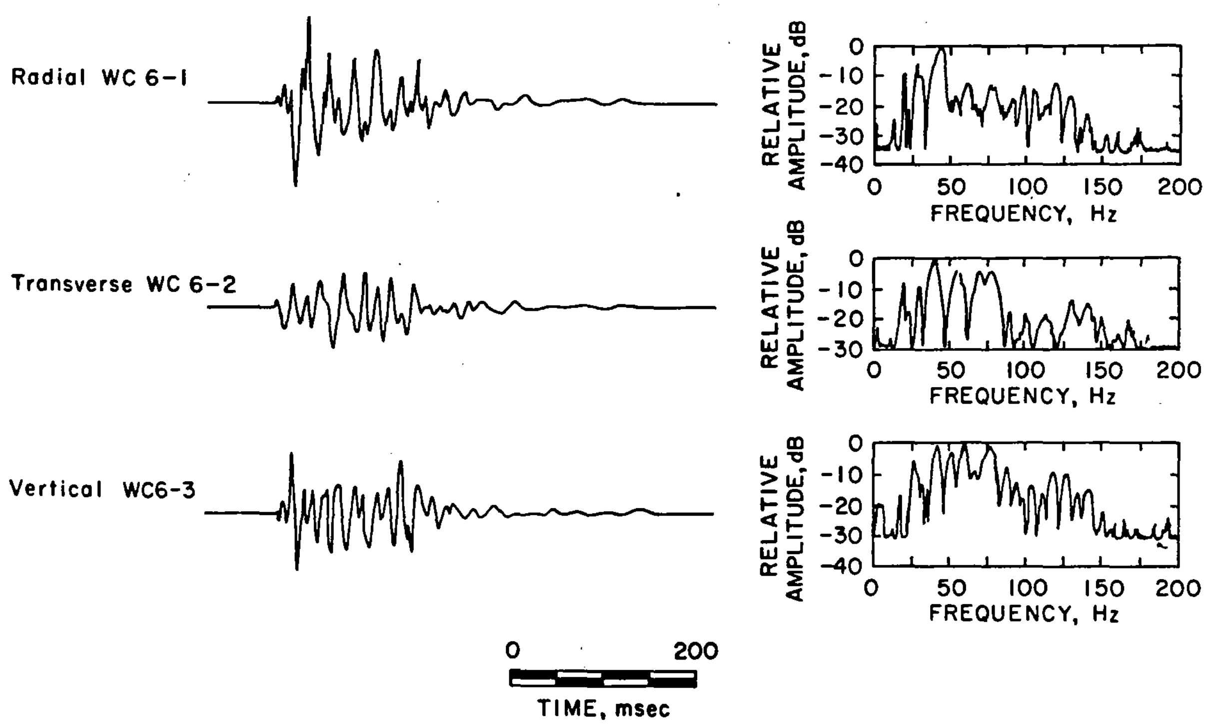

Figure 5.—Construction blast time histories and spectra measured at 75 ft.

GENERATION AND PROPAGATION

Much research has been conducted on ground vibrations. Generation and propagation of ground vibrations have been studied extensively to determine the effects of blast design and geology on vibration amplitudes and frequency character. In Bulletin 656, Nicholls summarized the Bureau's investigation of vibrations produced by blasting in 25 stone quarries, dating back to 1959 (*37*). The Bureau also conducted a series of studies of vibrations generated in four operating underground metal mines in 1974 (*45*). A major study was recently completed by Wiss that quantifies the influence of many of the blast design parameters on both ground vibration and airblast generation and propagation in five surface coal mines (*56*). Lucole also recently published the results of a year of routine monitoring of vibration levels generated by various types of blasting (*29*).

Prior to the last two studies, no data existed on vibrations generated by blasting in surface coal mines. It has been standard practice to apply the blast design rules developed for the small-hole, hard-rock quarry blasting to surface coal mines. Blast holes in surface coal mines have typical diameters exceeding 6 in, and in large area mines they are typically 9 to 15 in. These diameters are larger than those used in most quarries. The highwall blasts of surface coal mines are heavily confined, since they are used only to loosen the overburden and produce little or no throw. Decking is often used with complex timing systems, combining electronic and pyrotechnic delays. The rock being blasted is highly layered and of lower sonic velocity and strength than that in aggregate and lime quarries. Distances to houses are usually greater than for quarries, which are often in or near urban centers. Soil and incompetent rock overburden beneath structures near coal mines is normally tens of feet thick, far more than at most quarries.

Consequently, coal mine blasting is normally characterized as follows:

1. Relatively large charge weights per delay.
2. Complex delay systems that are optimized for efficient fragmentation but that may produce adverse ground vibration frequencies.
3. Relatively high ground vibration levels close-in from heavy confinement of highwall shots.
4. Relatively rapid falloff of ground vibration levels with distance because of attenuation in weak rock.
5. Ground vibrations having predominantly low frequencies because of thick soil overburdens, strong geologic layering that favors surface waves, and large blast-to-structure distances.

BLAST DESIGN AND GROUND VIBRATION GENERATION

As in studies on quarry blasting, most blast design parameters for surface coal mine blasts have little influence on the generated vibrations. Charge weights per delay were again the most influential parameter. A small decrease in ground vibrations was noted for shallow as opposed to great depths of burial. Also, the location of the receiver relative to both the face and direction of blast initiation influenced the delay intervals at which constructive wave interference was experienced (*56*).

The Bureau of Mines vibration data are given in table 1. Included are charge weights, distances, ground vibration, and structure vibration levels for the predominantly coal mine blasts. The two horizontal components of motion were alined with the walls of the nearby structures for analysis of response and did not necessarily correspond to the traditional "radial" and "transverse." The "structure number" of table 1 is for identification, and the "structure type" is the number of stories.

Vibration levels generated from one surface coal mine are shown in figure 6. The maximum horizontal and vertical ground motions were plotted for each blast. Equations and statistics for the various vibration propagations, including Site A (fig. 6), are given in table 2. All particle velocities are in inches per second, distances in feet, and charge weights in pounds. Propagation curves from a variety of surface coal mines are given in figures 7–9. Six of the propagation curves (Nos. 1–2 and 6–9) are from vertical hole blasts studied by Wiss (*56*). The remaining propagation curve (No. 19) is from a single Bureau of Mines site, where actual radial and transverse values were available.

Table 1.—Production blasts and ground vibration measurements

Shot	Facility	Shot type	Total charge, lb	lb per delay	Sealed distance, $ft/lb^{1/2}$	Peak ground vibration, in/sec			Peak structure motion, in/sec							Structure number (table 3)	Structure type
									Low corner			High corner		Midwall			
						H_1	H_2	V	H_1	H_2	V	H_1	H_2	H_1	H_2		
1	Coal	Highwall ---	6,000	500	38.00	1.07	1.07	0.80				0.76	0.49		1.41	27	1
2	Coal	---- do ------	7,200	600	33.00	1.38	1.19	.68				.87	.75		1.57	27	1
3	Coal	---- do ------	7,800	650	29.00	1.89	1.74	.59				.79	.54		1.55	27	1
4	Coal	---- do ------	7,200	1,200	20.00	1.91	1.85	.95				.81	.67		2.19	27	1
5	Coal	---- do ------	7,800	1,300	18.10	2.07	2.33	.94				.87	.56	2.37	3.18	27	1
6	Coal	---- do ------	7,800	650	24.00	3.73	1.73	.73				.82	.60	2.79	2.83	27	1
7	Coal	---- do ------	7,800	650	23.00	5.31	3.82	1.04				1.29	.70	4.96	1.55	27	1
9	Coal	---- do ------	6,600	550	22.00	2.34	1.97	.88				.82	.42	2.63	1.67	27	1
10	Coal	---- do ------	5,400	450	26.00	1.20	1.22	.61				.76	.39	1.24	1.72	27	1
11	Coal	---- do ------	3,600	300	33.00	.72	.52	.28				.33	.24	.82	.60	27	1
13	Quarry	Highwall ---	2,033	280	24.00	.76	.66	.49						1.02		1	1
14	Quarry	---- do ------	4,353	218	61.00	.29	.22	.32	0.90		0.85					1	1
15	Quarry	---- do ------	1,995	303	52.00	.18	.22	.36						.11		2	1
16	Quarry	---- do ------	2,850	187	88.00	.49	.24	.26						.37		3	2
17	Quarry	---- do ------	5,047	200	100.00	.21		.14						.33		1	1
17	Quarry	---- do ------	5,047	200	129.00	.16								.15		4	2
18	Quarry	---- do ------	2,367	305	22.90	1.00		3.82						1.53		1	1
18	Quarry	---- do ------	2,367	305	45.70	.53								.30		4	2
19	Quarry	---- do ------	2,450	160	86.00	.44		.33						.26		5	2
19	Quarry	---- do ------	2,450	160	119.00	.50								.32		6	1
33	Quarry	---- do ------	8,762	700	124.70	.15	.13	.07						.30		7	1
33	Quarry	---- do ------	8,762	700	124.70	.05								.16		8	1
35	Iron	Highwall ---		4.200	17.90		1.86								1.74.	10	2
35	Iron	---- do ------		4,200	17.90	.07		.09						.45		11	2
35	Iron	---- do ------		4,200	17.90	.07		.09						.33		12	2
35	Iron	---- do ------		4,200	17.90	.07		.09						.14		13	1
36	Iron	---- do ------		21,000	132.50	.02		.01						.04		14	2
36	Iron	---- do ------				.02		.01						.06		15	1
36	Iron	---- do ------		21,000	48.30	.03								.05		16	1
37	Iron	---- do ------		2,184	85.60	.18								.38		18	1
38	Iron	---- do ------		15,530	337.80	.01		.01	.01	0.01				.02		14	2
39	Coal	---- do ------	20,300	2,300	64.00	.25	.23	.12	.42	.11	.30			.46	.97	19	2
40	Coal	Parting -----	648	72	767.00	.01	.01	.01							.04	19	2
41	Coal	Highwall ---	21,800	2,600	58.00	.28	.20	.15	.40	.24	.24			.44	.79	19	2
43	Coal	---- do ------	20,700	2,600	56.00	.30	.39	.26	.34	.14	.34			.54	1.49	19	2
43	Coal	---- do ------	20,700	2,600	43.95	.87								1.37		20	1
44	Coal	---- do ------	20,600	2,300	57.00	.21	.36	.28	.29	.10	.42			.45	1.71	19	2
44	Coal	---- do ------	20,600	2,300	47.69	.91								1.20		20	1
45	Coal	Highwall ---	20,700	2,300	55.00	.33	.41	.20	.32	.10	.35			.68	2.27	19	2
45	Coal	---- do ------	20,700	2,300	48.94	1.13								.73		20	1
46	Coal	Ditch --------	3,600	600	91.00	.07	.11	.03	.05	.03	.14			.10	.84	19	2
46	Coal	---- do ------	36,000	600	71.57	.06								.23		20	1
47	Coal	Highwall ---	21,600	2,600	50.00	.26	.29	.24	.25	.10	.71			.54	1.09	19	2
47	Coal	---- do ------	21,600	2,600	47.32	1.10								.93		20	1
48	Coal	---- do ------	20,600	2,300	51.00	.24	.33	.25.	19	.10	.80			.48	1.00	19	2
48	Coal	---- do ------	20,600	2,300	51.71	.79								.68		20	1
49	Coal	---- do ------	19,800	2,200	54.00	.39	.28	.22	.28	.19	.29	.61	.35	1.07		20	1
50	Coal	---- do ------	19,700	2,200	56.00	.24	.15	.25	.22	.17	.36	.40	.28	.87		20	1
51	Coal	---- do ------	19,300	2,200	57.00	.13	.14	.13	.11	.08	.21	.26	.13	.67	.32	20	1
53	Coal	Parting -----	264	24	621.00	.01	.01	.01	.00	.01	.01	.01	.01	.05		20	1
54	Coal	---- do ------	360	36	425.00	.02	.02	.01	.01		.01	.03		.02		20	1
55	Coal	Highwall ---	18,400	2,100	60.00	.14	.13	.18	.13		.30	.21		.51	.36	20	1

56	Coal	---- do	17,700	2,000	64.00	.16	.08	.15	.08	.23	.16	.26		.51		20	1
57	Coal	---- do	6,000	2,000	65.00	.18	.08	.12			.18	.21		.18	.27	20	1
58	Coal	Parting	480	30	444.00	.02	.01	.01			.02	.05		.02	.04	20	1
59	Coal	---- do	294	30	788.00	.01	.01	.01			.01	.01	.01	.01	.06	19	2
60	Coal	Highwall	21,400	2,000	38.00	.49	.82	.88			.98	.31	.20	.52	1.12	19	2
61	Coal	---- do	24,700	2,100	35.00	.44	.90	.93		.65	.93	.42	.30	.67	2.51	19	2
62	Coal	Sweetner	1,500	150	138.00	.12	.20	.06		.23	.09	.12	.06	.23	.43	19	2
64	Coal	Highwall	24,600	2,100	33.00	.51	.62	.85		.51	.96	.43	.26		1.02	19	2
65	Coal	---- do	15,700	2,200	30.00	.45	.59	1.06		.47	1.06	.76	.26		1.33	19	2
66	Coal	---- do	15,800	1,900	31.00	.62	.77	1.53		.54	1.56		.30		1.45	19	2
67	Coal	---- do	13,540	1,900	29.00	.66	.81	.78		.59	.89	.25	.30		1.92	19	2
68	Coal	Parting	300	30	713.00	.01	.01	.01		.01					.07	19	2
69	Coal	Highwall	11,040	2,000	26.00	.53	.70	.94		.45		.29	.26		1.76	19	2
70	Coal	Sweetner	2,100	300	86.00	.19	.16	.07		.11	.10	.12	.04		.49	19	2
71	Coal	Hilltop	9,020	410	67.00	.21	.28	.17		.27	.26	.17	.10		.91	19	2
72	Coal	Ditch	3,060	510	93.00	.07	.09	.03		.03	.07	.07			.60	19	2
73	Coal	Highwall	19,600	2,000	24.00	1.24	1.24	2.24	.78	.97	2.22	.44	.33	2.08	2.77	19	2
74	Coal	---- do	17,100	2,000	23.00	.75	1.12	1.23	.62	.78	1.28	.38	.27	1.06	2.20	19	2
75	Coal	Ditch				.09	.07	.08	.07	.06	.14	.05	.05	.18	.35	19	2
76	Coal	---- do	3,360	280	93.00	.08	.12	.12			.18	.07	.08	.29	.50	19	2
77	Coal	---- do	1,200	220	102.00	.07	.07	.05			.08	.05	.03	.16	.36	19	2
78	Coal	Highwall	22,200	2,100	20.00	.68	1.14	1.58			1.79	.50	.39	1.66	2.38	19	2
79	Coal	---- do	24,900	2,200	18.20	1.58	1.69	2.45			2.93	.87	.71	2.55	3.24	19	2
80	Coal	Highwall	25,100	2,300	16.70	1.14	1.03	0.70			1.04	.63	.54	1.09	2.38	19	2
81	Coal	Sweetner	3,240	360	37.00	.35	.45	.24			.35	.25	.21	1.08	1.79	19	2
82	Coal	Hilltop	27,000	1,000	22.00	1.98	1.85	1.65			4.01	1.34	.84	3.26		19	2
83	Coal	Ditch	2,040	340	81.00	.06	.06	.05						.06	.12	19	2
84	Coal	Highwall	25,600	2,200	16.10	1.37	1.05	1.48			2.33	.87	.54	2.96	2.50	19	2
85	Coal	---- do	25,400	2,200	15.60	2.20	1.27	1.91			1.15	.87	.58	3.76	3.76	19	2
86	Coal	---- do	25,900	2,200	15.30	1.89	1.23	2.21			3.08	.95	.40	3.66	3.04	19	2
87	Coal	Ditch	1,320	220	98.00	.08	.05	.06			.07	.05	.03	.24	.30	19	2
89	Coal	Parting	360	36	372.00	.01	.01	.01			.02	.02	.02	.03	.04	19	2
90	Coal	Highwall	25,500	2,200	15.40	1.68	1.53	2.51			3.37	.94	.51	2.72	3.23	19	2
91	Coal	---- do	31,500	2,200	15.70	1.99	1.60	2.45			2.69	.74	.41	2.92	3.67	19	2
92	Coal	Ditch				.16	.12	.11			.19	.08	.04	.44	.62	19	2
93	Coal	Parting	114	12	626.00	.00	.01	.00						.02	.02	19	2
94	Coal	Highwall	30,700	2,200	17.10	.79	1.25	1.41			2.75	.63	.57	2.88	1.73	19	2
95	Coal	---- do	26,600	2,200	17.90	2.08	1.14	1.35			2.06	.63	.49	5.07	1.83	19	2
96	Coal	---- do	20,500	2,000	19.30	1.22	1.18	.99			2.41	.73	.49	3.07	1.66	19	2
97	Coal	---- do		450	118.00	.03	.01	.04	.06	.02				.11		21	1
98	Coal	---- do	14,400	450	127.00	.05	.01	.04	.04	.04				.16		21	1
99	Coal	Parting	20,880	773	50.00	.27	.19	.15	.34	.26				.61		21	1
100	Coal	---- do	18,000	200	53.00	1.26	.88	.72	.46	.59				1.68		21	1
101	Coal	---- do	17,500	350	96.00	.08	.05	.08	.13	.05				.29		21	1
102	Coal	---- do	27,040	208	48.00	1.20	.79		.69	.58				2.50		21	1
103	Quarry	Highwall	4,956	632	62.00	.32	.27	.19				.15	.14	.41	.28	22	2
103	Quarry	---- do	4,956	632	28.00	.82	.76	.53			.67	.49	.58	.90		23	1
104	Quarry	---- do	5,752	632	59.00	.22	.41	.13	.47	.22		.40	.24	.55	.62	22	2
104	Quarry	---- do	5,752	632	26.00	1.09	.77	.44			.60	1.04	.70	1.32		23	1
105	Quarry	---- do	4,350	615	22.00	.85	.61	.42			.70	.47	.52	.72		23	1
106	Quarry	---- do	17,604	852	144.00	.16	.19	.14	.12	.13		.26	.15	.44	.34	23	1
106	Quarry	---- do	17,604	852	79.00	.04	.03	.03	.03	.03		.03	.04	.08	.10	22	2
107	Coal	---- do				.17	.26	.20	.13	.26	.29			.53	.42	.26	1
108	Coal	---- do				.21	.20	.24	.21	.17	.20	.37	.22	.99	.92	28	1
109	Coal	---- do		300	105.00	.09	.04	.08	.08	.15		.11	.32	.30	.31	29	2
110	Coal	Parting	21,600	240	52.00	1.33	1.02	.52		.50		.33	.35	1.85	1.49	21	1
111	Coal	---- do		320	56.00	.79	.69	.34	.60	.28	.26	.57	.57	1.54	.80	21	1
112	Coal	Highwall		300	81.00	.43	.39	.20					.28	.93	1.02	30	1
113	Coal	Parting		320	61.00	.45	.69	.33			[illegible]			.86		21	1
114	Coal	---- do	23,680	370	68.00	.47	.51	.47			.26			.93	.17	21	1
116	Coal	Highwall	12,000	300	38.00	.24	.22	.23	.29	.25	.24	.37	.42	.53	.48	31	1
117	Coal	Parting	14,400	360	158.00	.04	.02	.02						.07	.02	21	1

Additional Info. in ERRATA

Table 1.—Production blasts and ground vibration measurements—Continued

Shot	Facility	Shot type	Total charge, lb	lb per delay	Scaled ~~Sealed~~ distance, $ft/lb^{1/2}$	Peak ground vibration, in/sec			Peak structure motion, in/sec							Structure number (table 3)	Structure type
									Low corner			High corner		Midwall			
						H_1	H_2	V	H_1	H_2	V	H_1	H_2	H_1	H_2		
119	Quarry	Highwall	16,608	782	154.00	0.03	0.04					0.04	0.04	0.04	0.11	32	2
120	Coal	do	15,120	120	137.00	.19	.09	0.11	0.25	0.09	0.18					31	2
122	Coal	do		15	430.00	.03	.05	.03	.02	.02	.02	.09	.13	.17	.27	28	1
124	Coal	Parting	1,340	20	447.00	.02	.02	.02	.03	.09	.05	.04				33	2
125	Coal	Highwall	10,200	200	141.00	.13	.13	.21	.09	.09	.01	.16		.72	.32	33	2
126	Coal	Parting	1,200	20	391.00	.02	.02	.03	.01	.02	.02					34	1
127	Coal	Highwall	12,000	400	88.00	.16	.13	.08	.15	.11	.16			.34	.36	34	1
129	Coal	do	15,000	350	166.00	.06	.09	.04	.06	.05	.06			.36	.30	35	1
130	Coal	Parting	890	20	391.00	.02	.02	.01	.05	.04	.07			.04	.05	34	1
131	Coal	Highwall	10,800	400	88.00	.15	.14	.10	.11	.10	.20			.36	.24	34	1
132	Coal	Parting	1,300	30	219.00	.05	.06	.04	.04	.03	.03	.09	.09	.24	.13	33	2
133	Coal	Highwall	24,000	400	60.00	.07	.07	.04	.07	.05	.05		.15	.12	.09	33	2
134	Coal	Parting	2,300	400	60.00	.23	~~.36~~ .32	.16	.22	.19	.12	.32	.23		.49	33	2
135	Coal					1.14	1.00	.02	.76	.66	.75	.61	.75	1.52	2.41	21	1
136	Coal	Parting	29,700	900	16.70	1.54	1.12	1.59	.94	.65		.70	.56	2.07	1.84	21	1
137	Coal	do	2,300	20	447.00	.03	.04	.02	.02	.02	.01	.03	.02	.20	.00	33	2
138	Coal	do	2,300	20	447.00	.03	.04	.02	.01	.01	.01	.05	.02	.20	.04	33	2
139	Coal	Highwall	19,200	400	100.00	.10	.12	.06	.11	.09	.07	.15	.12	.51	.20	33	2
140	Coal	Parting	1,000	20	783.00	.00	.01	.00	.04	.04	.02	.06	.03	.06	.05	35	1
141	Coal	do	1,000	20	537.00	.00	.00	.00		.00				.02		36	1
142	Coal	do	1,000	20	537.00	.00	.00	.00		.01				.02		36	1
143	Coal	Highwall	40,000	400	120.00	.06	.03	.02		.07	.03			.14	.17	36	1
144	Coal	Parting	2,400	10	750.00	.00	.00	.01		.00	.00			.02	.01	36	1
145	Coal	Highwall	40,000	400	120.00	.05	.05	.04	.03	.06	.05			.10	.19	36	1
146	Iron	do		4,580	86.00	.13	.22	.09	.13					.40		37	2
146	Iron	do		4,580	86.00	.05	.05	.04		.04				.08			2
146	Iron	do		4,580	86.00	.13	.22	.09	.42	.20				.50	.67		1
147	Iron	Highwall		8,800	74.00	.15	.17	.04	.15	.15	.03			.27	.22		1
147	Iron	do		8,800	74.00	.15	.17	.04	.39	.28				.70	.62	38	2
147	Iron	do		8,800	74.00	.15	.17	.04	.17	.11	.06			.14	.16	39	1
148	Iron	do		8,230	74.00	.11	.11	.03	.12	.12	.03		.14		.19	38	2
148	Iron	do		8,230	74.00		.11	.04	.11	.10	.03			.18			2
149	Iron	do	58,000	2,500	221.00	.00	.03	.00	.03	.01	.01	.04	.02	.05	.04	41	2
150	Iron	do		3,260	102.00	.07	.11	.07	.03	.04	.02	.07	.04	.16	.14	37	2
151	Coal	do					.02	.01	.03	.01	.01	.03	.05	.07	.05	42	2
152	Coal	do	3,585	255	132.00		.05	.05	.05	.04	.06	.07	.08	.11	.14	42	2
153	Coal	do	3,783	152	171.00		.09	.04	.09	.10	.06	.11	.15	.18	.25	42	2
154	Coal	do	3,000	125	51.00		.34	.51	.55	.38	.79	.44		.98	1.26	43	2
157	Coal	do	4,500	75	127.00		.14		.14	.11					.31		2
157	Coal	do	4,500	75	52.00	.34	.44	.26	.33	.38				.48	.58		1
158	Coal	do	2,450	41	180.00		.10		.10	.09				.25		45	2
158	Coal	do	2,450	41	56.00	.41	.32	.25	.52	.45				.66	.61		1
159	Coal	do	920	23	250.00		.04		.05	.03				.13		45	2
159	Coal	do	920	23	52.00	.33	.24	.33	.27	.25				.57	.46		1
160	Coal	do	5,460	78	51.00	.29	.23	.13	.11	.12		.17		.33	.55	47	1
161	Coal	do	3,280	41	34.00	1.17	.64	.64	.52	.37	.66	.62		2.02	1.72	48	2
162	Coal	do	13,040	602	61.00	.18	.19	.16	.12	.16				.41		49	2
163	Iron	do		8,530	6.50	.73	.53	.85	.81	.99	.87	.96	.61		1.15	50	1
164	Coal	do	3,510	351	45.00	.19	.15	.10	.16	.12	.19		.20	.37	.21	49	2
165	Coal	do	4,914	351	44.00	.25	.36	.13	.26		.25	.41	.48	.76	.64	49	2
166	Coal	do				.18	.17	.20	.13	.17	.19	.20	.23	.28	.32	49	2
167	Coal	do	1,750	35	51.00	.33	.42	.50	.38	.43	.49	.23	.44	.86	.94	51	2
168	Coal	do	4,300	86	27.00	.85	1.16	.72	.98	1.29	.77	[illegible]	1.03	2.51	3.12	51	2

169	Coal	---- do ------	4,300	86	19.20	2.11	1.81	1.45	1.92	1.34	1.27		1.86	6.50	5.10	51	2
170	Coal	---- do ------	4,300	86	16.20	2.84	1.85	1.65	1.72	1.27	1.63	1.01	1.63	3.64	3.71	51	2
171	Coal	---- do ------	1,775	71	17.80	1.23	1.24	.97	.43	.62	.72	.82	.47	2.36	.79	51	2
172	Coal	---- do ------				.20	.17	.21	.19	.26	.29			1.04	.62	49	2
174	Coal	---- do ------	4,300	86	21.00	1.38	1.86	.85	.67	1.15	1.90	1.20	2.06	3.84	2.91	51	2
175	Coal	---- do ------	5,150	212	9.90	10.21	6.92	5.65	3.18	4.02	3.19	3.89	4.09	6.99	10.27	51	2
178	Coal	---- do ------	1,320	33	45.00	1.04	.64	.83	.33	.30	.64					51	2
179	Coal	---- do ------	2,145	33	31.00	1.84	2.08	1.47	1.38	1.32	1.78					51	2
180	Coal	---- do ------	1,620	18	4.00	10.58	2.02	2.92	3.69	1.33	2.12					51	2
181	Coal	---- do ------	1,980	22	18.50	7.25	4.90	4.76	1.65	2.55	2.75					51	2
182	Coal	---- do ------	1,620	18	3.30	6.37	3.46	3.46	3.06	2.60	2.70					51	2
183	Coal	---- do ------	2,375	125	206.00	.02	.02	.02	.02	.02				.16		52	1
186	Coal	---- do ------	350	35	127.00	.06	.04	.03	.05	.03						54	1
187	Coal	---- do ------	350	35	127.00	.04	.04	.04	.06	.03						54	1
189	Coal	Highwall ---	360	40	119.00	.05	.03	.07	.04	.01					.06	54	1
190	Coal	---- do ------	720	40	119.00	.06	.03	.03	.06					.22	.04	54	1
191	Coal	---- do ------	400	40	119.00	.04	.02	.06						.06	.07	54	1
192	Coal	---- do ------	960	40	119.00	.06	.03	.05						.18	.07	54	1
193	Coal	---- do ------	3,780	60	36.00	2.67	2.11	3.20	.81	.72				.72		55	2
194	Coal	---- do ------	320	40	174.00	.02	.02	.02				.01		.07		56	2
195	Coal	---- do ------	424	40	174.00	.02	.01	.02				.01		.08		56	2
196	Coal	---- do ------	680	40	174.00	.03	.02	.03	.02			.02		.12		56	2
197	Coal	---- do ------	4,160	80	38.60	.80	.94	.59								49	2
198	Coal	---- do ------	1,200	30	32.90	1.02	.92	.43								57	1
199	Coal	---- do ------	1,200	30	31.00	1.08	.98	1.20								57	1
200	Coal	---- do ------	5,510	276	66.20	.25	.35	.25								49	2
201	Coal	---- do ------	1,200	30	28.70	1.19	1.13	.77								57	1
202	Coal	---- do ------	1,200	30	25.00	2.06	1.13	1.29								57	1
203	Coal	---- do ------		100	24.70	1.35	.77	.58								58	1
204	Coal	---- do ------		100	24.20	2.23	.68	.65								58	1
205	Coal	---- do ------		100	24.20	1.05	.66	.39	.85		1.00				.43	58	1
206	Coal	---- do ------	1,800	100	24.50	.73	.75	.55		.75				.87		58	1
207	Coal	---- do ------	1,800	100	24.50	1.88	1.76	.49		1.02	.50			.76		58	1
208	Coal	---- do ------		80	19.00	1.45	1.38	1.92								58	1
W 1	Constr	Excavation -	80	6	65.30	.18	.21	.26				.04	.06	.31	.27	59	1
W 2	Constr	---- do ------	14	2	45.40	.49	.58	.67	.44	.04		.28	.12	.92		60	2
W 3	Constr	---- do ------	12	1	60.00	.05	.03	.03	.02				.01	.02		60	2
W 4	Constr	---- do ------	110	7	60.50	.68	.60	.77	.39	.69	.36	.18	.29	.45		61	1
W 5	Constr	---- do ------	110	7	20.80	1.94	2.03	2.23			1.84	.57	.47			61	1
W 6	Constr	---- do ------	32	6	30.60	.35	.19	.29		.31	.27	.09	.18		.28	62	2
W 7	Constr	---- do ------	120	12	46.20	.24	.23	.10	.28	.21	.14	.15	.09	.47	.64	63	2
W 8	Constr	---- do ------	100	6	49.00	.27	.27	.13	.19	.13	[illegible]	[illegible]	.06	.39	.37	63	2
W 9	Constr	---- do ------	1	1	49.20	.04	.06	.08		.07	.05	.05	.03	.20	.26	64	2
W 10	Constr	---- do ------	4	1	30.00	.11	.10	.22	.22	.21	.20	.12	.06	.38	.32	64	2
W 11	Constr	---- do ------	18	4	98.90	.37	.32	.40	.15	.07	.06	.09	.07		.14	65	1
W 12	Constr	---- do ------	20	4	96.20	:25	.20	.22	.07	.06	.08	.07	.07		.20	65	1
W 13	Constr	---- do ------	27	8	17.50	.47	1.09	.52		.73	.41	.24	.47		1.81	66	1
W 14	Constr	---- do ------	30	9	23.00	.40	.40	.40		.65	.31	.38	.47		1.30	66	1
W 15	Constr	---- do ------	30	9	25.40	.15	.32	.18		.27	.14	.24	.32		.72	66	1
W 16	Constr	---- do ------	41	12	11.50		2.47	1.25	1.30	.64	1.17	.40	.18	1.18	1.01	67	2
W 18	Constr	---- do ------	119	10	44.80	.46	.69	.51		.11	.13	.18	.16	.22	.17	68	1
W 19	Constr	---- do ------	127	10	36.80	.72	.84	.93	.19	.47	.31	.21	.25	.29	.21	68	1
W 20	Constr	---- do ------	22	3	39.20	.53	.53	.30		.20		.14	.09	.28	.34	69	1
W 21	Constr	---- do ------	24	3	16.60	1.09	.77	.80	.19	.24	.12	.15	.17	.62	.64	69	1
W 22	Constr	---- do ------	46	7	38.50	1.56	.76	1.43	.54	.32	.45	.15	.13	.56	.55	70	1
W 23	Constr	---- do ------	42	7	11.70	3.73	2.08	3.20	2.49	1.44	2.70		.77		1.53	71	1
W 24	Constr	---- do ------	51	6	28.00	.64	.81	1.76	.55	.48	.73	.26	.41	.52	.35	72	2
W 25	Constr	---- do ------	50	6	63.30	.96	.85	.49	.30	.21	.39	.26	.43	.65	.24	73	1
W 26	Constr	Excavation -	70	6	64.00	1.61	1.32	.67	.47	.27	.58	.47	.53	.92	.26	73	1
W 27	Constr	---- do ------	70	6	61.20	1.16	1.20	.75	.38	.42	.25	.32	.46	.63	.25	73	1
W 28	Constr	---- do ------	43	5	41.60	1.14	.85	1.26	.62	.73	.52	.71	.17	1.09		74	1
W 29	Constr	---- do ------	58	7	30.20		1.44	1.80	.84	1.04	.70	.85	.29	.89	1.46	74	1
W 30	Constr	---- do ------	27	6	42.60	.27	.28	.21	.04	.17	.07	.09	.07	.30	.40	75	1
W 31	Constr	---- do ------	85	6	65.30	.53	1.22	.75	.23	.32	.39	.12	.29	.15	.89	76	1
W 32	Constr	---- do ------	85	6	32.00	1.82	1.19	1.55	.46	.50	.73	.15	.47	.19	1.09	76	1

*2σ → PPV= $438(SD)^{-1.52}$

Table 2.—Equations and statistics for ground vibration propagation

Site and component	Equation	Correlation coefficient	Standard error, pct
Site A:			
Maximum horizontal	$GV = 84.5\ (D/W^{1/2})^{-1.324}$	NA	NA
Vertical	$GV = 134.1\ (D/W^{1/2})^{-1.569}$	NA	NA
Radial:			
Site 1.	$GV = 82\ (D/W^{1/2})^{-1.324}$	0.977	35
Site 2	$GV = 68\ (D/W^{1/2})^{-1.324}$	.971	35
Site 6	$GV = 54\ (D/W^{1/2})^{-1.493}$	.973	35
Site 7	$GV = 44\ (D/W^{1/2})^{-1.447}$	.902	85
Site 8	$GV = 135\ (D/W^{1/2})^{-1.475}$	.981	42
Site 9	$GV = 281\ (D/W^{1/2})^{-1.729}$	.980	47
Site 19	$GV = 79.2\ (D/W^{1/2})^{-1.383}$	.937	41
Vertical:			
Site 1	$GV = 137\ (D/W^{1/2})^{-1.551}$	.973	52
Site 2	$GV = 80\ (D/W^{1/2})^{-1.551}$	.968	52
Site 6	$GV = 56\ (D/W^{1/2})^{-1.553}$	.960	52
Site 7	$GV = 79\ (D/W^{1/2})^{-1.676}$	.972	34
Site 8	$GV = 110\ (D/W^{1/2})^{-1.512}$	.963	29
Site 9	$GV = 298\ (D/W^{1/2})^{-1.823}$	.984	42
Site 19	$GV = 335\ (D/W^{1/2})^{-1.825}$	.942	54
Transverse:			
Site 1	$GV = 64\ (D/W^{1/2})^{-1.234}$	.951	66
Site 2	$GV = 51\ (D/W^{1/2})^{-1.234}$	.931	66
Site 6	$GV = 55\ (D/W^{1/2})^{-1.362}$	.975	44
Site 7	$GV = 40\ (D/W^{1/2})^{-1.425}$	.944	54
Site 8	$GV = 50\ (D/W^{1/2})^{-1.257}$	.937	45
Site 9	$GV = 106\ (D/W^{1/2})^{-1.480}$	.940	59
Site 19	$GV = 64.2\ (D/W^{1/2})^{-1.381}$	.946	37
All Bureau of Mines coal mine data:			
Maximum horizontal	$GV = 133\ (D/W^{1/2})^{-1.50}$	.933	83
Vertical	$GV = 79\ (D/W^{1/2})^{-1.46}$	.923	88
Total	$GV = 119\ (D/W^{1/2})^{-1.52}$	.936	92
Mines[1]:			
Radial	$GV = 52\ (D/W^{1/2})^{-2.37}$	NA	58
Vertical	$GV = 51\ (D/W^{1/2})^{-2.49}$	NA	59
Transverse	$GV = 73\ (D/W^{1/2})^{-3.13}$	NA	55
Quarries[1]:			
Radial	$GV = 14\ (D/W^{1/2})^{-1.22}$	NA	57
Vertical	$GV = 13\ (D/W^{1/2})^{-1.31}$	NA	61
Transverse	$GV = 10\ (D/W^{1/2})^{-1.11}$	NA	57
Construction[1]:			
Radial	$GV = 5.0\ (D/W^{1/2})^{-1.09}$	NA	85
Vertical	$GV = 8.9\ (D/W^{1/2})^{-0.99}$	NA	72
Transverse	$GB = 5.9\ (D/W^{1/2})^{-1.12}$	NA	80

NA = Not available
GV = Ground vibration, in/sec.
[1] From Lucole and Dowding (*29*).
D = Distance, ft.
W = Charge weight per delay, lb.

All Bureau coal mine vibration data are shown in figure 10. A vibration level of 1.0 in/sec was typically observed at a square root scaled distance of 23 ft/lb$^{1/2}$ and never observed beyond 60 ft/lb$^{1/2}$. The equivalent scaled distances for 0.5 in/sec peak particle velocity are 38 and 80 ft/lb$^{1/2}$. Wiss found that square root and cube root scaled distances required to enclose or envelope all his vibration data at 1.0 in/sec were 75 ft/lb$^{1/2}$ and 300 ft/lb$^{1/3}$, respectively (*56*). Two standard deviations of the summary data in figure 10 should leave roughly 2.5 pct of the points outside the upper limit. This corresponds to scaled distances of 55 and 90 ft/lb$^{1/2}$ at 1.0 and 0.5 in/sec, respectively. As alternatives to vibration monitoring or for statistical predictive purposes, the maximums represented by the envelopes (e.g., fig. 10) or two standard deviations from the mean regressions can be used; however, these will result in conservative vibration levels.

The Bureau of Mines coal data, as well as all of Lucole's (*29*), consist of relatively few measurements at each of a large variety of sites. Consequently, the pooled data representing each industry as a whole tends toward large scatter (high standard deviations).

Both Wiss (*56*) and Nicholls (*37*) utilized arrays of gages and found that the propagation from individual sites could reliably be quantified (fig. 7–9) and that vibration levels for individual sites could be reasonably predicted from scaled distances.

VIBRATION COMPARISONS: MINE AND QUARRY BLASTS

Vibrations from quarry blasting have been discussed extensively in Bulletin 656 (*37*). That report recommended two scaled distances intended to prevent the exceeding of 2 in/sec. For a site where propagation conditions were shown to be normal, a square root scaled distance of 20 ft/lb$^{1/2}$ was recommended. In the absence of any vibration monitoring, a scaled distance of 50 ft/lb$^{1/2}$ was to be used, based on the envelope of maximum observed values.

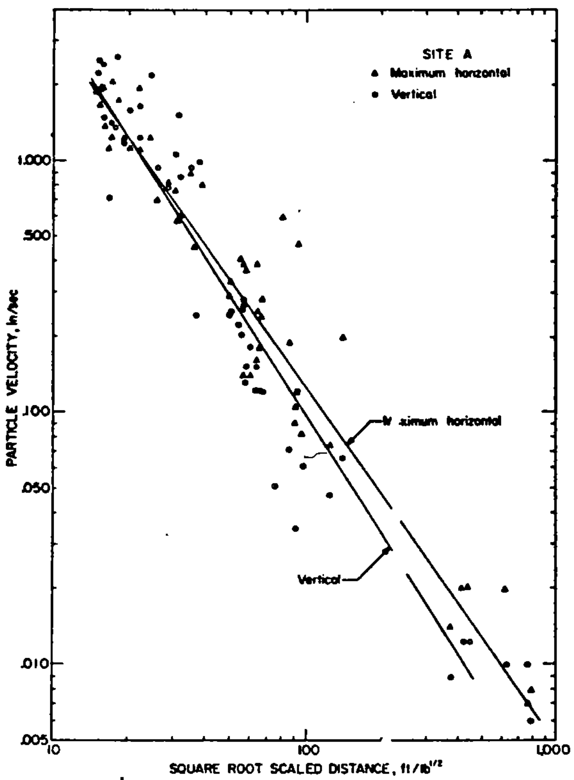

Figure 6.—Ground vibrations from a single coal mine. Equations are given in table 2.

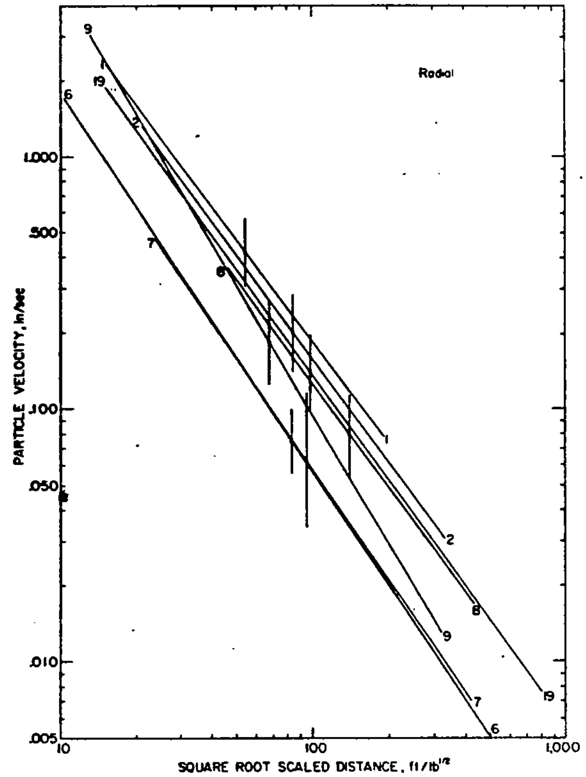

Figure 7.—Radial ground vibration propagations from surface coal mines.

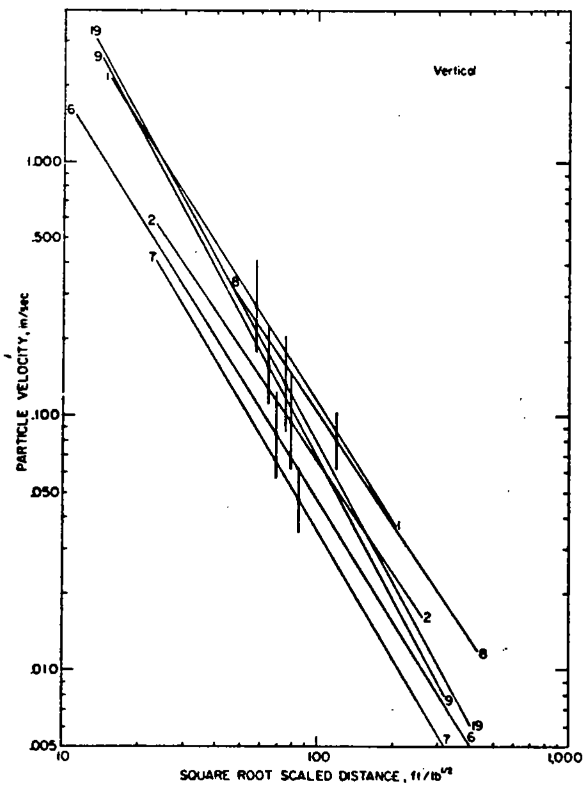

Figure 8.—Vertical ground vibration propagations from surface coal mines.

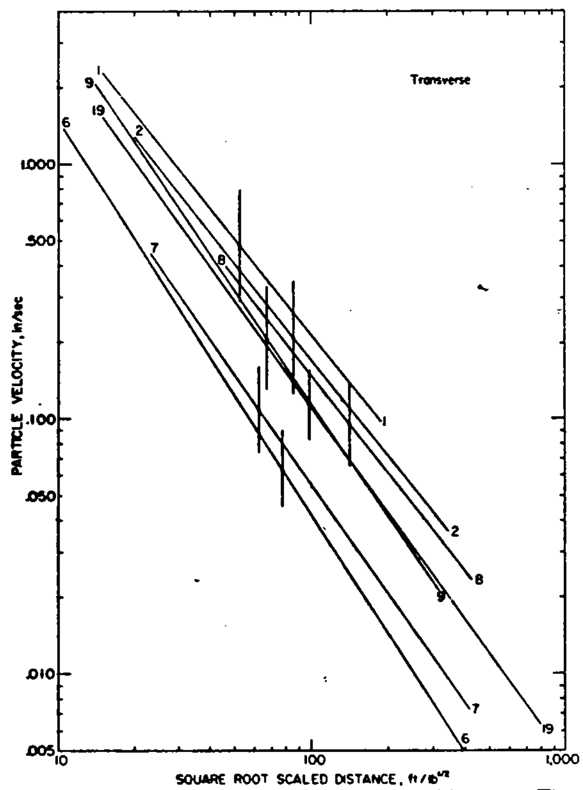

Figure 9.—Transverse ground vibration propagations from surface coal mines.

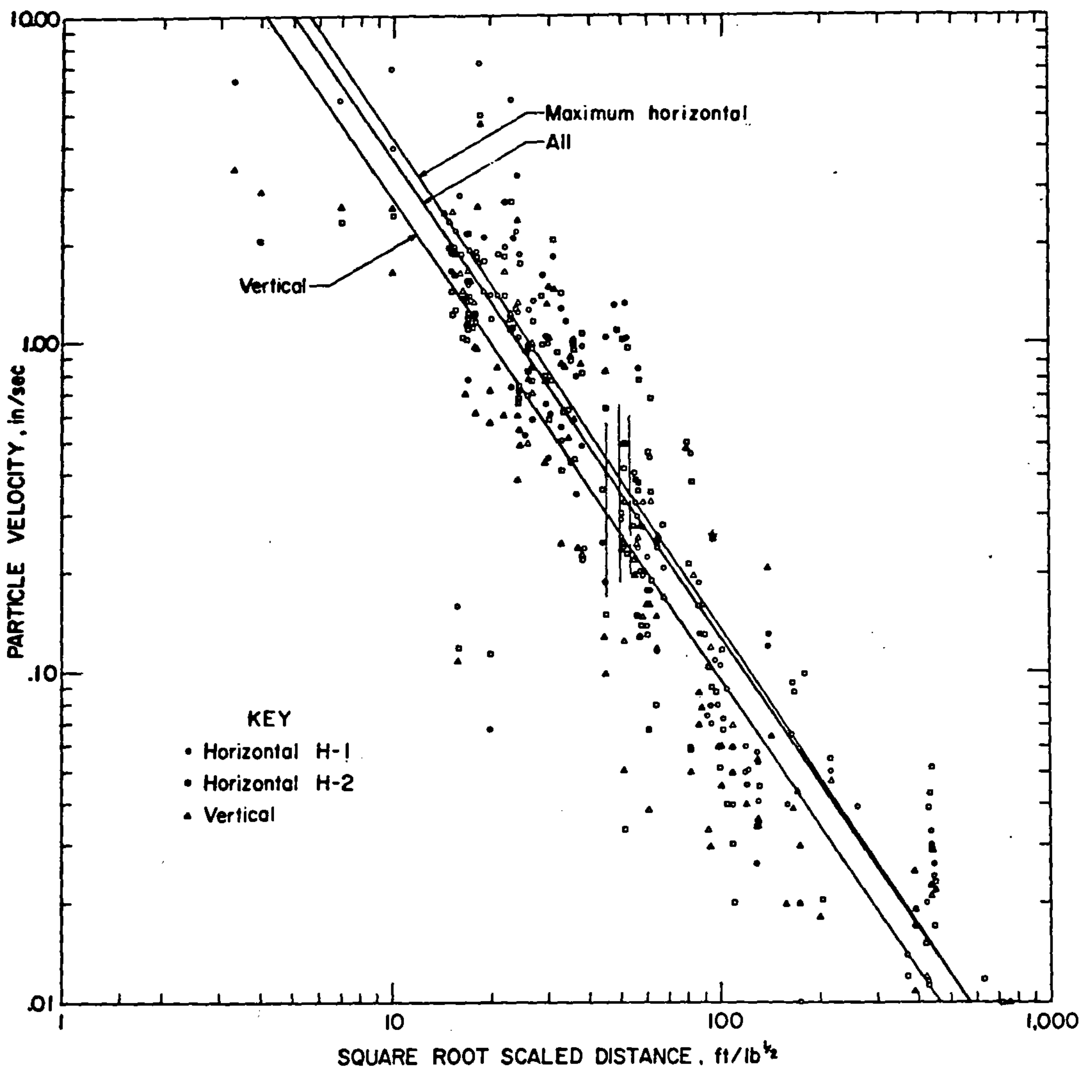

Figure 10.—Summary of ground vibrations from all surface coal mines. The component H–1 approximates "radial" and H–2 "transverse".

The overall zones encompassing the propagation regression lines for the radial motion (usually the largest) for coal mine and quarries are shown in figure 11. It is obvious that the vibration levels for coal and quarry blasting are similar, particularly at the smaller scaled distances that warrant most concern. Contrary to expectations, the coal mine vibrations were of greater amplitude than quarry vibrations at larger scaled distances. This is probably the result of larger absolute distances involved (for the relatively large charge weights) and the possible existence of slower decaying surface waves and dispersion-produced interference between delays at these distances. The Lucole study found different relative amplitudes between coal and quarry blasting to be more in agreement with the theoretical predictions (fig. 12). However, their data were also characterized by larger scatter and only a rough approximation to a Gaussian distribution (*29*). Their maximum envelope at 1.0 in/sec exceeded 200 ft/lb$^{1/2}$ for all kinds of blasting. Two standard deviations (95 pct) of the propagation data at 2 in/sec was less than 41 ft/lb$^{1/2}$ for coal mines and 33 ft/lb$^{1/2}$ for quarries and construction. These are both significantly lower than the Bureau's coal mine summary value of 55 ft/lb$^{1/2}$ from figure 10.

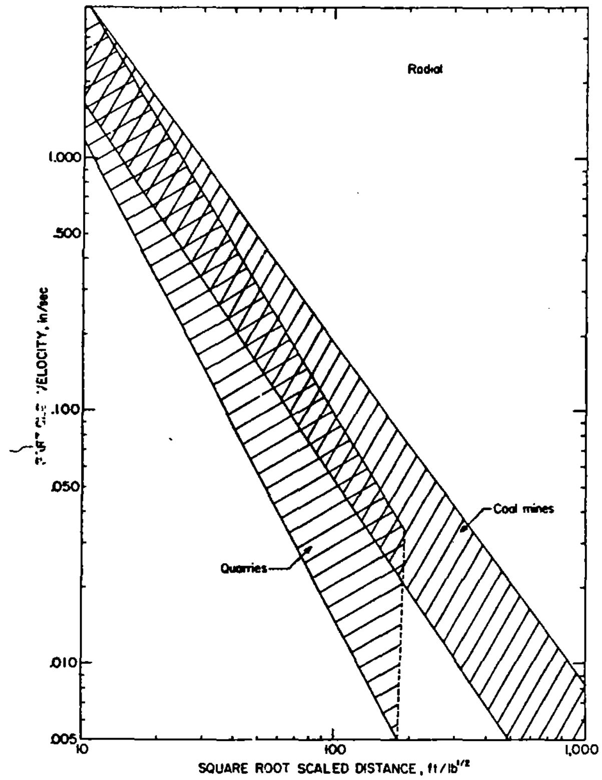

Figure 11.—Zones of mean propagation regressions for two major types of blasting.

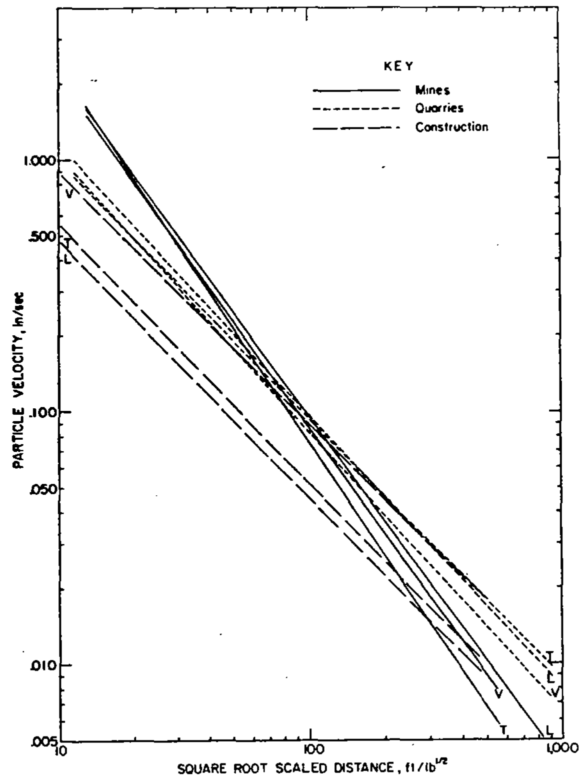

Figure 12.—Ground vibration propagation for three types of blasting as found by Lucole (*29*). Longitudinal (L), transverse (T), and vertical (V) components.

RESPONSE OF RESIDENTIAL STRUCTURES

The measured response of residential structures is a critical indicator of troublesome or potentially damaging ground vibrations. Corner motion measurements were used to assess the racking motions (shearing) of the gross structure (fig. 13). Essentially, cracking from blasts occurs where excessive stresses and strains are produced within the planes of the walls or between walls at the corners. Consequently, the vibration in the corners is assumed to indicate cracking potential, because it corresponds to whole-structure response. Other types of response cause different but consequential results. Midwall motions (normal to the wall surface) were also measured and are primarily responsible for window sashes rattling, picture frames tilting, dishes jiggling, and knick-knacks falling. Structures are designed to resist normal vertical load; however, differential vertical motions can produce high strains in floors and ceilings. Vertical floor motions are also of concern for potential human response.

RESPONSE SPECTRUM ANALYSIS TECHNIQUES

A simple method for predicting structural responses to vibrations has developed from studies of building response to earthquakes. It is based upon the single degree of freedom (SDF) model of a structure shown in figure 13 (*8, 10, 13, 24, 30, 32, 42*). The relative displacement between the mass and the ground, u(t), can be mathematically calculated from a knowledge of the time-varying ground displacements, y(t). The simplifying assumptions behind this mathematical idealization are as follows:

1. The structure can be represented by a lumped mass, m.
2. The relative displacement and deformation of the structure produces a restoring force proportional to the stiffness of the structure, k.
3. During vibration, energy is dissipated through viscous friction, C, which is constant regardless of the amplitude of the motion.

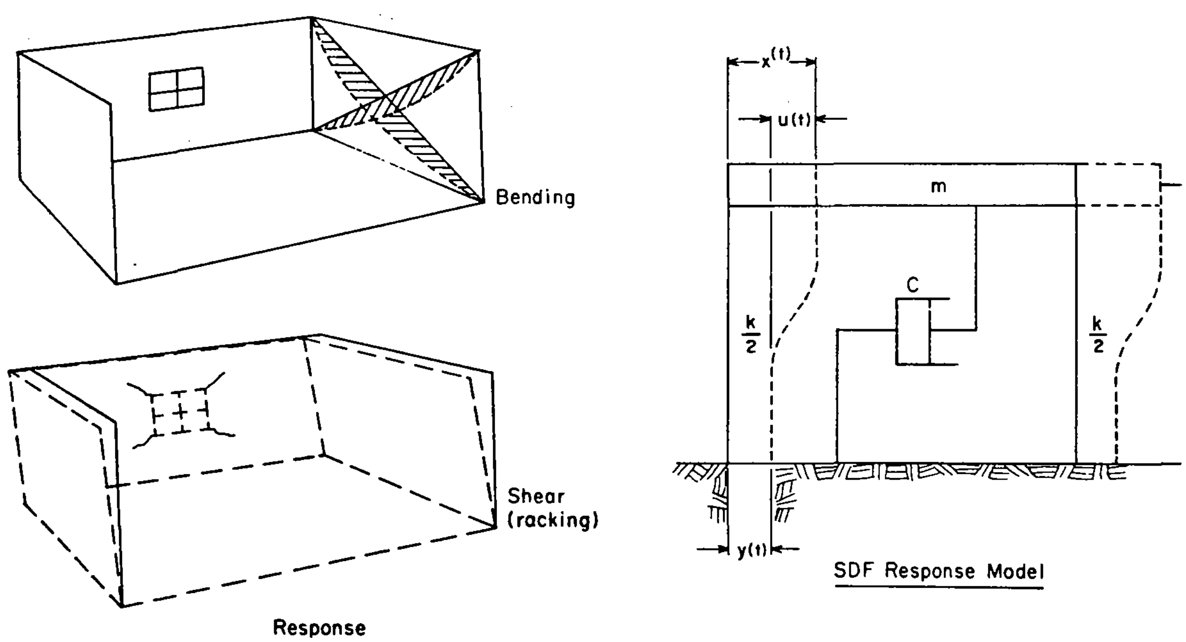

Figure 13.—Single degree of freedom (SDF) model and types of structures response. SDF symbols are explained in the text.

4. The structure responds or translates only in a single direction—hence the name single degree of freedom (SDF). Incorporation of simultaneous torsional rotation or additional components of motion requires additional degrees of freedom.

In an actual structure, m is the mass of the walls, floor, and roof; the restoring force is that produced by the walls resisting shear deformation, and frictional dissipation of energy results from portions of the structure working against each other. Nail pulling is one consequence. The equation of motion of the SDF system, subjected to a time varying motion, is

$$\ddot{u} + 2\beta\omega_n\dot{u} + \omega_n^2 u = -\ddot{y} \qquad (1)$$

where $\ddot{u}$, $\dot{u}$, u, are relative acceleration, velocity, and displacement,
$\ddot{x}$, $\dot{x}$, x are absolute acceleration, velocity, and displacement of mass,
$\ddot{y}$, $\dot{y}$, y are absolute acceleration,velocity, and displacement of the ground,
ω_n is the circular natural frequency (also $2\pi f_n$) and related to stiffness (k) and mass (m) by: $\omega_n = \sqrt{k/m}$, and
β is the damping ratio (pct of critical /100) and equal to $C/\sqrt{km}$,
where C is the viscous damping and is equal to $\sqrt{km}$ when critical.

The natural frequency, ω_n, describes the rate at which the mass will freely oscillate when displaced. The damping, β, controls the decay of the oscillation. When a structure is critically damped (β = 1.0), it will return to its equilibrium position without oscillating.

Equation 1 can be solved for the relative displacement at any time, t, when given a transient ground particle velocity time history, $\dot{y}$. The solution is shown in equation 2:

$$u(t) = \int_0^t \dot{y}(\tau)e^{-\beta\omega_n(t-\tau)} \left\{\cos\left[\omega_n\sqrt{1-\beta^2}\,(t-\tau)\right] + \frac{\beta}{\sqrt{1-\beta^2}}\sin\left[\omega_n\sqrt{1-\beta^2}\,(t-\tau)\right]\right\} d\tau \qquad (2)$$

When a ground particle-velocity time history, such as shown in figure 3, is processed by computer with this equation, the modeled time history is produced.

The time history produced by equation 2 is one of relative displacements, u, rather than the absolute velocity $\dot{x}$, which is normally measured on the structure. In this relative displacement time history there will be a maximum, u_{max}. If that maximum relative displacement is multiplied by ω_n (or $2\pi f$), the resulting product, $2\pi f u_{max}$, is called the pseudo velocity, the PSRV, or the pseudo spectral response velocity. This pseudo velocity is a close approximation of the relative velocity, $\dot{u}$, when the assumption of simple harmonic motion is valid.

A response spectrum of a single ground motion, such as that of a hard-rock construction blast shown in figure 14, is generated from u_{max}'s from a number of different SDF systems. Consider two different components of the same structure, the 10 Hz gross structure and the 20 Hz wall. If the ground motions, $\dot{y}(t)$, of the construction blast are processed twice by equation 2 with β held constant at 5 pct and ω_n set to $2\pi(10)$ for the first time and $2\pi(20)$ for the second, two u_{max}'s will result: 0.01 in (0.25 mm) and 0.02 in (0.05 mm).

These u_{max}'s can be converted to two maximum pseudo velocities, $2\pi(10)$ (0.01) = 0.62 in/sec (15.7 mm/sec) and $2\pi(20)$ (0.02) = 2.5 in/sec (63.5 mm/sec); they are plotted in figure 14 as points *1* and *3*. If the ground motions from the construction blast are processed a number of times for a variety of ω's with β constant, the resultant pseudo velocities will form the solid line in figure 14.

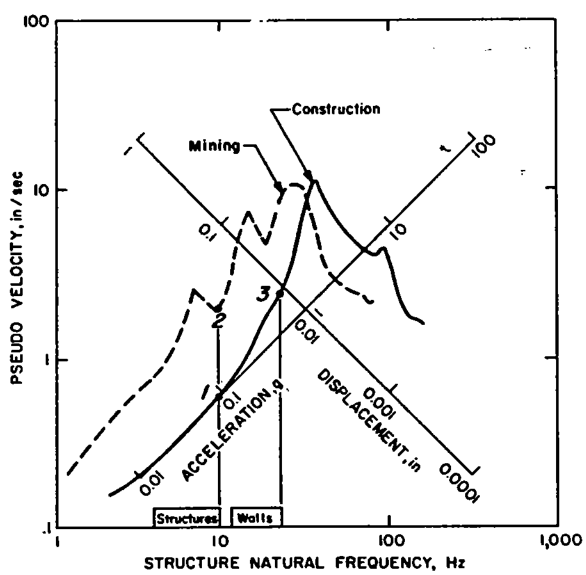

Figure 14.—Response spectra for mining and construction shots, after Corser (*8*).

The response spectra in figure 14 are plotted on four-axis tripartite paper. These four axes take advantage of the sinusoidal approximation involved in calculating a pseudo velocity. They are constructed so that the axis of the maximum relative displacement, u_{max}, is inclined upward to the left such that

$$u_{max} = PV/2\pi f,$$

where PV is the pseudo velocity, and that the axis of pseudo acceleration, PA, is inclined upward to the right such that

$$PA = PV \cdot 2\pi f.$$

The portion of a spectrum that is quasi-parallel to lines of constant displacement (less than 20 Hz for the mining blast in figure 14) is called the displacement bound. Likewise, the spectrum for the mining blast for frequencies greater than 50 Hz is the acceleration bound.

The response spectrum is similar to a Fourier frequency spectrum, since it shows the spectral content of a vibration time history. However, it is more useful as the pseudo velocity is calculated from a simplified measure of the maximum relative displacement, and as such it is related to wall strains that induce cracking.

Values of structure damping (β) must be assumed for computations of response spectra, and this value is 5 pct of critical in figure 14. This is a good approximation for a residence; however, the model response of residences is much more dependent on small changes in natural frequency than on small changes in damping (*32*).

Several researchers have applied response spectra techniques to blasting. Dowding examined responses from construction blasting (*10*). He shows the important relationship between the two frequencies (structure and ground motion) and how the ground motion descriptors of displacement, velocity, and acceleration affect response spectra of blasting vibrations. Most significant for blasting is that the principal frequencies of the ground motion almost always equal or exceed the gross structure natural frequencies of 4 to 10 Hz. This suggests either a displacement- or velocity-bound system in the 5- to 10-Hz range and supports the use of these motion descriptors to assess cracking potential. Earthquakes and nuclear blasts generate low principal frequency motions at the large distances of concern, and the 4- to 10-Hz range falls on the acceleration bound of the spectra.

Medearis developed response spectra for a variety of production blasts (*30*). This was one of the first attempts to show statistically that the structural response of residences (and consequently the cracking potential) is related to frequency content of the blasts. Medearis recommended safe particle velocities based on distances from the blasts that implicitly include the above-described frequency dependencies. These range from 3.20 in/sec (10 ft from a 2-story residence) to 0.62 in/sec (10,000 ft from a 1-story residence) and are based upon a 5-pct tolerance of damage. Medearis' suite of time histories was taken from quarry, excavation, and construction blasts, with an average spectral peak of 40 Hz. He therefore predicted that the relatively higher frequency 1-story homes with natural frequencies nearer 10 Hz are more damage-prone than taller 2-story homes with natural frequencies near 5 Hz. These results would not apply to mine blasts having ground vibrations at lower frequencies.

Corser calculated response spectra for a variety of blasts recorded by the Bureau of Mines (*8*). He found that, in the 5- to 10-Hz range (fundamental frequencies for wood frame structures), mining blasts generated SDF relative displacements that averaged 5.7 times (2.9 to 9.3) those of close-in construction shots. The time histories analyzed had peak particle velocities of 0.66 to 2.23 in/sec. Since the relative structure velocities will have similar ratios, the safe vibration levels for these two classes of blasts could differ by that same factor (5 to 6).

Figure 14 compares spectra from ground motions generated from surface coal mining and construction blasting in hard rock. Even though these two blasts produced peak particle velocities of 2.3 in/sec, the gross structure of a 1-story residence (represented by the 10 Hz response) would respond to the surface mining vibrations with relative displacements 3 times that of the higher frequency motions produced by the construction blasts.

Response-spectra analysis techniques are a powerful tool for research, engineering, and design because they include the important frequency effects. They can predict responses of a variety of structures for any type of time history. However, they do have some serious limitations in that their validity depends on how closely the structures fit the SDF model. They are not required for situations where responses can be determined empirically. They are not practical for regulatory purposes, as they are too complex and time consuming for agencies responsible for measurement and monitoring compliance. Where responses and damage potentials have been established for one type of structure, response spectra analysis allows predictions for quite different structures with unknown vibration character. Since taller structures better fit the SDF model, these techniques have been used widely for predictions of earthquake and nuclear blast effects on such structures.

DIRECT MEASUREMENT OF STRUCTURE RESPONSES

Measurements were made of structure motions, produced by both the ground-borne vibration and airblast, as part of the assessment of potentially damaging blasts. The measurement and recording systems have been described in Bureau reports (*45, 50*). Both ground and structure measurements were made with 2.50- and 4.75-Hz velocity transducers (Vibra-Metrics[6] 120 and 124) with flat frequency responses (-3 dB) of 3 to 500 Hz and 5 to 2,000 Hz, respectively. A few accelerometers, having low-frequency response down to 1 Hz, and a variety of blasting seismographs were used (*50*).

Test Structures

A total of 76 different structures were studied for ground vibration and airblast response and damage (table 3). All were houses except Nos. 13, 15, 16, and 50, which were 1- and 2-story structures somewhat larger than single-family residences, and No. 54, which was a mobile home. Some structures (Nos. 19 and 20) were studied in conjunction with highwall, parting, and surface blasts. The response of structures 1–6 was described in an earlier study (*45*). Of the 76 structures, only 14 were subjected to high enough levels for significant damage and nondamage data, although levels of response were measured for every structure. The 14 significant test houses are shown in figures 15–28.

[6] Reference to specific brand names is made for identification only and does not imply endorsement by the Bureau of Mines.

Figure 15.—Test structure 19, near a coal mine.

Table 3.—Test structures and measured dynamic properties

Structure	No. of stories	Dimensions, ft: Plan NS × EW	Dimensions, ft: Overall height	Construction: Superstructure	Construction: Exterior covering	Construction: Interior covering	Construction: Foundation	Natural frequency of structure, Hz: N-S	Natural frequency of structure, Hz: E-W	Damping, pct: N-S	Damping, pct: E-W	Midwall natural frequencies, Hz	Midwall damping, pct	Shots (table 1)
1	1	22×30	14	Wood frame	Wood siding	Gypsum wallboard	Full basement					16		13,14,17,18
2	1	30×70	14	Masonry and wood	Stone	do	do							15
3	1½	35×35	16	Wood frame	Brick and wood	do	Partial basement					13		16
4	2	30×40	22	do	Wood siding	do	Full basement	8		2		19,22		17,18
5	2	40×40	22	do	Brick and wood siding.	do	Partial basement					19		19
6	1	40×40	14	do	Wood siding	do	Full basement	9				32		19
7	1	48×25	15	do	Asbestos siding	do	do							33
8	1	15×10	12	do	Wood siding	do	Concrete slab							33
9	1	61×29	14	do	do	do	Full basement							34
10	2	44×29	22	do	Asphalt sheathing	Plaster	do							35
11	2	26×32	30	do	Masonite siding	Gypsum wallboard	do					36		35
12	1½	27×36	20	do	Cedar shakes	do	do					25		35
13	1	34×100	16	do	Brick and stucco	do	Slab and crawlspace							35
14	1½	35×35	23	do	Wood siding	do	Full basement	10		7		14		36,38
15	1	125×25	12	Steel frame	Steel	do	Concrete slab	6		3		17		36,38
16	1	80×80	17		Brick and stucco	do	Full basement					8.3		36
17	1½	19×40	20	Wood frame	Wood shingles	do	do	10	9	5	7	18		37,146
18	1	44×28	13	do	Wood siding	do	Pillars in dirt	6	10	7	7	11.4		37,146
19	2	33×35	24	do	Wood siding	Plaster and lath	Partial basement	4	4	13	13	13,17	4.5,5.1	39–48,59–96
20	1½	39×29	21	do	do	Gypsum wallboard	Full basement	8	7	3	8	20	3.1	42–58
21	1	48×28	15	do	do	do	do	7	7	2	7	13.4,14.5	2.9,2.3	97–102,110, 111,113, 114,117, 135,136
22	2	27×76	26	do	Brick and masonite	Gypsum and paneling.	Crawl space	8	6	3	4	12.3,13.1	2.0,3.0	103,104
23	1	62×26	14	do	Asbestos shingles	Gypsum wallboard	do	9	7	2	5	18.5		103–105
24	1	24×55	15	do	Brick	do	Crawl space	10	10	2	4			106
25	1½	41×24	22	do	Wood siding	do	Full basement	8	10	8	3	13.7,16.3	1.8,3.6	106
26	1	40×31	15	do	Aluminum siding	do	Crawl space	7	8	6	4			107
27	1	51×30	15	do	Wood siding	Plaster and lath	Partial basement	7	6	10	6	17,24		1–11
28	1	42×28	14	do	Wood and aluminum.	Gypsum wallboard	Crawl space	7	8	6	4			108,122
29	2	26×35	22	do	Wood panel	do	do	7	8	2	2	17.7,13.0	1.1,2.2	109,120,121
30	1	34×48	16	do	Stone	do	Full basement							112
31	1	35×44	13	do	Wood siding	do	Crawl space	8	6	2	2	12.2,16.6	1.5,1.2	115,116,118
32	1½	58×26	22	do	Brick and masonite	Paneling and wallboard.	Concrete slab							119
33	1½	69×27	24	do	Stone	Gypsum wallboard	Full basement	8	9	2	2	16.0,19.7	1.5,2.1	124,125,132–134,137–139
34	1	33×33	18	do	Asphalt sheathing	Plaster	Crawl space	7	6	3	4			126,127, 130,131
35	1	32×37	18	do	do	Gypsum wallboard	do	7	6	1	4			128,129,140
36	1	28×40	14	do	Asphalt shingles	do	do	6	7	3		14,17		141–145
37	1½	32×26	20	do	Wood siding	Plaster and lath	Full basement	9	10	2	2	18.5,20		146,150
38	2	28×32	20	Masonry and wood.	Brick and aluminum.	Wood paneling	Concrete slab	4	6	5	3			147,148

SEE ERRATA

Table 3.—Test structures and measured dynamic properties—Continued

Structure	No. of stories	Dimensions, ft		Construction				Natural frequency of structure, Hz		Damping, pct		Midwall natural frequencies, Hz	Midwall damping, pct	Shots (table 1)
		Plan NS × EW	Overall height	Superstructure	Exterior covering	Interior covering	Foundation	N-S	E-W	N-S	E-W			
39	1	34×29	15	Wood frame	Masonite siding	Paneling and wallboard	Full basement	5	5	7		14		147
40	1½	28×31	18	do	Stucco	Plaster and lath	Partial basement	5	8	7	2	13.6		148
41	2	40×28	22	do	Wood siding	Gypsum and plaster	Full basement	10	8	4	2	16.6		149
42	1½	44×30	20	do	do	Paneling	do	5	7	5	4	11.9,13.9		151–153
43	1½	28×46	23	do	do	do	do	8	5			18,18		154
44	1	...	15	do	do	...	do					11,11		155–156
45	2	55×44	32	Solid brick	Brick	Plaster on brick	do	9	10	3	3			157–159
46	1½	38×40	21	Concrete block	Concrete block	Plaster	do	10		4		11,11		157–159
47	1	87×38	15	Wood frame	Brick	Gypsum wallboard	do					12.5,13.3		160
48	1½	36×24	22	do	Wood siding	do	do					16.7,16.7		161
49	1½	41×35	27	do	do	Gypsum wallboard and plaster on lath						18.2,18.2		162,164–166, 172,197,200.
50	1	48×180	14	do	Aluminum siding	Gypsum wallboard	Concrete slab	9		2				163
51	2	50×43	28	Solid brick	Brick	Plaster on brick and lath	Full basement							167–171, 173–182
52	1	37×24	16	Wood frame	...	Wood paneling	do							183
53	1	24×35	15	do	Wood siding	...	Crawl space							184
54	1	12×60	15	Metal walls	Metal	Paneling	None							186,187, 189–192
55	1½	40×31	23	Wood frame	Wood siding	...	Full basement							193
56	1½	34×57	20	do	Wood siding	...	do							194,196
57	1	40×24	20	Wood frame	Aluminum siding	Plaster and lath and paneling	Sandstone blocks partial basement		8		9.6			198,199, 201,202 203–209
58	1	40.4×31	26	Brick and masonry	Brick and masonry	Brick and gypsum wallboard	Masonry basement							W–1
59	1	30.5×54		Wood frame	Wood siding	Gypsum wallboard	Continuous concrete footings							W–2
60	2	54×26.5		do	Aluminum siding	do	do							W–4,W–5
61	1	28.5×55.5		do	Brick and plywood	Gypsum wallboard and plaster	Concrete block							W–6
62	2	34.5×48		do	Board and bat	Gypsum wallboard	Slab on grade	11	5	3	8			W–7,W–8
63	2	76.8×80		do	Wood siding	Plaster	Wooden piers on spread footings							W–9,W–10
64	2	34.5×48		do	Board and bat	Gypsum wallboard	Slab on grade							W–11,W–12
65	1	26×25		do	Aluminum siding	do	Continuous concrete footings	8		6				W–13,W–14, W–15
66	1	26.5×34.5		do	Wooden shingles	do	do							W–16,W–17
67	2	19.5×46.5		do	Wood siding	Wood paneling except kitchen ceilings	Concrete block	8		6				W–18,W–19
68	1	55×34		do	Board and bat	Gypsum wallboard	do							W–20,W–21
69	1	41×37.5		do	Aluminum siding	do	do							W–22
70	1	33×44.5		do	Wood panels	do	Continuous concrete footings							W–23
71	1	23.5×23.5		do	Board and bat	Unfinished	do							W–24
72	2	41.5×28.5		do	do	Wallboard paneling	do							W–25,W–26, W–27
73	1	30.5×26.5		do	Asphalt shingles	Plaster	Concrete							W–28,W–29
74	1	28×45		do	do	Wallboard	Slab and concrete block	7	7	6	9			W–28,W–29
75	1	36.5×34		do	Plywood	Gypsum wallboard	Concrete							W–30
76	1	38.5×40.5		do	Wood plank	Wallboard	do							W–31,W–32

Figure 16.—Test structure 20, near a coal mine.

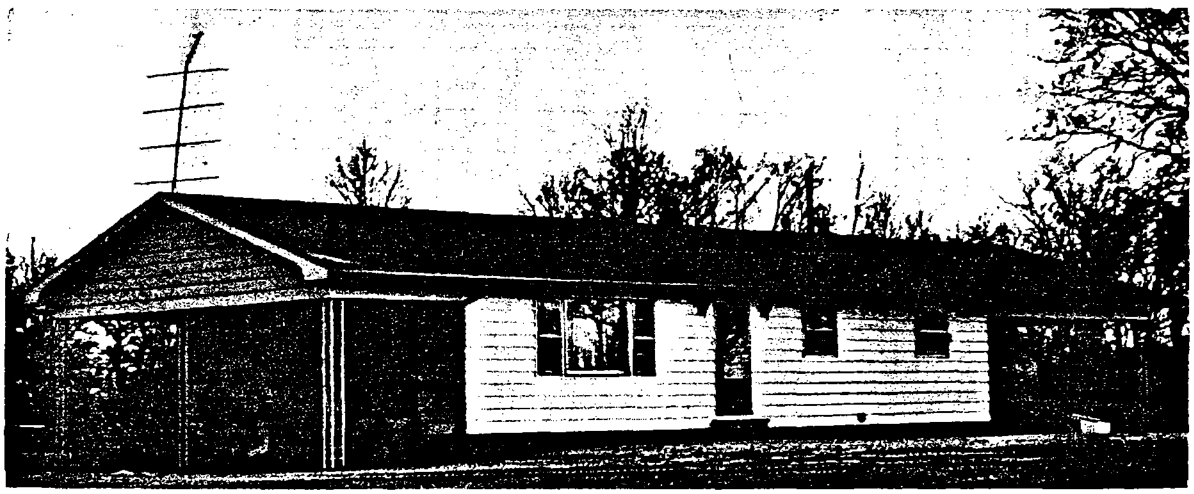

Figure 17.—Test structure 21, near a coal mine.

Figure 18.—Test structure 22, near a quarry.

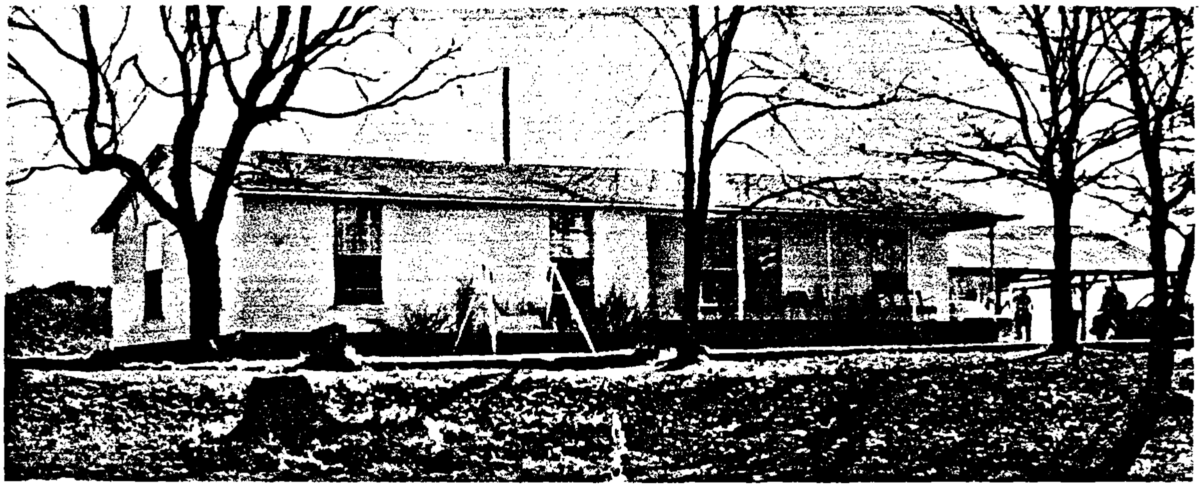

Figure 19.—Test structure 23, near a quarry.

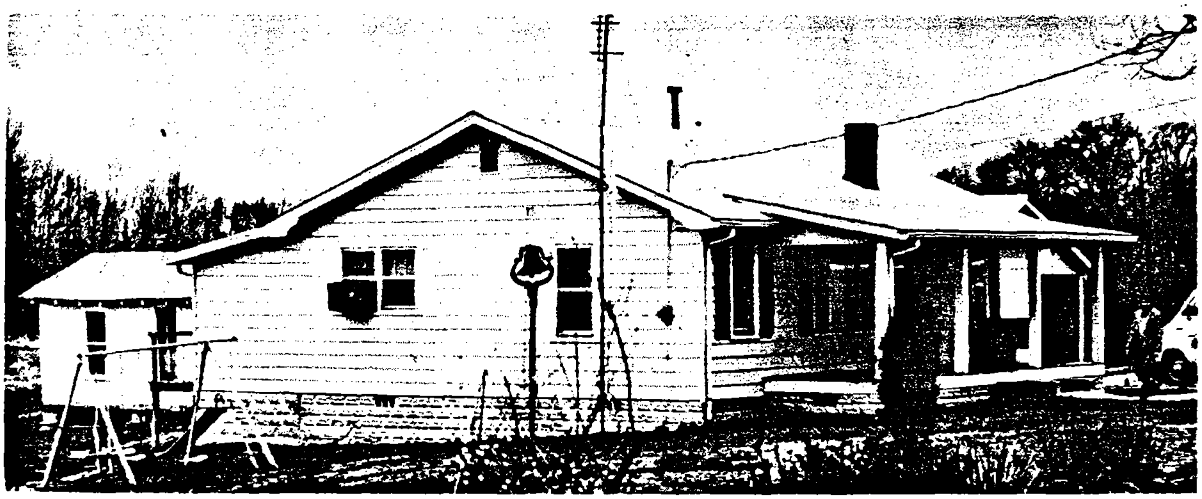

Figure 20.—Test structure 26, near a coal mine.

Figure 21.—Test structure 27, near a coal mine.

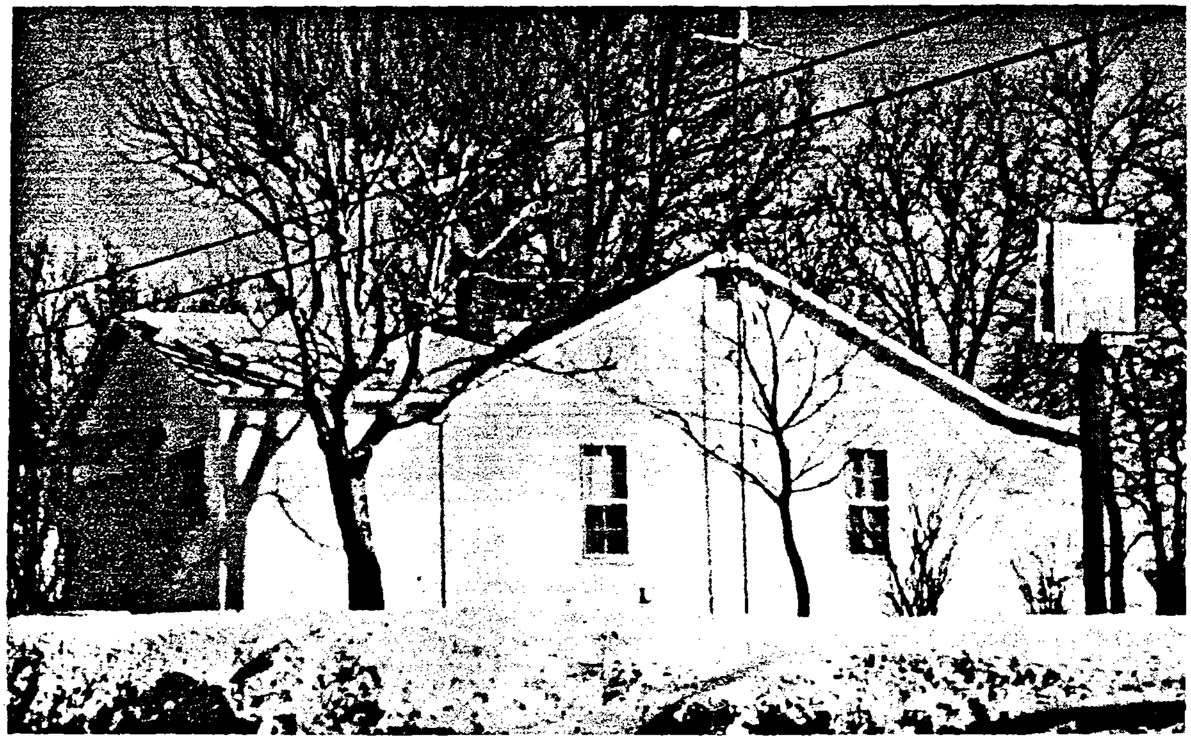

Figure 22.—Test structure 28, near a coal mine.

Figure 23.—Test structure 29, near a coal mine.

Figure 24.—Test structure 30, near a coal mine.

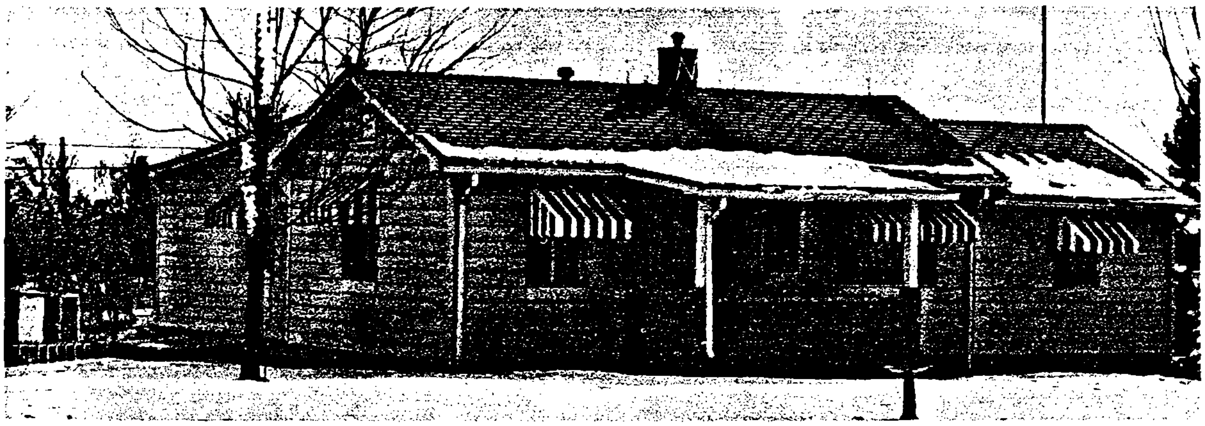

Figure 25.—Test structure 31, near a coal mine.

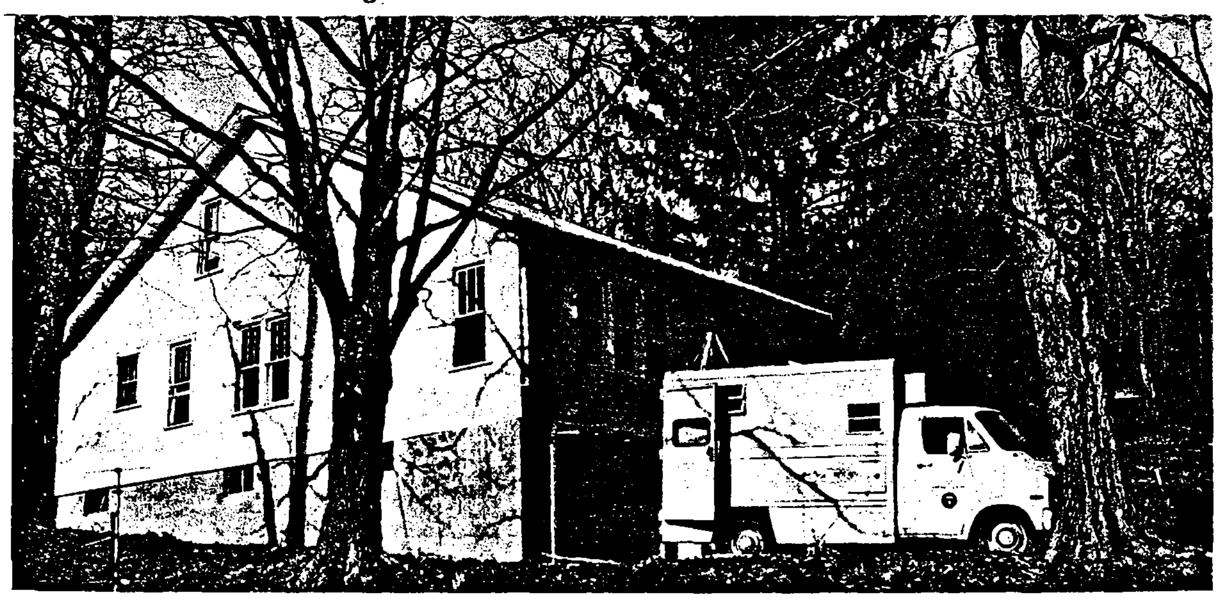

Figure 26.—Test structure 49, near a coal mine.

Figure 27.—Test structure 51, near a coal mine.

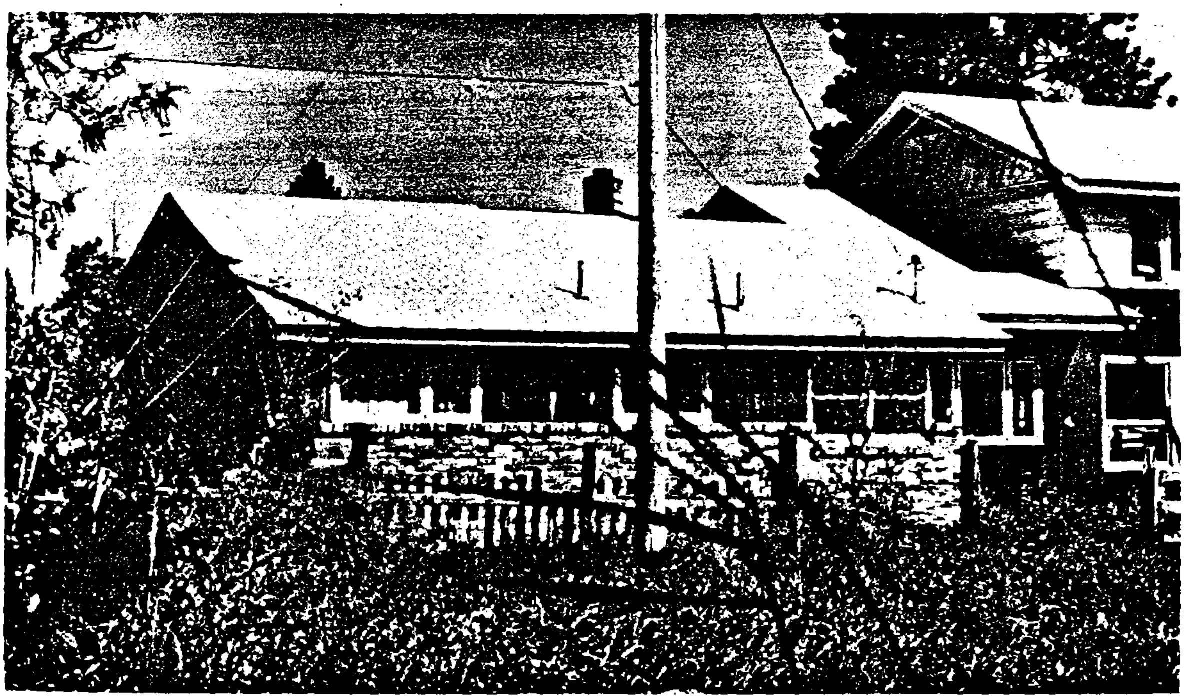

Figure 28.—Test structure 61, near a ~~coal mine~~.

Construction Site

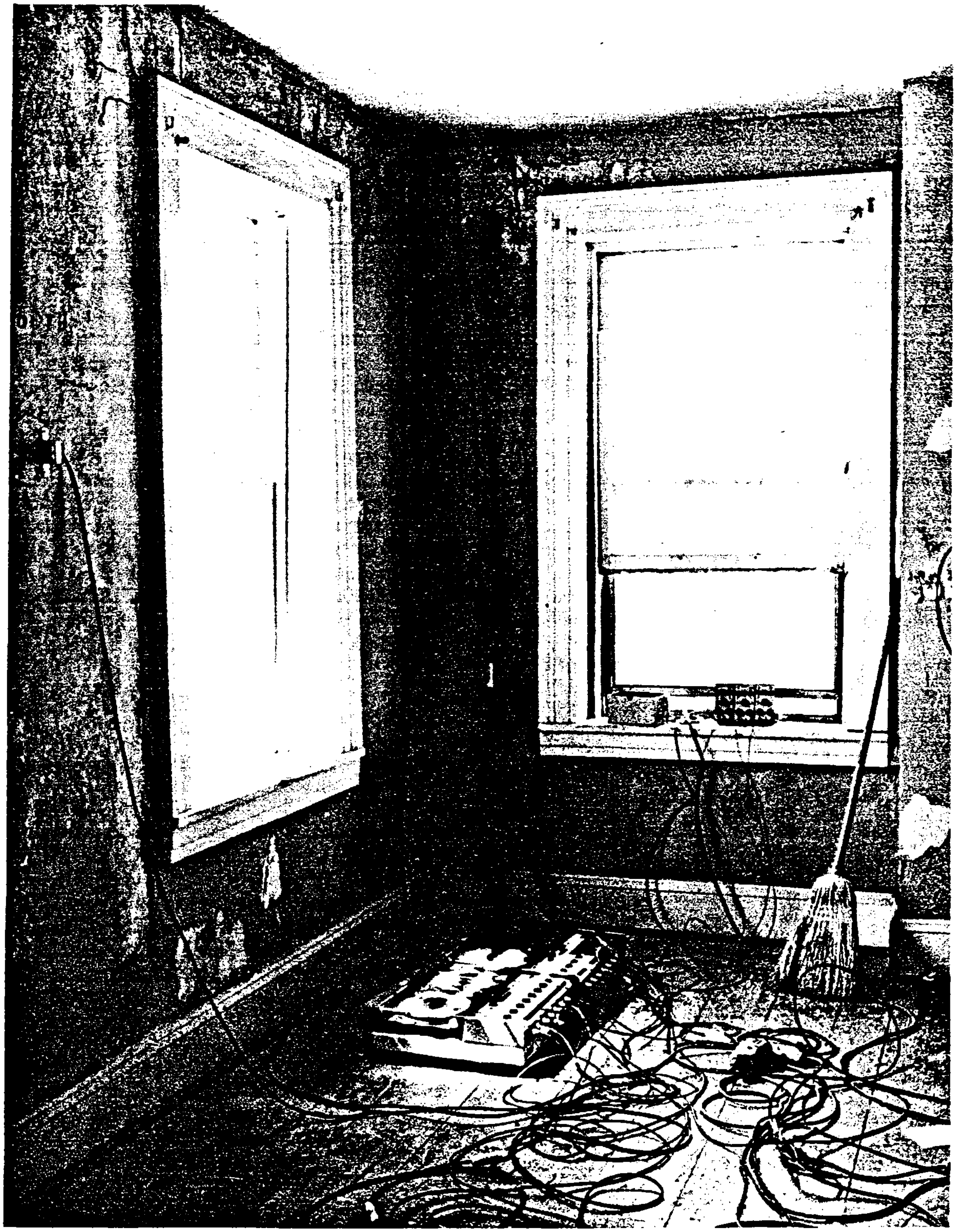

Figure 29.—Vibration gages mounted in corners and on walls for measuring structure response in structure 51.

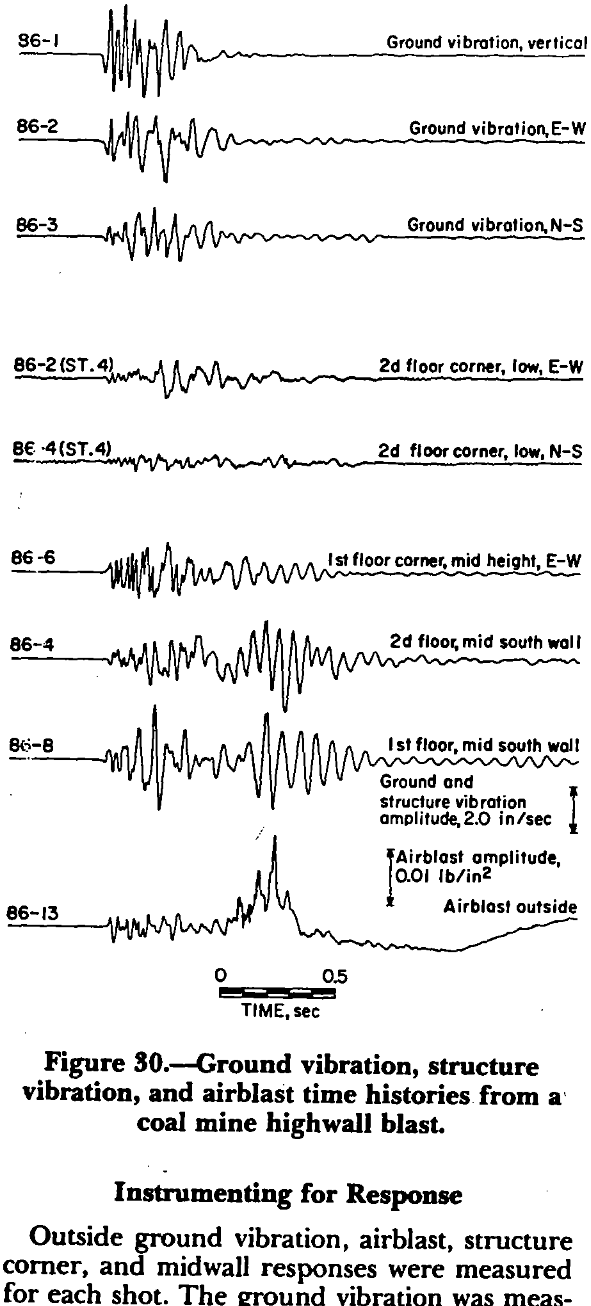

Figure 30.—Ground vibration, structure vibration, and airblast time histories from a coal mine highwall blast.

Instrumenting for Response

Outside ground vibration, airblast, structure corner, and midwall responses were measured for each shot. The ground vibration was measured by three orthogonal 2.5-Hz velocity gages buried about 12 inches in the soil next to the foundation (*50*). Outside airblasts were measured with at least one pressure gage and two sound level meters, one reading C-slow (*46*). The structures were instrumented for horizontal motions by a pair of gages mounted on the first-floor vertical walls in the corner closest to blasts and on one or more midwalls (fig. 29). Typically, the vertical motion was also measured in the same corner. Extra recording channels that were available were used for additional corner motions (at midheights, near the ceiling, or on the next floor); additional floor motions (e.g., midfloor verticals); basement wall horizontals; opposite corner responses (for torsional motions); and inside noise. A typical set of time histories is shown in figure 30. This particular shot produced strong airblast responses of the midwalls.

Natural Frequency and Damping

Natural frequency, ω_n, and damping, β, are the most important structure response characteristics. The structural natural frequencies as measured from blast-produced corner motions are summarized in figure 31, with individual values listed in table 3. Structures continue to vibrate after the sources (ground vibration and airblast) decay, and natural frequencies and damping can be measured from these free vibration time histories. The variations of structures, especially midwalls, are approximately sinusoidal; therefore, the natural frequencies are the inverse of the periods in seconds. Damping values calculated from free vibration motions are given by:

$$\beta = \frac{100}{2\pi m} \mathrm{Ln}(A_n/A_{n+m}),$$

where β is the percent of critical damping, A is the peak amplitude at the nth cycle, and m is any number of cycles later. Dowding (*13*) and Langan (*24*) discuss the general problem of structure frequencies and damping. Their works include transfer function methods for calculating ω_n and β as well as amplitude-dependence of the damping value. Murray (*32*) computed many of the damping and frequency values in table 3, some of which were later reanalyzed by Langan (*24*).

Little difference in natural frequencies was observed among 1- and 1½-story homes; however, that for the 2-story homes was lower. Dowding (*13*) found average natural frequencies for the three types of homes of 8.0, 7.4, and 4.2 Hz, respectively. Medearis (*30*) measured frequencies and damping values for 61 houses and found similar results, except for some higher frequencies for the 1- and 1½-story homes. He found frequency ranges of 8 to 18 Hz (1-story), 7 to 14 Hz (1½-story) and 4 to 11 Hz (2-story). Damping, found by both investigators to vary between 2 and 10 pct, is summarized in figure 32.

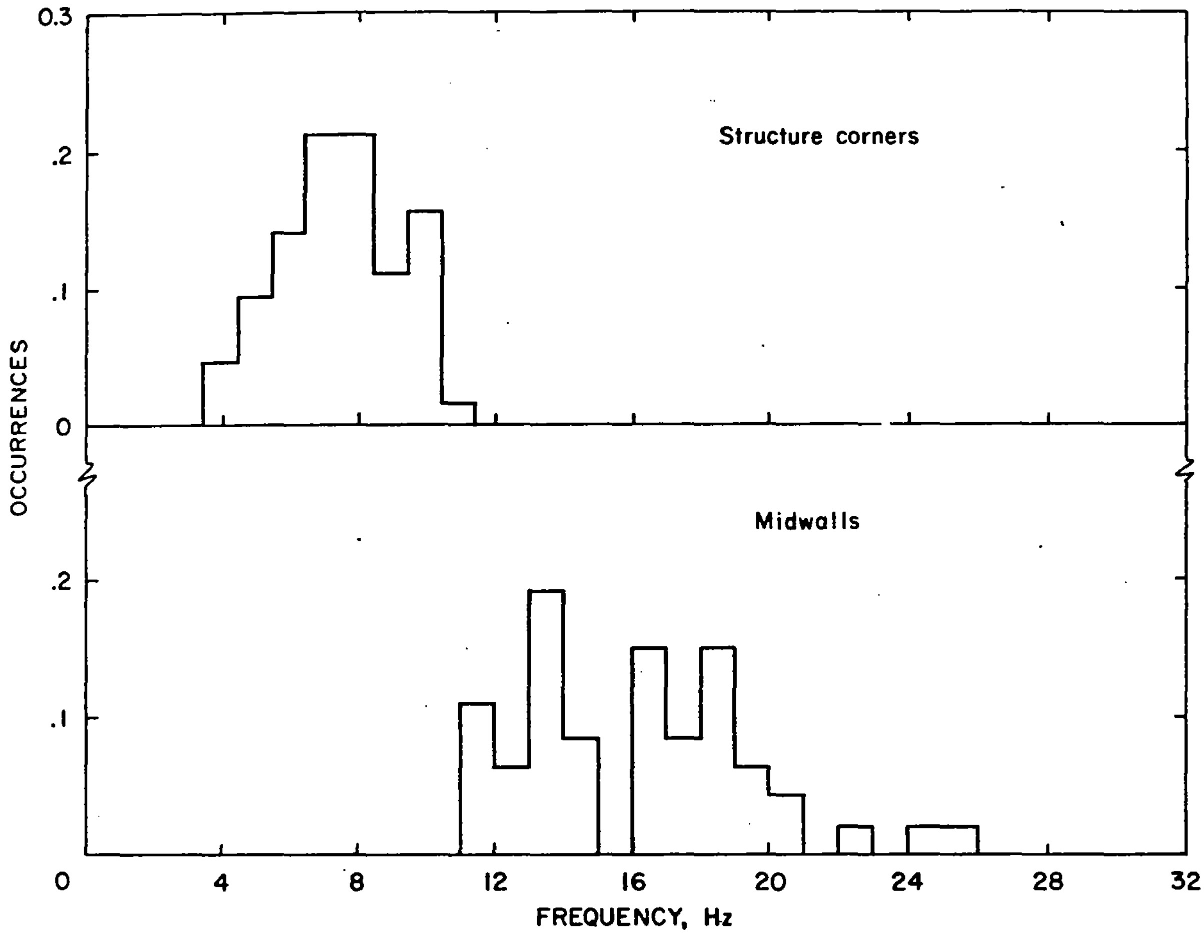

Figure 31.—Residential structure natural frequencies.

Production Blasting

Levels of structure response and incidents of damage were sought for 225 production blasts (table 2). A wide range of charge sizes, distances, geologies, and blast types produced vibrations of various peak values, durations, and frequency character. Quarries in urban areas had high free faces, used multiple decks, and had hole diameters seldom exceeding 5 in. Shots 21 to 30 were in an isolated quarry with high vibration levels at the close-in locations, but no house vibration measurements were made.

Coal mine highwall blasts varied from well-confined blasts producing no throw whatsoever, to quarry-type blasts with three free faces (top, front, and one side). Where ground vibration appeared to be more serious than airblast, design emphasis for production blasts was placed on sufficient relief (maximum number of free faces). Parting shots involved blasting a thin and often hard rock layer, and often produced high levels of airblast and low ground vibration. An extensive study of blast design and resulting vibration levels and character was made by Wiss (*56*) and will not be discussed further in this report.

Velocity Exposure Levels

In addition to analyzing particle velocity time histories for peak values and frequency character, ground vibrations were also processed for velocity exposure levels (VEL), which are analogous to sound exposure levels (SEL) for noise (*22, 49*). These methods measure the energy of a signal within specified frequency limits and time intervals. The use of VEL to assess structure response is a possible alternative technique to using the simple peak levels of the particle

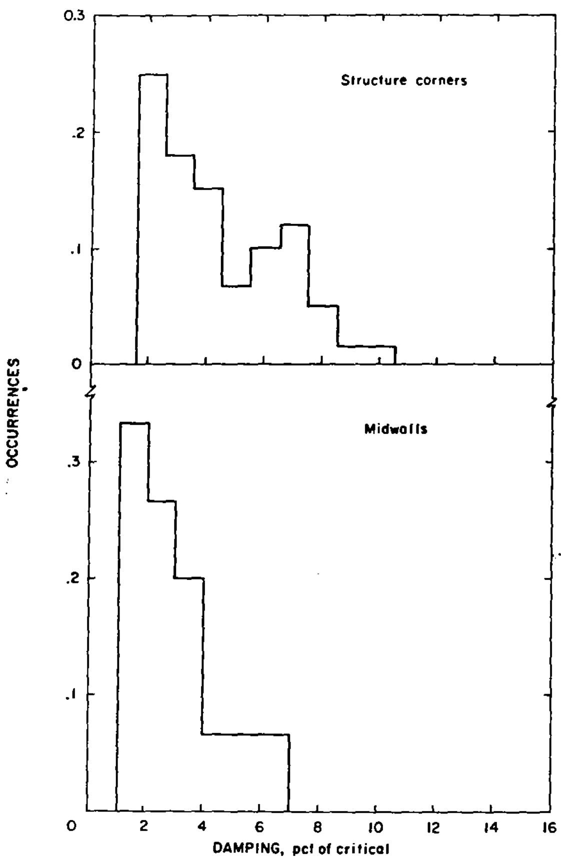

Figure 32.—Residential structure damping values.

velocity and also to response spectra techniques. The ideal VEL is normalized to 1 sec; therefore, this penalizes excessively long events (3 dB per doubling of duration) and allows higher levels for short-duration events. Current field practice involves the use of an rms system (e.g., sound level meter) with either ⅛- or 1-sec time constants and optional filtering.

Velocity exposure levels were determined for 200 of the measured blasts, with an rms detecting and filtering system described by Stachura (*49*) and defined by:

$$\mathrm{VEL} = 10 \log_{10} \left[\frac{1}{t_o} \int_o^T v^2 (t)\, dt \right]$$

where $t_o = 1$ sec, v(t) the time-varying filtered particle velocity, and T the various integration times. A filter range of 1 to 12 Hz was employed to include the range of whole-structure natural frequencies. Integration times were ⅛, ¼, 1, and 2 sec. The 1-sec time was an overall compromise that was long enough to include all the significant energy in a typical mine blast vibration measure near the source. VEL values were also determined for structure as well as ground motions.

Structure Responses From Blasting

Structure and midwall responses from production mine blasting are shown in figures 33–37, with the statistics given in table 4. In all cases, the corner and midwall responses from any given blast were plotted against the corresponding ground vibration components. The horizontal vibration components did not necessarily correspond to the true radial (or longitudinal) and transverse, since the velocity gages were oriented parallel to the structure walls.

Most interesting is that the racking response (absolute corner horizontal vibration) as shown in figures 33 and 34 is significantly lower than the input ground vibration velocity, when measured at either the first or second floor, or low or high in the corner. The vertical ground and structure corner vibrations were roughly equal as expected (figs. 33 and 36). The differences in the responses between types of blasts were significant. However, very little difference was observed between the 1- and 2-story structures.

All the responses discussed in this paper are applicable to residential-type structures with wood frame superstructures. The values do not apply to multistory steel frame structures or large structures with masonry load-supporting walls. The natural frequencies of vibration of these structures could be considerably lower than the 4 to 24 Hz range for residences and their midwalls.

The ground motion VEL did not correlate significantly better to the measured peak or VEL of the structure than the use of simple peak versus peak. Consequently it is recommended that peak velocities continue to be the primary measure of ground motion to assess the damage potential to residential-type structures and for regulatory purposes. However, it is recognized that for engineering, design, and research involving a variety of types of structures and sources, a measurement of simple peak particle velocity is an oversimplification. Some type of direct measurement of response (preferably dynamic strain) or model prediction (such as response spectra) would be appropriate in such cases.

Amplification Factors

Several analyses were made of structure response amplifications of the ground vibrations. The Bureau of Mines structure motion data were analyzed by Murray (*32*), Langan (*24*), and Dowding (*13*) for Fourier transfer functions and response characteristics. They discussed the problem of "ghost" resonances (dividing a small apparent response in the spectrum of the structure's motion by an even smaller spectral value in the ground motion).

A simpler amplification factor was determined directly from the vibration time histories. Maximum structure velocities and their times of occurrence were noted. Ground velocities and frequencies were then picked off the records at the corresponding moments of time or immediately preceding the time of the peak structure vibrations. The ratios of the two velocities are plotted in figures 38–40 against the frequency of the corresponding ground motion peak. Amplification factors for the racking response of a 1-story and a 2-story structure are shown in figure 38. Maximum amplifications were found to be associated with ground motions between 5 and 12 Hz, as expected from the natural resonance frequencies of the residences. Because

Table 4.—Equations and statistics f ›r peak structure responses from ground vibrations

Descriptor[1] and mine type	Stories, home	Equation	Correlation coefficient	Standard error, in/sec	Normalized std. error, in/sec	Regression line (figs. 33–37)	Number of points
Max.H SV versus Max. H GV:							
Coal	1	SV = 0.049 + 0.557GV	0.936	0.084	0.090	NAp	36
Do	2	SV = .075 + .553GV	.870	.151	.174	NAp	34
Do	All	SV = .060 + .559GV	.898	.120	.120	1	70
Construction	All	SV = .136 + .230GV	.599	.140	.234	2	13
Iron range	All	SV = .052 + [illegible]976GV	.894	.117	.130	3	10
All	1	SV = 0.87 + [illegible]435GV	.741	.169	.228	NAp	50
All	2	SV = .082 + [illegible]61GV	.862	.141	.163	NAp	53
All	All	SV = .084 + .496GV	.800	.157	.197	4	103
Vert. SV versus Vert. GV:							
Coal	1	SV = .048 + .771GV	.928	.063	.068	5	26
Do	2	SV = .070 + 1.124GV	.880	.335	.335	6	62
Do	All	SV = .044 + 1.131GV	.892	.286	.320	NAp	88
Construction	1	SV = .112 + .230GV	.568	.127	.223	7	11
Do	2	SV = .090 + .529GV	.859	.233	.271	8	7
Do	All	SV = .054 + .424GV	.741	.193	.260	NAp	18
All	1	SV = .035 + .738GV	.905	.208	.230	NAp	37
All	2	SV = .115 + .942GV	.896	.364	.406	NAp	69
All	All	SV = .073 + .907GV	.893	.330	.370	NAp	106
Max.H midwall, SV versus Max.H GV:							
Coal	1	SV = .154 + 1.347GV	.927	.228	.246	9	47
Do	2	SV = .153 + 1.636GV	.920	.358	.389	10	53
Do	All	SV = .146 + 1.534GV	.918	.310	.337	NAp	100
Construction	1	SV = .191 + .300GV	.754	.121	.160	NAp	8
Do	2	SV = .170 + .928GV	.754	.202	.268	NAp	7
Do	All	SV = .269 + .275GV	.524	.194	.371	11	15
Quarry	All	SV = .025 + 1.106GV	.886	.202	.228	12	19
Iron range	All	SV = .029 + 2.546GV	.722	.147	.203	13	16
All	1	SV = .196 + .904GV	.868	.331	.382	NAp	77
All	2	SV = .218 + 1.181GV	.776	.498	.642	NAp	82
All	All	SV = .217 + 1.002GV	.803	.431	.537	NAp	159
Coal, single home:							
Max.H SV versus MaxH GV	2	SV = .114 + .472GV	.894	.114	.161	14	35
H_1 SV versus H_1 GV	2	SV = .114 + .472GV	.894	.144	.161	NAp	35
H_2 SV versus H_2GV	2	SV = .019 + .370GV	.906	.091	.101	NAp	37
Max.H SV versus Max VEL H GV	2	SV = .128 + 2.451GV	.812	.189	.232	15	37
H_1 SV versus VELH$_1$GV	2	SV = .128 + 2.451GV	.812	.189	.232	NAp	37
H_2 SV versus VELH$_2$ GV	2	SV = .057 + 1.563GV	.854	.113	.132	NAp	38
Max.H SV versus TVS GV	2	SV = .110 + :299GV	.789	.143	.181	16	28
Max.HSV versus VELTVS GV	2	SV = .158 + 1.171GV	.763	.211	.276	NAp	29
Vert.SV versus Vert.GV	2	SV = .140 + 1.119GV	.852	.403	.472	17	33
Max.H midwall SV versus MaxH. GV	2	SV = .152 + 1.567GV	.905	.428	.472	18	28
Midwall H_1 SV versus H_1 GV	2	SV = .151 + 1.567GV	.905	.428	.472	NAp	28
Midwall H_2 SV versus H_2 GV	2	SV = .514 + 1.517GV	.830	.431	.519	NAp	37
Max.H SV versus PVS GV	2	SV = .092 + .267GV	.781	.128	.164	19	26

NAP = Not applicable.

[1] Symbols SV = Structure vibrations, in/sec (unless specified "midwall" all SV are corner vibrations).
GV = Ground vibration.
Max.H = Maximum horizontal component of vibration.
Vert. = Vertical component of vibration.
H_1 = Horizontal component of vibration best approximating radial.
H_2 = Horizontal component of vibration perpendicular to H_1.
VEL = Velocity exposure level (1-second integration, 1–12Hz).
TVS = True vector sum.
PVS = Pseudo vector sum.

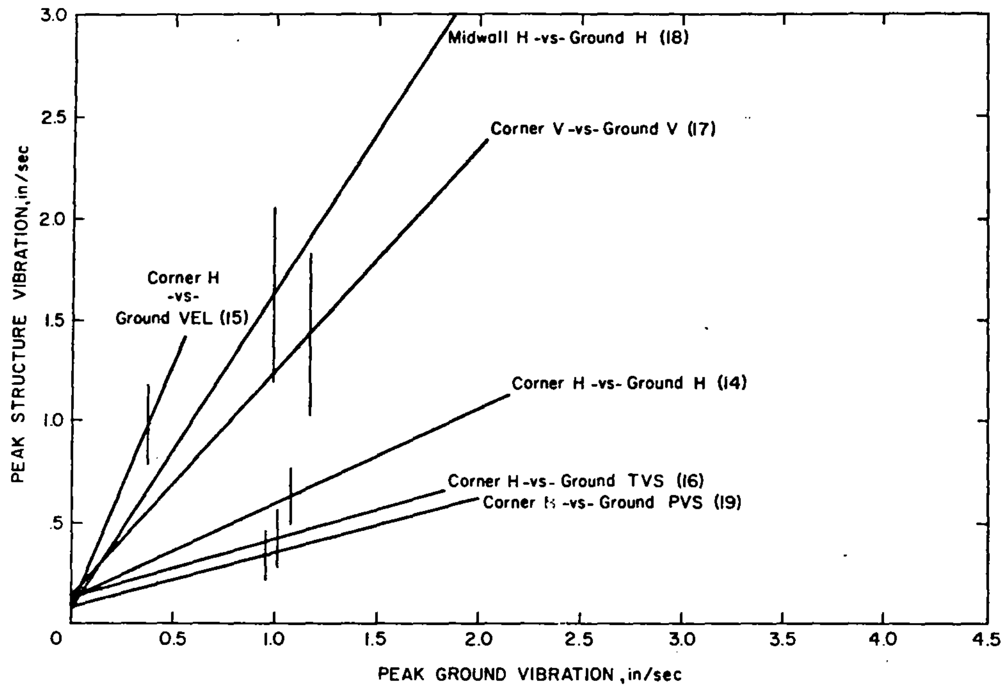

Figure 33.—Corner and midwall responses for a single structure (No. 19). Symbols, equations, and statistics are given in table 4.

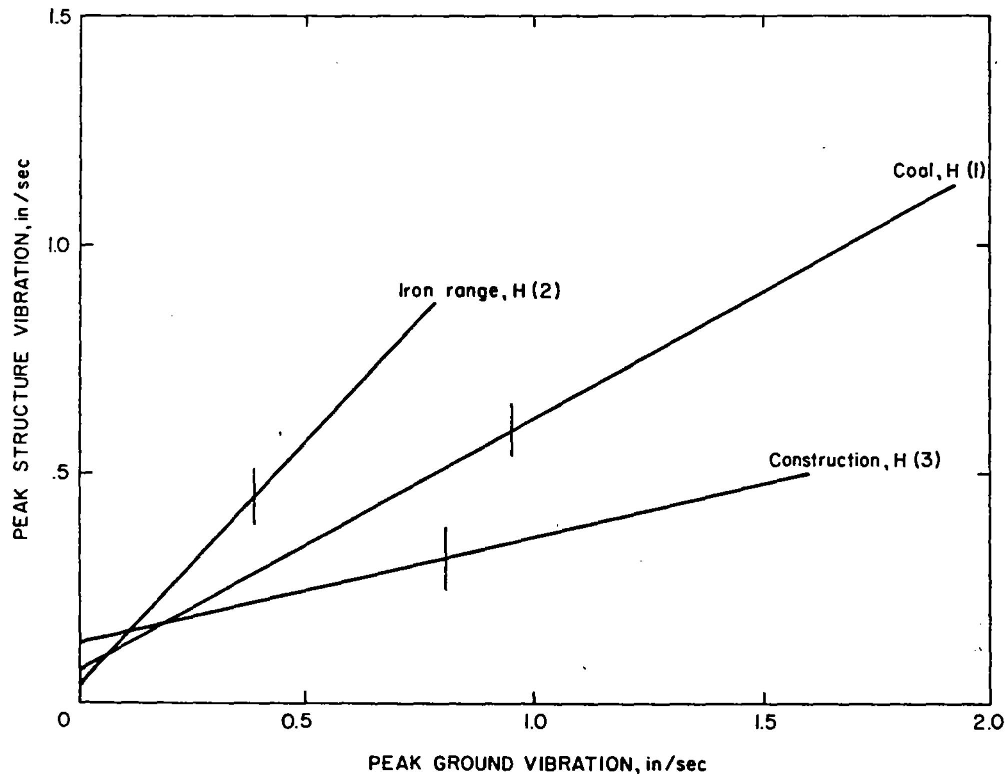

Figure 34.—Structure responses (corners) from peak horizontal ground vibrations, summary. Symbols, equations, and statistics are given in table 4.

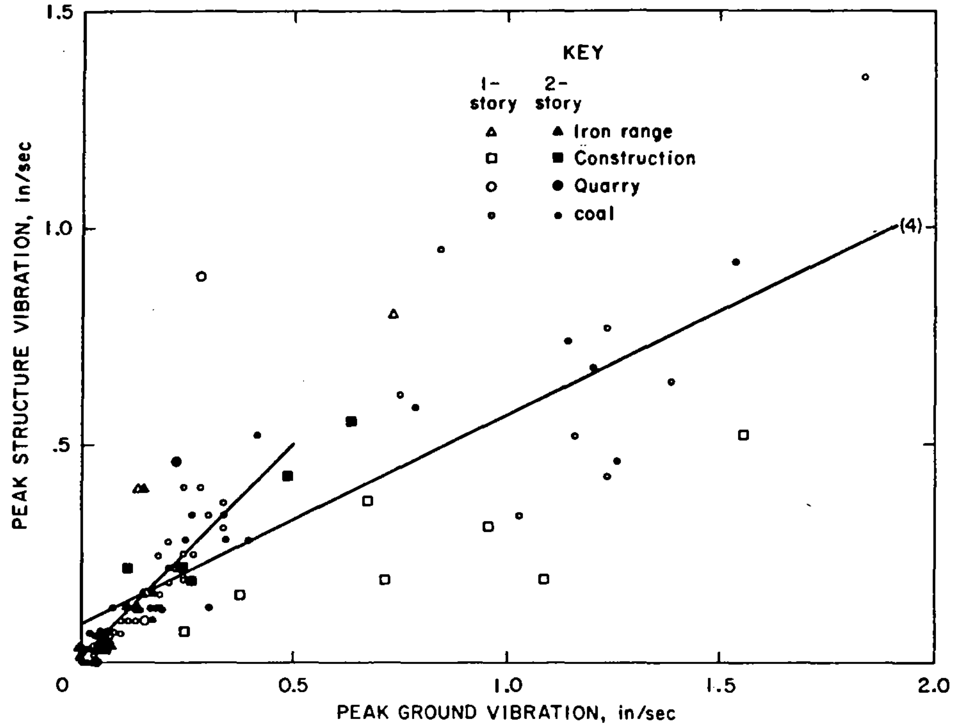

Figure 35.—Structure responses (corners) from peak horizontal ground vibrations with measured values. Equations and statistics are given in table 4.

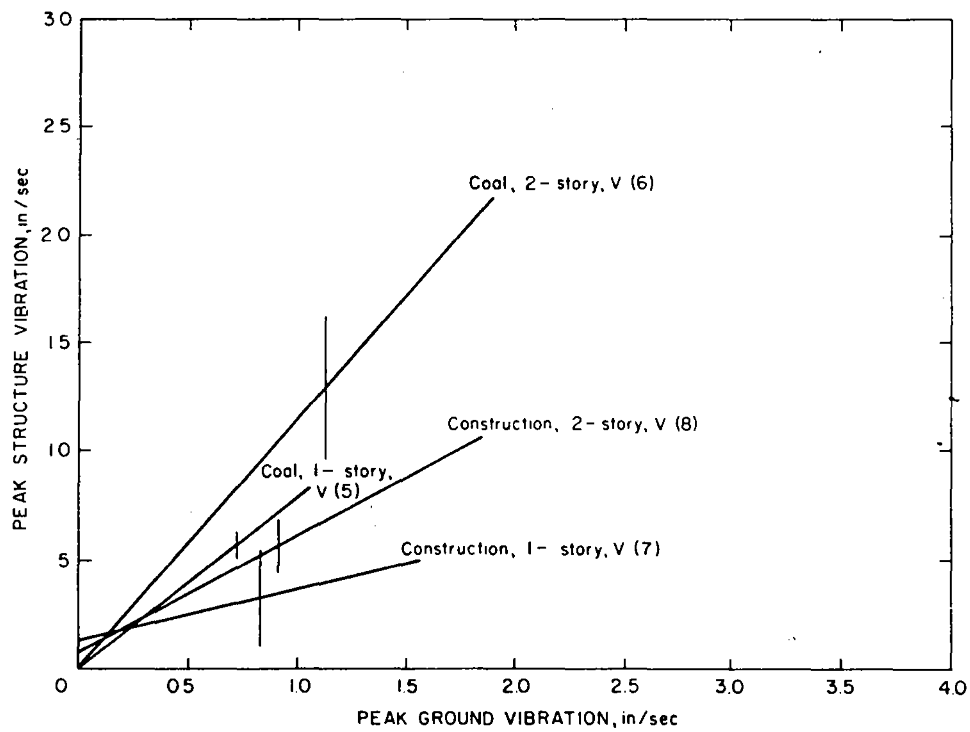

Figure 36.—Structure responses (corners) from peak vertical ground vibrations. Symbols, equations, and statistics are given in table 4.

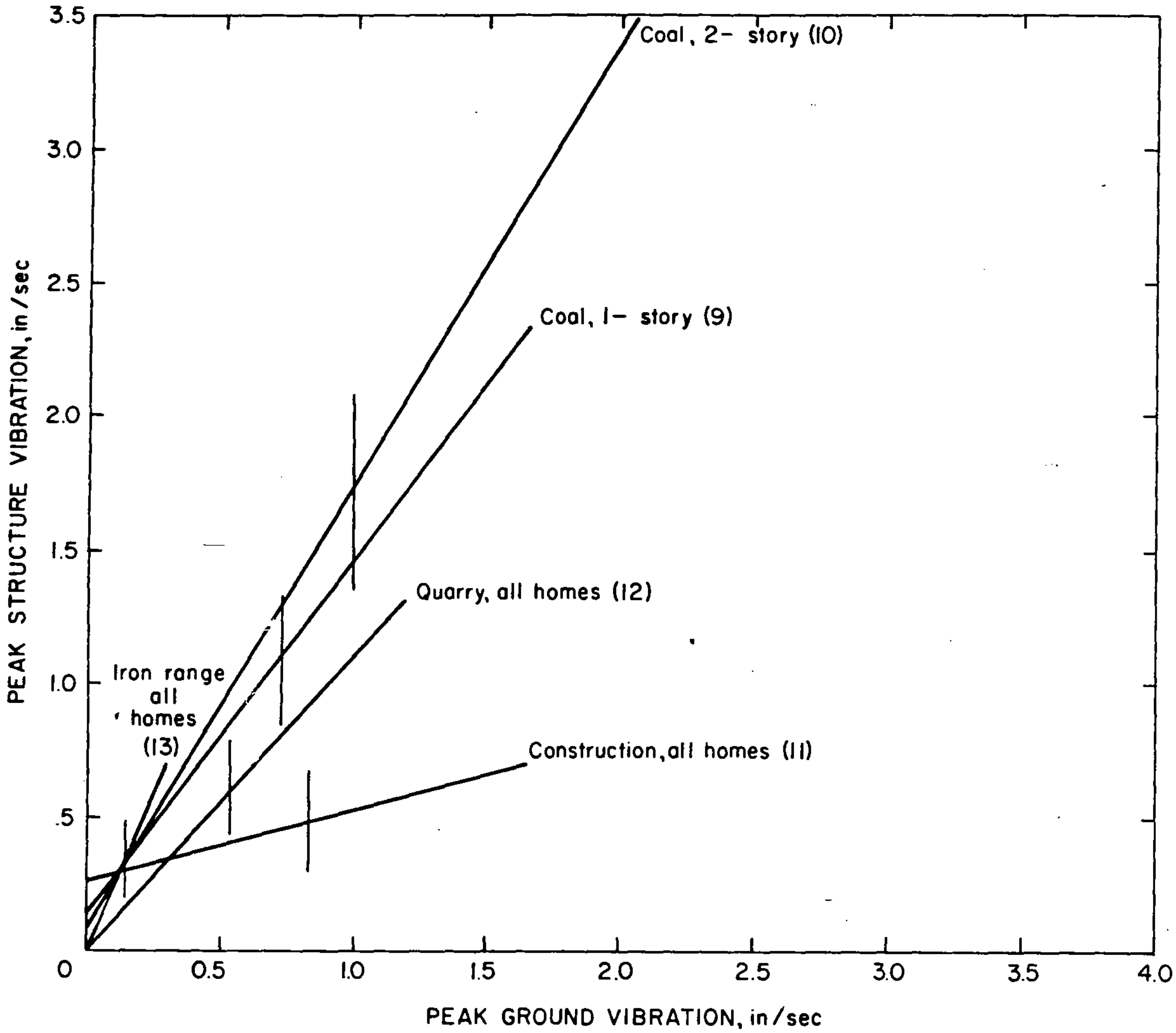

Figure 37.—Midwall responses from peak horizontal ground vibrations. Equations and statistics are given in table 4.

absolute, rather than relative, structure motions were measured, the responses at ground motion frequencies lower than the resonant frequencies theoretically should be unity; however, no ground motions with significant energy at frequencies lower than 5 Hz were encountered in this investigation. A summary of corner motion amplification factors for all of the homes studied is shown in figure 39. The highest amplifications were approximately 4, with 1.5 being a typical value. Ground motions above about 45 Hz produced little or no amplification of the corner-measured structure motion.

Midwall motion amplification factors are shown in figure 40. The maximum amplifications are greater than for the corners, with many responses occurring at higher frequencies, particularly up to 25 Hz. As with corner motions, amplification factors for ground motions above 45 Hz were less than unity.

These results suggest that frequencies below 10 Hz are most serious for potential damage from structure racking. Vibrations below about 25 Hz can excite high levels of midwall motion (typically wall motions are amplified 4 times that of the ground motions) and generate most of

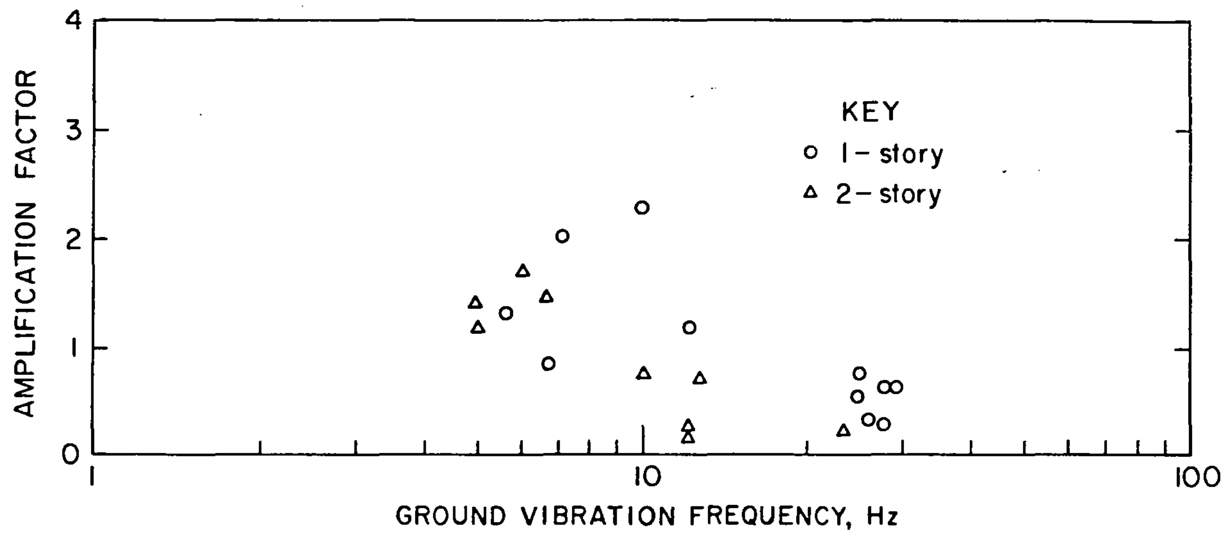

Figure 38.—Amplification factors for blast-produced structure vibration (corners) of a single 1-story and a single 2-story house.

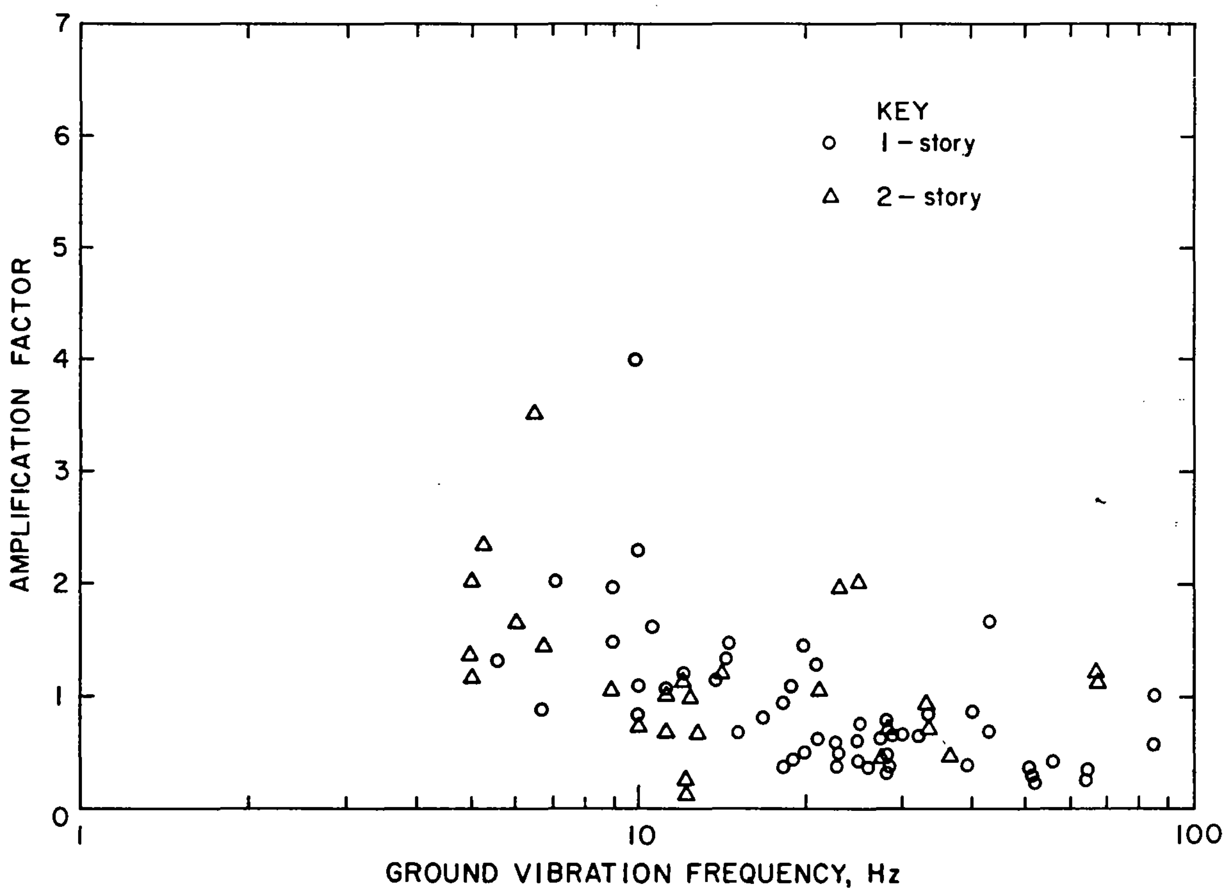

Figure 39.—Amplification factors for blast-produced structure vibration (corners), all homes.

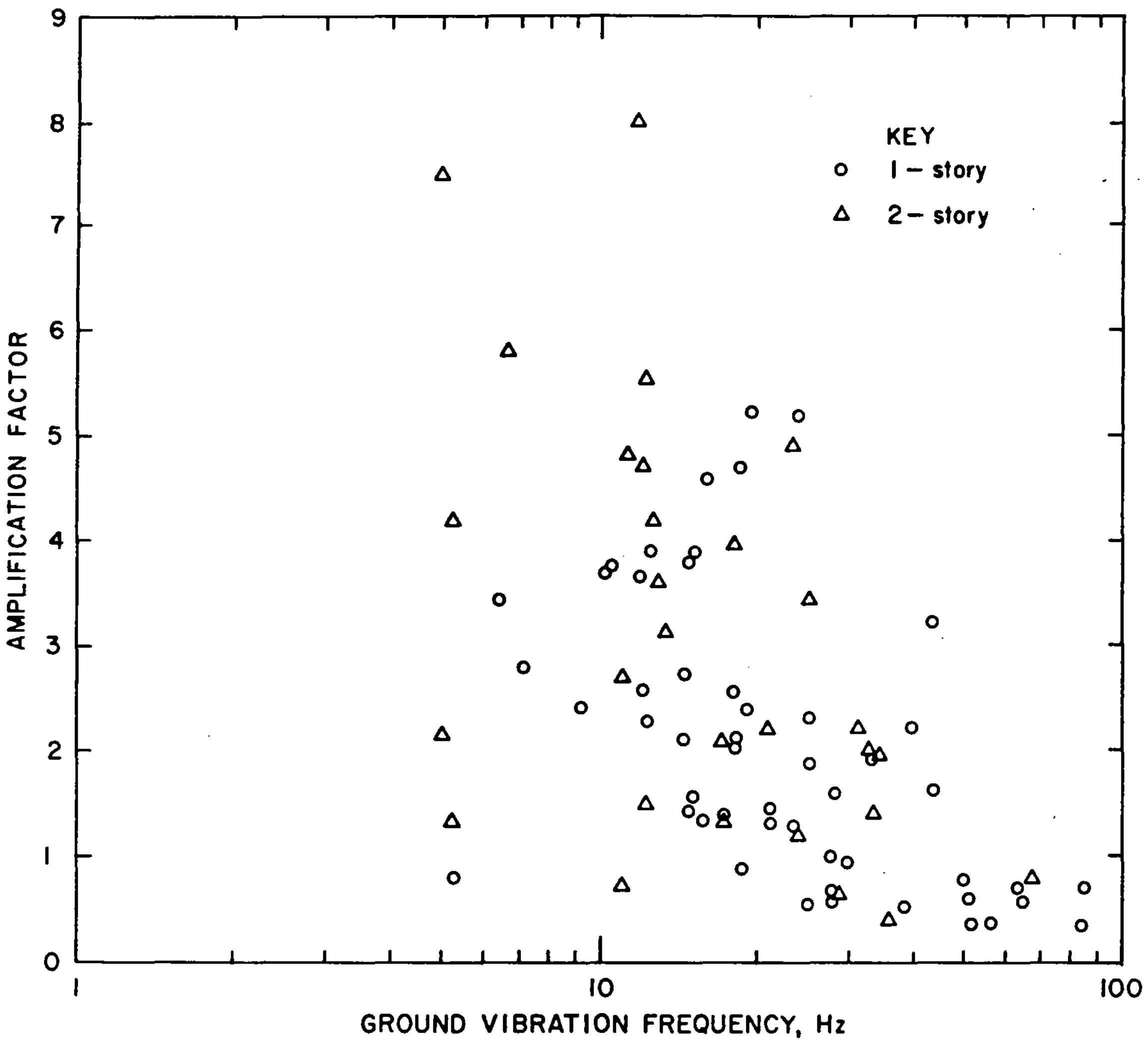

Figure 40.—Amplification factors for blast-produced midwall vibration, all homes.

the secondary noises, rattling, and other annoyances.

Kamperman studied transfer functions for residences subjected to quarry blasts (*22*). His concern was primarily with human response to midspan vertical floor motions, and an assessment of various airblast measurement descriptors. Kamperman made 23 comparisons between measured outside ground and inside floor motions from 18 blasts. He found amplification factors of 1.60 for vertical peak particle velocity and 1.04 for horizontal velocity (lateral or radial).

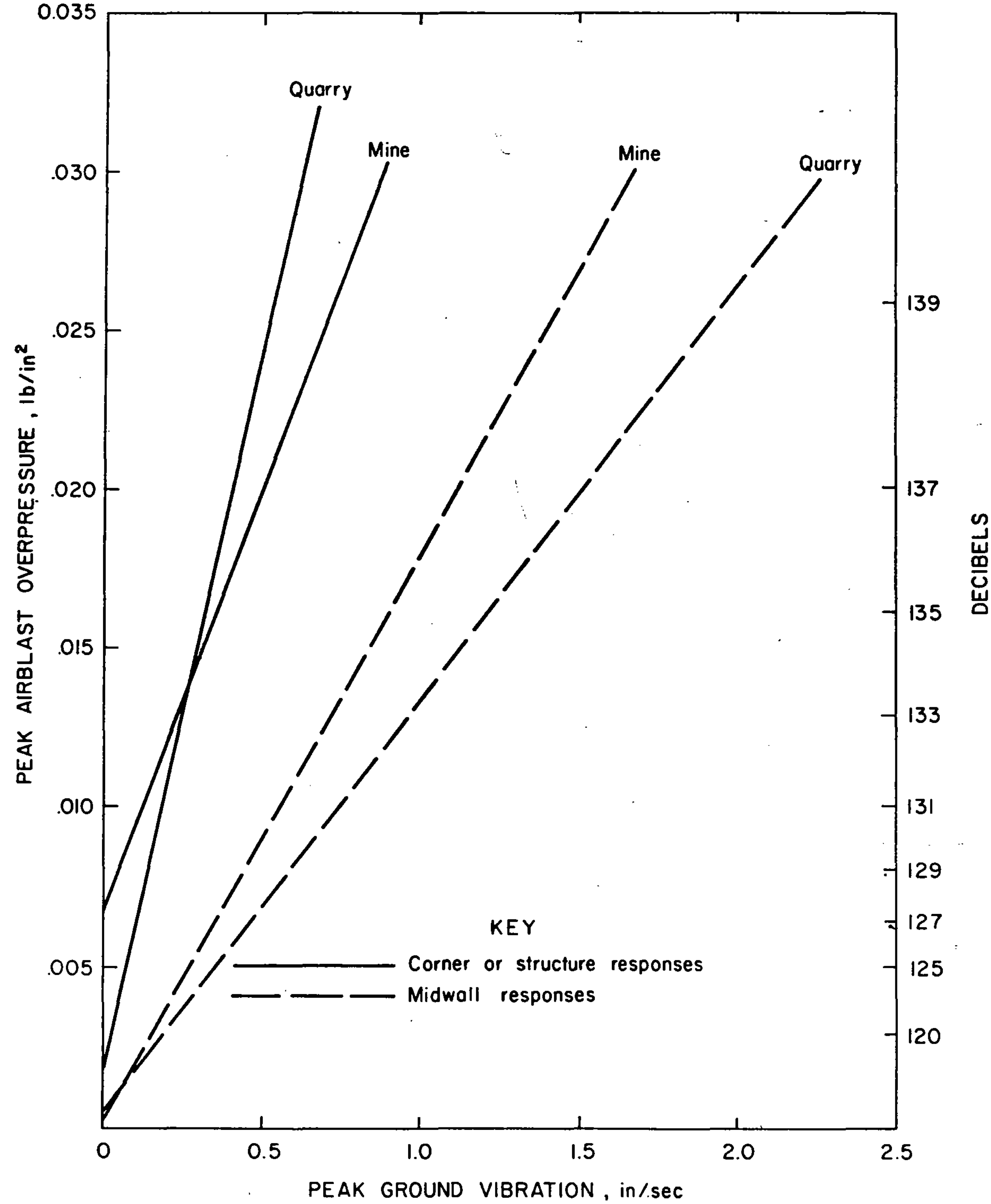

Figure 41.—Ground vibration and airblast that produce equivalent amounts of structure response, in frame residential structures of up to 2 stories.

Figure 42.—Test residential fatigue structure near surface coal mine. AYRSHIRE

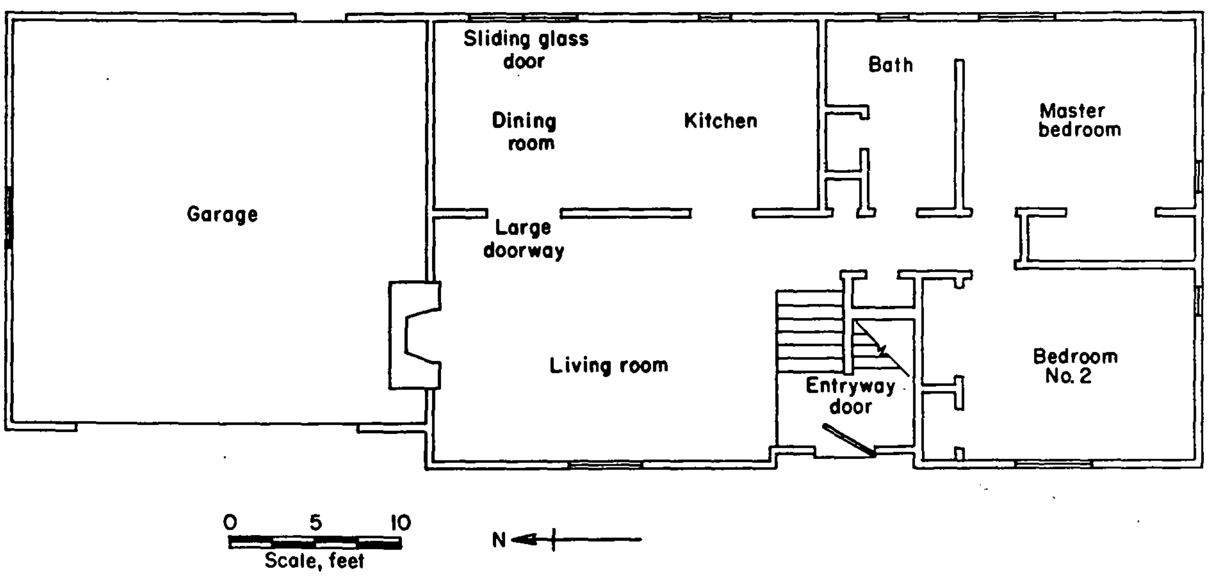

Figure 43.—Plan of main floor of test fatigue structure shown in figure 42.

Airblast Response

Structure responses from airblasts and sonic booms have been described in an extensive analysis of airblast from surface mine blasting (*46*). Levels of ground vibration and airblast that produce the equivalent structure motions are shown in figure 41, based on mean observed responses. The airblasts are those measured with 0.1-Hz low-frequency response systems. Typical 2- and 5-Hz commercial systems would give airblasts with sound levels in the range of 1 to 5 dB lower. Airblasts are relatively strong sources of midwall vibrations and poor sources of corner (whole-structure racking) vibration. The airblast levels producing the same amounts of corner vibration as 0.50 in/sec ground vibration are 0.020 to 0.024 lb/in^2 (137 to 138 dB). Relatively strong midwall vibrations are produced by airblasts, with only 0.007 to 0.009 lb/in^2 (128 to 130 dB) required to produce wall vibration equivalent to that from 0.50 in/sec ground vibration. From these equivalencies, airblast appears less likely to crack walls than ground vibration, as cracking occurs predominantly from shear and tensile wall strains that are produced by shearing rather than bending. Airblasts, however, are often responsible for the secondary rattling and annoyance effects produced by midwall motions (perpendicular to the planes of the wall surface).

Differences between mine and quarry blast-produced corner responses are not significant in the critical airblast range of 0.010 to 0.016 lb/in^2 (131 to 135 dB). By contrast, the midwall responses are very much different, probably because the relatively less confined quarry blasts produce more and higher frequency airblasts.

Structure Responses From Everyday Activities

Houses are subjected to a variety of vibrations and strains from human-produced transients and from slower processes of settlement from soil consolidation and changes in both the house and ground from natural environmental influences. The Bureau of Mines has measured strain and vibration from both human activities and from five mine blasts as the beginning of a study on fatigue effects in a residential structure.

The test structure and plan view are shown in figures 42 and 43. Strains were measured at critical places over windows and doorways using gages developed from a Northwestern University model (*11*). The maximums of the three strains measured at each location are given in table 5. The maximum principal strains would be slightly greater. Vibrations were measured in low and high corners, midfloors, and midwalls for both the blasts and the other activities (table 6).

Surprisingly high levels of strain and vibration were generated by the human activities. Comparisons between the blast- and human-produced effects suggests that house superstructures are continuously subjected to transients producing localized strains equivalent to ground vibrations of up to 0.50 in/sec. Additionally, it was found that effects produced in one part of the house (i.e., a front door slam) could produce significant strains all over the structure. No measurements have yet been made on the masonry facade or the basement floor or walls.

Table 5.—Strains in fatigue test structure from blasting and human activity

Strain locations	Maximum structure strains, µin/in						
				Door slams			
	Mine blasts	Jumps	Heel drops	Entrance	Sliding glass	Nail pounding	Walking
Over sliding glass door	[1]22,[2]15	24	9.2	13	22	21	Low
Over south window in master bedroom	[3]18	42	20	12	19	9.3	9.1
Over large doorway in living room	[4]24,[5]11	17	6.1	8.3	6.2	28	Low
Over picture window	[4]33	17	11	21	3.6	32	3.2
Over entrance door	[4]36,[5]43	13	5.8	140	Low	Low	Low

[1] From peak ground vibration of 0.300 in/sec, 129 dB airblast.
[2] From peak ground vibration of 0.210 in/sec, 124 dB airblast.
[3] From peak ground vibration of 0.290 in/sec, 124 dB airblast.
[4] From peak ground vibration of 0.470 in/sec, ~~111~~ dB airblast. 119
[5] From peak ground vibration of 0.320 in/sec, 125 dB airblast.

Table 6.—Structure vibrations in test fatigue structure from blasting and human activity

Vibration location	Mine blasts	Maximum structure vibrations, in/sec					
		Jumps	Heel drops	Door slams: Entrance	Door slams: Sliding glass	Nail hammering	Walking
NW corner, low horizontal living room	[1]~~0.472~~ .377 [2].483	0.190	0.055	0.220	0.110	0.100	0.056
NW corner, low vertical living room	—	.200	.069	.120	.041	.180	.180
NW corner, high horizontal living room	[1].316 [2].345	.170	.037	.260	.100	.064	.054
SE corner, low horizontal master bedroom	[3].227 [4].222	.310	.139	.182	.164	.508	.157
SE corner, low vertical master bedroom	[5]~~.392~~ .314 [3].194	.286	.133	.121	.029	.118	.126
Midsouth wall, master bedroom	[5].508 [4].700	1.44	.783	1.29	.136	.241	.225
Mideast wall, master bedroom	—	2.63	1.42	.934	.111	3.81	.285
Midwest wall, living room	[1].964 [2]1.37	1.00	.486	1.05	.124	.365	.086
Midfloor, [illegible] room	—	5.58	4.08	1.25	.031	.063	1.49
Midfloor, living room	[1]1.18 [2].85	10.1	5.84	.453	.272	.067	.286

[1] From peak ground vibration of 0.470 in/sec, ~~117~~ dB airblast. 119
[2] From peak ground vibration of 0.320 in/sec, 125 dB airblast.
[3] From peak ground vibration of 0.210 in/sec, 124 dB airblast.
[4] From peak ground vibration of 0.300 in/sec, 129 dB airblast.
[5] From peak ground vibration of 0.290 in/sec, 124 dB airblast.

FAILURE CHARACTERISTICS OF BUILDING MATERIALS

Most of the damage concern from the relatively low-level blasting vibrations involves cosmetic cracking of the interior walls of residences. Modern construction uses interior walls of gypsum plaster board (Drywall) with a covering of paint, wallpaper, or a plaster wash. Older homes often have interior walls of thick plaster over wood lath support. The strength of interior construction materials is not well understood, as they are not explicitly used as shear force resisting elements and homes tend to be nonengineered structures. However, it is evident that wall coverings stiffen their responses to forces acting in the planes of the walls. Early Bureau of Standards work on the strength of construction materials is discussed by Beck (*3*).

GYPSUM WALLBOARD FAILURE

Gypsum wallboard or Drywall consists of a panel of ⅜- to ⅝-in-thick gypsum plaster with a paper laminate covering on both sides. The 0.015-in-thick paper contributes greatly to the strength of the board and conceals cracking of the plaster core.

Strength tests on gypsum wallboard and plaster are summarized in table 7. Included are tests with and without paper laminates, preloaded static, and fatigue tests for various thicknesses of boards. Initial cracking could be seen on uncovered plaster but was masked by the laminate paper on covered wallboard.

Leigh studied plaster panels subjected to simulated sonic booms (*28*). In his fatigue study, he found only one failure out of 13 panels tested, and this he attributed to the experimental design. He also performed static failure tests.

Wiss measured strains on the walls of a home as part of his study of damage from blasting on the Mesabi Iron Range in Minnesota (*57*). His is the only failure strain measured under field blasting conditions. Wiss related his measured strains to peak ground particle velocities and found that 1.0 in/sec corresponded to interior strains of up to 50 μin/in, with 15 μin/in being a typical value. Drywall failure strains were also determined from laboratory tests of samples removed from the structure. Failure strains were very high but compare well with results of Bureau of Mines tensile tests on Drywall sections.

Table 7.—Failure characteristics of plaster and gypsum wallboard

Author and type for failure[1]	Strain, μin/in	Stress, lb/in²	Material	Thickness, in	Prestrain, μin/in	Cycles to failure
Leigh (*28*): Tensile	460	300	Plaster beam	NA	0	Static.
Do	365	300	Plaster panel	⅜	0	1
Do	260	200	---- do	⅜	0	10,000
Wiss and Nichols (*57*): Tensile	[2]1,230	[2]920	Gypsum wallboard with longitudinal section.	⅜	0	Static.
Do	[3]3,300	[3]1,460	---- do	⅜	0	Static.
Do	[2]1,100	[2]650	---- do	½	0	Static.
Do	[3]4,700	[3]1,100	---- do	½	0	Static.
Do	[2]840	[2]580	Gypsum wallboard with transverse section.	⅜	0	Static.
Do	[3]3,770	[3]785	---- do	⅜	0	Static.
Do	[2]910	[2]380	---- do	½	0	Static.
Do	[3]2,400	[3]580	---- do	½	0	Static.
Do (in situ)	1,162	NA	Gypsum wallboard	NA	NA	Blasting.
Dowding and Beck (*11*): Shear[4]	130	NA	Gypsum wallboard core with paper laminate removed.	⅝	0	Static.
Do	80	NA	---- do	⅝	0	1,000
Do	50	NA	---- do	⅝	0	18,000
Do	90	NA	---- do	⅝	26	330
Do	76	NA	---- do	⅝	26	1,900
Do	56	NA	---- do	⅝	26	8,500
Do	[2]340	NA	Gypsum wallboard	⅝	26	Static.
Do	[3]>1,400	NA	---- do	⅝	0	Static.
Bureau of Mines (this study):						
Tensile	[2]1,240	[2]175	---- do	⅜	0	Static.
Do	[3]3,400	[3]285	---- do	⅜	0	Static.
Do	[2]1,420	[2]170	---- do	½	0	Static.
Do	[3]3,210	[3]250	---- do	½	0	Static.
Do	[2]1,445	[2]140	---- do	⅝	0	Static.
Do	[3]3,450	[3]230	---- do	⅝	0	Static.
Shear	[2]3,000	[2]95	---- do	½	0	Static.
Do	[3]8,450	[3]136	---- do	½	0	Static.

NA = Not available.
[1] All laboratory tests except as noted in parentheses.
[2] Initial gypsum core failure.
[3] Ultimate failure, paper laminate damage.
[4] Beck's strains involved measurement on test sample. Others used platen displacement.

Beck sheared gypsum panels to failure, while investigating both fatigue behavior and the effects of preloading (*3, 11*). Most of his tests were on commercially cast panels from which the paper laminate had been removed. He found that after 5,000 cycles the panel would fail at about half the maximum strain that corresponds to static failure. Beck also found that preloading or prestraining reduced the number of cycles required for failure and also the failure strain.

The principal failure strains for this study and the two points from Wiss' study are plotted in figure 44, along with observed static failure levels. Large variances are shown for Drywall core failures (e.g., 340 to 1,200 μin/in), which can be attributed to experimental load setup, moisture differences, and method of strain determination. Additional fatigue testing of building materials is needed.

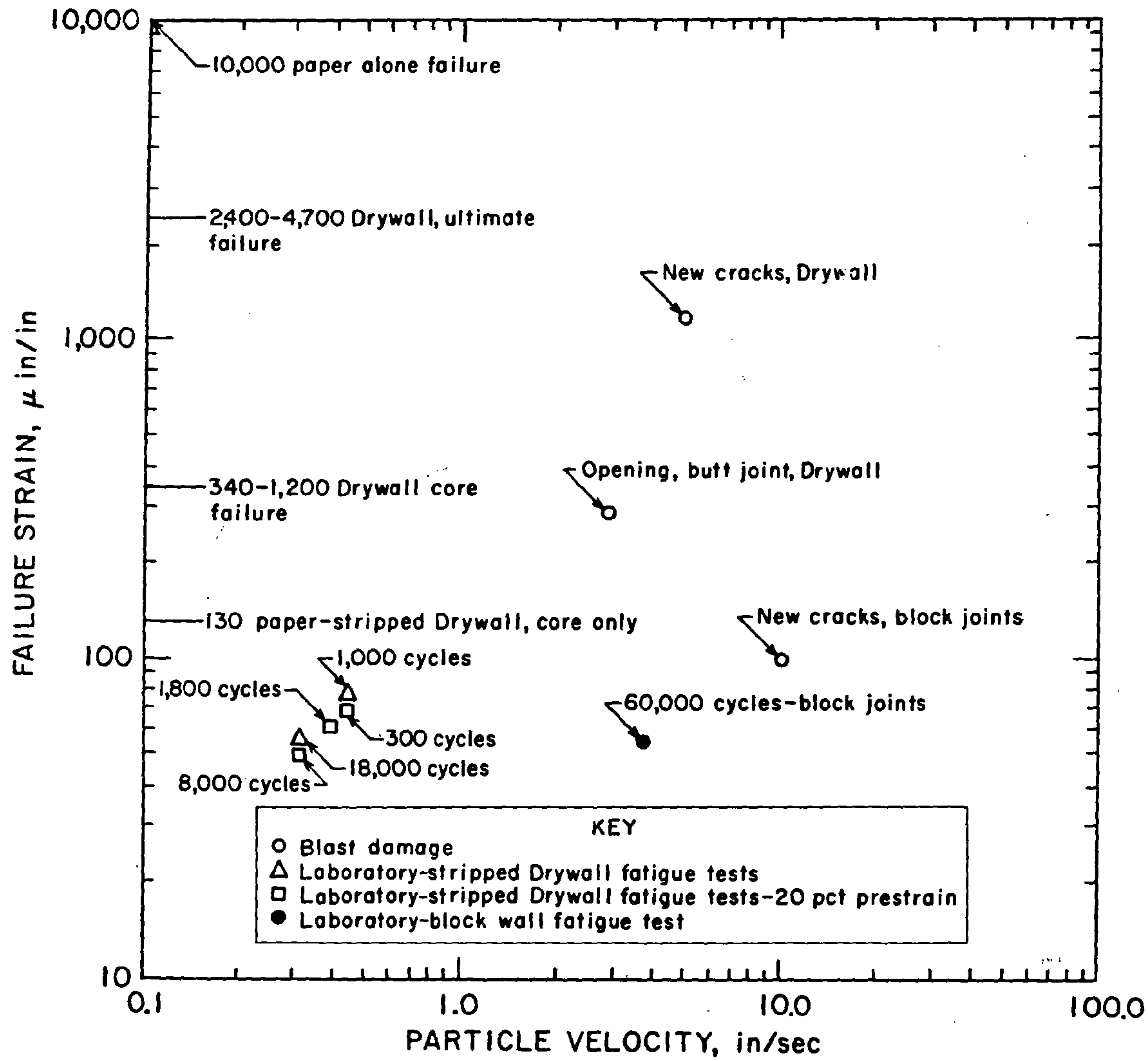

Figure 44.—Failure strains for residential construction materials from a variety of sources (tables 7 and 8).

The ultimate tensile failure strain for typical gypsum wallboard appears to be about 1,000 µin/in (*57*). Assuming that a stress concentration of 10 corresponds to the space above doorways or large windows, a shear deformation producing a uniform 100 µin/in would be potentially damaging. Projecting this over a typical house wall length (30 ft) gives peak differential displacements of approximately 0.036 in.

Complicating comparisons between different studies is that some measurements are made directly on the test specimens, while others are made using the machine platens. These values can differ by a wide margin.

MASONRY AND CONCRETE FAILURE

The two Canadian studies of blasting vibration damage included measurements of strains in basement walls of thick stone and mortar (table 8). Edwards and Northwood (*16*) found dynamic strains corresponding to initial cracking of > 375 µin/in and permanent induced strains of > 150 µin/in. Later measurements by Northwood found very much lower cracking thresholds of 45 µin/in (*38*).

Crawford and Ward studied masonry cracking induced by blasts in an 8- by 8-foot block and poured concrete box filled with sand (*9*). They found that poured concrete walls were much stronger than block walls and required high levels of both strain and particle velocity to induce cracking. The mortar joints of the concrete block wall failed at considerably lower strains, but the blocks themselves had the same ratio of strain to velocity as the concrete walls. The walls of concrete block and mortar did not act as monolithic bodies but as concentrated strains at the mortar joints. Crawford and Ward measured strain levels across the mortar joints that were 10 times those on the adjacent blocks (*9*).

Table 8.—Failure of masonry and concrete

Author and type of material	Dynamic strain at failure, µin/in	Particle velocity, in/sec	Type of cracking
Edwards and Northwood (*16*):			
On stone mortar basement walls, 18 to 24 in thick	375	3.1	Threshold.
Do	[1]150	3.1	Do.
Northwood, Crawford, and Edwards (*38*): On stone and mortar walls perpendicular to shot (radial)	40	3.4	None.
Do	45	4.5	Threshold.
Do	75	7	Minor.
Do	80	10	Major.
Crawford and Ward (*9*):			
8- and 10-in concrete block	30	3	Threshold.
Mortar joints	300	NAp	Do.
7- and 9-in poured concrete	100	10	Do.

NAp = Not applicable.
[1] This is permanent strain. All the remaining are dynamic.

Cracks appeared in the mortar joints when strains of 30 µin/in were measured on the blocks, consistent with Northwood's values (*38*). The strains across the joints were 300 µin/in. These results are consistent with the observations that cracks in the mortar between the blocks or bricks are the first signs of damage in masonry. Crawford and Ward recommended particle velocity as an index of damage independent of masonry type, with failure at 3 in/sec measured radially to the blasting and perpendicular to the block surface. This corresponds to surface strains of 35 to 40 µin/in on the blocks. Monolithic concrete, on the other hand, did not crack until particle velocities exceeded 10 in/sec and strains of 100 µin/in. Even then, the concrete cracked at the corners of the box. This location of cracking suggests that expanding gas pressures may have deformed the box and cracked the concrete at strain concentrations in the corners.

The measurement of strain is a useful engineering tool. It may provide the most appropriate method of assessing cracking potential for instances where locations of maximum strains can be predicted beforehand and material failure characteristics are understood.

FATIGUE

A very limited amount of work has been done on fatigue or damage from long-term repeated blasting. For engineered materials, fatigue strengths are typically a significant fraction of the ultimate strengths (e.g., 50 pct).

The U.S. Army Corps of Engineers, Civil Engineering Research Laboratory (CERL), conducted a fatigue damage test for the Bureau of Mines as the first phase of a full-scale fatigue study (*54*). An 8-foot-square by 8-foot-high test structure (model room) was built on the CERL 12- by 12-foot biaxial vibration table (fig. 45). This structure represented a typical residential room with a 7-foot doorway and two window openings. It was constructed of 2- by 4-inch wood studs and ⅜-inch-thick gypsum wallboard. Joints were taped and finished in the standard manner, with metal beads on the outside corners.

The vibration simulator that shook the base was programed with one of the horizontal components and the vertical component of an actual

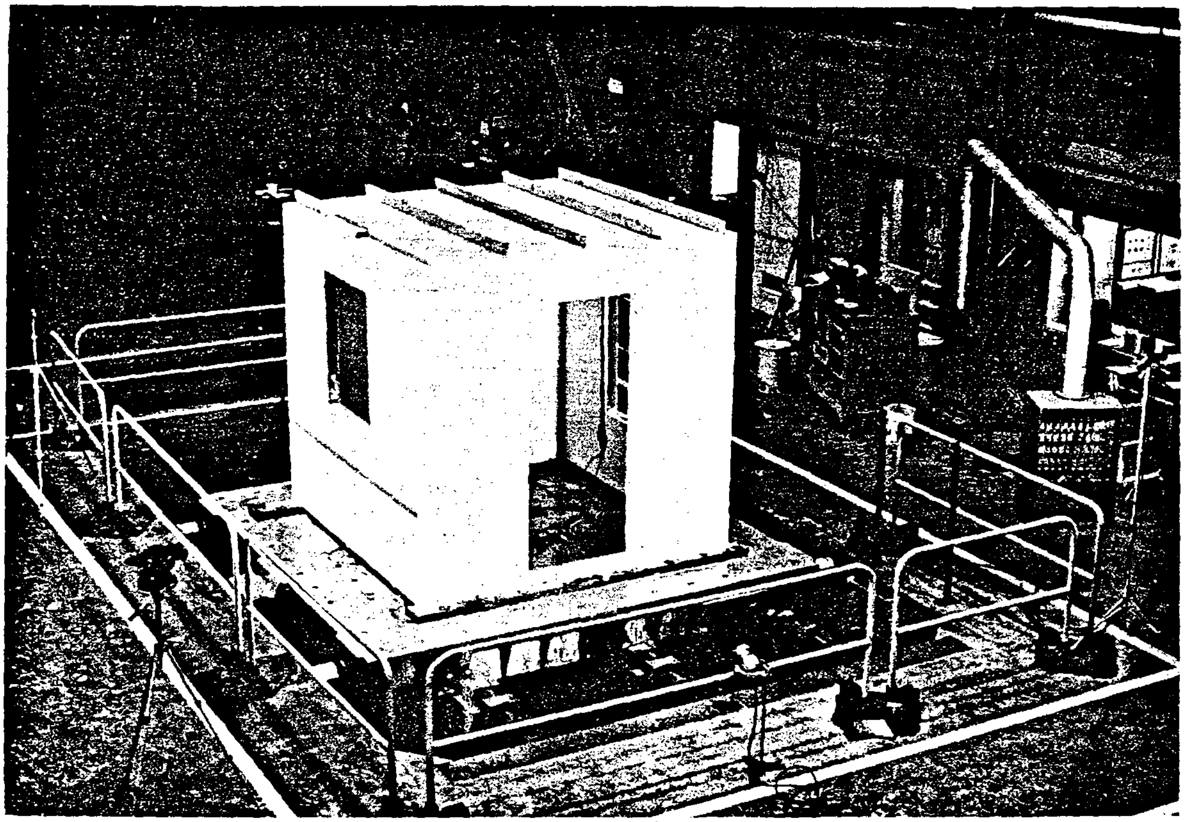

Figure 45.—Fatigue test model on biaxial vibrating table.

quarry blast from Bulletin 656 (*37*). The predominant horizontal and vertical component frequencies were 26 and 30 Hz, respectively. Testing consisted of a series of "blasts" at increasing platform vibration levels with inspections between each series. The sequence of number of events for each level of vibration was 1, 5, 10, 50, 100, and 500. The vibration levels run were 0.1, 0.5, 1.0, 2.0, 4.0, 8.0, and 16.0 in/sec. The first damage was observed after six events (blasts) at 4.0 in/sec, when the Drywall pulled away from the bottom plate. After six events at 8.0 in/sec nails began to work out, and after 66 events the corners cracked. A level of 16 in/sec produced cracks at window openings. The vibration levels from this study cannot be directly related to the full-scale case, because the excitation motions were not scaled (e.g., the natural frequency of the model was too high because the mass was too low). However, the existence of fatigue was demonstrated as each new degree of damage was observed after several complete events at that vibration level.

Fatigue and cracking of masonry walls have been studied by Koerner (*23*). He subjected 1/10-scale block masonry walls to sinusoidal vibrations at their resonant frequencies of 40 to 50 Hz. Failure was observed after approximately 10,000 cycles at peak particle velocities of 1.2 to 2.0 in/sec. More cycles were required for damage at frequencies outside of resonance. Recent tests by Koerner on 1/4-scale block walls also found fatigue effects, including the cracking of three walls at particle velocities of 1.69 to 1.95 in/sec, requiring 60,000 to 400,000 vibration cycles. Koerner predicted that the prototype natural frequency values would be half those of his model walls, and that the failure particle velocities would then be double the model results (*23*). Applied to full scale, these results correspond to more than a thousand 1-sec-long, 40-Hz events. In addition to Koerner's study, other fatigue studies are in progress to quantify the failure potentials from long-term blasting as well as the other stress-producing environmental factors.

SAFE VIBRATION LEVELS FOR RESIDENTIAL STRUCTURES

There are a large number of publications on ground vibrations and blasting; however, few contain actual observations of damage[7] and corresponding measurements of ground motions. In 1962, the Bureau of Mines published RI 5968 by Duvall and Fogelson (*14*). This was a summary analysis of the three existing blasting damage studies, one from Canada (*16*), one from Sweden (*26*), and data from Bureau of Mines Bulletin 442 dating back to 1942 (*51*). RI 5968 was revolutionary in several respects. It recommended the use of a single motion descriptor, particle velocity, in place of displacement and acceleration. Based on the use of particle velocity, a single safe value damage criterion of 2.0 in/sec was recommended, which was frequency independent over the wide range of 2.5 to over 400 Hz.

In 1971, the Bureau of Mines published Bulletin 656, a comprehensive summary of the many problems of blasting, including generation, propagation, and damage from both ground vibration and airblast (*37*). The ground vibration damage data in Bulletin 656 were those collected for RI 5968. A single new point from a study by Wiss (*57*) was included, but no new statistical analysis was conducted to include studies made since the 1962 report. It later became evident that the Bureau-recommended vibration criterion was not applicable under some conditions and that damage was occurring below 2 in/sec. Consequently, in 1974 the Bureau of Mines started a new program to examine damage from blasting. This included an analysis of data that had become available since 1962, and also the collection of new damage data, particularly from large-scale blasting operations in coal mines.

Review of the RI 5968 indicated that low-frequency vibrations (e.g., 2.5 to 40 Hz) were a significant problem and required additional study, such as response spectrum analysis. The 2.0-in/sec safe level had been based on a mixture of both high- and low-frequency damage data. Consequently, the inferred 5-pct damage probability was somewhat artificial and depended on the relative amount of each kind of data available. Using any given number of standard deviations from the mean of the high- and low-frequency data separately would give widely differing safe values for the two cases. The derivation of 2.0 in/sec as the safe level was based on 2.0 standard deviations from the 5.4-in/sec mean of all the minor damage points. Five values for minor damage were outside the 2.0 standard deviation damage envelope (at approximately 1.2, 1.36, 1.24, 0.75, and 0.32 in/sec), all from Bureau of Mines shaker tests that only approximately modeled transient blast loads (*51*). The last of these values was dropped for statistical reasons. Because 2.0 in/sec was also lower than all the individual major damage points, and because it included all actual blasting damage data, it was recommended as a boundary between damage and nondamage.

The large amount of scatter in the summary analysis at low frequencies is undoubtedly caused by the presence of structure resonances and initial strain states. The lower frequency vibrations also result in large displacements (and strains), and it is strain that ultimately produces cracking. RI 5968 had not presented sufficient data for separate analyses of the low and high frequencies because it was based upon only three studies, one of which was not blasting. Since the 1962 report, four major sets of additional data have become available, including new damage data obtained from Bureau of Mines research. Three other studies have supplied a few new damage points each, bringing the total number of relevant studies to 10 (table 9). Direct statistical treatment of the type used in RI 5968, probability analysis, and response spectra analysis were all applied to quantify blasting damage potentials.

PREVIOUS DAMAGE STUDIES

Few studies have been made that actually produced data useful for determination of thresholds and probabilities of damage. Required are actual structures near enough to blasts for damage and careful preblast and postblast inspections. All homes are cracked from natural causes, including settlement and periodic changes of humidity, temperature, and wind. Soil moisture changes are notorious for causing foundation cracks (e.g., from tree roots). The widths of old cracks change seasonally and often daily; however, the number of cracks continues to increase with age, independent of blasting.

[7] The term "damage" is used in this report and those referenced (*14, 16, 26, 37, 51*) to refer to cracking of either interior superstructure walls or masonry. The special nature of the damage is discussed in later sections of this report (and in table 10); however, it is understood that the observed damage refers to cosmetic and superficial effects, and that the structural integrity of the homes is not being questioned here.

Table 9.—Studies of damage to residences from blasting vibrations

Study	Damage classifications	Types of damage	Overburden type	Structures studied	Distances to shots, ft	Shot sizes, lb/delay	Frequency range, Hz	Total shots	Damage observed, uniform classification				Instrumentation
									Non-damage	Threshold	Minor	Major	
Thoenen and Windes, Bureau of Mines (51).	Threshold and minor.	Plaster cracks and fall of plaster.	None	6 frame, brick, and stone, 1 to 3 story.	None	None	4–40	[1]163	103	26	34	0	Displacement.
Langefors, Westerberg, and Kihlstrom (26).	Minor and major.	do	Rock	NA	NA	NA[2]	48–420	105	57	0	32	16	NA.
Edwards and Northwood (16).	Threshold, minor, and major.	Cracks in masonry, bricks, or stone basement walls.	Soft, wet sand with clay 20 ft down, and well-consolidated glacial till.	6 total: 4 with 12-in brick and plaster interiors, 2 frame.	30–200	47–750	2.5–25	22	22	6	8	5	Displacement and acceleration measured on basement walls.
Northwood, Crawford, and Edwards (38).	do	Basement wall damage close in, and super-structure plus basement damage far out.	Glacial till and limestone overlain by thin till layer.	6 total: 1 frame, 1 stone, 4 9- to 12-in brick.	3–300	0.3–1,600	[3]7–120	60	51	10	4	5	Velocity, MB-120 gage, measured on basement walls.
Thoenen and Windes, Bureau of Mines (51).	Threshold and minor.	None	10 quarries	14 total	715–2,500	36–1,200	3–16	43	11	0	0	0	Displacement and acceleration.
Morris and Westwater (31).	Threshold	Plaster and partition cracks.	1 quarry and 1 surface coal mine.	2 stone with plaster interiors.	115–820	200–14,000	3.7–5.7	3	1	2	0	0	Displacement.
Dvorak (15)	Threshold, minor, and major.	Plaster and masonry cracks.	Semihard clay with sand lenses.	4 brick and masonry.	30–164	2.2–44	1.5–15	58	7	25	15	11	Do.
Wiss and Nicholls (57).	Minor	Drywall cracks	Glacial till	Single structure, rubble stone foundation.	35–200	1–85	NA	10	9	0	1	0	Velocity, MB-120 gage.
Jensen and Rietman (~~37~~). 21	do	do	Rock with 0 to 7 ft of soil overburden.	18 frame structures.	[4]30–185	1.75–12.75	[5]11–126	29	27	0	2	0	Do.
Bureau of Mines new data.	Threshold and minor.	Plaster, Drywall, and masonry cracks.	Various, usually with soil overburdens.	17 frame structures.	14–2,500	18–2,600	6.3–71	225	~~37~~ 76	~~23~~ 28	3	0	Do.

[1] Shaker tests.
[2] Excavation in rock, small shots.
[3] Predominantly 12 to 26 Hz for damage data.
[4] Plus 1 at 5 ft.
[5] Mostly >30 Hz.
NA = Not available.

Analysis of damage probabilities is particularly difficult because of the low probabilities being sought. For example, reliable determination of the 2-pct damage probability theoretically requires 49 nondamage measurements for every one of damage. Consequently, it is necessary to pool all the available data while avoiding the use of data that are clearly not similar to actual blasting. Examples of the latter are teleseismic blast vibrations and earthquakes, whose low-frequency content and long durations make them more likely to produce damage to structures. Thoenen and Windes' (*51*) early analyses recognized the nonapplicability of the Mercalli intensity scale developed for earthquakes, and Richter's observations on duration effects were discussed in the section on ground vibration characteristics. The shaker damage results of Thoenen and Windes are also questionably applicable, being of longer duration than actual blasting.

All the applicable blast-vibration damage studies are summarized in table 9, all involving preblast and postblast inspections. A detailed analysis of these studies is not made in this paper. Many are discussed in Bulletin 656 (*37*), and only the last two represent entirely new data. The first three studies in the table had been analyzed in RI 5968; summary results are in figure 3.4 of Bulletin 656 and figure 6 of RI 5968 (*14*). In some cases, measurements were made on foundation walls, and in others in the ground next to the structure. Obviously, uniform measurements are highly desirable. Stagg (*50*) discusses measurement methodology. The degrees of damage (threshold, minor, and major) are given in table 10.

The Canadian researchers made the second study of damage from blasting (*38*) published after RI 5968. This followed the Edwards and Northwood investigation (*16*), involved more shots and a wider range of both shot-to-house distances and shot sizes, and utilized similar experimental design.

Thoenen and Windes reported on a series of quarry blasts intended to study damage to residences (*51*). In the absence of damage, they used structure vibrators to induce cracking. The quarry nondamage data were not useful in the mean square analyses of damage thresholds performed for RI 5968; however, they are useful for probability analysis where numbers of damage and nondamage observations are compared.

Morris and Westwater described early studies on blast damage at a time when all measurements and damage criteria were based on ground displacements (*31*). In addition to discussing the Thoenen and Windes study, they describe three monitored blasts in Britain where inspections were made. They concluded that 0.040-in peak displacement would be a safe value criterion, and that a previously recommended maximum of 0.008 in had a considerable margin of safety. The damage data all involved low frequencies (3.7 to 5.7 Hz) with the 0.040-in displacement corresponding to a 1.0 in/sec particle velocity at 4 Hz, assuming simple harmonic motion. Prior to the use of particle velocity and going back to 1947, the State of Pennsylvania had a maximum safe blasting criterion of 0.030-in peak displacement for vibration frequencies below 10 Hz (*27*).

Dvorak (*15*) examined damage to masonry residences in a study published soon after RI 5968. Bulletin 656 discusses the Dvorak study, but did not include it in the summary analysis. The Bulletin raised questions about the old instrumentation used by Dvorak. It is not possible to verify the reliability or accuracy of any of the old studies, particularly those that published few of their actual data and for which the original time histories have been lost.

Recognizing the problems caused by old instrumentation, and particularly the low levels of damage observed by Dvorak, the analyses for this study were run both with and without the Dvorak data.

Table 10.—Damage classification

Uniform classification	Description of damage	Studies of blasting damage
Threshold	Loosening of paint; small plaster cracks at joints between construction elements; lengthening of old cracks.	Threshold: Dvorak (*15*); Edwards and Northwood (*16*); Northwood, Crawford, and Edwards (*38*). Minor: Thoenen and Windes (*51*).
Minor	Loosening and falling of plaster; cracks in masonry around openings near partitions; hairline to 3-mm cracks (0 to ⅛ in.); fall of loose mortar.	Minor: Dvorak (*15*); Edwards and Northwood (*16*); Northwood, Crawford, and Edwards (*38*); Jensen and Rietman (*21*); Langefors, Westerberg, and Kihlstrom (*26*). Major: Thoenen and Windes (*51*).
Major	Cracks of several mm in walls; rupture of opening vaults; structural weakening; fall of masonry, e.g., chimneys; load support ability affected.	Major: Dvorak (*15*); Edwards and Northwood (*16*); Northwood, Crawford, and Edwards (*38*); Langefors, Westerberg, and Kihlstrom (*26*).

Wiss and Nicholls (*57*) examined the blast damage characteristics of a single well-constructed residence on a soil type similar to that of the Canadian studies (*16, 38*). Their single damage observation was from a very high particle velocity for this damage-resistant, rubblestone foundation structure with gypsum Drywall. This point was shown in the Summary of Bulletin 656 (*37*, fig. 3.8) for comparison to the other three studies.

Jensen and Rietman measured vibration effects from construction blasts for the Bureau of Mines (*21*). The goal was to collect response data for residences from small-scale excavation blasting for comparisons of the relative responses from shots of widely differing frequency character. Damage observations were also made, and the resulting values were used in this study. One shot was so close to the foundation (5 ft) that damage was caused by permanent ground strain, or inelastic effects. This value was not used in the analyses.

Two recent studies in Sweden became available too late for the analyses in this paper (*4, 6*). They involved structures on solid rock, and their damage observations agreed with previous Swedish results (*26*). Bergling described a test of blast damage to a concrete and brick residence (*4*). Shots were in the range of 1 to 50 m distance, and the lowest level at which damage was observed was 110 mm/sec (4.33 in/sec). Bergling also discussed the strict German DIN 4150 Standards and British 117 (1970) Standards (appendix A). Bogdanoff described a house of similar construction, also directly founded on granite-gneiss bedrock (*6*). From 38 rounds at distances less than 100 m, he indicated no damage below a vertical peak particle velocity of 90 mm/sec. They concluded that 30 mm/sec was safe for this structure (and geology), since many nondamaging shots occurred at this level.

The Salmon nuclear blast generated damage and complaint data (*39*), as well as the structural responses discussed previously (*5*). The damage observed was at large distances and occurred at lower levels than those observed for blasting. Particle velocity was estimated to have been approximately 5 mm/sec in Hattiesburg, 34 km away from the blast. Complaints about damage were also very high, with 1 pct of all families complaining at particle velocities of 2 mm/sec (0.08 in/sec), and 10 pct at 10 mm/sec (0.40 in/sec). Little justification exists to applying the Salmon results to typical mine blasting. As discussed in the section on Ground Vibration Characteristics, the 90-sec-long, low-frequency wave is far more typical of earthquake ground motions than of blasting. As no preblast surveys were available, damage causation was impossible to determine.

J. F. Wall studied masonry structures in Mercury, Nev. (*53*). He tabulated rates of cracking and concluded that they were higher during times of blasting. He concluded that the nuclear blasts at 33 to 78 km, which produced peak particle velocities of 1 to 3 mm/sec, were generating 4 to 30 cracks in concrete block structures over the natural rate of 2.5 cracks/day (for all 43 structures). As in the Salmon study, there were no direct damage observations that could be attributed to the specific events. Also, as in the Salmon study, the vibration time histories were of character similar to teleseismic vibrations; that is, dispersed to long durations and dominated by low-frequency surface waves. Even if the damage observed were caused by the nuclear blasts, it provides no reliable insight into damage potentials from conventional blasts. Nelson (*36*) monitored crack widths in six of the Mercury structures. He observed that crack width changes during intervening periods (from wind, temperature, sun, and humidity variations) were larger than those attributed to the seismic events.

The Rulison 40-kiloton nuclear shot also provided damage data where the event durations (of 5.5 to 7 sec) were somewhat typical of mine or quarry blasting (*43*). Frequencies were probably again very low because of the long absolute distances. As with the other nuclear blast studies, no preblast inspections had been made and crack observations were based on postblast evaluations. Scholl's survey of five nearby towns found damage ratios of 3 to 6 pct at peak particle velocities of 0.79 to 1.07 in/sec, based only on postblast inspections. This is in fair agreement with the Bureau of Mines summary blast damage results discussed later in this report.

Scholl also studied the Handley nuclear blast and other similar events for complaints and damage (*42*). He related pseudo absolute accelerations and complaint ratios for these events of very low frequency ground motion, in the range of 0.25 to 1.5 Hz. No determinations were made of damage claim validity.

Esteves describes damage to a single concrete and tile residence near a quarry (*17*). The first damage observed was plaster cracks at 60 mm/sec (2.35 in/sec).

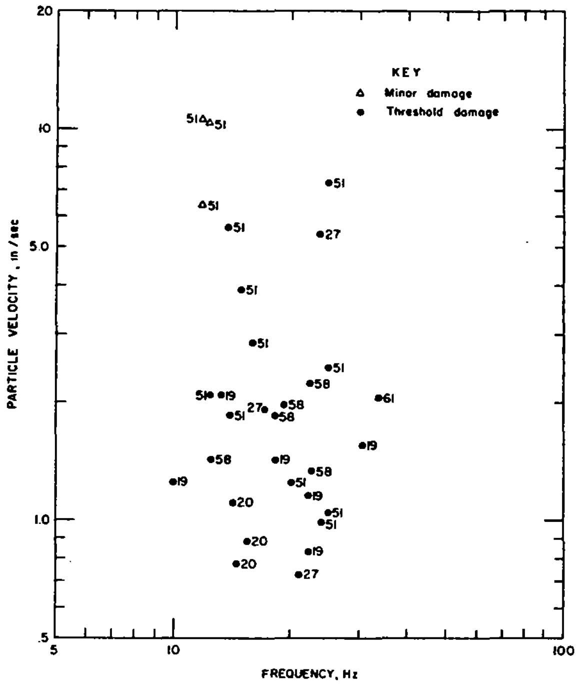

Figure 46.—Damage observations, new Bureau of Mines data from production blasting in surface mines. (Houses are listed by number in table 3.)

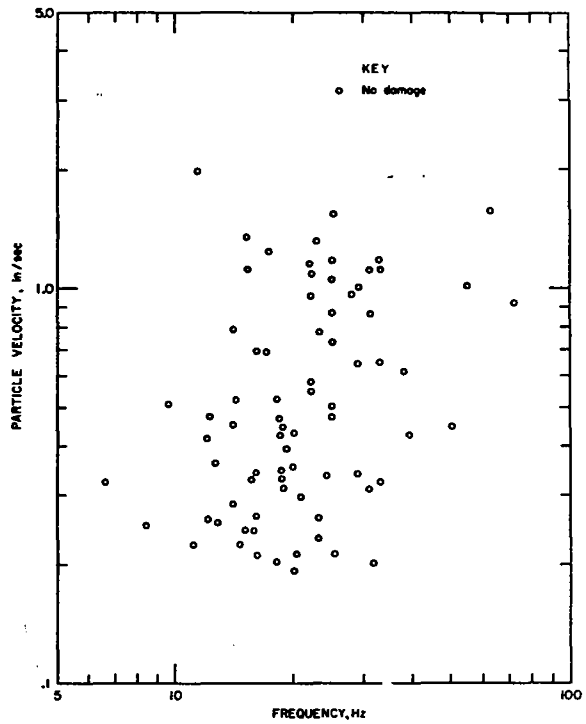

Figure 47.—Nondamage observations, new Bureau of Mines data from surface mine blasting.

NEW BUREAU OF MINES DAMAGE STUDIES

The Bureau conducted a series of field studies of ground vibration and airblast damage and responses from 1976 to 1979. Efforts were concentrated on actual measurements of wall, floor, and racking responses and the observations of damage that could be correlated to specific vibration events. A significant part of the work was done near large surface coal mines, with thick soil overburdens and large-diameter blastholes; cases of this sort had not been studied previously.

The production shots monitored for the damage analysis are listed in table 1. At five sites, houses were in the paths of the advancing mines and eventual damage was inevitable. Most of the homes, however, were not owned by the mines, and the blasts had been designed to protect them from damage. In all, 63 shots out of 225 produced useful high-level damage and nondamage data. Most of the other shots provided data on structural responses and airblast effects. Thirty-two of the shots (labeled "W" in table 1) were measured by Jensen and Rietman (*21*) under a Bureau of Mines contract. A total of 76 houses were studied (including 18 by Jensen and Rietman) and are listed in table 3. The houses that were subjected to high ground vibration levels and produced useful damage data are shown in figures 15–28.

Summaries of the damage and nondamage data from the high-level blasts are given in figures 46 and 47. Most of the damage was observed in homes with interior walls of plaster on wood lath (Nos. 19, 27, 51) and consisted of extensions of existing cracks and new hairline cracks. House 20 was notable in being a modern 1-story home with gypsumboard interior walls. Unfortunately, this structure was sold by the mine and moved before more than superficial cracking could be inflicted. The lowest level for observed damage in this structure was 0.79 in/sec (shot 48).

House 21 was also a modern 1-story residence and had been subjected to nine large blasts including six exceeding 1.0 in/sec. No damage was observed that could be correlated to specific blasts. However, this home had a significant number of cracks around windows and doors. The block basement wall on the mine side had been falling inward and was being supported by steel bracing. The foundation deformation undoubtedly contributed to the superstructure's cracking.

House 61 was also a modern 1-story structure with both gypsum wallboard and plaster interior walls. This home was subjected to a peak particle velocity of 2.23 in/sec, and several cracks propagated over windows and doors.

House 67 was also damaged (by shot W–17); however, the blast was within 5 feet and the cracking was likely produced by permanent ground strain rather than elastic energy. This shot was not considered useful for damage analysis.

Frequencies were determined directly from the vibration time histories and by real-time spectral analysis. In some cases, the records showed two dominant frequencies; high-frequency for the first few hundred milliseconds, and then a significantly longer low-frequency wave train. The values of amplitude and frequency used corresponded to the part of the vibration record that produced the larger structure response, which was invariably the low frequency (7 to 30 Hz).

Some long-term observations were made of numbers of cracks, and their widths and lengths. None of these parameters could be related quantitatively to the blasting. The number of cracks increased with time regardless of the vibration levels, and their widths varied irregularly from a variety of environmental stresses. Consequently, blast damage was assumed only when immediate preblast and postblast inspections found additional cracks or extensions.

In all cases, except three shown in figure 45, blast damage was superficial cracking of the same type as caused by natural settlement, drying of building materials (shrinkage), and variations in wind, temperature, humidity, and soil moisture. The three minor damage points in figure 46 represent cracks in masonry and large, new interior cracks exceeding 2 mm in width.

SUMMARY DAMAGE ANALYSIS

A summary analysis of damage was made using the 10 studies listed in table 9. To facilitate comparisons, a uniform classification of damage was adopted based on three levels of observed effects (table 10). The 10 studies of damage to residences from blasting produced a total of 553 observations, including 228 of various degrees of damage. These studies represent a variety of geologies, distances, and measurement methods. Data were analyzed in sets in order to group similar studies (table 11). Sets 1 and 3 were not unique enough to describe separately. Analysis involved both mean square fits and probability techniques.

Mean and Variance Analysis

The first analysis was made to determine mean and variance for the various damage classifications in terms of displacements as a function of frequency (figs. 48 to 52). This is analogous to the analyses performed for RI 5968 (*14*) and Bulletin 656 (*37*). A slope of minus 1 corresponds to a constant particle velocity, and a slope of minus 2 to a constant acceleration. A slope of zero is, of course, constant displacement.

Set 2 combines the two Canadian studies and that by Wiss, all giving similar results on glacial till. Sets 4 and 5 are the remainder of the low-frequency results with and without Dvorak's data, respectively. Set 6 is the high-frequency ground vibration data from Sweden (*26*) and from construction excavation (*21*). Set 7 is an overall summary of all the damage data.

Table 11.—Data sets used for damage analyses

Set and figures	Studies	Experimental conditions
1. (No plots)	Edwards and Northwood (*16*); Northwood, Crawford, and Edwards (*38*).	Low-frequency vibrations; glacial till soil/wallpaper on walls.
2. (Figs. 48, 53, and 55).	Edwards and Northwood (*16*); Northwood, Crawford, and Edwards (*38*); Wiss and Nicholls (*57*).	Do.
3. (No plots)	Morris and Westwater (*31*); Thoenen and Windes (*51*), quarry; Thoenen and Windes (*51*), shaker.	Low-frequency vibrations; walls stripped of wallpaper; plaster walls; shaker tests.
4. (Figs. 49 and 56).	Morris and Westwater (*31*); Thoenen and Windes (*51*), quarry; Thoenen and Windes (*51*), shaker, new Bureau of Mines (this study).	Do.
5. (Figs. 50, 53, and 57).	Dvorak (*15*); Morris and Westwater (*31*); Thoenen and Windes (*51*), quarry; Thoenen and Windes (*51*), shaker; new Bureau of Mines (this study).	As set 4 but with addition of masonry damage.
6. (Figs. 51, 53, and 58).	Jensen and Reitman (*21*); Langefors, Westerberg and Kihlstrom (*26*).	High-frequency vibrations.
7. (Figs. 52, 54, and 59).	Dvorak (*15*); Edwards and Northwood (*16*); Jensen and Reitman (*21*); Langefors, Westerberg, and Kihlstrom (*26*); Morris and Westwater (*31*); Northwood, Crawford and Edwards (*38*); Thoenen and Windes (*51*), quarry; Thoenen and Windes (*51*), shaker; new Bureau of Mines (this study).	Summary.

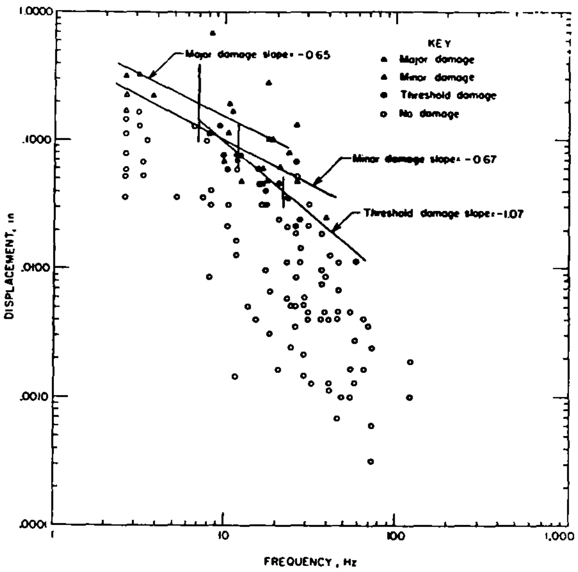

Figure 48.—Displacement versus frequency for low-frequency blasts in glacial till, set 2 mean and variance analysis.

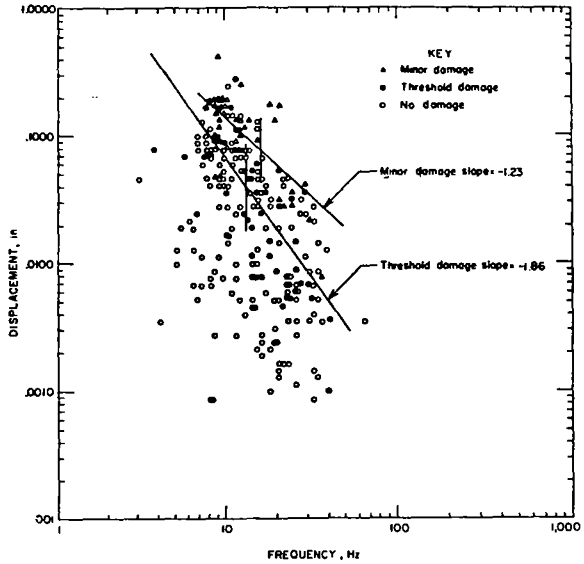

F gure 49.—Displacement versus frequency fc.: low-frequency blasts and shaker tests, set 4 mean and variance analysis.

Damage data for set 2 are shown in figure 48. The three mean regressions approximate constant particle velocities, particularly for the threshold case. All the individual damage points correspond to levels over 3 in/sec, with 2 in/sec roughly equal to three standard deviations[8] below the threshold line. The minor and threshold lines cross because of the occurrence of some minor damage at levels below some of the threshold points observed from other shots.

Set 4 analysis shows the low-frequency data, consisting mainly of the old Bureau of Mines mechanical shaker damage and new coal mine blast damage (fig. 49). All the damage points are included, even that anomalous 0.001-in displacement, 40-Hz observation from the shaker experiment (equivalent to 0.31 in/sec).

[8] The use of these statistical techniques is based on the assumption of a Gaussian distribution about the mean square regression fit. For damage data, which have an increasing monotonic probability at increasing levels, this is not rigorously accurate. Since the observations were in categories (or degrees), the means are roughly halfway between the damage onset for that category and the onset of the next category. This makes the damage means somewhat approximate except for the open-ended "major" classification. Statistical theory puts the following probabilities on occurrences lying outside a given number of standard deviations:

Standard deviations	Total probability outside high and low limit,pct	Probability outside low limit only,pct
1	32	16
1.64	10	5.0
2	4.6	2.3
2.33	2.0	1.0
3	.4	.2

Problems involved in this type of statistical analysis were discussed in Bulletin 656 (37).

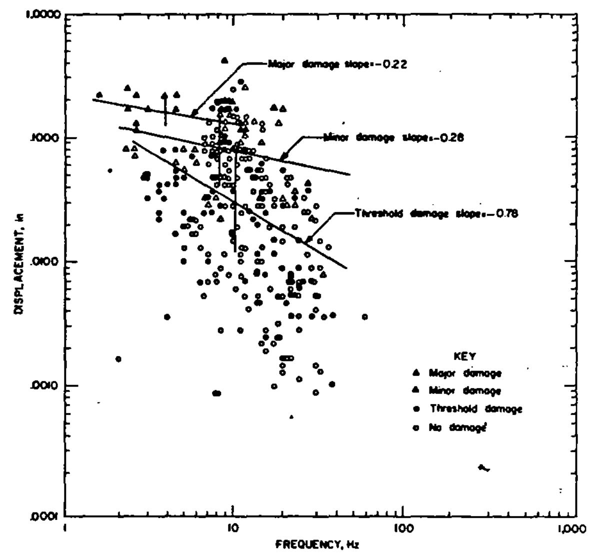

Figure 50.—Displacement versus frequency for low-frequency blasts, shaker tests, and masonry damage, set 5 mean and variance analysis.

Other than that single point, the lowest damage observed corresponded to approximately 0.72 in/sec, with quite a few points below 2 in/sec. The slopes are somewhat high, with the threshold line being almost equivalent to a constant acceleration that would have a slope of −2. The standard deviations are large, with 2

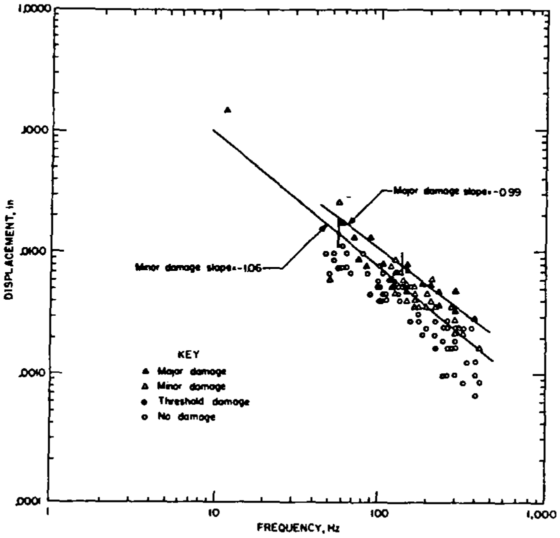

Figure 51.—Displacement versus frequency for high-frequency blasts, set 6 mean and variance analysis.

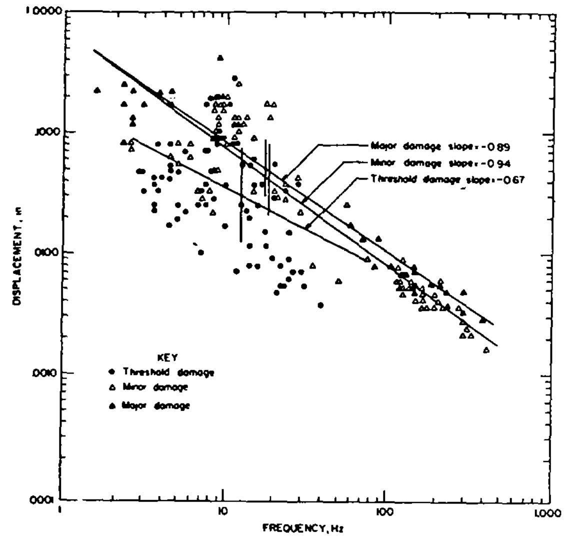

Figure 52.—Displacement versus frequency summary, set 7 mean and variance analysis.

and 3 deviations from the mean threshold giving approximately 0.7 and 0.3 in/sec, respectively.

Set 5 (fig. 50) is a rerun of set 4, but with the addition of Dvorak's data (*15*). Standard deviations increased as expected, but the slopes are reduced. The threshold line approximates a constant particle velocity of 2 in/sec, with 1 and 2 standard deviations corresponding to roughly 0.7 and 0.3 in/sec, respectively (1 standard deviation lower than the set 4 results). The lower limit of the cracking data is enveloped by the 0.51 in/sec, excluding the single maverick point. The shallow slopes suggest that these low-frequency data approximate a displacement-bound condition, which is consistent with the observation that low-frequency vibrations (e.g., 5 Hz) produce large displacements (and strains). As an example, 1 in/sec at 5 Hz is equivalent to 0.032-in displacement, which is twice the British recommended maximum of 0.016 in for vibrations below 5 Hz. The large amount of scatter in the low-frequency data is undoubtedly related to the structure response frequencies being in the same range. Between 4 and 25 Hz, the response, hence the damage for any given structure, will depend strongly on frequency. Therefore, the large amount of scatter is to be expected in a summary involving many shots and structures.

The high-frequency damage cases are shown by set 6 analysis (fig. 51), with the observation of only two classes of damage. Most notable are the minus 1 slopes (constant particle velocities), small scatter, and relatively high vibration levels for damage. No damage was observed below 2 in/sec. This level also corresponds to >3 standard deviations from the minor damage mean (lowest class of damage observed).

Set 7 (fig. 52) is an overall summary of all the damage data. The nondamage points have been omitted for clarity. This figure is analogous to the similar damage summaries in RI 5968 (*14*, fig. 6) and Bulletin 656 (*37*, fig. 3.4). The statistics corresponding to this summary analysis are somewhat arbitrary, being an artifact of the relative amount of high- and low-frequency data available. The large amount of scatter for the low frequencies shows that greater caution is required for equivalent damage probability as compared with that for high-frequency vibrations, those exceeding approximately 50 Hz. Regressions of the mean damage levels for the various sets have been plotted as particle velocities versus frequencies in figure 53, with the overall summary shown in figure 54. The maverick low point from figures 49 and 50 has been omitted as experimental error in the summary figures (figs. 52 and 54).

Probability Analysis

Probability analyses were also applied to the damage data as an alternative to regression analysis and were expected to produce more meaningful predictions. The number of damage observations within particle velocity intervals were plotted for the various sets of data. Four sampling methods were used on the damage and nondamage observations:

1. Simple counting of the numbers of points within an interval.
2. Smoothed sampling with variable-width particle velocity windows.
3. Assuming that every damage point excludes the possibility of higher level nondamage for that particular test with the reverse for nondamage.
4. Using only damage points and accumulated damage at increasing levels, and the same assumption for nondamage as for observation 3 above.

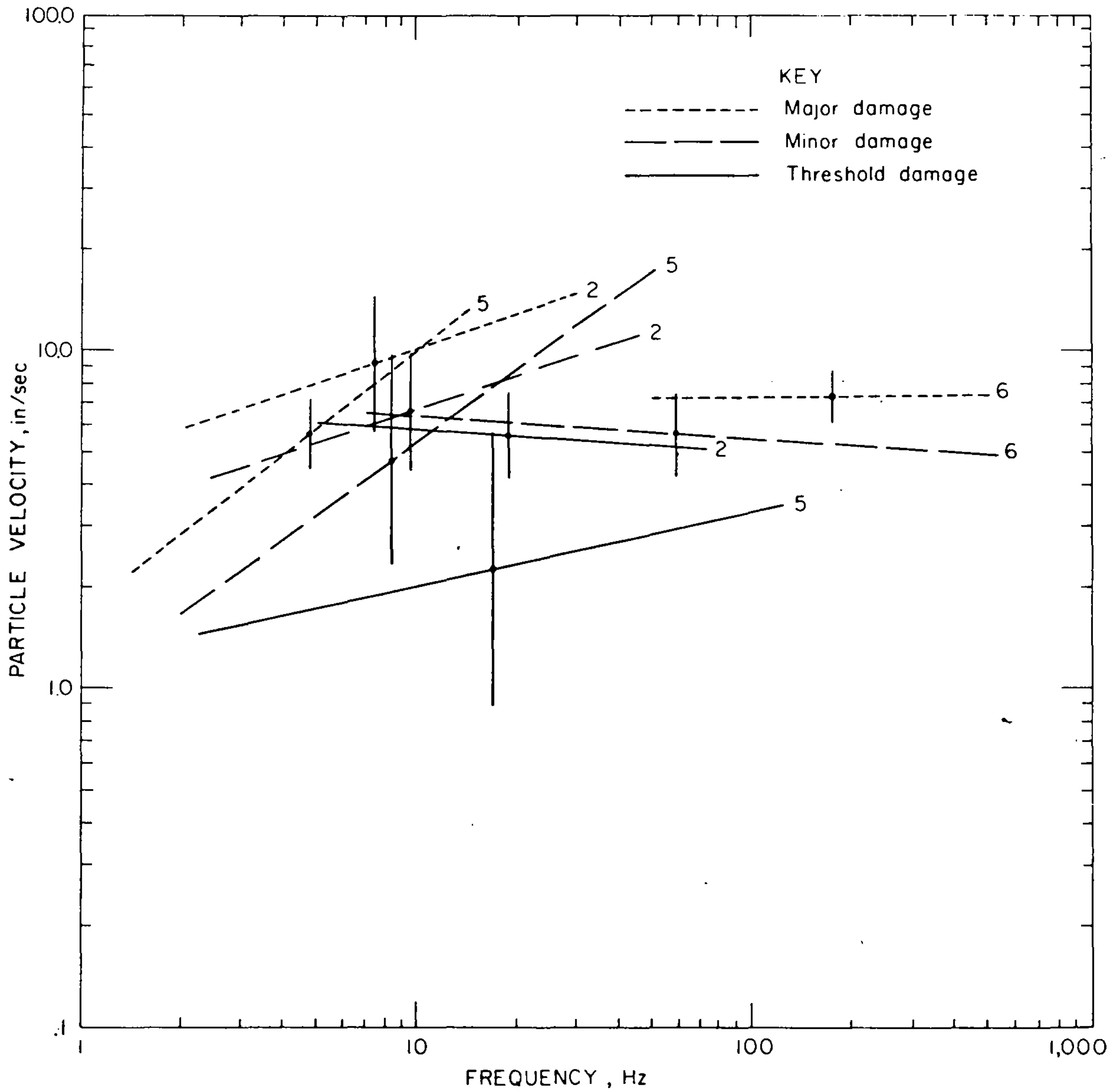

Figure 53.—Velocity versus frequency for the various damage data sets, mean and variance analysis. Sets are given in table 11.

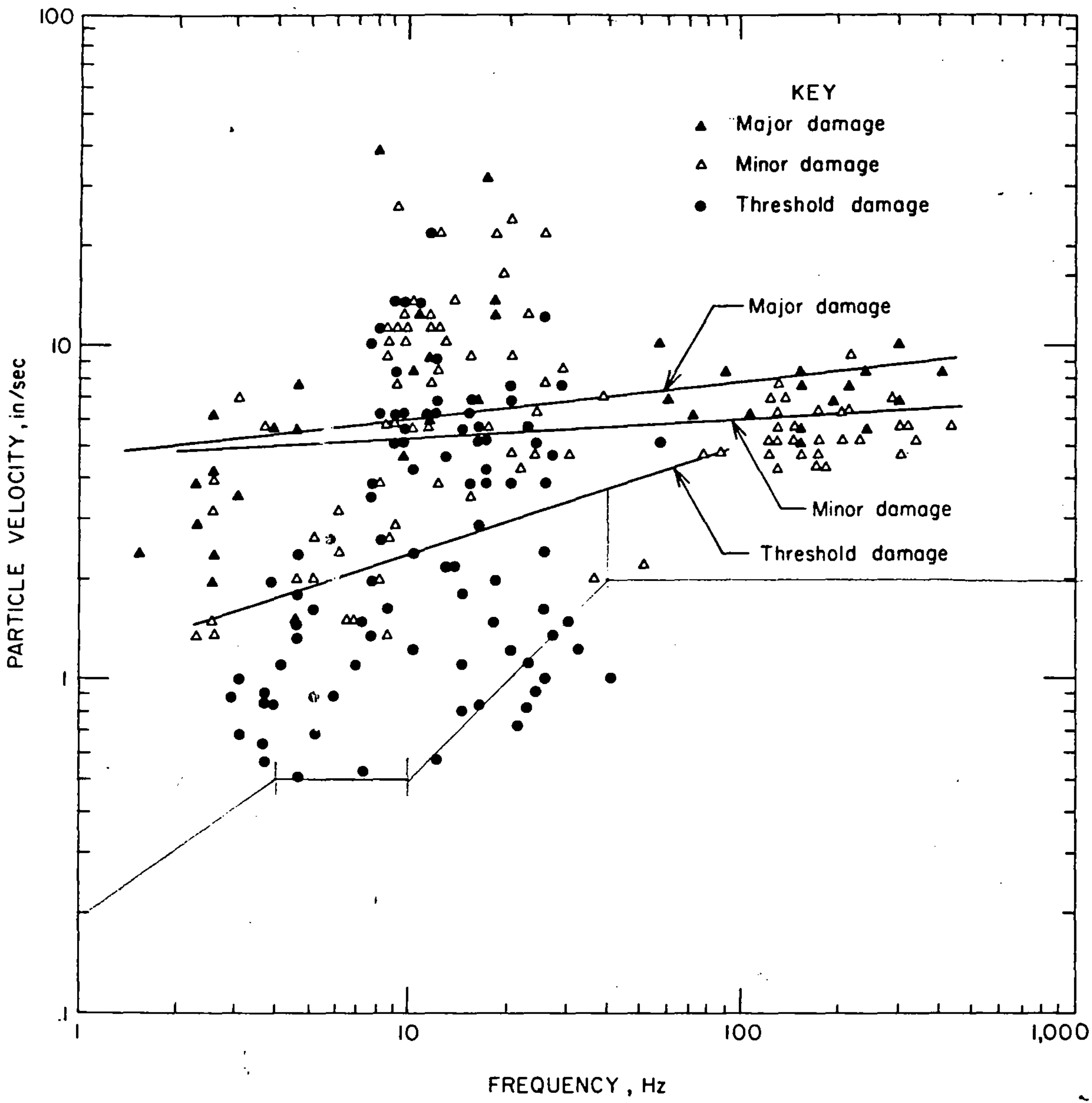

Figure 54.—Velocity versus frequency summary, set 7 mean and variance analysis.

All the sampling methods except the last violated one or more of the basic principles: (1) that the probability of damage must be independent of the sampling interval or (2) independent of the number of points (of damage or nondamage) in a given sample, and (3) that the number of new damage points must increase as levels increase. The first two principles are essential, that the probabilities concern the physics of the problem and are not a statistical artifact. The last is a result of the experimental design that involves steadily increasing levels of vibration until damage is observed. This places the observations on the upward curving part of the probability plot. When the cumulative damage was initially plotted on linear scales, they showed very little (essentially zero) damage at low levels and all damage (essentially 100 pct) at high levels. Between these extremes is the familiar S-shaped probability curve. On a log-normal ruled probability scale, the data plot as a straight line if they have the kind of log-normal distribution found for sonic boom glass breakage (*46*).

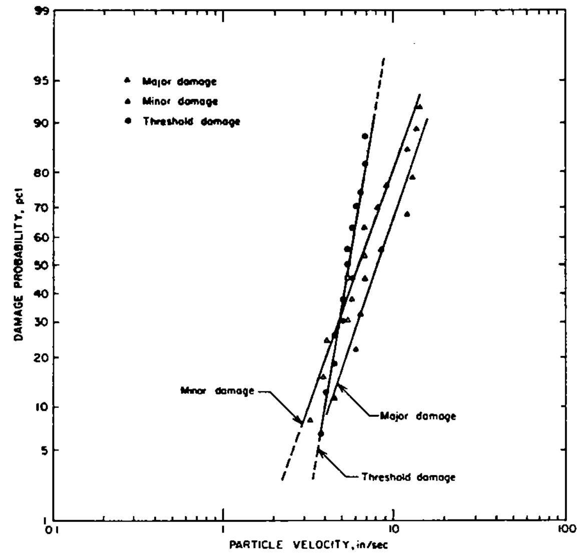

Figure 55.—Probability damage analysis for low-frequency blasts in glacial till, set 2.

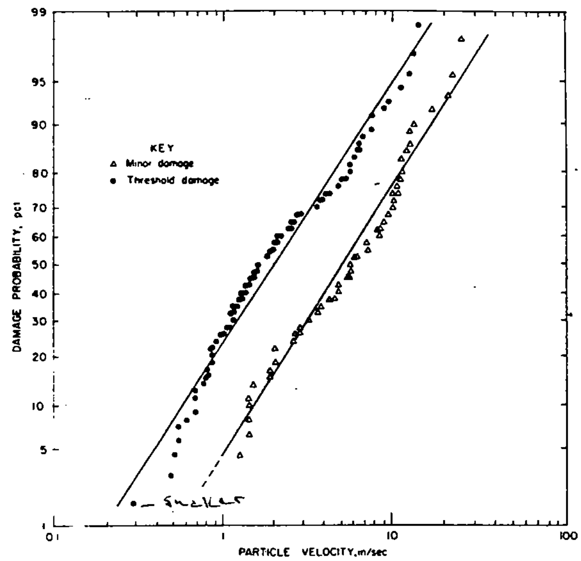

Figure 57.—Probability damage analysis for low-frequency blasts, shaker tests, and masonry damage, set 5.

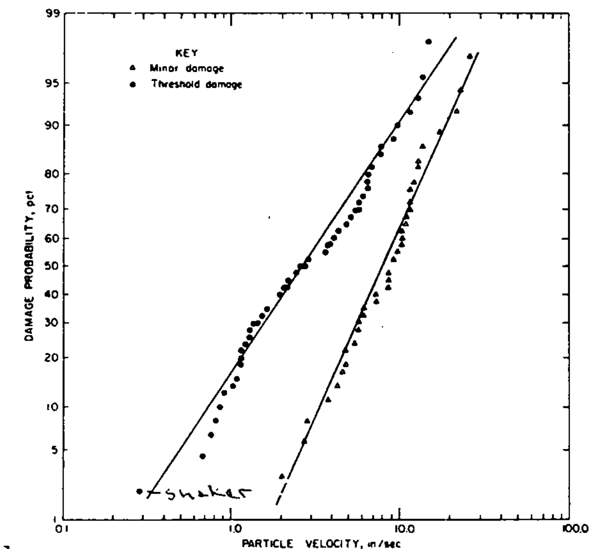

Figure 56.—Probability damage analysis for low-frequency blasts and shaker tests, set 4.

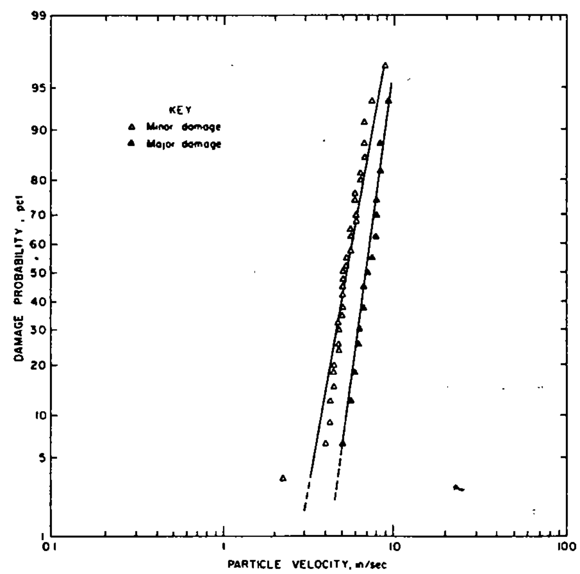

Figure 58.—Probability damage analysis for high-frequency blasts, set 6.

Log normal-scaled damage probability curves are shown in figures 55 to 59, for the same sets of studies analyzed for mean regressions. Data from the individual studies plotted as good straight-line fits, and even combining studies with apparent experimental differences still yielded high correlation coefficients.

The set 2 damage probabilities are shown in figure 55. This is primarily the two Canadian studies (*16, 38*), and as with the analysis of mean and variance, the threshold and minor damage lines cross. Projection of the probability lines for these data shows a low probability of damage below 2.0 in/sec (2 pct or less).

Sets 4 and 5 are shown in figures 56 and 57, respectively. These are again the low-frequency damage cases and the early Bureau of Mines shaker data. Set 5 includes Dvorak's study (*15*).

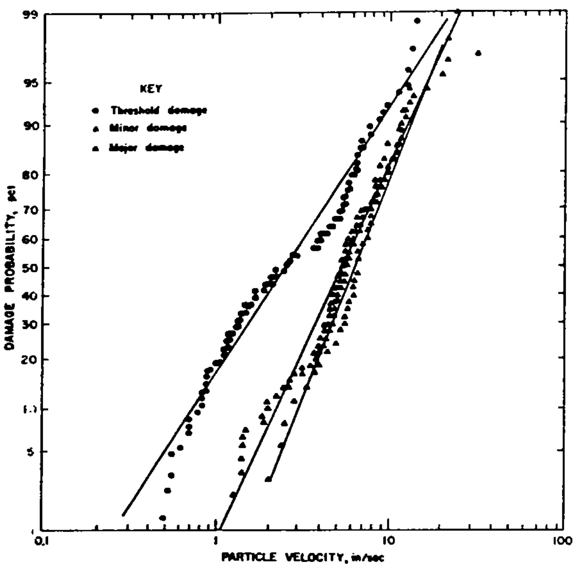

Figure 59.—Probability damage analysis summary, set 7.

The single very low valued maverick point is still included, and it produces the apparent discontinuity at the lowest vibration level. For both sets 4 and 5 probability plots, the mean line, and the trend from the individual points differ considerably at the lower probabilities. Statistical reliability increases results when the actual statistical points rather than the mean line is used for predictions. Consequently, the 5-pct damage probabilities from sets 4 and 5 are 0.80 and 0.53 in/sec, respectively.

The probability of damage from high-frequency vibrations is shown in figure 58 for set 6 data. By contrast to sets 4 and 5, data for set 6 form an excellent straight-line fit and have very steep slopes. The damage occurs over a narrow range of particle velocities, and as with the mean analysis of damage (fig. 51), it strongly supports the use of particle velocity. The vibration levels are again very high, exceeding approximately 2 in/sec for probabilities of 5 pct and below. The Swedish data alone would support a somewhat higher level, such as 3.5 in/sec for 5 pct and 3.0 in/sec for 1 pct.

The set 7 analysis (fig. 59) again represents the overall summary of all 10 sets of data. That single odd point was removed for the same reasons that it was dropped in the earlier analyses *(14, 37)*.

Most notable is the downward turn of the damage probabilities at low vibration levels, suggesting a departure from log-normal predictions and some kind of asymptotic probability toward zero damage. However, precise predictions at increasingly lower levels must necessarily become less reliable. Accurate probability figures require a large number of observations, and even this summary analysis does not have excess data, particularly for each of the principal experimental variables.

SAFE BLASTING LEVELS

The damage statistics from figures 48–59 are summarized in table 12. Safe vibration levels are suggested by the three sets of values, two from statistical analyses and a third from the simple observation of the lowest level at which damage occurred. The mean and variance values are of limited use, owing to several problems with the data. They show (for set 2) that minor damage is predicted at lower vibration levels than threshold damage. This is caused by the crossing of the means and different relative magnitudes of the standard deviations. They also produced particle velocity levels that are frequency dependent for cases where the slopes do not approximate minus 1 (set 4, threshold; set 5, minor and major; set 2, minor and major). For predictive purposes, the probability analysis results are more reliable. The lowest values of damage actually observed correspond quite closely to the 5-pct damage probabilities, except for the high-frequency data (set 6).

Safe vibration levels for blasting are given in table 13, being defined as levels unlikely to produce interior cracking or other damage in residences. Implicit in these values are assumptions that the structures are sited on a firm foundation, do not exceed 2 stories, and have the dimensions of typical residences, and that the vibration wave trains are not longer than a few seconds.

A minimum safe level of 0.50 in/sec for blasting was adopted from table 12 based on the probit analyses of set 5 (low-frequency shots) and set 7 (overall summary). This assumes a 5-pct probability for very superficial cracking. However, this vibration level is also lower than the lowest level in cases where damage was observed. The almost-constant particle velocities for the lower damage probabilities of 2 and 1 pct (threshold, set 7) strongly suggest that the

Table 12.—Summary of damage statistics by data sets

Type of damage[1]	Peak particle velocities, in/sec						
	Mean and variance analysis, standard deviations			Probability analysis			Envelope of lowest observed damage
	1.64(5 pct)	2.05(2 pct)	2.33(1 pct)	5 pct	2 pct	1 pct	
Threshold:							
Set 2	3.4	3.0	2.8	3.5	[2]3.2	[2]3.0	3.8
Set 4	.88	.63	.50	.70	NA	NA	.72
Set 5	.46	.31	.24	.52	.32	NA	.51
Set 7	.54	.36	.28	[3].53	[3].48	[3].46	.51
Minor:							
Set 2	3.0	2.6	2.3	[2]2.5	[2]2.1	[2]1.7	3.1
Set 4	3.0	2.3	2.0	2.5	[2]2.0	NA	2.0
Set 5	1.3	.98	.80	1.3	[2]1.0	NA	1.4
Set 6	3.3	3.0	2.8	3.1	NA	NA	2.2
Set 7	1.6	1.2	1.0	1.4	[2]1.2	[2]1.1	1.4
Major:							
Set 2	2.6	1.9	1.6	[2]3.3	[2]2.7	[2]2.4	4.5
Set 5	2.6	2.2	2.1	NA	NA	NA	2.0
Set 6	5.0	4.6	4.2	4.8	4.4	NA	5.5
Set 7	2.3	1.9	1.6	2.3	1.8	1.6	2.0

NA = Not available.
[1] No threshold analysis exists for set 6; no major analysis exists for set 4.
[2] Extrapolated line.
[3] Maverick point was deleted.

0.50-in/sec level will provide protection from blast damage in > 95 pct of the cases. The damage probabilities realistically refer to numbers of homes being affected by a given shot rather than the number of shots required to damage a single home. This results from the much wider variation of damage susceptibilities among structures with various degrees of prestrain as compared with a time-dependent susceptibility for a given structure. Additional work on fatigue and special soil and foundation types may later justify stricter criteria.

Data are insufficient for a thorough analysis of the damage potentials in structures of various construction types. However, the values in table 13 are obviously dominated by houses that are susceptible to cracking. Most of the observed damage listed in table 9 involved plaster cracking in older structures. Modern Drywall (gypsumboard) interior-walled homes are apparently more capable of withstanding vibrations, since the paper-backed wallboard is relatively stiff and nonbrittle. Only two studies specifically examined Drywall damage from blasting, Wiss' (57) and the new Bureau of Mines measurements. The lowest vibration level corresponding to very minor crack extensions was 0.79 in/sec (structure 20), and many nondamage observations were made at levels exceeding 2.0 in/sec. Consequently, there is little justification in using the conservative 0.50 in/sec or anything lower for modern construction, and in this case 0.75 in/sec is a good minimum criterion. The conservative 2.0 in/sec is justified for the high-frequency blasts, even though the 5-pct value is 3.2 in/sec. This is based on the lowest observed damage value of 2.2 in/sec and the fact that no observations were made of damage corresponding to the "threshold" criteria of the other studies. Construction and excavation blasting will often fall in this high-frequency category.

Table 13.—Safe levels of blasting vibrations for residential type structures

Type of structure	Ground vibration—peak particle velocity, in/sec	
	At low frequency[1] (<40 Hz)	At high frequency (>40 Hz)
Modern homes, Drywall interiors	0.75	2.0
Older homes, plaster on wood lath construction for interior walls	.50	2.0

[1] All spectral peaks within 6 dB (50 pct) amplitude of the predominant frequency must be analyzed.

Estimation of the predominant frequency is still a problem. Where the wave train is simple, the period corresponding to the peak level can be directly measured. Otherwise, some kind of spectral analysis is required. Complex vibration time histories consist of a variety of frequencies and amplitudes, so a visual estimate of frequency can be misleading. Occasionally, the peak level occurs early in the wave and at a high frequency, with a long-duration wave train of somewhat lesser amplitude following. The safest approach is to consider the low-frequency part of the time history separately, and where it is below 40 Hz, use the 0.75 in/sec or 0.50 in/sec criteria. If Fourier spectral analysis is used, any spectral peak occurring below 40 Hz and within

6 dB (half amplitude) of the peak at the predominant frequency justifies the use of the lower criteria.

A more complex scheme of assessing the damage potential of blast vibrations is possible, using a combination of particle velocity and displacement (appendix B). This permits higher levels for the intermediate-frequency cases (15 to 40 Hz) but requires lower particle velocities for the lowest frequencies (< 4 Hz). The measurement complexity will make this impractical for many situations.

RESPONSE SPECTRA ANALYSIS OF DAMAGE CASES

Damaging and nondamaging blast vibration time histories were examined for single degree of freedom response by Corser (*8*). Four old houses were analyzed, Wiss' single structure (*57*) and three from the new Bureau analysis (houses 19, 27, and 51). Corser found that the shapes of the response spectra were not noticeably different for those that produced damage and for similar blasts that did not, but they had higher pseudo velocities. The response spectra were mostly displacement-bound at the lower frequencies (less than 20 Hz), which includes the range of whole-structure response frequencies.

The lowest damage line was equivalent to structural displacements of roughly 0.012 to 0.014 in, consistent with the old British practice of taking special precautions where ground vibration levels exceed 0.016 in at frequencies below 5 Hz.

EXISTING STANDARDS FOR VIBRATIONS

A variety of vibration standards are in use or under consideration. They are intended to prevent damage to structures as well as to a great variety of other objects (e.g., computers), and also to control annoyance effects. Establishing safe and appropriate levels for all situations is well beyond the scope of this study. However, these blast vibration studies represent a major part of the research effort in this technical area. The results are often applied to situations far removed from cracking prediction in houses from short-duration, ground-transmitted vibrations. For this reason, existing blast vibration standards and reported vibration tolerances are presented in the section on Human Response and in appendix A.

HUMAN RESPONSE

The tolerance and reactions of humans to vibrations are important when standards are based on annoyance, interference, work proficiency, and health. Humans notice and react to blast-produced vibrations at levels that are lower than the damage thresholds. Similar problems also exist for annoyance from sonic booms and airblasts, and these are discussed in a related study of airblasts (*46*). The technical problem of quantifying responses is complicated by the simultaneous presence of both ground vibration and airblast and the many secondary effects of wall-produced window, dish, and bric-a-brac rattling. Persons inside buildings will hear and feel the predominantly 5- to 25-Hz structure midwall and midfloor response vibrations (*45*). Ground vibrations are occasionally blamed for house vibrations when long-range airblasts propagating under favorable weather conditions are responsible. The very infrasonic airblast itself cannot be heard, but the house responds as if subjected to a ground vibration.

Critical to levels of response are the vibration characteristics (duration, peak level, vibration frequency, and frequency of occurrence), reaction descriptors (startle, fright, fear of damage, sleep, or other interference), and tolerance descriptors (health and safety endangered, work or proficiency, and comfort or annoyance boundaries). Running like a thread through the already complex fabric are social, economic, and legal factors, typified by the importance of the vibration source to the Nation, community, or individuals involved. Examples are the temporary or indefinite nature of this environmental intrusion, beliefs in the inevitability of the source, and the social consciousness of the blaster (as shown by his public relations program and blast design efforts that minimize ground vibrations and airblast).

Most studies of human tolerance to vibrations have been of steady-state sources or those of relatively longer duration than typical mine, quarry, and construction blasting. In the absence of data on tolerance to impulsive vibrations, these results have been assumed to be applicable to blasting. Additionally, most useful data are from tests involving human subjects directly, when not in their homes. The duration and frequency of occurrence of the events are obviously critical. The vibration limits required for reasonable comfort from a long-term vibration source (e.g., air conditioning, machinery, building elevators, and vehicle traffic) are certainly more restrictive than for sources of short duration and infrequent occurrence.

The classical study of subjective human tolerance to vibratory motion was done by Reiher and Meister in 1931 (*40*). They subjected 15 people to 5-min duration vertical and horizontal vibrations in a variety of body positions and established levels of perception and comfort. Responses of "slightly perceptible" occcurred at 0.010 to 0.033 in/sec, and the threshold of "strongly perceptible" was 0.10 in/sec, all essentially independent of frequency over the range 4 to 25 Hz.

More recent research on the effects of vibration on man have produced results similar to those of Reiher and Meister (*2, 18, 55*). Goldman analyzed human response to steady-state vibration in the frequency range of 2 to 50 Hz (*18*). His results were converted to particle velocities and presented in Bulletin 656 (*37*, fig. 3.9), where the lines represent means within each response category. One standard deviation of the reactions was at approximately half the level of the means. Goldman's "slightly perceptible" and "strongly perceptible" (unpleasant) levels at 1.65 standard deviations (including all but 5 pct at the low end) are approximately 0.0086 and 0.074 in/sec, respectively, at 10 Hz. Taking these as thresholds, they agree quite well with Reiher and Meister's data.

Several researchers recognized that the duration of the vibration was critical to its undesirability. Most evident was that a higher level could be tolerated if the event was short. Consequently, steady-state vibration data could not be realistically applied to blasting, except for events that exceed several seconds' duration. A good example of a long event was the Salmon nuclear blast (*37, 39*). This was technically a transient; however, the 90-sec-long, low-frequency wave train produced at large distances resulted in numerous complaints (10 pct of all families at 0.40 in/sec). This duration exceeds that of any kind of mining blasts. Chang analyzed the human vibration response literature with particular attention to event durations (*7*). He noted that Reiher and Meister's responses could be multiplied by a factor of 10 for short events. Atherton studied impact- and walking-

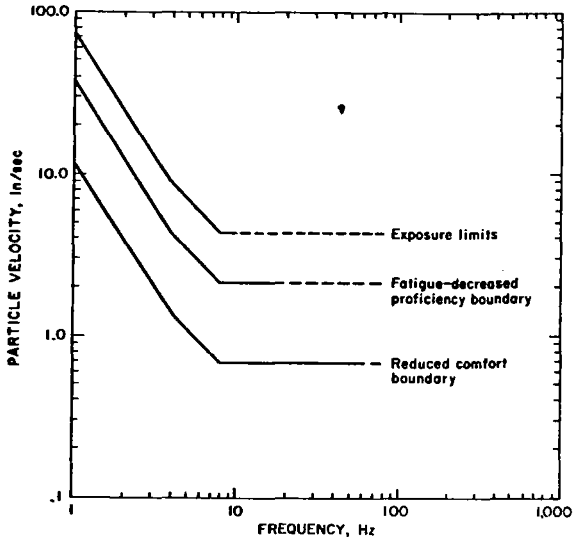

Figure 60.—Human tolerance standards for rms vibrations exceeding 1-minute-duration ISO 2631.

produced floor motions. His impact tests consisted of 3 to 5 cycles of motion at 19 Hz (the floor resonance), or events of approximately 200-msec duration. His "disturbing" level mean was 3.5 to 4.4 in/sec, or over 5 times Goldman's steady-state "intolerable" level of 0.77 in/sec at 20 Hz.

The International Standards Organization (ISO) published tolerable levels for whole body vibration in 1978 (*19*). The scope of their standard included durations of 1 min and longer, frequencies of 1 to 80 Hz, three-axis vibrations, and human tolerances for comfort, working efficiency, fatigue, and health and safety. Their recommendations for 1-min-duration events are shown in figure 60, having been converted from accelerations to particle velocities and corresponding to the worst-case body orientation (longitudinal or Z-axis). All values are rms and are constant particle velocities for frequencies above 8 Hz. Peak values would be larger by a factor of 1.4 to 3. The dashed part of the lines in figure 60 represent peak accelerations in excess of 1 g.

Wiss and Parmelee studied the responses of 40 people to transient vibrations consisting of damped 5-sec sinusoidal pulses (*58*). Damping ranged from zero to 16 pct and frequencies from 2.5 to 25 Hz. All subjects were standing on an open platform and subjected to vertical vibrations. They found that responses depended on vibration levels and damping but were independent of frequency, when plotted in units of frequency times displacement (velocity). Their results, and the two steady-state vibration studies, are shown in figure 61. The various experimental factors for the three studies are listed in table 14. The reaction descriptors were different, a sign of the subjective nature of this kind of work. "Thresholds" correspond to the responses of the most sensitive people tested. "Means" are the responses of the "average subject" within each response descriptor category. Between Goldman's "unpleasant" and "intolerable" (G–2 and G–3) lies the ISO "reduced comfort boundary". Wiss and Parmalee's results were reanalyzed for duration-of-vibration effects, with damping frequency and duration being interrelated. It was assumed that the vibration duration is the time during which the vibration level exceeds 10 pct of the peak (−20 dB). The following relationship was derived:

$$\tau = \frac{0.{:}67}{f\beta} + 0.018$$

where τ is the duration (sec), f the frequency (Hz), β is the damping ratio, and 0.018 the average input rise time (sec). Application of this equation to Wiss and Parmelee's test runs allows durations to be calculated for the various reactions that become slightly frequency dependent when plotted as particle velocities (fig. 62), and very much so when plotted as accelerations (fig. 63).

Table 14.–Studies of human response to vibration

Authors	Vibration duration, sec	Curve representations, response descriptors, and curve label for data plotted in figure 61
Goldman (*18*):		Mean values of subject response:
Various body positions, 5 sources	5	Perceivable (curve G–1).
Do	5	Unpleasant (curve G–2).
Do	5	Intolerable (curve G–3).
Reiher and Meister (*40*):		Thresholds:
Standing with vertical vibration	300	Barely noticeable (curve R–1).
Do	300	Objectionable (curve R–2).
Do	300	Uncomfortable (curve R–3).
Wiss and Parmalee (*58*):		Mean values of subject response:
Standing with vertical vibration	5	Barely perceptible (curve W–1).
Do[1]	5	Distinctly perceptible (curve W–2)
Do[1]	5	Strongly perceptible (curve W–3).
		Thresholds:
Do[1]	5	Barely perceptible (curve W–4).
Do[2]	5	Distinctly perceptible (curve W–5).
Do[2]	5	Strongly perceptible (curve W–6).
Do[2]	5	Severe (curve W–7).

[1] Transient with 1 pct damping. 5-sec duration is maximum.
[2] Zero damping.

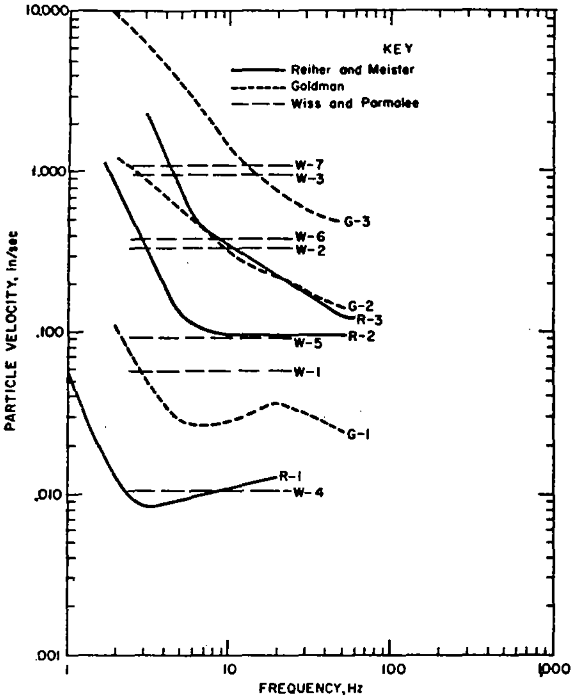

Figure 61.—Human response to steady-state and transient vibrations. Labels refer to measurements listed in table 14.

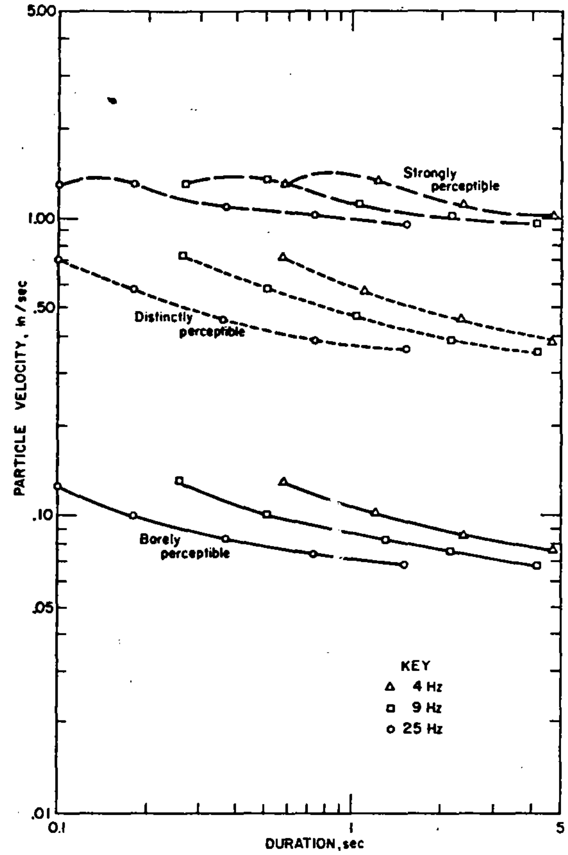

Figure 62.—Human response to transient vibration velocities of various durations.

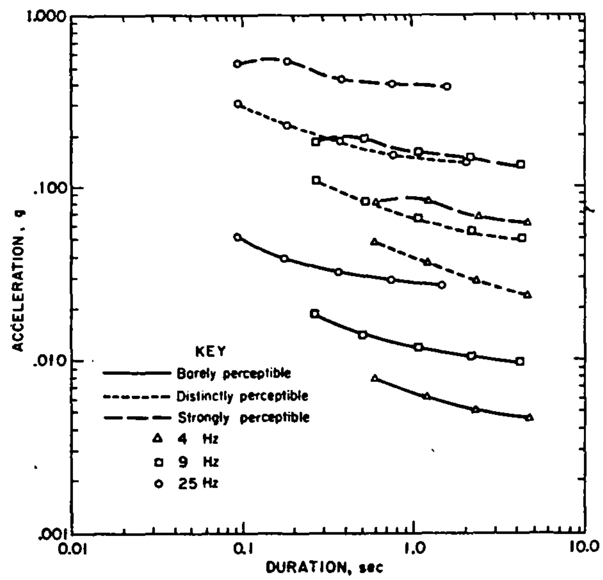

Figure 63.—Human response to transient vibration accelerations of various durations.

T. M. Murray investigated human reactions to vibrations of concrete floors (*33*). His summary of 91 observations of acceptable versus unacceptable cases indicated strong influences for amplitude times frequency (same units as particle velocity) and damping levels. He derived the following relationship for an acceptable concrete floor:

$$\beta \geq 35Af_0 + 2.5$$

where β is percent of critical damping (damping ratio × 100), A is initial amplitude from a heel-drop impact (in), and f_0 is the first natural frequency (Hz). Murray's data were converted to peak particle velocities and are shown in figure 64. The line represents the equation above and is Murray's eyeball separation between acceptable and unacceptable cases. Acceleration and displacement plots were also made from Murray's data and, unlike the particle velocity data, they showed a strong frequency influence.

As with Wiss' data, Murray's 91 points were converted into duration-amplitude form using the relationship:

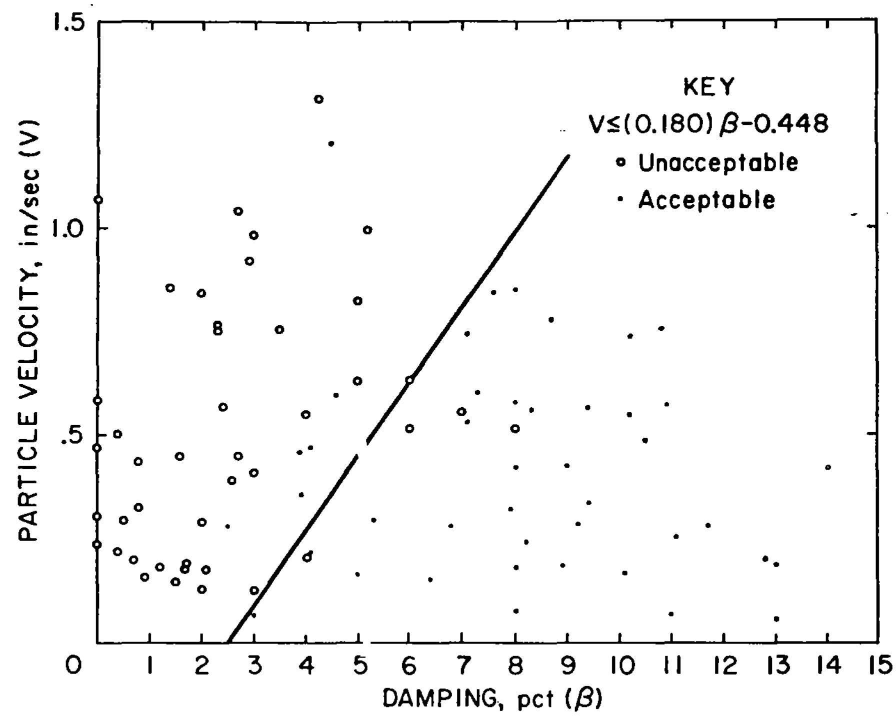

Figure 64.—Human response to vib ations of damped concrete floors, after Murray (*33*). Equatior defines acceptable zone.

$$\tau = \frac{36.7}{\beta f}$$

where β is the percentage of critical damping.

The results, given in figure 65, show a strong influence on acceptability of both floor velocity and vibration duration. As in Murray's analysis, a separation of cases was derived by visual means and produced the following acceptability criterion:

$$V \leqslant 0.415\ \tau^{-1.29}$$

where V is the peak floor vibration (in/sec) and τ is the time (sec) from the peak to the minus 20-dB level (or 10 pct of peak amplitude). The amplitude-duration acceptability line shows a better defined separation of cases than Murray's original amplitude-damping version.

As with Murray's damping version of the data, the duration version did not produce simple relationships when plotted as accelerations and displacements, with frequency factors and nonlinear plots required. Murray suggests that his acceptability criteria for concrete floors may be conservative compared with that for wooden floors, where a greater amount of vibration is normally expected.

Human reactions to events of varying durations are summarized in figure 66, with the values given in table 15. In cases where "distinctly perceptible" applies (i.e., infrequent and short-duration events), these results suggest that levels of over 0.5 in/sec could be tolerated. The barely perceptible levels are still below 0.1 in/sec; consequently, it is impractical for blasting ever to be totally unobtrusive.

The studies just discussed all involve people in a test situation rather than in their own homes. None of the problems of damage fear, startle, house rattle, and other secondary effects were present. Undoubtedly, the addition of such effects lowers the thresholds at which people react. Relationships have been developed for people subjected to sonic booms and airblasts in their "normal" environment (*46*).

An estimate of annoyance from indoor-perceived ground vibration can be made by comparing airblast and ground vibration-produced midwall response (fig. 41), and the annoyance curves from airblast study. Estimated ground-vibration-produced human reactions are given in figure 67 based on the airblast responses from figure I–1 of RI 8485 (*46*). These are for coal mining; quarry levels are 20 pct higher. The three lines of the figure show the distribution

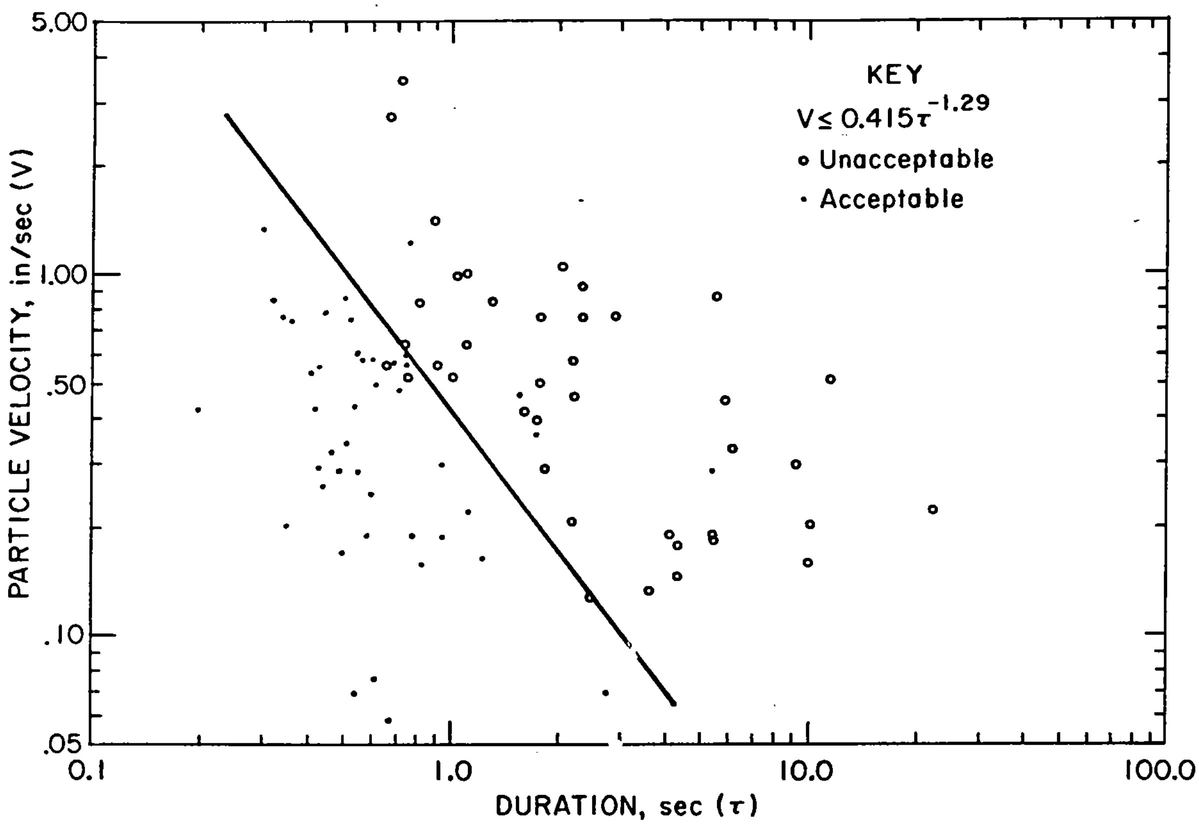

Figure 65.—Human response to concrete floor vibrations of various durations. Equation defines acceptable zone.

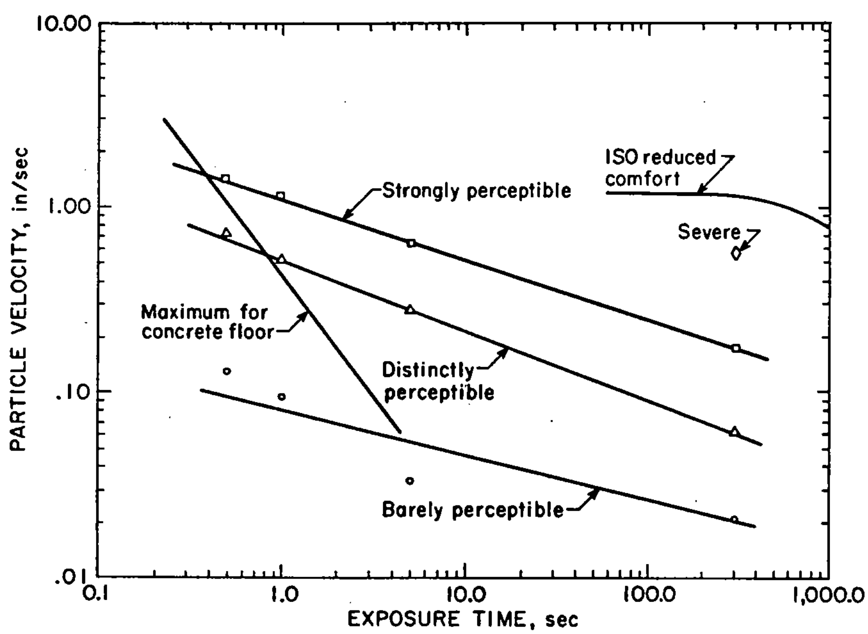

Figure 66.—Human response to vibrations of various durations, summary. ISO values are from Standard 2631.

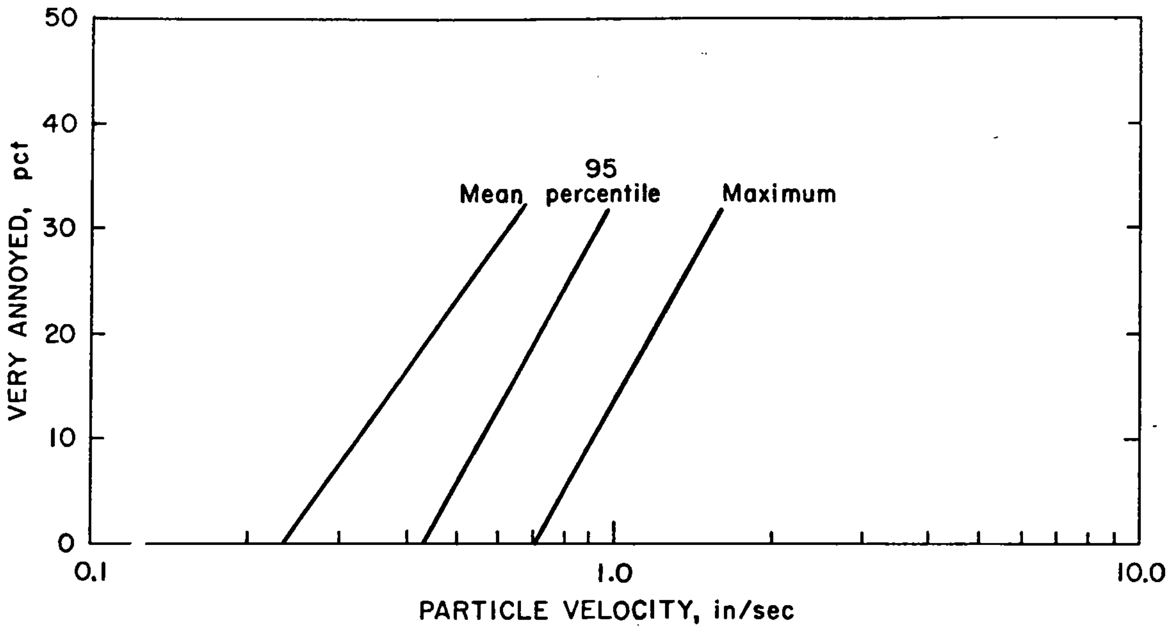

Figure 67.—Reactions of persons subjected to blasting vibration in their homes.

of the particle velocities. Since reactions are most likely from stronger events, actual public reaction would occur somewhere between that corresponding to the mean vibration level and the maximum, probably close to the 95th percentile. Exact determination of the airblast-produced human reactions (and also those produced by ground vibration) is not possible without knowing how closely the reported subjective reactions correspond to various levels of sonic boom experienced during the three test periods. It is possible and even likely that those interviewed reacted more to the higher level booms (e.g., maximum values). More work is needed to quantify reactions and specific levels. The potential for ground vibrations to produce strong public reaction is evident from figure 67. In the absence of a public relations program, it is expected that a mean ground vibration level of 0.50 in/sec in a community will produce 15 to 30 pct "very annoyed" neighbors. The 95-pct line gives 5 pct very annoyed at 0.5 in/sec. The blaster must convince the nearby homeowners that the rattling is to be expected and is not damaging. He can also demonstrate his sincerity by blasting as unobtrusively as possible, and using the best blast design principles.

Table 15.—Subjective responses of humans to vibrations of various durations

Type of response	Duration, sec	Particle velocity, in/sec	Source
Barely perceptible:			
Mean	0.5	0.130	Wiss and Parmelee (*58*).
Do	1	.095	Do.
Do	5	.033	Do.
Do	300	.020	Reiher and Meister (*40*).
Threshold	5	.011	Wiss and Parmelee (*58*).
Do	300	.011	Reiher and Meister (*40*).
Disticly perceptible:			
Mean	.5	.700	Wiss and Parmelee (*58*).
Do	1	.500	Do.
Do	5	.280	Do.
Do	300	.060	Reiher and Meister (*40*).
Threshold	.5	.300	Wiss and Parmelee (*58*).
Do	1	.230	Do.
Do	5	.100	Do.
Do	300	.033	Reiher and Meister (*40*).
Strongly perceptible:			
Mean	.5	1.400	Wiss and Parmelee (*58*).
Do	1	1.150	Do.
Do	5	.630	Do.
Do	300	.170[1]	Reiher and Meister (*40*).
Threshold	.5	.910	Wiss and Parmelee (*58*).
Do	1	.810	Do.
Do	5	.390	Do.
Do	300	.102	Reiher and Meister (*40*).
Severe:			
Mean	300	.550[1]	Do.
Threshold	5	1.13	Wiss and Parmelee (*58*).
Do	300	.301	Reiher and Meister (*40*).
Acceptable	0.2–4	$\leqq 0.415\tau^{1.29}$	Murray (*33*).[2]

[1] At 9 Hz.
[2] τ = duration (sec).

CONCLUSIONS

The problems of blasting vibration damage to residential structures and human tolerance to vibrations have been analyzed using data from a wide variety of studies. Statistical techniques of mean and variance analysis and probability plots have both been applied to the damage data from the 10 studies and demonstrated the following:

1. Particle velocity is still the best single ground motion descriptor.
2. Particle velocity is the most practical descriptor for regulating the damage potential for a class of structures with well-defined response characteristics (e.g., single-family residences).
3. Where the operator wants to be relieved of the responsibility of instrumenting all shots, he could design for a conservative square root scale distance of 70 ft/lb$^{1/2}$. The typical vibration levels at this scaled distance would be 0.08 to 0.15 in/sec.
4. Damage potentials for low-frequency blasts (< 40 Hz) are considerably higher than those for high-frequency blasts (> 40 Hz), with the latter often produced by close-in construction and excavation blasts.
5. Home construction is also a factor in the minimum expected damage levels. Gypsumboard (Drywall) interior walls are more damage resistant than older, plaster on wood lath construction.
6. Practical safe criteria for blasts that generate low-frequency ground vibrations are 0.75 in/sec for modern gypsumboard houses and 0.50 in/sec for plaster on lath interiors. For frequencies above 40 Hz, a safe particle velocity maximum of 2.0 in/sec is recommended for all houses.
7. All homes eventually crack because of a variety of environmental stresses, including humidity and temperature changes, settlement from consolidation and variations in ground moisture, wind, and even water absorption from tree roots. Consequently, there may be no absolute minimum vibration damage threshold when the vibration (from any cause, for instance slamming a door) could in some case precipitate a crack about to occur.
8. The chance of damage from a blast generating peak particle velocities below 0.5 in/sec is not only small (5 pct for worst cases) but decreases more rapidly than the mean prediction for the entire range of vibration levels (almost asymptotically below about 0.5 in/sec).
9. Human reactions to blasting can be the limiting factor. Vibration levels can be felt that are considerably lower than those required to produce damage. Human reaction to vibration is dependent on event duration as well as level. Particle velocities of 0.5 in/sec from typical blasting (1-sec vibration) should be tolerable to about 95 pct of the people perceiving it as "distinctly perceptible". Relevant to whole-body vibration reaction is the degree that the vibration interferes with activity (sleep, speech, TV viewing, reading), presents a health hazard, and affects task proficiency. For people at home, the most serious blast vibration problems are house rattling, fright (fear of damage or injury), being startled, and for a few, activity interference. Complaints from these causes can be as high as 30 pct at 0.5 in/sec, and this is where good public relations attitudes and an educational program by the blaster are essential.

REFERENCES

1. Ashley, C. Blasting in Urban Areas. Tunnels and Tunneling, v. 8, No. 6, September/October 1976, pp. 60–67.
2. Atherton, G. H., A. Polensek, and S. E. Corder. Human Response to Walking and Impact Vibration of Wood Floors. Forest Prod. J., v. 26, No. 10, October 1976, pp. 40–47.
3. Beck, W. K. Fatigue Cracking of Drywall to Model Blast Loading. M.S. Thesis, Dept. Civil Eng., Northwestern Univ., Evanston, Ill., June 1979, 131 pp.
4. Bergling, J. O., K. Eklund, and C. Sjoberg. A Villa Built of Light Concrete and Concrete Exposed to Vibrations From Blasting. Swedish Council for Bldg. Res., Bldg. Res. Summaries, R 32, 1977, 85 pp.
5. Blume, John A. and Associates, Research Division. Response of Tall Industrial and Residential Structures to an Underground Nuclear Detonation. VELA Uniform Program, Project Dribble, Salmon Event RPT, VUF–1031. Final Rept. to the Advanced Res. Agency of the Department of Defense and the Atomic Energy Commission, Nov. 15, 1965, 31 pp.
6. Bogdanoff, I., T. Larson, and R. Nilsson. Lightweight Concrete Buildings Exposed to Vibrations From Blasting Operations. Swedish Council for Bldg. Res., Bldg. Res. Summaries, R 42, 1975, 47 pp.
7. Chang, F. Human Response to Motions in Tall Buildings. Proc. ASCE, v. 99, No. 2, June 1973, pp. 1259–1272.
8. Corser, P. Wall Cracking in Residential Structures From Surface Mining and Hard Rock Construction Blasts. M.S. Thesis, Dept. Civil Eng., Northwestern Univ., Evanston, Ill., August 1979, 199 pp.
9. Crawford, R., and H. S. Ward. Dynamic Strains in Concrete and Masonry Walls. Div. Bldg. Res., National Res. Council, Ottawa, Canada, Bldg. Res. Note 54, December 1965, 13 pp.
10. Dowding, C. H. Response of Buildings to Ground Vibrations Resulting From Construction Blasting. Ph.D. Thesis, Univ. Illinois, Urbana, Ill., 1971, 204 pp.
11. Dowding, C. H., W. K. Beck, and D. K. Atmatzidis. Blast Vibration Implications of Cyclic Shear Behavior of Model Plaster Panels. Geotechnical Testing J., ASTM, v. 3, No. 2, June 1980.
12. Dowding, C. H., and P. G. Corser. Cracking and Construction Blasting. Importance of Frequency and Free Response. J. Construction Div., ASCE, March 1981 (in press).
13. Dowding, C. H., P. D. Murray, and D. K. Atmatzidis. Dynamic Properties of Residential Structures Subjected to Blasting Vibrations. J. Structural Div., ASCE, 1981 (in press).
14. Duvall, W. I., and D. E. Fogelson. Review of Criteria for Estimating Damage to Residences From Blasting Vibrations. BuMines RI 5968, 1962, 19 pp.
15. Dvorak, A. Seismic Effects of Blasting on Brick Houses. Prace geofyrikeniha Ustance Ceskoslovenski Akademie Ved. No. 169. Geofysikalni Sbornik, 1962, pp. 189–202.
16. Edwards, A. T., and T. D. Northwood. Experimental Studies of the Effects of Blasting on Structures. The Engineer, v. 210, Sept. 30, 1960, pp. 538–546.
17. Esteves, J. M. Control of Vibrations Caused by Blasting. Laboratorio National De Engenharia Civil, Lisboa, Portugal, Memoria 498, 1978, 11 pp.
18. Goldman, D. E. A Review of Subjective Responses of Vibrating Motion of the Human Body in the Frequency Range, 1 to 70 Cycles per Second. Naval Medical Res. Inst., Proj. NM 004001, Rept. 1, Mar. 16, 1948, 17 pp.
19. International Standards Organization. Guide for the Evaluation of Human Exposure to Whole-Body Vibration. ISO 2631–1978 (E), 1978, 15 pp.
20. Jackson, M. W. Thresholds of Damage Due to Ground Motion. Proc. Internat. Symp. on Wave Propagation and Dynamic Properties of Earth Materials, Univ. New Mexico, Albuquerque, N. Mex., Aug. 23, 1967, pp. 961–969.
21. Jensen, D. E., and J. D. Rietman. Collection of Ground and Structure Vibration Data Generated From Small Charge Residentially Adjacent Construction Blasting. Woodward-Clyde Consultants, Proj. 410741. Final report to the Bureau of Mines, Nov. 9, 1978, 71 pp.; available for consultation at the Twin Cities Research Center, Bureau of Mines, Twin Cities, Minn.
22. Kamperman. G., and M. A. Nicholson. The Transfer Function of Quarry Blast Noise and Vibration Into Typical Residential Structures. Kamperman Associates, Inc. Final Report to the Environmental Protection Agency, Washington, D.C., EPA 550/9–77–351, February 1977, 43 pp.; National Technical Information Service, Springfield, Va., PB 288 892.
23. Koerner, R. M., J. N. Deisher, and R. P. Scheller. Laboratory Study of Cracking in Model Block Masonry Walls. Proc. 3d Ann. Conf. on Explosives and Blasting Techniques, Soc. Explosive Eng., Pittsburgh, Pa., Feb. 23, 1977, pp. 227–237.
24. Langan, R. T. The Use of Single-Degree-of-Freedom System as a Dynamic Model for Low-Rise Residential Structures Subjected to Blast Vibrations. M.S. Thesis, Northwestern Univ., Evanston, Ill., 1980, 79 pp.
25. Langefors, U., and B. K. Kihlstrom. Rock Blasting. John Wiley and Sons, Inc., New York, 1963, 405 pp.
26. Langefors, U., B. Kihlstrom, and H. Westerberg. Ground Vibrations in Blasting. Water Power, February 1958, pp. 335–338, 390–395, 421–424.
27. Leet, D. L. Vibrations From Construction Blasting. Hercules Powder Co., Wilmington, Del., 1960, 24 pp.
28. Leigh, B. R. Lifetime Concept of Plaster Panels Subjected to Sonic Boom. Univ. Toronto, Canada, UTIAS–TN–191, July 1947, 78 pp.
29. Lucole, S., and C. H. Dowding. Statistical Analysis of Blast Emission. Records From Quarrying, Mining, and Construction Operations in the State of Illinois. Illinois Inst. of Nat. Res., Doc. 79/02, Proj. 30.013, January 1979, 200 pp.
30. Medearis, K. The Development of Rational Damage Criteria for Low-Rise Structures Subjected to Blasting Vibrations. Kenneth Medearis Associates, Final Rept. to National Crushed Stone Assn., Washington, D.C., August 1976, 93 pp.
31. Morris, G., and R. Westwater. Damage to Structures by Ground Vibrations Due to Blasting. Mine and Quarry Eng., April 1953, pp. 116–118.
32. Murray, P. D. Dynamic Properties of Residential Structures Subjected to Blasting Vibrations. M.S. Thesis, Dept. Civil Eng., Northwestern Univ., Evanston, Ill., June 1978, 142 pp.

33. Murray, T. M. Acceptability Criteria for Occupant-Induced Floor Vibrations. Sound and Vibration, v. 13, No. 11, November 1979, pp. 24–30.
34. Nadolski, M. E. Architectural Damage to Residential Structures From Seismic Disturbances. Bull. Seis. Soc. Am., v. 59, No. 2, April 1969, pp. 487–502.
35. Navarro, R. Old Reliable Mine Project Seismic Measurements. NOAA Tech. Memo, ERL ESL–19, July 1972, 17 pp.
36. Nelson. W. H. Movement of Building Element Cracks in Six Mercury Nevada Structures. John A. Blume and Associates, Research Div., San Francisco, Rept. NVO–99–20 to The Nevada Operations Office. U.S. Atomic Energy Comm., December 1957, 45 pp. (contract AT (26–1)–99).
37. Nicholls, H. R., C. F. Johnson, and W. I. Duvall. Blasting Vibrations and Their Effects on Structures. BuMines Bull. 656, 1971, 105 pp.
38. Northwood, T. D., R. Crawford, and A. T. Edwards. Blasting Vibrations and Building Damage. The Engineer, v. 215, No. 5601, May 31, 1963, pp. 973–978.
39. Power, D. V. A Survey of Complaints of Seismic Related Damage to Surface Structures—Salmon Event. Bull. Seis. Soc. Am., v. 56, No. 6, December 1966, pp. 1413–1428.
40. Reiher, H., and F. J. Meister. (The Effect of Vibration on People.) Forschung auf dem Gebeite des Ingenieurwesens (Germany), v. 2, No. 11, 1931, p. 381; transl. by Headquarters Air Material Command, Wright Field, Ohio, Rept. F–TSL–616–RE, 1946.
41. Richter, C. F. Elementary Seismology. W. H. Freeman and Co., San Francisco, 1958, 768 pp.
42. Scholl, R. E. Low-Rise Building Damage From Low Amplitude Ground Motions. John A. Blume and Associates, Research Div., San Francisco, Rept. JAB–99–117 to U.S. Atomic Energy Comm., April 1974, 22 pp. (contact AT(26–1)–99).
43. Scholl, R. E., and I. Farhoomand. Statistical Correlation of Observed Ground Motion With Low-Rise Building Damage. Bull. Seis. Soc. Am., v. 63, No. 5, October, 1973, pp. 1515–1537.
44. Seismore, C. J. Analyzing of Surface-Motion Data From Old Reliable Mine Blast. Lawrence Livermore Lab., Rept. UDIC–16314, July 19, 1973, 19 pp.
45. Siskind, D. E., V. J. Stachura, and K. S. Radcliffe. Noise and Vibrations in Residential Structures From Quarry Production Blasting. Measurements at Six Sites in Illinois. BuMines RI 8168, 1976, 17 pp.
46. Siskind, D. E., V. J. Stachura, M. S. Stagg, and J. W. Kopp. Structure Response and Damage Produced by Airblast From Surface Mining. BuMines RI 8485, 1980.
47. Skipp, B. O. Ground Vibration Instrumentation—A General Review. Instrumentation for Ground Vibration and Earthquakes. Proc., Conf. for Earthquake and Civil Eng. Dynamics, Keele, England, July 4, 1977, pp. 11–34.
48. Snodgrass, J. J., and D. E. Siskind. Vibrations From Underground Blasting. BuMines RI 7937, 1974, 31 pp.
49. Stachura, V. J., D. E. Siskind, and A. J. Engler. Airblast Instrumentation and Measurement Techniques for Surface Mine Blasting. BuMines RI 8508, 1981 (in press).
50. Stagg, M. S., and A. J. Engler. Ground Vibration Measurement and Seismograph Calibration. BuMines RI 8506, 1980 (in press).
51. Thoenen, J. R., and S. L. Windes. Seismic Effects of Quarry Blasting. BuMines Bull. 442, 1942, 83 pp.
52. Tynan, A. E. Ground Vibrations, Damaging Effects to Buildings. Australian Road Res. Bd., Spec. Rept. 11, 1973, 61 pp.
53. Wall, J. F., Jr. Seismic-Induced Architectural Damage to Masonry Structures at Mercury, Nevada. Bull. Seis. Soc. Am., v. 57, No. 5, October 1967, pp. 991–1007.
54. Wendler, B. H., M. J. Rosenfield, J. B. Gambill, W. E. Fischer, R. G. Merritt, and J. A. Gill. Shock Environment Test of Model Drywall Room (Bureau of Mines Test Package No. 1). U.S. Army Constr. Eng. Res. Lab., Champaign, Ill., Tech. Rept. M–152, August 1975, 81 pp.
55. Whiffin, A. C., and D. R. Leonard. A Survey of Traffic-Induced Vibrations. Road Res. Lab., Dept. Environment, Crowthorne, Berkshire, England, Rept. RRL LR 418, 1971, 58 pp.
56. Wiss, J. F., and P. Linehan (Wiss, Janney, Elstner and Associates, Inc.). Control of Vibration and Blast Noise From Surface Coal Mining. BuMines Open File Rept. 79–103, 1979, v. 1, 159 pp.; v. 2, 280 pp.; v. 3, 624 pp.; v. 4, 48 pp.; available for consultation at the BuMines libraries in Denver, Colo., Twin Cities, Minn., Pittsburgh, Pa., and Spokane, Wash.; U.S. Dept. Energy facilities in Carbondale, Ill., and Morgantown, W. Va.; Nat. Mine Health and Safety Academy, Beckley, W. Va.; and Nat. Library of Natural Resources, U.S. Dept. Interior, Washington, D.C. Contract JO 255022; Nat. Tech. Inf. Service, Springfield, Va., PB 299 886/AS.
57. Wiss, J. F., and H. R. Nicholls. A Study of Damage to a Residential Structure From Blast Vibrations. Res. Council for Performance of Structures, ASCE, New York, 1974, 73 pp.
58. Wiss. J. F., and R. A. Parmelee. Human Perception of Transient Vibrations. J. Structural Div., ASCE, v. 100, No. ST4, Proc. Paper 10495, April 1974, pp. 773–787.

APPENDIX A.—EXISTING VIBRATION STANDARDS AND CRITERIA TO PREVENT DAMAGE

The German vibration standards (DIN 4150) are intended to protect buildings but are so strict as to be unworkable (table A–1). Reportedly, they are not enforced, at least for blasting. No technical data have been given to justify the levels specified (*4, 52*).[1]

The Australian standard (CA 23–1967) specifies maximums of

(1) 0.008-in displacement for frequencies less than 15 Hz and

(2) 0.75 in/sec resultant peak particle velocity for frequencies greater than 15 Hz.

The 0.008-in maximum displacement corresponds to 0.5 in/sec at 10 Hz and 0.25 in/sec at 5 Hz.

Skipp (*47*) lists a variety of national vibration limits, including the Czechoslovakian maximum code of 10 mm/sec (0.40 in/sec). Skipp states, "in countries without formal codes, good practice usually takes into account the intrusive element without specifying a particular damage state. In the U. K. for example for tunnel blasting, 10 mm/sec has been the aim in densely populated areas and 25 mm/sec in sparsely populated areas." The British Secretary of State specified that 12 mm/sec (0.47 in/sec) be used for surface coal mine blasts that generate frequencies below 12 Hz.

[1] Italic numbers in parentheses refer to items in the list of references preceding the appendixes.

Table A–1.—German vibration standards, DIN 4150

Type of construction	Peak pseudo vector sum particle velocity	
	mm/sec	in/sec
Ruins, ancient and historic buildings given antiquities protection	2	0.08
Buildings with visible damage and cracks in masonry	4	.16
Buildings in good condition, possibly with cracks in plaster	8	.32
Industrial and concrete structures without plaster	10–40	.39–1.56

Bogdanoff's damage paper (*6*) summarizes safe values from the text "Rock Blasting," by Langefors and Kihlstrom (*25*), given in table A–2. The propagation velocity (c) is related to particle velocity (V) and ground strain (e) according to:

$$e = \frac{V}{c}$$

Table A–2.—Damage levels from blasting, after Langefors and Kihlstrom (*25*)

Damage effects	Peak particle velocity					
	Sand, gravel, clay below water level; c = 1,000 – 1,500 m/sec[1]		Moraine, slate, or soft limestone; c = 2,000 – 3,000 m/sec		Granite, hard limestone, or diabase; c = 4,500 – 6,000 m/sec	
	mm/sec	in/sec	mm/sec	in/sec	mm/sec	in/sec
No noticeable crack formation	18	0.71	35	1.4	70	2.8
Fine cracks and falling plaster threshold	30	1.2	55	2.2	100	~~3.9~~ 4,3
Crack formation	40	1.6	80	3.2	~~150~~ 160	~~5.9~~ 6,3
Severe cracks	60	2.4	115	4.5	~~225~~ 230	~~8.9~~ 9,1

[1] Propagation velocity in media is given by c.

Table A–3.—Limiting safe vibration values of pseudo vector sum peak particle velocities, after Esteves (*17*)

Type of construction	Peak particle velocity					
	Incoherent loose soils, soft coherent soils, rubble mixtures: c < 1,000 m/sec[1] c < 3,300 ft/sec[1]		Very hard to medium consistence coherent soils, uniform or well-graded sand: c = 1,000–2,000 m/sec c = 3,300–6,600 ft/sec		Coherent hard soils and rock: c > 2,000 m/sec c > 6,600 ft/sec	
	mm/sec	in/sec	mm/sec	in/sec	mm/sec	in/sec
Special care, historical monuments, hospitals, and very tall buildings	2.5	0.10	5	0.20	10	0.40
Current construction	5	.20	10	.40	20	.80
Reinforced construction, e.g., earthquake resistant	15	.60	30	1.20	60	2.40

[1] Propagation velocity in media given by c.

Consequently, low-velocity materials will have higher ground strains (and potentials for failure) for a given particle velocity. Langefors and Kihlstrom did not give the experimental data to support their thresholds of table A–2. Esteves' study (*17*) includes safe values for a variety of conditions, including types of soil, construction, and frequency of blasting (table A–3). As with Langefors and Kihlstrom (table A–2), Esteves does not give the supporting experimental data. Ashley lists maximum particle velocities for a variety of structure types (*1*). Again, technical data to derive or support the recommended values are not given (table A–4).

Several survey papers have been written that combined nuclear blast, earthquake, and blasting data without pointing to the variations among vibration characteristics and the resulting response and damage potentials (*20, 34*). The worst-case experimental data are from the Salmon nuclear blast and the Mercury, Nev., studies. These results are overly conservative for blasting, and their use cannot be justified on technical grounds.

Cases occasionally arise where blasting vibration is considered a potential problem to equipment, or concern is expressed about the vibration sources such as traffic. The safe level criteria established for blasting are often applied to these situations with little justification. Traffic is usually a steady-state source of low amplitude. Appropriate safe levels would have to be lower than for blasting, which is relatively infrequent and of shorter duration. The British criterion for architectural damage from steady-state sources is 5 mm/sec (0.20 in/sec) (*55*). Vibration standards for laboratory instruments are given in table A–5.

Table A–4.—Limiting safe vibration values, after Ashley (*1*)

Type of construction	Peak particle velocity	
	mm/sec	in/sec
Ancient and historic monuments	7.5	0.30
Housing in poor repair	12	.47
Good residential, commercial, and industrial structures	25	1.0
Welded gas mains, sound sewers, engineered structures	50	2.0

Table A–5.—Vibration limits for laboratory instruments, after Whiffin and Leonard (*55*)

Dimensional and electrical physical reference standards	g[1]	0.01
Do	in/sec	[2]0.031
Dimensional working standards	g	0.02
Do	in/sec	[2]0.062
Electrical, physical working standards	g	0.03
Do	in/sec	[2]0.093
General electronic apparatus	in/sec	0.19
Mettler analytical balance	in/sec	[2]0.0125
Sartorius analytical balance	in/sec	[2]0.10
Leeds—Northrup Reflection Galvanometer	in/sec	[2]0.0125
Photo microscope	in/sec	1.44
Phillips EM 300 electron microscope	in/sec	0.00013
HAAS standards barometer	in/sec	0.08

[1] g = acceleration of gravity 9.8 m/sec^2 (32.2 ft/sec^2).
[2] At 20 Hz.

APPENDIX B.—ALTERNATIVE BLASTING LEVEL CRITERIA

Safe blasting vibration criteria were developed for residential structures, having two frequency ranges and a sharp discontinuity at 40 Hz (table 13). There are blasts that represent an intermediate frequency case, being higher than the structure resonances (4 to 12 Hz) and lower than 40 Hz. The criteria of table 13 apply equally to a 35-Hz and a 10-Hz ground vibration, although the responses and damage potentials are very much different.

Using both the measured structure amplifications (fig. 39) and damage summaries (figs. 52 and 54), a smoother set of criteria was developed. These criteria have more severe measuring requirements, involving both displacement and velocity (fig. B–1).

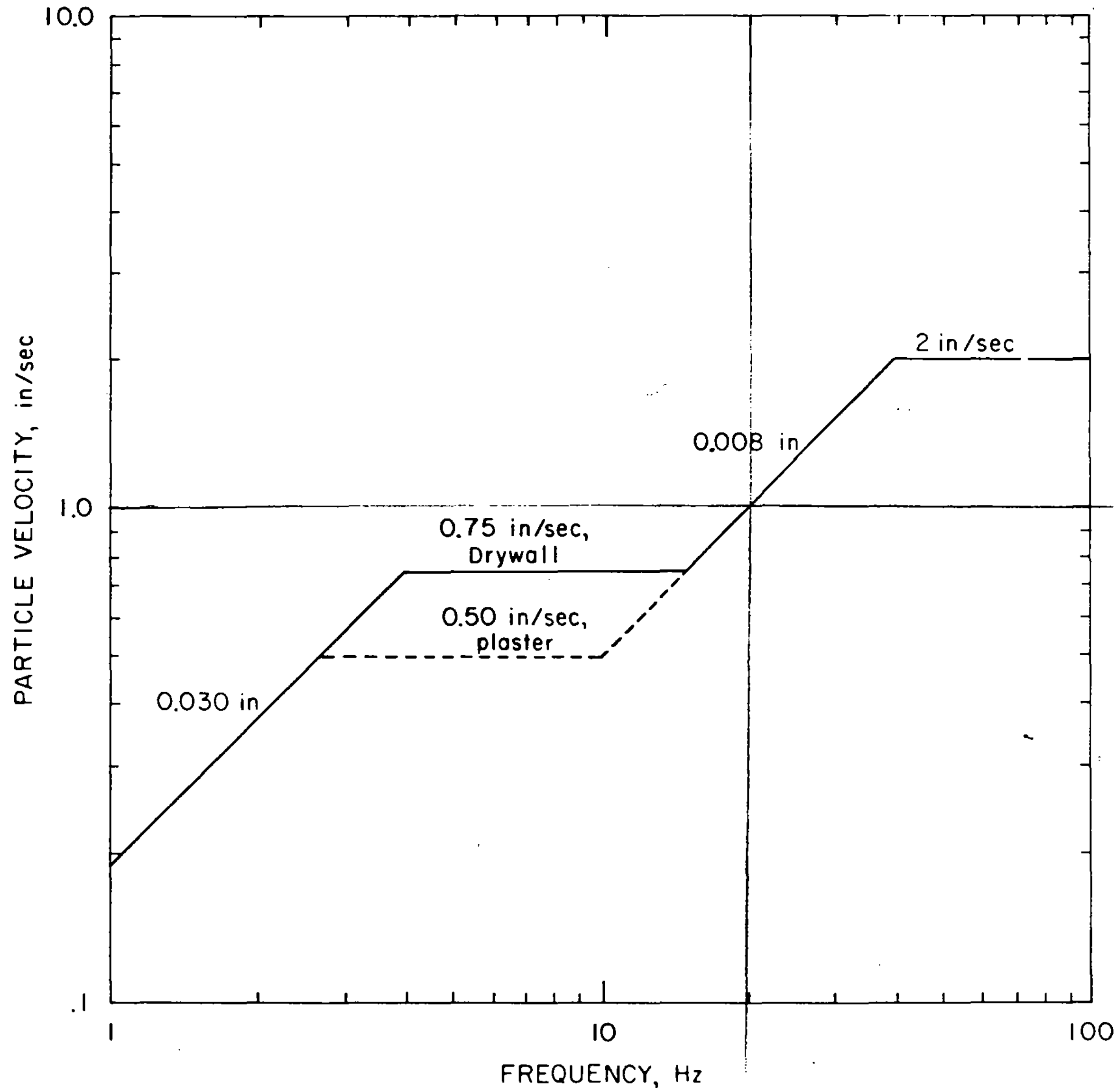

Figure B–1.—Safe levels of blasting vibration for houses using a combination of velocity and displacement.

Above 40 Hz, a constant peak particle velocity of 2.0 in/sec is the maximum safe value. Below 40 Hz, the maximum velocity decreases at a rate equivalent to a constant peak displacement of 0.008 in. At frequencies corresponding to 0.75 in/sec for Drywall, and 0.50 in/sec for plaster, constant particle velocities are again appropriate. An ultimate maximum displacement of 0.030 in is recommended, which would only be of concern where very low frequencies are encountered (< 4 Hz).

This scheme is based on the response and damage data, recognizes the displacement-bound requirement for house responses to blast vibrations, and provides a smooth transition for the intermediate frequency cases. This method of analyzing the damage potential of blasting vibrations has the disadvantage of possibly underestimating annoyance reactions. Midwall responses (fig. 40) do not decrease nearly as fast as structure (corner) responses as frequencies increase from 10 to 40 Hz. A very nearly linear decrease of velocity amplification was observed for the gross structure; however, the higher midwall response frequencies will make the 20- to 35-Hz vibrations relatively annoying if the maximum levels shown on figure B–1 are attained.

☆U.S. GOVERNMENT PRINTING OFFICE: 1983-705-020/105

INT.-BU.OF MINES,PGH.,PA. 25077

Bureau of Mines
Report of Investigations 8507

STRUCTURE RESPONSE AND DAMAGE
PRODUCED BY GROUND VIBRATION
FROM SURFACE MINE BLASTING

by

David E. Siskind, Mark S. Stagg,
John W. Kopp, and Charles H. Dowding

ERRATA

Page 1, line 14 should read "Safe levels" instead of "Save levels."

Page 3, footnote should read "Italic numbers" instead of "Underlined numbers."

Page 12 (table 1): Seven shots that were omitted are given on the attached page. In addition, for shot 134 "Peak ground vibration (H_2)" should be 0.32 instead of 0.36, and the column heading labeled "Sealed distance" should read "Scaled distance."

Page 19 (equation 2): Sign before $\frac{\beta}{\sqrt{1-\beta^2}}$ should be minus instead of plus.

Page 23 (table 3): Structures numbered 58 and above have some of the shots improperly indicated. The attached table shows the correct values, and is consistent with table 1.

Page 28, caption of figure 28 should be "Test structure 61, near a construction site."

Page 41 (table 5): Footnote 4 should show 119 dB airblast instead of 111 dB.

Page 42 (table 6): Values in "Mine blasts" column should read 0.377 instead of 0.472 and .314 instead of .392. Footnote 1 should have 119 dB airblast instead of 111 dB.

Page 48 (table 9): Jensen and Rietman reference number should be 21 instead of 57. Also, under "Damage observed, uniform classification," Nondamage and Threshold values for "Bureau of Mines new data" should be 76 and 28, respectively, not 37 and 23.

Page 71 (table A-2): Values in the "Granite, hard limestone, or diabase" column should be as follows:

mm/sec	in/sec
70	2.8
110	4.3
160	6.3
230	9.1

ADDITIONAL VALUES FOR TABLE 1 OF RI 8507

Production blasts and ground vibration measurements

Shot	Facility	Shot type	Total charge lb.	Lb per delay	Scaled distance $ft/lb^{1/2}$	Peak ground vibration, in/sec			Peak structure motion, in/sec							Structure number (table 3)	Structure type
									Low corner			High corner		Midwall			
						H_1	H_2	V	H_1	H_2	V	H_1	H_2	H_1	H_2		
155	Coal	Highwall..	5,400	120	43.0		0.43	0.55						0.84		44	1
156	Coal	....do....	3,600	80	41.0		0.96	0.57						0.76		44	1
173	Coal	....do....	2,150	86	27.0	0.59	0.96	1.01	0.56	0.66	1.19			0.74	2.55	51	2
176	Coal	....do....	3,550	71	6.9	5.58	2.34	2.61	2.85	1.32	4.09	3.43	1.41	9.14	2.69	51	2
177	Coal	....do....	3,240	36	9.7	3.90	2.44	1.65	2.13	2.2	2.60	3.53	2.28	7.06	2.82	51	2
209	Coal	....do....		80	19.0	4.50	1.17	[illegible]								58	1
W-17	Constr	Excavation	50	13	1.4	5.83	11.87	6.49	8.05	[illegible]	9.62	2.77	2.03	5.8	8.69	67	2

CORRECTIONS FOR TABLE 3 OF RI 8507

Test structures and measured dynamic properties

Structure	Shots (table 1)
57	201,202
58	203-209
59	W-1
60	W-2, W-3
61	W-4, W-5
62	W-6
63	W-7, W-8
64	W-9, W-10
65	W-11, W-12
66	W-13, W-14, W-15
67	W-16, W-17
68	W-18, W-19
69	W-20, W-21
70	W-22
71	W-23
72	W-24
73	W-25, W-26, W-27
74	W-28, W-29
75	W-30
76	W-31, W-32